



Selma GREBOVIC, MoE

Energy Stresses of Transmission Line Surge Arresters Due to Lightning Discharges

DOCTORAL THESIS

to achieve the university degree of
Doktorin der technischen Wissenschaften

submitted to

Graz University of Technology

Supervisor

Ao.Univ.-Prof. Dipl.-Ing.Dr.techn. Stephan PACK

Institute of High Voltage Engineering and System Performance

AFFIDAVIT

I declare that I have authored this thesis independently, that I have not used other than the declared sources/resources, and that I have explicitly indicated all material which has been quoted either literally or by content from the sources used. The text document uploaded to TUGRAZonline is identical to the present doctoral thesis.

Date

Signature

*To my dear parents,
and in loving memory of
Professor Salih Sadovic*

Abstract

Although we can say nowadays that we understand lightning more than ever, this phenomenon is still left to be conquered and fully understood. In this work we have discovered and identified some features of lightning for the first time. Our main aim of this work was transmission lines surge arrester energy duty calculation and consideration due to bipolar and multicomponent lightning flashes.

For the first time we have identified bipolar lightning current parameters which are needed for modelling, simulations and analysis of transients in power systems. Those are: positive and negative charge transfer, two current peaks (for positive and negative part), two front and two tail times (for positive and negative part) and duration of positive and negative part of bipolar stroke. We have extracted some specific lightning flashes from large number of lightning location system data, such as: flashes that involve return strokes of opposite polarity, flashes with currents of subsequent strokes larger than the current of the first stroke and flashes that consist of more than 30 components.

In this work for the first time we have also created and solved complete transmission line in the EMTP-RV software for the purpose of the transient analysis. Our transmission line model included modelling of: phase conductors, shield wire (for shielded line design), transmission line tower, and tower footing resistance, line surge arresters, lightning current source and substation.

The major contributions of this work are calculation and consideration of transmission line surge arrester energy duty due to bipolar and multicomponent lightning flashes. Energy stresses of transmission line surge arresters due to bipolar and multicomponent lightning flashes are analysed for the first time in this work. Then we have made an analogy between calculation of line surge arrester energy duty in EMTP – RV and MATLAB.

We have also created transmission line surge arrester energy duty calculation procedure (due to bipolar and multicomponent lightning flashes). In order to select the appropriate arrester, parametric analysis was carried out, considering different parameters that affect arrester's energy calculation. Together with usually considered parameters, line surge arrester energy duty calculation and consideration have been made in the case of non – uniform tower footing resistance distribution.

In the end we have come to two important results: that we have identified parameters of bipolar lightning current and conclusion that the arrester energy rises up as the bipolar or multicomponent lightning current arrives at the arrester. Bipolar and multicomponent lightning flashes are very dangerous and destructive for line surge arrester as well as for complete transmission line. With our work we have hopefully answered some questions considering lightning phenomenon and opened more new ones.

List of keywords – bipolar lightning flashes, multicomponent lightning flashes, direct measurements at towers, lightning location systems, gapless line surge arresters, line surge arrester energy duty, shielded line, unshielded line, modelling, simulation, EMTP – RV, MATLAB, parametric analyses.

Acknowledgments

Writing a thesis is often considered a solitary act. However, there are a lot of persons involved in the process of writing a thesis, some without even noticing it.

Firstly, I would like to express my sincere gratitude to my supervisor Professor Stephan Pack for the continuous support of my PhD study and related research, for his patience, motivation, and immense knowledge. His guidance helped me throughout the research and writing of this thesis. The technical problems always were easier when discussing with a person of such great talent and intelligence. I could not have imagined having a better advisor and mentor for my PhD study.

Besides my supervisor, I would like to express my deep appreciation and gratitude to Professor Salih Sadovic. Professor Sadovic had a huge influence on my life, inspired me to study Electrical Power Engineering and encouraged me to begin my PhD study at Graz University of Technology. But besides that, he gave me the most precious gifts – his time, friendship and sincere care for me. With my future work I will try to elevate all that this virtuoso gave me, first of all knowledge and professionalism, but also sincere human values which he unselfishly shared with all those willing and ready to hear.

My sincere thanks also goes to Professor Lothar Fickert for his advices, support, friendship and for his tremendous hospitality during my stays to Graz.

I would like to express my gratitude to Professor H. D. Betz and his company Nowcast GmbH, Germany, for the authorization of using their LINET – Lightning Location System data for the purposes of this work. Also, I would like to express my thanks to Dr. Tarik Sadovic and Professor Salih Sadovic for the support and to Sadovic Consultant company, France, for the authorization of using their measured lightning current data for the purposes of this work.

My special gratitude to: Professor Ivo Uglesic, Dr. Alain Xemard, Dr. Wolfgang Schulz, Dr Bozidar Filipovic-Grcic, Dr. Stephan Pedebay and many other experts for their participation in many discussions regarding my work and for their kindness during the conferences.

I would also like to thank all of my friends who supported me in writing, and incited me to strive towards my goal. Just to name a few: Djana, Sanda, Selma, Miro and Samira.

A special thanks to my family. Words cannot express how grateful I am to my mother Elvedina and father Kasim for all of the sacrifices that they have made on my behalf. I know that success is in my stride, because I have parents like you by my side. Thanks for everything.

Table of Contents

Abstract	<i>i</i>
Acknowledgements	<i>ii</i>
Table of Contents	<i>iii</i>
List of Abbreviations and Symbols	<i>vii</i>
List of Figures	<i>xi</i>
List of Tables	<i>xx</i>
1. Chapter 1	1
Introduction	1
1.1. Contributions of Thesis	3
1.2. Chapter Summaries	4
2. Chapter 2 – Lightning Phenomenon	5
2.1. Introduction	5
2.2. Lightning Terminology	5
2.3. Types of Lightning Discharges	6
2.4. Models of Charge Transfer to Ground	7
2.5. Bipolar Lightning	8
2.5.1. Bipolar Lightning Definition	8
2.5.2. Bipolar Lightning Occurrence	9
2.5.3. Types of Bipolar Discharges	11
2.5.4. Definition of Parameters	12
2.5.5. Bipolar Lightning in Austria	13
2.5.6. A Possible Explanation of Observed Bipolar Lightning	13
2.6. Multicomponent Flashes	16

3. Chapter 3 – Line Surge Arresters	18
3.1. Introduction	18
3.2. Types of Line Surge Arresters	18
3.2.1.Externally Gapped Line Arresters (EGLAs)	19
3.2.2.Gapless Line Arresters (NEGLAs)	19
3.3. Metal Oxide Block and Housing	20
3.4. U – I characteristics	21
3.5. Energy Handling Capability, Temperature and Degradation	22
3.5.1.Thermal Energy Handling Capability	23
3.5.2.Temperature of MO Varistor Materials	24
3.5.3.Factors Affecting Rate of Degradation	25
3.6. Illustration of LSA Cooling and Energy Absorption	26
3.7. Discussion NEGLA vs EGLA	27
3.8. The NEGLA Selection Process	28
4. Chapter 4 – Recorded Bipolar and Multicomponent Flashes Analysis	31
4.1. Introduction	31
4.2. Lightning Activity Monitoring System and Lightning Location System	32
4.3. Bipolar Lightning Current Shape	34
4.4. Multicomponent Flashes Data	36
4.5. Lightning Parameters Comparison	39
5. Chapter 5 – Modelling Procedures	40
5.1. Introduction	40
5.2. Fundamental Mathematical Models	41
5.2.1.Phase Conductors and Shield Wire Model	41
5.2.2.Transmission Line Tower Model	42
5.2.3.Tower Footing resistance Model	44
5.2.4.Line Surge Arrester Model	45
5.2.5.Line Surge Arrester Energy Duty Calculation	45

5.2.6.	Lightning Current Model	46
5.2.7.	Substation Model	47
5.3.	EMTP – RV Models	51
5.3.1.	Model for Phase Conductors and Shield Wire in EMTP – RV	51
5.3.2.	Transmission Line Tower Model in EMTP – RV	53
5.3.3.	Tower Footing Resistance Model in EMTP – RV	55
5.3.4.	Line Surge Arrester Model in EMTP – RV	56
5.3.5.	Analogy between Calculation of Line Surge Arrester Energy Duty in MATLAB and EMTP – RV	57
5.3.6.	Lightning Current Model in EMTP – RV	59
5.3.7.	Substation Model in EMTP – RV	60
5.4.	Modelling of Complete Transmission Line and EMTP – RV 's Grouping Elements into Subcircuits	62
5.5.	Summary of Modelling and Calculation Procedure for Transient Studies	65
6.	Chapter 6 – Simulations and Results	68
6.1.	Introduction	68
6.2.	Line Surge Arrester Energy Duty Calculations – Conducted Simulations	69
6.2.1.	Unshielded and Shielded Transmission Line Designs – Description	69
6.2.2.	Effect of Bipolar Lightning Stroke on Arrester Energy Duty – Unshielded Line Design	70
6.2.3.	Effect of Bipolar Lightning Stroke on Arrester Energy Duty – Shielded Line Design	72
6.2.4.	Multicomponent Flashes	74
6.2.5.	Effect of Multicomponent Lightning Flashes on Arrester Energy Duty – Unshielded Line Design	76
6.2.6.	Effect of Multicomponent Lightning Flashes on Arrester Energy Duty – Shielded Line Design	80
6.3.	Arrester Energy Sharing and Importance of Complete Transmission Line Modelling	83
6.4.	Parametric Analysis	85

6.4.1. Influence of Uniform Tower Footing Resistance Distribution on Line Surge Arrester Energy Duty – Unshielded Line Design	86
6.4.2. Influence of Uniform Tower Footing Resistance Distribution on Line Surge Arrester Energy Duty – Shielded Line Design	89
6.4.3. Arrester Energy Duty Consideration for Different Arrester Installation Configuration – Unshielded Line Design	91
6.4.4. Arrester Energy Duty Consideration for Different Arrester Installation Configuration – Shielded Line Design	93
6.4.5. Influence of Lightning Channel Impedance on Line Surge Arrester Energy Duty – Unshielded Line Design	97
6.4.6. Influence of Lightning Channel Impedance on Line Surge Arrester Energy Duty – Shielded Line Design	99
6.4.7. Influence of Non – Uniform Tower Footing Resistance Distribution on Line Surge Arrester Energy Duty – Unshielded Line Design	101
6.4.8. Influence of Non – Uniform Distributed Tower Footing Resistance on Line Surge Arrester Energy Duty for Nearest and Farthest Tower	108
6.4.9. Influence of Front Time, Tail Time and Current Peak on Arrester Energy Duty	112
7. Chapter 7 – Summary of results, conclusions and recommendations	116
References	128
Appendix A.	
Lightning Current Shape Parameters, Bipolar and Multicomponent Flashes	A1
A.1. Lightning current shape parameters	A1
A.2. Bipolar Lightning Current Shapes	A3
A.3. Multicomponent Flashes Data	A14
A.4. Basic Flowcharts of Software for Lightning Data Analyses	A22
Appendix B.	
MATLAB Code for Line Surge Arrester Energy Duty Calculation	B1

List of Abbreviations and Symbols

Abbreviations	Description
AC	Alternating current
BIL	Basic insulation level
CC	Cloud to cloud lightning discharges
CFO	Critical Flashover Voltage
CG	Cloud to ground lightning discharges
CP	Constant parameter
CPU	Central processing unit
DC	Direct current
EGLA	Externally gapped line surge arresters
EMTP – RV	ElectroMagnetic Transient Program – Restructured Version
GM	Geometrical mean
GMT	Greenwich mean time
IC	Cloud lightning discharges (intracloud, intercloud, and cloud-to-air)
IS	Lightning current initial stage
LSA	Line surge arrester
MCOV	Maximum continuous operating voltage
MO	Metal oxide
NEGLA	Gapless line surge arresters
RAM	Random access memory
SiC	Silicon carbide
SVU	Series varistor unit
TOV	Temporary overvoltage
ZnO	Zinc oxide

Symbol	Unit	Description
A, B	--	Constants needed for computation of power transformer surge capacitance
b	m	Distance
C_B	nF	Breaker total surge capacitance to ground
C_E	nF	Disconnecter switches and bus support insulators surge capacitance to ground
C_{MT}	nF	Measuring transformer surge capacitance to ground
C_{PT}	nF	Power transformer surge impedance to ground
E	kJ	Arrester energy
E_g	kV/m	Soil ionisation critical electric field
h	m	Tower height
h_1	m	Tower height from base to waist
h_2	m	Tower height from waist to top
h_c	m	Conductor average height
I	kA	stroke current through the resistance
i_{ar}	kA	Arrester current
$I_{CIGRE}(t)$	kA	CIGRE lightning current shape model
I_g	kA	Limiting current to initiate sufficient soil ionization
i_k	kA	Current vector determined from line surge arrester U – I characteristic
I_{max+}	kA	Peak of positive part of bipolar stroke
I_{max-}	kA	Peak of negative part of bipolar stroke
k	--	Parameter depends upon the dimensions of valve block
L_n	H	Branch inductance
l_n	m	Length of tower section
Q_-	As or C	Negative charge transfer
Q_+	As or C	Positive charge transfer

Symbol	Unit	Description
Q_{total}	As or C	Summary of the negative and positive charge transfers
r	m	Tower base radius
r_1	m	Tower top radius
r_2	m	Tower radius at waist
r_3	m	Tower base radius
r_{avg}	m	Weighted average of the tower radius
r_c	m	Conductor radius
R_i	Ω	Tower footing impulse resistance
R_0	Ω	Footing resistance at low current and low frequency
S_{PT}	MVA	Power transformer rating per phase
t_{f+}	μs	Front time for positive part of bipolar stroke
t_{f-}	μs	Front time for negative part of bipolar stroke
t_{h+}	μs	Tail time for positive part of bipolar stroke
t_{h-}	μs	Tail time for negative part of bipolar stroke
T_+	μs	Positive current component duration
T_-	μs	Negative current component duration
$T_{instrnc}$	ms	Interstroke time interval
T_{nc}	ms	No – current time interval
T_{total}	μs	Summary of the negative, positive current component duration, no – current interval and interstroke interval
u_{ar}	kV	Arrester voltage
U_i	kV	Interpolated voltage vector
u_k	kV	Voltage vector determined from line surge arrester U – I characteristic
V	cm^3	Volume of metal oxide block
v	m/ μs	propagation velocity
W	J	Energy of metal oxide block
Z_{ch}	Ω	Lightning channel impedance

Symbol	Unit	Description
Z_m	Ω	Mutual impedance
Z_s	Ω	Self impedance
Z_T	Ω	Tower surge impedance
\mathbf{Z}_T	Ω	Thevenin impedance matrix
α	--	Parameter depends upon the valve block material
g	$^{\circ}\text{C}$	Temperature of metal oxide block
ρ	Ωm	Soil resistivity

List of Figures

2.3.1	Classification of cloud discharges [1,3]	6
2.3.2	Four types of lightning effectively lowering cloud charge to ground. Only the initial leader is shown for each type. In each lightning-type name given below the sketch, the direction of propagation of the initial leader and the polarity of the cloud charge effectively lowered to ground are indicated. [3]	6
2.4.1	Schematic representation of current versus height profiles for three modes of charge transfer to ground in negative lightning subsequent strokes: (a) dart-leader–return-stroke sequence, (b) continuing current, and (c) M-component. The corresponding current versus time waveform represents the current at the ground. [1]	8
2.5.1.	The first type of bipolar lightning discharge [3]	11
2.5.2.	The second type of bipolar lightning discharge [3]	11
2.5.3.	The third type of bipolar lightning discharge [3]	12
2.5.4.	Definitions of the negative current component duration, positive current component duration, total duration and their associated charge transfers of bipolar flashes. [4] ..	12
2.5.5.	A possible explanation of observed bipolar lightning currents. Currents of both polarities follow, in turn, the same channel to the ground, with negative charge transfer from the cloud charge region labelled “1” being followed by positive charge transfer from the charge region labelled “2”. [1, 3]	13
2.5.6.	Electrical structure of a convective cloud. Note pockets of positive and negative charge (numerous smaller encircled plus and minus signs) at different altitudes, while the net charge at the top of the cloud is positive and that at the bottom of the cloud is negative (larger encircled and minus signs). Adapted from Imyanitov et al. (1971). [1, 3]	14
2.5.7.	Illustration of the mechanism proposed to explain natural bipolar cloud-to-ground flashes. The two minus signs represent a single charge region, partially inside the cloud and partially outside the cloud [5, 6]	15
3.2.1.	Design concept and standard configuration of an EGLA [28, 32]	19
3.2.2.	Installations of an NEGLA [35]	19
3.3.1.	Typical ZnO block [35, 40]	20
3.4.1.	Typical varistor/arrester U-I characteristics [44]	21
3.5.1.	Heat loss – input diagram for steady state operation of a ZnO surge arrester [41]	23

3.5.2.	Metal-oxide resistor energy per volume vs. Temperature [46]	24
3.6.1.	Illustration of case when line surge arrester absorbs energy due to bipolar or multicomponent lightning flash as well as LSA's cooling process	26
3.8.1.	Selection of an NEGLA in six steps	30
4.2.1.	Block diagram of lightning monitoring system installed on Corsica [62]	32
4.2.2.	Current transformer installed on lightning rod of the telecom base station at Milccia and monitoring system [62].....	32
4.2.3.	LINET sensor installation	33
4.3.1.	Shape of bipolar current for event recorded on the 11 th of December 2011 at 16:08:15.855 GMT	34
4.4.1.	Display and histogram of interstroke time interval data for flash 3	38
5.1.1.	Information required for system modelling	40
5.2.1.	Distributed parameter line model [75]	41
5.2.2.	Tower representation	42
5.2.3.	Tower shapes [77]	43
5.2.4.	Lightning stroke representation with Norton equivalent circuit	47
5.2.5.	Power transformer representation [87]	48
5.2.6.	Circuit breaker representation [87]	49
5.2.7.	Measuring transformer representation [87]	49
5.3.1.	Transmission line model	51
5.3.2.	EMTP – RV CP line multiphase	51
5.3.3.	EMTP – RV CP line three phase	52
5.3.4.	Input data for EMTP – RV CP line multiphase – Shielded line model	52
5.3.5.	Input data for EMTP – RV CP line 3 – phase – Unshielded line model	53
5.3.6.	Tower surge impedance calculator – C#	53
5.3.7.	Tower model in EMTP – RV	54
5.3.8.	EMTP – RV symbol for tower subcircuit	54
5.3.9.	EMTP – RV tower footing resistance representation for nonlinear soil ionization model	55
5.3.10.	Three basic metal oxide arrester types	56

5.3.11.	Modelling procedure of arrester in EMTP – RV	56
5.3.12.	Arrester $U - I$ characteristic	57
5.3.13.	Arrester current and voltage (interpolated in MATLAB and calculated in EMTP – RV)	58
5.3.14.	Analogy between calculation of line surge arrester energy duty in MATLAB and EMTP – RV	58
5.3.15.	Modelling procedure of ideal current source in EMTP – RV	59
5.3.16.	Lightning stroke representation with Norton equivalent circuit in EMTP – RV	59
5.3.17.	Substation model in EMTP –RV	60
5.3.18.	EMTP – RV symbol for substation subcircuit	61
5.3.19.	EMTP – RV block for substation modelled as the voltage sources with a Thevenin impedance	61
5.4.1.	Main idea of the EMTP – RV modelling	62
5.4.2.	Span division in two segments	62
5.4.3.	Elements needed for modelling complex subcircuit (line section)	63
5.4.4.	EMTP – RV section of transmission line	63
5.4.5.	Illustration of complete transmission line model in EMTP – RV	64
5.5.1.	Flowchart of procedure for transient studies of transmission lines	65
6.1.1.	EMTP – RV and MATLAB in simulation process	68
6.2.1.	Lightning flash is injected to the middle of the span of top phase conductor	69
6.2.2.	Lightning flash is applied to the tower top	69
6.2.3.	Illustration of bipolar lightning effect on arrester energy duty – unshielded line design	70
6.2.4.	Arrester current and energy duty calculated for arrester installed on the middle phase conductor – unshielded line design	71
6.2.5.	Arrester current and energy duty calculated for arrester installed on the bottom phase conductor – unshielded line design	71
6.2.6.	Illustration of bipolar lightning effect on arrester energy duty – shielded line design	72
6.2.7.	Arrester current and energy duty from figure 6.2.6 – shielded line design	72

6.2.8.	Arrester current and energy duty calculated for arrester installed on the top phase conductor – shielded line design	73
6.2.9.	Arrester current and energy duty calculated for arrester installed on the middle phase conductor – shielded line design	73
6.2.10.	Multicomponent flash #1 from chapter 4	74
6.2.11.	Multicomponent flash #2 from chapter 4	75
6.2.12.	Multicomponent flash #3 from chapter 4	75
6.2.13.	Arrester current due to flash # 1 – unshielded line design	76
6.2.14.	Arrester current due to flash # 1, and flash #1 current comparison – unshielded line design	76
6.2.15.	Arrester energy duty due to flash # 1 – unshielded line design	77
6.2.16.	Arrester energy duty due to flash # 1 zoomed – in	77
6.2.17.	Arrester current due to flash # 2 – unshielded line design	78
6.2.18.	Arrester energy duty due to flash # 2 – unshielded line design	78
6.2.19.	Arrester current due to flash # 3 – unshielded line design	79
6.2.20.	Arrester energy duty due to flash # 3 – unshielded line design	79
6.2.21.	Arrester current due to flash # 1 – shielded line design	80
6.2.22.	Arrester energy duty due to flash # 1 – shielded line design	80
6.2.23.	Arrester current due to flash # 2 – shielded line design	81
6.2.24.	Arrester energy duty due to flash # 2 – shielded line design	81
6.2.25.	Arrester current due to flash # 3 – shielded line design	82
6.2.26.	Arrester energy duty due to flash # 3 – shielded line design	82
6.3.1.	Percentage (with respect to energy absorbed by arrester at tower first to the point of lightning impact) of energy shared by adjacent arresters at towers along the line – 10 towers case	83
6.3.2.	Percentage (with respect to energy absorbed by arrester at tower first to the point of lightning impact) of energy shared by adjacent arresters at towers along the line – 30 towers case	84
6.3.3.	Percentage (with respect to energy absorbed by arrester at tower first to the point of lightning impact) of energy shared by adjacent arresters at towers along the line – comparison 10 and 30 towers	84
6.4.1.	Arrester energy duty for different values of tower footing resistance – on the first tower to the point of lightning impact – unshielded line design	86

6.4.2.	Arrester energy change due to bipolar lightning for different values of tower footing resistance – on the first tower from the point of lightning impact – unshielded line design	86
6.4.3.	Arrester energy duty for different values of tower footing resistance – on the second tower to the point of lightning impact – unshielded line design	87
6.4.4.	Arrester energy change due to bipolar lightning for different values of tower footing resistance – on the second tower to the point of lightning impact – unshielded line design	87
6.4.5.	Arrester energy duty for different values of tower footing resistance – on the third tower to the point of lightning impact – unshielded line design	87
6.4.6.	Arrester energy change due to bipolar lightning for different values of tower footing resistance – on the third tower from the point of lightning impact – unshielded line design	88
6.4.7.	Maximum arrester energy for different values of tower footing resistance along unshielded transmission line	88
6.4.8.	Arrester energy duty for different values of tower footing resistance – shielded line design	89
6.4.9.	Arrester energy change due to bipolar lightning for different values of tower footing resistance – shielded line design	89
6.4.10.	Bottom phase arrester energy for different values of tower footing resistance along shielded transmission line	90
6.4.11.	Energy of arrester installed on all three phases along unshielded transmission line – tower footing resistance 10 Ω	91
6.4.12.	Energy of arrester installed on all three phases along unshielded transmission line – tower footing resistance 100 Ω	91
6.4.13.	Energy of arrester installed on the top and middle phases along unshielded transmission line – tower footing resistance 10 Ω	92
6.4.14.	Energy of arrester installed on the top and middle phases along unshielded transmission line – tower footing resistance 100 Ω	92
6.4.15.	Energy of arrester installed on all three phases along shielded transmission line – tower footing resistance 10 Ω	93
6.4.16.	Energy of arrester installed on all three phases along shielded transmission line – tower footing resistance 100 Ω	93
6.4.17.	Energy of arresters installed on the middle and bottom phase conductors along shielded transmission line – tower footing resistance 10 Ω	94
6.4.18.	Energy of arresters installed on the middle and bottom phase conductors along shielded transmission line – Tower footing resistance 100 Ω	94

6.4.19.	Energy of arresters installed on the bottom phase conductor along shielded transmission line –resistance 10 Ω	95
6.4.20.	Energy of arresters installed on the bottom phase conductor along shielded transmission line – tower footing	95
6.4.21.	Arrester energy for different values of lightning channel impedance – unshielded line design	98
6.4.22.	Percentage of energy decrease in regard to case when ideal current source is used – unshielded line design	98
6.4.23.	Arrester energy for different values of lightning channel impedance – shielded line design	100
6.4.24.	Percentage of energy decrease in regard to case when ideal current source is used – shielded line design	100
6.4.25	Arrester energy vs. distance from the point of lightning impact – towers have same footing resistance	101
6.4.26.	Illustration of low and high tower footing resistance regions	101
6.4.27.	Energy of arresters for 50 Monte Carlo simulations	102
6.4.28.	Tower footing resistance for 5 simulation cases	103
6.4.29.	Arrester energy for 5 simulation cases	103
6.4.30.	Arrester energy and tower footing resistance for 1 simulation case	104
6.4.31.	Examples of uniform and non-uniform tower footing resistance distributions	104
6.4.32.	Arresters energies for uniform and non-uniform tower footing resistance distributions from figure 6.4.31.	105
6.4.33.	Tower footing resistance for 5 simulation cases	106
6.4.34.	Arrester energy for 5 simulation cases	106
6.4.35.	Arrester energy and tower footing resistance for 1 simulation case	107
6.4.36.	Examples of uniform and non-uniform tower footing resistance distributions	107
6.4.37.	Arresters energies for uniform and non-uniform tower footing resistance distributions from figure 6.4.36.	108
6.4.38.	Change of tower footing resistance for tower nearest to the point of lightning impact	109
6.4.39.	Change of energy of arrester installed on tower nearest to the point of lightning impact	109

6.4.40.	Histogram of tower footing resistance for tower nearest to the point of lightning impact	109
6.4.41.	Histogram of energy for arrester installed on tower nearest to the point of lightning impact	110
6.4.42.	Change of tower footing resistance for tower farthest of the point of lightning impact	110
6.4.43.	Change of energy of arrester installed on tower farthest to the point of lightning impact	111
6.4.44.	Histogram of tower footing resistance for tower farthest to the point of lightning impact	111
6.4.45.	Histogram of energy for arrester installed on tower farthest to the point of lightning impact	111
6.4.46.	Arrester energy duty due to different front times – unshielded line design	112
6.4.47.	Arrester energy duty due to different tail times – unshielded line design	113
6.4.48.	Arrester energy duty due to different tail times – unshielded line design	115
7.1.1.	Analogy between calculation of line surge arrester energy duty in EMTP – RV and MATLAB	118
7.1.2.	Percentage of energy (with respect to energy absorbed by arrester at tower placed first to the point of lightning impact) shared by adjacent arresters at towers along the line – comparison 10 and 30 towers	119
7.1.3.	Illustration of bipolar lightning effect on arrester energy duty – unshielded and shielded line designs respectively	120
7.1.4.	Arrester current due to flash #1 and zoomed in diagram of comparison between arrester current due to flash #1 and flash #1 current – unshielded line design	121
7.1.5.	Arrester energy duty due to flash #1 and zoomed in diagram of arrester energy duty due to flash #1	121
7.1.6.	Arrester current and arrester energy duty due to flash #1 – shielded line design	122
7.1.7.	Arrester energy duty for different values of tower footing resistance (left) and arrester energy change due to bipolar lightning for different values of tower footing resistance (right) – for nearest arrester from the point of lightning impact – unshielded line design	122
7.1.8.	Arrester energy change due to bipolar lightning for different values of tower footing resistance – on the second tower from the point of lightning impact (left) and on the third tower from the point of lightning impact (right) – unshielded line design	123

7.1.9.	Arrester energy duty for different values of tower footing resistance and arrester energy change due to bipolar lightning for different values of tower footing resistance – for nearest arrester from the point of lightning impact – shielded line design	123
7.1.10.	Examples of uniform and non-uniform tower footing resistance distributions – region of low tower footing resistance (left) and region of high tower footing resistance (right)	124
7.1.11.	Arresters energies for uniform and non-uniform tower footing resistance distributions – region of low tower footing resistance (left) and region of high tower footing resistance (right)	124
7.1.12.	Arrester energy for different lightning channel impedance values – unshielded line design (left) and shielded line design (right)	125
7.1.13.	Arrester energy duty due to different front times (left) and arrester energy duty due to different tail times (right) – unshielded line design	125
7.1.14.	Arrester energy duty due to flash # 1 (left) and flash #3 (right) – unshielded line design	126
A.1.1.	Definition of current shape parameters (illustrated for a negative impulse)	A1
A.2.1.	Shape of bipolar current for event 1	A3
A.2.2.	Shape of bipolar current for event 2	A4
A.2.3.	Shape of bipolar current for event 3	A4
A.2.4.	Shape of bipolar current for event 4	A5
A.2.5.	Shape of bipolar current for event 5	A5
A.2.6.	Shape of bipolar current for event 6	A6
A.2.7.	Shape of bipolar current for event 7	A6
A.2.8.	Shape of bipolar current for event 8	A7
A.2.9.	Shape of bipolar current for event 9	A7
A.2.10.	Shape of bipolar current for event 10	A8
A.2.11.	Shape of bipolar current for event 11	A8
A.2.12.	Shape of bipolar current for event 12	A9
A.2.13.	Shape of bipolar current for event 13	A9
A.2.14.	Histogram of current peaks for positive parts of bipolar lightning currents	A10
A.2.15.	Histogram of current peaks for negative parts of bipolar lightning currents	A10
A.2.16.	Histogram of positive charge transfer of bipolar lightning strokes	A11

A.2.17.	Histogram of negative charge transfer of bipolar lightning strokes	A11
A.2.18.	Histogram of time duration for positive parts of bipolar lightning strokes	A12
A.2.19.	Histogram of time duration for negative parts of bipolar lightning strokes	A12
A.3.1.	Display and histogram of interstroke time interval data for flash 3	A15
A.3.2.	Display and histogram of interstroke time interval data for flash 4	A17
A.3.3.	Display and histogram of interstroke time interval data for flash 5	A19
A.3.4.	Display and histogram of interstroke time interval data for flash 6	A21
A.4.1.	Basic flowchart for measured bipolar lightning current analysis	A22
A.4.2.	Basic flowchart of software for extraction of specific multicomponent lightning flashes	A23

List of Tables

2.5.1.	Bipolar lightning occurrence	10
2.6.1.	Average number of strokes per negative flash	16
3.3.1.	Example of correlation between block diameter and energy capability	21
3.7.1.	EGLA advantages and disadvantages	27
3.7.2.	NEGLA advantages and disadvantages	27
4.3.1.	Bipolar events recorded on Corsica	34
4.3.2.	Parameters of bipolar stroke from figure 4.2.1	35
4.4.1.	Average number of strokes per flash for two locations in Montenegro	36
4.4.2.	LINET data for flash 1	36
4.4.3.	LINET data for flash 2	37
4.4.4.	Interstroke time interval for flash 2	37
4.4.5.	LINET data for flash 3	37
4.4.6.	Interstroke time interval for flash 3	38
4.4.7.	Summary of basic data for flash 3	38
5.2.1.	Tower surge impedance formulas [64, 78]	43
5.2.2.	Constants used for the computation of the power transformers surge capacitance	48
5.2.3.	Power transformer surge capacitance to ground (nF)	48
5.2.4.	Dead tank breaker total surge capacitance to ground	49
5.2.5.	Measuring transformer surge capacitance to ground C_{MT} (nF)	49
5.2.6.	Disconnecter switches and bus support insulators surge capacitance to ground C_E (nF)	50
5.3.1.	Shielded line conductor data [90]	52
5.3.2.	Guidelines to represent metal oxide surge arresters	57

5.3.3.	Line surge arrester energy calculated in EMTP – RV and MATLAB	59
6.2.1.	Maximum values of lightning current, arrester current and arrester energy	70
6.3.1.	Percentage of absorbed energy	84
6.4.1.	Middle phase arrester energy for different LSA installation configuration (resistance 10 Ω)	95
6.4.2.	Bottom phase arrester energy for different LSA installation configuration (resistance 10 Ω)	96
6.4.3.	Middle phase arrester energy for different LSA installation configuration (resistance 100 Ω)	96
6.4.4.	Bottom phase arrester energy for different LSA installation configuration (resistance 100 Ω)	96
6.4.5.	Maximum line surge arrester energy for different values of lightning channel impedance and percentage of energy decrease – unshielded line design	97
6.4.6.	Maximum line surge arrester energy for different values of lightning channel impedance and percentage of energy decrease – shielded line design	99
6.4.7.	Input and output data for simulation 1 – different front time	112
6.4.8.	Input and output data for simulation 2 – different front time	112
6.4.9.	Input and output data for simulation 3 – different front time	113
6.4.10.	Input and output data for simulation 4 – different front time	113
6.4.11.	Input and output data for simulation 1 – different tail time	114
6.4.12.	Input and output data for simulation 2 – different tail time	114
6.4.13.	Input and output data for simulation 3 – different tail time	114
6.4.14.	Input and output data for simulation 4 – different tail time	114
6.4.15.	Input and output data for simulation 4 – different tail time	114
6.4.16.	Energy duty values due to bipolar lightning flash for unshielded and shielded line design	115
6.4.17.	Energy duty values due to multicomponent lightning flash for unshielded and shielded line design	115
A.3.1.	LINET data for flash 1	A14
A.3.2.	LINET data for flash 2	A14
A.3.3.	LINET data for flash 3	A14
A.3.4.	Interstroke time interval for flash 3	A15

A.3.5.	Summary of basic data for flash 3	A15
A.3.6.	LINET data for flash 4	A16
A.3.7.	Interstroke time interval for flash 4	A16
A.3.8.	Summary of basic data for flash 4	A17
A.3.9.	LINET data for flash 5	A17
A.3.10.	A.3.10. Interstroke time interval for flash 5	A18
A.3.11.	Summary of basic data for flash 5	A18
A.3.12.	LINET data for flash 6	A19
A.3.13.	Interstroke time interval for flash 6	A20
A.3.14.	Summary of basic data for flash 6	A20

Chapter 1.

INTRODUCTION

Lightning influences our everyday life. Although lightning is one of the most common natural phenomenon, it is very poorly understood. The study and understanding of lightning is important in areas that range from environmental sciences to different engineering fields. The preliminary understanding of the lightning phenomenon was established by Benjamin Franklin early in the 18th century. From Benjamin Franklin's period until 20th century this phenomenon was insufficiently explored. During 1950s and 1960s, extensive experimental data recorded by professor Berger and his team on the top of two instrumented towers in Monte San Salvatore (Switzerland) resulted in a complete statistical characterization of lightning current parameters, which are still considered to be the reference in lightning protection standards. However, the results obtained by professor Berger and his team suffered from the technological limitations of the instruments, in particular an insufficient frequency bandwidth of a few hundred kHz, despite the fact that the spectrum of lightning current exhibits significant frequencies up to a few MHz. Thanks to researches conducted in 20th and 21st century we are beginning to grasp the complexity of this phenomenon. Nowadays, with data gathered so far and more advanced technology, we can say that we understand lightning more than ever, but this phenomenon is still left there to be conquered and fully understood.

Four types of cloud – to – ground lightning were identified by professor Berger depending on the direction of the motion of the initial leader (upward or downward) and the sign of the charge deposited along the channel by the same initial leader (positive or negative). Previously mentioned classification of lightning discharges covers only “unipolar flashes” that transport charge of one polarity to ground. This classification should be extended, to additionally include bipolar lightning flashes that transport both negative and positive charges to ground. To date, the knowledge of the physics of bipolar lightning is not sufficient as that of negative or positive lightning. Thanks to development of lightning location and measurement systems on tall towers, three types of bipolar lightning discharge were identified (although some events may belong to more than one category). Bipolar lightning flashes are very dangerous and destructive. For example, the geometrical mean total absolute charge transfer of 15 bipolar lightning flashes recorded on Gaisberg tower is 93.6 C, which is almost three times larger than that geometrical mean value of 33 C for 457 negative upward lightning flashes observed from the Gaisberg tower.

The term multiplicity is often used to denote the number of strokes per flash. The average number of strokes per negative flash is typically 3 to 5, with the geometric mean interstroke interval being about 60 ms. Research done by Rakov confirmed that 80% of cloud – to – ground discharges contain more than one stroke per flash with up to 18 strokes per flash as observed in Russia and Florida. The largest number of strokes per flash observed in New Mexico is 26. The average number of strokes per flash observed in different locations is 6.4 in New Mexico, 4.6 in Florida, also 4.6 in Brazil, etc. Although positive lightning discharges account for 10% or less of global cloud-to-ground lightning activity, there are several situations for example winter storms who appear to be conducive to more frequent occurrence of positive lightning. Positive flashes are usually composed of a single stroke, although up to four strokes per flash were observed. Subsequent strokes in positive and negative flashes can occur both in new and in previously formed channel. It is very common that first strokes have larger currents than subsequent strokes, but that is not always the case. This means that more than one lightning stroke can hit the same place on the Earth in very short time interval.

Lightning is a main cause of transmission line outages. It is a very severe problem for transmission lines, especially for those located in the regions of high lightning incidence and high tower footing resistance. There are several methods used for the transmission line lightning performance improvement, such as: tower footing resistance reduction, increase of line insulation level, installation of additional ground and guy wires, addition of under-built ground wires, etc. Some of them have limited effect, while others are very often related to very high costs and the corresponding difficulties. Based on the development of line surge arresters it is possible to maintain complete control of line lightning performance. Many line surge arresters are in service today. Line surge arrester may fail in service if it is not correctly selected. In the selection of the line surge arrester for line lightning performance improvement it is very important to determine arrester energy duty. Expected arrester energy duty is of extreme importance for the selection of the arrester class (arrester block size). Line surge arrester energy duty is mainly related to the lightning stroke parameters, line surge arrester installation configuration, line design, tower footing resistance and stroke location. Any new equipment that needs to be installed into a power system is usually subjected to standard lightning impulse tests, so that its reliability and energy capability when exposed to lightning surges is assured. Lightning natural characteristics are entirely different from standard testing procedures which focus on impulse with specified impulse wave shape. Power system and its components were never analysed before due to bipolar and multicomponent lightning flashes.

The above mentioned considerations constitute the motivation for this thesis, the aim of which being to calculate and consider transmission line surge arrester energy duty due to bipolar and multicomponent flashes.

1.1. Contributions of Thesis

The first part of the research activity has been dedicated to:

- determination of bipolar lightning current parameters (from measured current shapes);
- identification and analysis of specific multicomponent flashes.

Bipolar lightning current parameters which are needed for modelling, simulations and analysis of transients in power systems are identified in this work for the first time. Bipolar lightning current is characterized with: positive and negative charge transfer, two current peaks (for positive and negative part), two front and two tail times (for positive and negative part) and duration of positive and negative part of bipolar stroke.

Some specific lightning flashes are extracted from large number of lightning location system data, such as:

- flashes that involve return strokes of opposite polarity – in literature known as bipolar lightning discharges of third type;
- flashes with currents of subsequent strokes larger than the current of the first stroke;
- flashes that consist of more than 30 components (examples with 42 and 45 components).

For determination of measured bipolar lightning current parameters and for extraction of specific multicomponent lightning flashes from lightning location system data, software was developed.

Simulations for transient analysis of transmission lines are commonly based on model that consist of only few towers on both sides from point of the lightning impact. As addition to the accurate modelling of transmission line, the development of entire transmission line is clearly necessary. Therefore, another novelty is that complete transmission line is created and solved in EMTP – RV for purposes of this thesis. This creates new possibilities in complete power system analysis. Also static energy duty consideration is possible. This is the first time that the complete transmission line is created and solved in the EMTP – RV for the purpose of the transient analysis.

The major contributions are calculation and consideration of transmission line surge arrester energy duty due to bipolar and multicomponent lightning flashes. Energy stresses of transmission line surge arresters are commonly analysed due to unipolar flashes that transport charge of one polarity to ground. Energy stresses of transmission line surge arresters due to bipolar and multicomponent lightning flashes are analysed for the first time. Transmission line surge arrester energy duty calculation procedure (due to bipolar and multicomponent lightning flashes) is also created. In order to select the appropriate arrester, parametric analysis was carried out, considering different parameters that affect arrester's energy calculation. Usually considered as line parameters for transient studies are: tower footing resistance and different arrester installation configuration. Usual lightning flash parameters which are considered: lightning channel impedance, front time, tail time, polarity, multiplicity and current peak. Together with usually considered parameters mentioned above, another important novelty is line surge arrester energy duty calculation and consideration with non – uniform tower footing resistance distribution.

1.2. Organization of the Thesis

The rest of this thesis is organized as follows:

Chapter 2 – This chapter presents lightning phenomenon literature review. The chapter starts with a brief presentation of phenomenology and classification of lightning discharges. The second part of this chapter is devoted to bipolar lightning. Bipolar lightning is defined, as well as its parameters. An overview of different types of bipolar lightning discharges is given. Bipolar lightning occurrence all over the world is summarized. A possible explanation of observed bipolar lightning is given. Then, a term multiplicity is explained. Basic facts regarding multicomponent lightning flashes are presented.

Chapter 3 – This chapter describes basic principles regarding transmission line surge arresters and provides explanation of the line surge arrester type which will be considered in this thesis.

Chapter 4 – The knowledge about lightning parameters and characteristics for different regions is very important for transient studies in electrical power systems. Current shape parameters are very important for modelling and simulations. True data recorded from direct measurements at towers and from lightning location systems are especially important for better protection design. Therefore, the aim of this chapter was to analyse data obtained from measurements using instrumented towers (at the telecom base station Miluccia – Corsica) and lightning location systems (LINET). The chapter starts with presentation of the bipolar lightning current shape. An analysis of current parameters for bipolar impulse is given. The second part of the chapter is devoted to description and analysis of the multicomponent flashes.

Chapter 5 – Modelling of transmission line for transient studies and for arrester energy duty consideration is described in this chapter. Firstly, basic mathematical models and circuit representation for transmission line components are described. Afterwards in this chapter, models for transmission line components are developed in EMTP – RV. Transmission line model includes modelling of: phase conductors, shield wire (for shielded line design), transmission line tower, tower footing resistance, line surge arresters, lightning current source and substation. An analogy between calculation of line surge arrester energy duty in EMTP – RV and MATLAB is presented. After that importance of modelling of a complete transmission line is explained. Complete transmission line is modelled thanks to EMTP – RV possibility of grouping elements into so called subcircuit elements. A summary of modelling and calculation procedure is also given in this chapter.

Chapter 6 – This chapter includes simulation cases description and results of simulations and discussions. Line surge arrester energy duty due to bipolar and multicomponent flashes is calculated and analysed. Shielded and unshielded line designs are considered. Also, line surge arrester current shapes are computed and presented for both line designs. Parametric analysis was carried out.

Finally, summary of results, conclusions and recommendations for future works are presented in **Chapter 7**.

Chapter 2.

LIGHTNING PHENOMENON

2.1. Introduction

From ancient times until today man was fascinated with lightning. It was always a mix of a deep admiration and fear. From ancient stories and legends to modern experiments and models we can see how our understanding of lightning was changing. People from many cultures were trying to explain lightning and thunder by postulating thunder gods, as personifications or sources of thunder and lightning. In Norse mythology that was Thor, in Hinduism Indra, in Greek mythology Zeus and in Slavic religion god Perun. Aware of devastating power of lightning and its influence on our daily lives, through history we were trying to protect ourselves. Most of the time, the means of protection were through prayer and sacrifices to mighty gods. Interesting fact is that in medieval France it was believed that ringing a church bell was somehow “breaking” lightning, so on many medieval bells “Fulgura frango” sign can be found, meaning “I break lightning”. As a result of this belief many bell-ringers were killed by lightning during thunderstorms, trying to conquer nature. A huge improvement in lightning protection was given in 1749 by Benjamin Franklin, who was first to detail the principles of lightning rod (conductor). Although lightning is one of the most common natural phenomenon it is very poorly understood. Thanks to researches conducted in 20th and 21st century we are beginning to grasp the complexity of this phenomenon. Nowadays, with data gathered so far and more advanced technology, we can say that we understand lightning more than ever, but this phenomenon is still left to be conquered and fully understood.

2.2. Lightning Terminology

A lightning discharge is a natural phenomenon whose very complex physics is not completely understood so far. Basic lightning terms, defined by Rakov and Uman (2003), are given in this section.

Lightning, or the lightning discharge, in its entirety, whether it strikes ground or not, is usually termed as a “lightning flash” or just a “flash”. A lightning discharge that involves an object on ground or in the atmosphere is sometimes referred to as a “lightning strike”. A commonly used non-technical term for a lightning discharge is a “lightning bolt”. The terms “stroke” or “component stroke” apply only to components of cloud-to-ground discharges. Each stroke involves a downward leader and an upward return stroke and may involve a relatively low level of “continuing current” that immediately follows the return stroke. Transient processes occurring in a lightning channel while it carries continuing current are termed M-components. First strokes are initiated by “stepped” leaders while subsequent strokes following previously formed channels are initiated by “dart” or “dart-stepped” leaders.

2.3. Types of Lightning Discharge

The global lightning flash rate is some tens to a hundred per second or so. The majority of lightning discharges, probably three-quarters, do not involve ground. These are termed cloud discharges and sometimes are referred to as ICs. Cloud discharges include intracloud, intercloud, and cloud-to-air discharges (see figure 2.3.1).

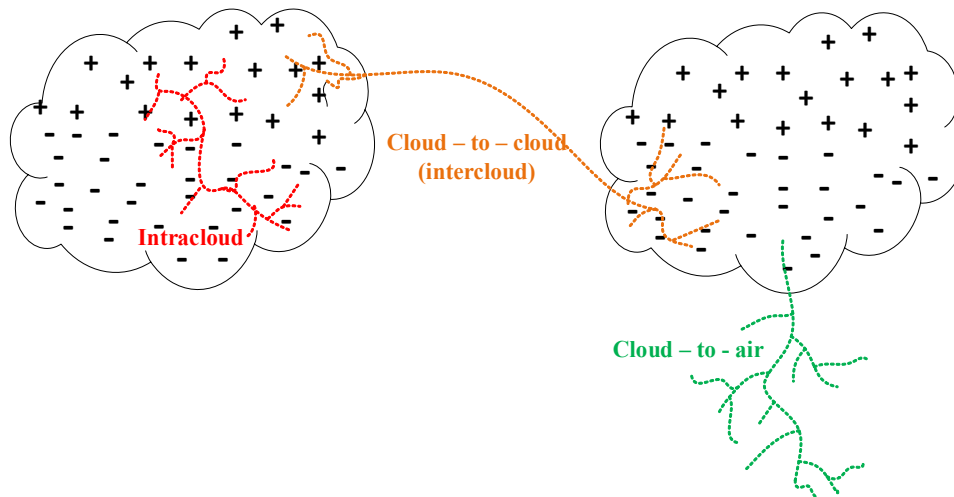


Figure 2.3.1. Classification of cloud discharges [1,3]

Four types of cloud – to – ground lightning were identified by Berger (1975) depending on the direction of the motion of the initial leader (upward or downward) and the sign of the charge deposited along the channel by the same initial leader (positive or negative), as illustrated in figure 2.3.2. Discharges of all four types can be viewed as effectively transporting cloud charge to the ground and therefore are usually termed cloud-to-ground discharges (sometimes referred to as CGs).

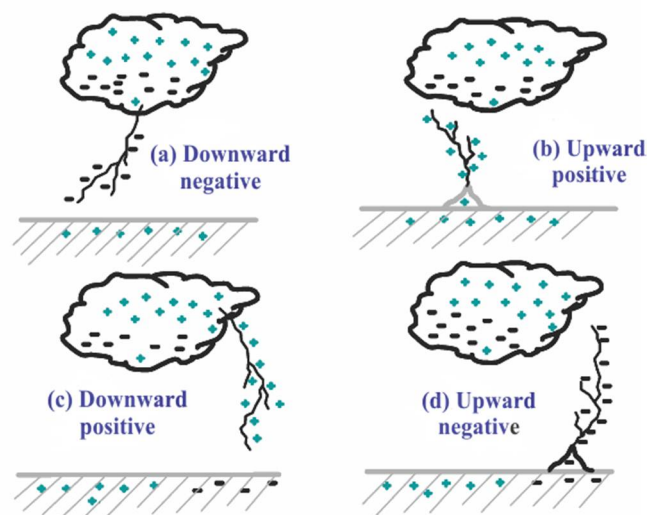


Figure 2.3.2. Four types of lightning effectively lowering cloud charge to ground. Only the initial leader is shown for each type. In each lightning-type name given below the sketch, the direction of propagation of the initial leader and the polarity of the cloud charge effectively lowered to ground are indicated. [3]

Category 1 – downward negative lightning discharges, type (a) from figure 2.3.2, account for about 90 percent or more of global cloud-to-ground lightning.

Category 2 – upward positive lightning discharges, type (b) from figure 2.3.2.

Category 3 – downward positive lightning discharges, type (c) from figure 2.3.2, account for less than 10 percent of cloud – to – ground lightning.

Category 4 – upward negative lightning discharges, type (d) from figure 2.3.2.

Upward lightning discharges, category 2 and category 4, are thought to occur only from tall objects (higher than 100 m or so) or from objects of moderate height located on mountain tops.

2.4. Models of Charge Transfer to Ground

Literature describes three possible modes of charge transfer to ground in lightning discharges. It is convenient to illustrate these for the case of negative subsequent strokes. In negative subsequent strokes these three modes are represented by (a) dart-leader–return-stroke sequences, (b) continuing currents, and (c) M-components. Figure 2.4.1 schematically shows current profiles corresponding to these three modes.

(a) dart-leader–return-stroke sequences

In a leader–return-stroke sequence, the descending leader creates a conductive path between the cloud charge source and ground, and it deposits negative charge along this path. The following return stroke traverses that path, moving from ground toward the cloud charge source, and neutralizes the negative leader charge. Thus, both leader and return-stroke processes serve to transport effectively negative charge from the cloud to ground.

(b) continuing currents

The lightning continuing current can be viewed as a quasi-stationary arc between the cloud charge source and ground. The typical arc current has a magnitude of tens to hundreds of amperes, and the duration is up to some hundreds of milliseconds.

(c) M-components

Lightning M-components can be viewed as perturbations (or surges) in the continuing current and in the associated channel luminosity. It appears that the M – component involves the superposition of two waves propagating in opposite directions (see figure 2.4.1). The spatial front length for the M-component waves is of the order of a kilometre (shown shorter in relation to the cloud height in figure 2.4.1, for illustrative purposes) while for dart-leader and return-stroke waves the spatial front lengths are of the order of 10 and 100 m, respectively. The M-component mode of charge transfer to ground requires the existence of a grounded channel carrying a continuing current that acts as a wave-guiding structure. In contrast, the leader–return stroke mode of charge transfer to ground occurs only in the absence of such a conducting path to ground. In this latter mode, the wave-guiding structure is not available and it is created by the leader. For all the processes shown in figure 2.4.1, the channel conductivity is of the order of 10^4 Sm^{-1} , except for the channel section between the dart – leader tip and ground shown by a broken line. For this latter channel section, the conductivity is about 0.02 Sm^{-1} (Rakov, 1998). Thus, the primary distinction between the leader – return – stroke and M – component modes is the availability of a conducting path to ground. It is possible that, as the conductivity of the conducting path to ground decreases, the downward M – component wave can transform to a dart leader.

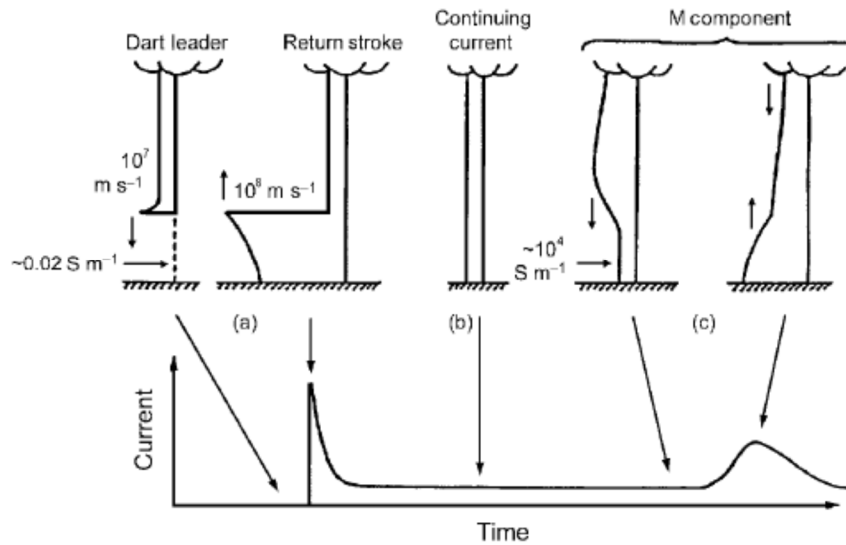


Figure 2.4.1. Schematic representation of current versus height profiles for three modes of charge transfer to ground in negative lightning subsequent strokes: (a) dart-leader–return-stroke sequence, (b) continuing current, and (c) M-component. The corresponding current versus time waveform represents the current at the ground. [1]

2.5. Bipolar Lightning

The classification of lightning discharges described in previous sections covers only “unipolar flashes” that transport charge of one polarity to ground. The classification should be extended, to additionally include bipolar lightning flashes that transport both negative and positive charges to ground. To date, the knowledge of the physics of bipolar lightning is not as sufficient as that of negative or positive lightning. Measurements of lightning currents on tall towers provide a useful way to investigate the occurrence of bipolar flashes.

2.5.1. Bipolar Lightning Definition

Four definitions of bipolar lightning are found in the papers published by Rakov and Uman (2003), Zhou et al. (2010) and Saraiva et al. (2014).

Definition 1:

Flashes with subsequent strokes of polarity opposite to the polarity of the first stroke are called bipolar flashes.

Definition 2:

Lightning flashes that transfer to ground both negative and positive charges are referred to as bipolar lightning.

Definition 3:

Bipolar lightning is defined as a lightning current waveform measured at the channel – base exhibiting a polarity reversal within the same flash.

Definition 4:

Bipolar lightning discharges are those that transfer both positive and negative electric charges to ground throughout their development.

2.5.2. Bipolar Lightning Occurrence

Most of the bipolar lightning events were identified in direct current measurements on tall grounded objects. Lightning current waveforms exhibiting polarity reversals were first reported by McEachron (1939, 1941) from his studies at the Empire State Building (New York). According to Hagenguth and Anderson (1952), the number of bipolar flashes observed at this object over a 10-year period was 11 (14%) from a total of 80 flashes for which polarity could be determined. Berger (1978) reported that 72 (6%) of 1196 discharges observed in 1963-1973 at Monte San Salvatore (Switzerland) were bipolar, with 68 of them being of the upward type. Gorin and Shkilev (1984) reported that 6 (6.7%) of 90 upward discharges initiated from the Ostankino tower (Russia) were bipolar; all of which initially transported negative charge to ground. The total number of bipolar lightning discharges observed on the Peissenberg tower (Germany) was two (Heidler et al., 2000), both of which initially transported negative charge to ground. Many bipolar current waveforms have been observed in winter lightning studies in Japan, the reported frequency of occurrence ranging from 5 to 33 percent. Zhou et al. analysed 21 upward – initiated bipolar lightning flashes at the Gaisberg tower in 2000 – 2009. Saraiva et al. (2014) reported two natural bipolar cloud – to – ground lightning flashes. Both of the flashes were recorded using high – speed video cameras and both of them began with a single positive return stroke that was followed by more than one subsequent weak negative stroke. At least one bipolar lightning discharge was reported from each of the triggered-lightning experiments in France, Japan, New Mexico, Florida, and China.

Table 2.5.1 represents the most significant bipolar lightning flashes recorded over the world.

Table 2.5.1. Bipolar lightning occurrence

Source	Place	Observation Period	Number of bipolar (%)	Total number of flashes (%)
McEachron 1952	Empire State Building (New York USA)	10-year	11 (14)	80 (100)
Berger 1978	Monte San Salvatore (Switzerland)	10-year	72 (6)	1196 (100)
Gorin and Shkilev 1984	Ostankino tower (Russia)	--	6 (6.7)	90 (100)
Miyake et al. 1992	Observation tower at Kashiwazaki and stack at Fukui (Japan)	8-year	6 (5)	125 (100)
Goto and Narita 1995	Meteorological tower at Maki (Japan)	11-year?	29 (20)	145 (100)
Nagai et al. 1996	500-kV Genden-Tsuruga transmission line tower (Japan)	6-year	8 (33)	24 (100)
Heidler et al., 2000	Peissenberg tower (Germany)	--	2 (--)	-- (--)
Miki et al. 2004	Stack at Fukui (Japan)	13-year	47 (22)	213 (100)
Wang and Takagi 2008	Windmill and its lightning protection tower	--	3 (--)	-- (--)
Hussein et al. 2009	Toronto CN tower (Canada)	10-year	2 (1.25)	160 (100)
Zhou et al. 2010	Gaisberg tower (Austria)	9-year	21 (3)	652 (100)
Ishii and Natsuno 2011	Wind turbines at 25 sites (Japan)	3-year	18 (6)	304 (100)
Wang and Takagi 2012	Windmill and its lightning protection tower	--	9 (25)	36 (100)
Romero et al. 2013	Säntis tower, (Switzerland)	2-year	3 (1.5)	200 (100)
Saraiva et al. 2014	Sao Jose dos Campos (Brazil)		2 (--)	-- (--)
Rakov and Uman 2003 [1]	Triggered-lightning experiments (France, Japan, New Mexico, Florida, and China)	--	1 ¹ (--)	-- (--)
Sadovic measurements (not published)	Telecom base station Miluccia (Corsica, France)	1.5 - year	13 (--)	-- (--)

¹ One bipolar lightning discharge was reported from each of the triggered-lightning experiments.

2.5.3. Types of Bipolar Discharges

There are basically three types of bipolar lightning discharge, although some events may belong to more than one category.

Type 1

The first type of bipolar discharge, illustrated in figure 2.5.1, is associated with a polarity reversal during a slowly varying (millisecond-scale) current component. The initial-stage current in figure 2.5.1 is followed by two return-stroke current pulses. Bipolar flashes of type 1 may be composed only of the initial stage. The polarity reversal may occur one or more times and may involve an appreciably long no-current (or unmeasurable-current) interval between opposite-polarity portions of the waveform.

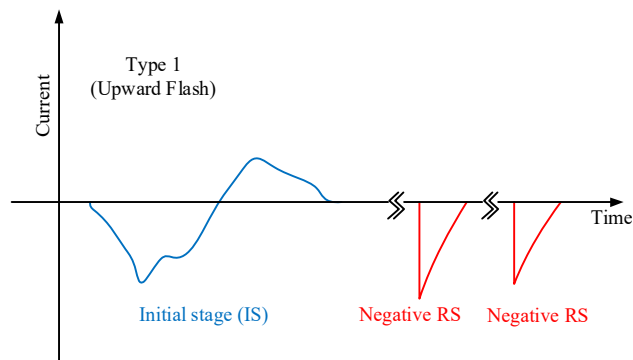


Figure 2.5.1. The first type of bipolar lightning discharge [3]

Type 2

The second type of bipolar discharge, illustrated in figure 2.5.2, is characterized by different polarities of the initial-stage current and of the following return stroke or strokes.

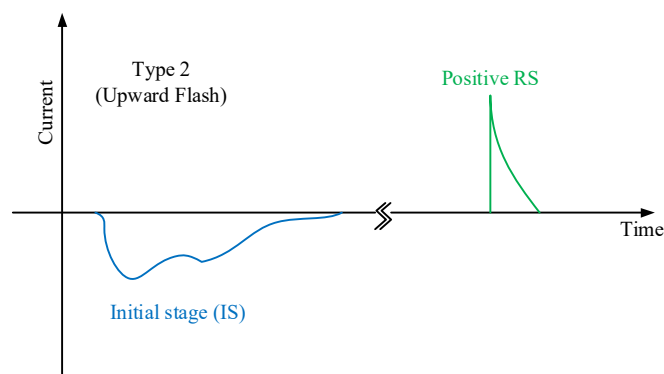


Figure 2.5.2. The second type of bipolar lightning discharge [3]

Type 3

The third type of bipolar discharge, illustrated in figure 2.5.3, involves return strokes of opposite polarity. All documented bipolar discharges in this category are of the upward type.

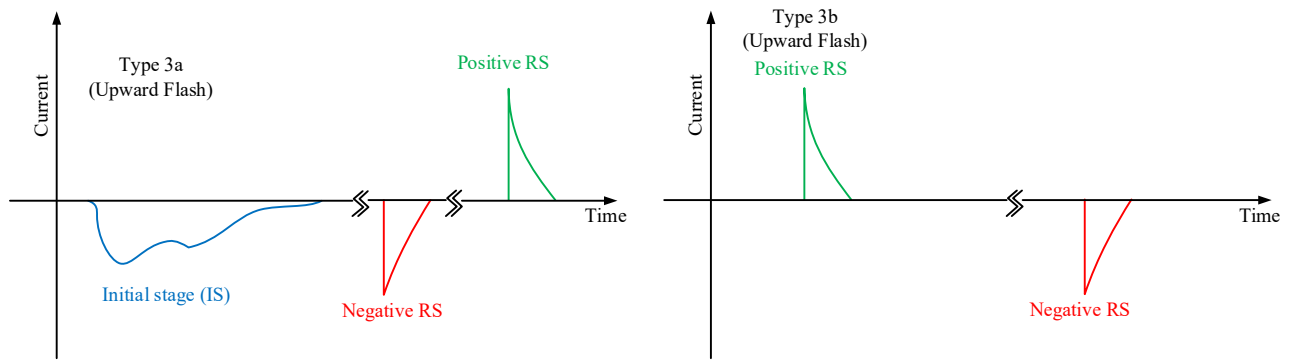


Figure 2.5.3. The third type of bipolar lightning discharge [3]

2.5.4. Definition of Parameters

Definitions of the negative current component duration, positive current component duration, total duration and their associated charge transfers of bipolar flashes are first time introduced in paper published by Zhou et al. (2010). These definitions are given below.

Upward lightning flashes are usually characterized by an initial stage (IS) composed of a long upward – propagating leader originating from elevated objects. After a no – current interval, the IS is often followed by one or more downward dart leader/upward return stroke sequences.

The negative current component duration (T_-) is a summary of negative polarity current parts, while the positive current component duration (T_+) is a summary of positive polarity current parts. The total duration (T_{total}) is a summary of the negative current component duration (T_-), positive current component duration (T_+), no – current interval (T_{nc}) and interstroke intervals ($T_{inrstmc}$).

The negative charge transfer (Q_-) is determined by integrating the absolute value of the current over the negative current component duration (T_-). The positive charge transfer (Q_+) is determined by integrating the current over the positive current component duration (T_+). The total transfer (Q_{total}) is summary of the negative (Q_-) and positive (Q_+) charge transfers.

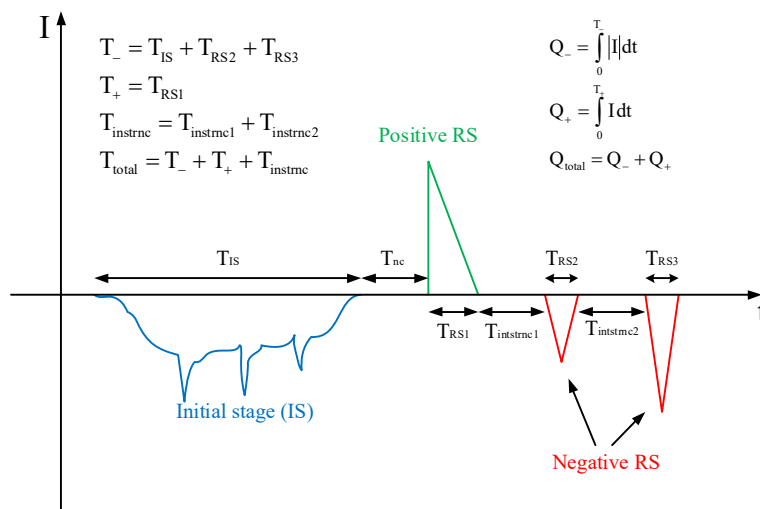


Figure 2.5.4. Definitions of the negative current component duration, positive current component duration, total duration and their associated charge transfers of bipolar flashes. [4]

2.5.5. Bipolar Lightning in Austria

During the observation period from 2000 to 2009, a total of 21 upward – initiated lightning are identified as bipolar flashes from measured current waveforms. It is shown in Austria that the monthly percentage of bipolar lightning flashes is almost consistent with that of all types of lightning initiated from the Gaisber tower. Additionally, it is interesting to note that the maximum percentage of bipolar flashes (each 19%) occurred in March, August and November, time when seasons change from one to the other. These seasonal transmission periods appear to provide more favourable meteorological conditions for the initiation of bipolar lightning discharges from the Gaisberg tower. Negative current component duration varies from 1.33 ms to 655 ms with a geometrical mean (GM) of 100 ms, the positive current component duration ranges from 0.252 ms to 303 ms with a GM of 49.4 ms, and the range of variation of total flash duration is from 55.9 ms to 800 ms with a geometrical mean (GM) being 320 ms. The negative charge transfer varies from 0.61 C to 156 C with a GM of 22.5 C, the positive charge transfer ranges from 0.241 C to 286 C with a GM of 28.6 C, and the range variation of total absolute charge transfer is from 18.4 C to 343 C with a geometrical mean (GM) being 99.5 C. The negative current component within one bipolar flash has a longer GM duration (100 ms) and less GM charge transfer (22.5 C), while the positive current component has a shorter GM duration (49.4 ms) and higher charge transfer (28.6 C). For all the 21 bipolar flashes examined in this study, the GM total absolute transfer is 99.5 C with relatively short GM total duration of 320 ms.

The GM total absolute charge transfer of 15 bipolar lightning flashes from years 2000 to 2007 is 93.6 C, which is almost three times larger than that GM value of 33 C for 457 negative upward lightning flashes observed from the Gaisber tower. A majority (76% or 16/21) of bipolar lightning current waveforms changes polarity from negative to positive. All of Type 1 bipolar flashes change polarity from negative to positive, while only one of five in Type 2 bipolar flashes changes polarity from negative to positive.

The GM of total absolute charge transfer of bipolar lightning is 99.5 C with a total time duration of 320 ms. It is indicative that bipolar flashes are characterized by a large charge transfer within a relatively short time duration.

2.5.6. A Possible Explanation of Observed Bipolar Lightning

For winter lightning in Japan, Narita et al. (1989) suggested that in a bipolar discharge, currents of both polarities follow the same channel to ground, but from different, oppositely charged regions in the cloud, as illustrated in figure 2.5.5.

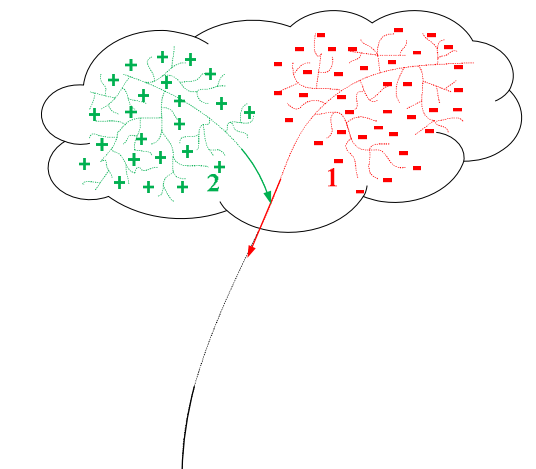


Figure 2.5.5. A possible explanation of observed bipolar lightning currents. Currents of both polarities follow, in turn, the same channel to the ground, with negative charge transfer from the cloud charge region labelled “1” being followed by positive charge transfer from the charge region labelled “2”. Adapted from Narita et al. (1989). [1,3]

It is likely that the explanation of bipolar current wave shapes suggested by Narita et al. (1989) for winter lightning also applies to summer bipolar lightning. The hypothetical scenario shown in figure 2.5.5 implies that the cloud charge structure cannot always be described by a simple, vertically stacked charge model. For this scenario to occur, positively and negatively charged regions should be displaced horizontally (they should exist at about the same height in the cloud). The existence of such charge distributions is confirmed by experimental data of Imyanitov et al. (1971) who reported, from aircraft measurements, pockets of relatively high charge density that appeared to be chaotically located in the cloud.

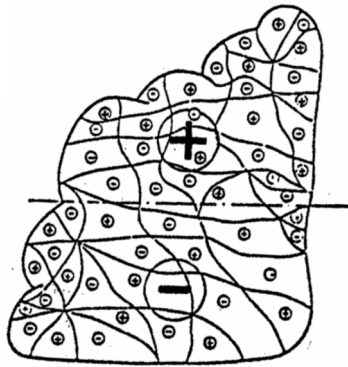


Figure 2.5.6. Electrical structure of a convective cloud. Note pockets of positive and negative charge (numerous smaller encircled plus and minus signs) at different altitudes, while the net charge at the top of the cloud is positive and that at the bottom of the cloud is negative (larger encircled and minus signs). Adapted from Imyanitov et al. (1971). [1,3]

The numerous pockets of positive and negative cloud charge observed by them are illustrated in figure 2.9. Note that average net charges at different heights usually formed the classical positive dipole (the positive charge above the negative charge; see larger plus and minus signs in figure 2.5.6). Although figure 2.5.6 was given by Imyanitov (1971) for cumulus clouds having heights up to 4 km, they stated that it also applies to cumulonimbus clouds (thunderclouds) if one adds a third, net positive charge layer near the bottom of the cloud. According to Imyanitov et al. (1971), the average dimensions of cloud regions (pockets) containing the largest charges in active thunderstorms are of the order of a few hundred meters. Further, Davis and Standring (1947) inferred the existence of oppositely charged regions separated by a horizontal distance of 300 m by measuring the currents in the cables of kite balloons flying at a height of 600 m under thunderstorm conditions. Also, Bateman et al. (1999) found, from in situ measurements, precipitation particles carrying charge of either polarity at nearly all altitudes. Thus, it appears that charges of both polarities can coexist in any cloud charge layer, regardless of the polarity of the net charge of that layer. The “lumpy” cloud charge structure illustrated in figure 2.5.6 should be conducive to the occurrence of bipolar flashes.

Figure 2.5.7 illustrates in detail the mechanism proposed to explain natural bipolar cloud-to-ground flashes described in the paper published by Saraiva et al in 2014. Both flashes initiated between 3 and 5 km altitude, where the respective negative and positive dominant charge regions were located. Each panel of figure 2.5.7 depicts the following processes:

(a) and (b): The cloud base is located at 3.2 km height, and the flash develops in a bidirectional fashion, with the positive end of the lightning tree propagating towards ground and the negative end developing inside the cloud. The ramifications in the positive end are usually fainter than in the negative end and are barely visible with the camera.

(c): The recoil leaders seem to take place when the faintest branches are about to stop their development for any reason, for example, when a current cut off happened at some point. The recoils act like a current surge on the branch, extending it a little further, therefore, the branch can propagate for itself again. Such bidirectional nature of the recoil leaders has been previously documented in detail by Warner et al. (2012) and Mazur et al. (2013). This process can occur on several branches and can repeat on the same one multiple times.

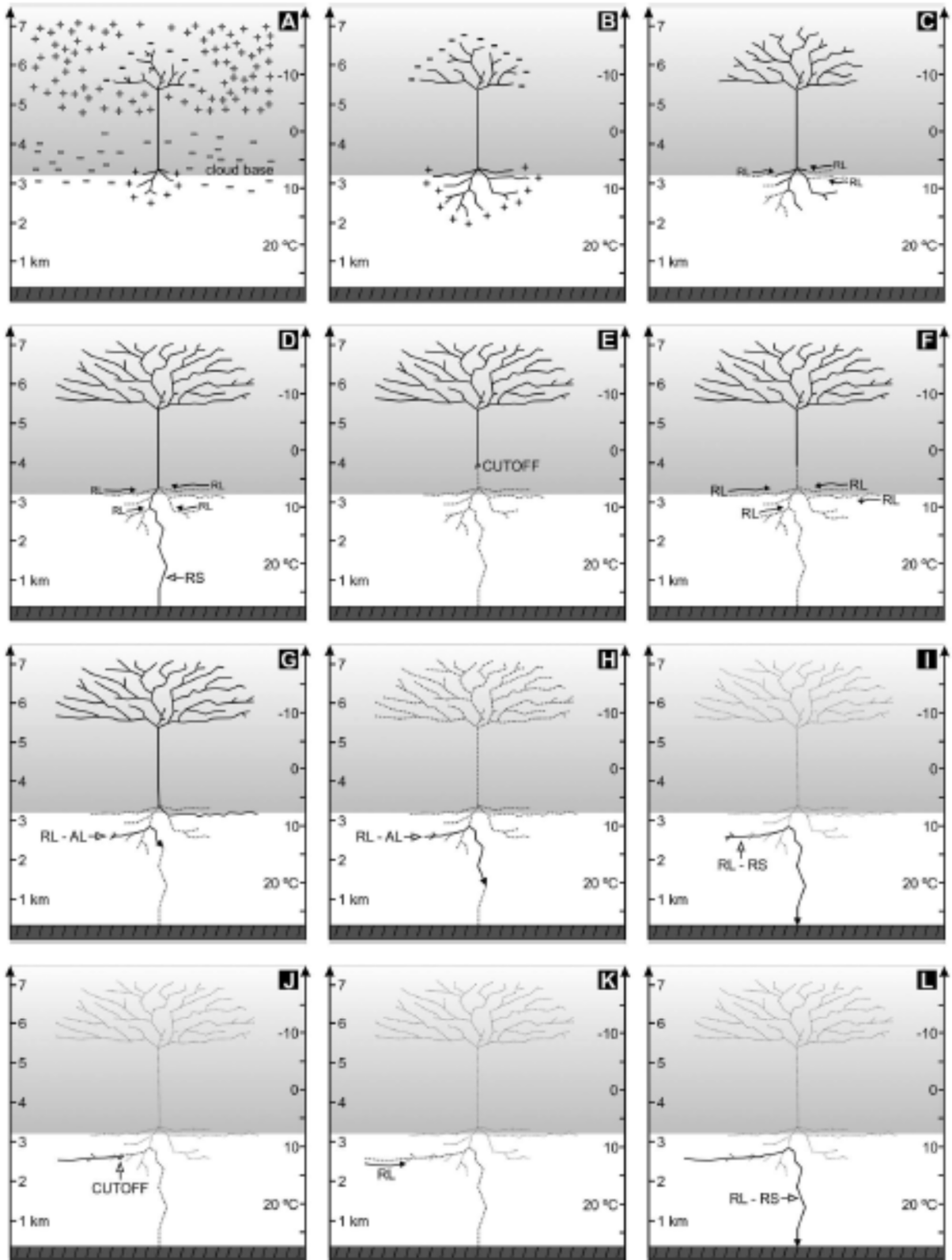


Figure 2.5.7. Illustration of the mechanism proposed to explain natural bipolar cloud-to-ground flashes. The two minus signs represent a single charge region, partially inside the cloud and partially outside the cloud [5,6].

(d): The lower end of the bidirectional leader continues to propagate until it touches ground, producing the initial positive return stroke. It is followed by a period of continuing current, which takes place simultaneously with recoil leader activity on positive leader branches that have been cut off once the return stroke occurred.

(e): Once the continuing current is finished, the lower section of the double-ended tree is presumed to be cut off from the in-cloud negative end. The positive charge transfer to ground stops, but the negative end of the in-cloud lightning tree continues to develop independently.

(f): A large number of recoil leaders (indicated as RL) occur in channel branches visible below cloud base that were previously ionized by the positive leader. Some can reconnect with the active in-cloud negative leader, forming an intracloud discharge, and others are not able to do so.

(g) and (h): Some of the recoil leaders, in particular, develop toward the vertical section of the channel to ground followed by the positive stroke, behaving as attempted leaders (indicated as RL-AL). Eventually, the in-cloud negative leader propagation is interrupted, as indicated by the VHF sources.

(i): One of the recoil leaders was capable of following the same path to ground as the initial positive stroke. It behaved as a regular dart leader and produced the first subsequent negative return stroke (indicated as RL-RS). It is important to notice that, from this point on, the horizontal end of the channel carries positive charges, and the descending channel carries negative charges to ground.

(j): Negative charge transfer to ground is finished after the channel cut off. The positive horizontal end, however, continues to propagate with a luminous emission below the camera sensitivity.

(k): At some point the positive leader propagation is terminated due to current cut off. This allows the initiation of another recoil leader, which propagates toward ground in bidirectional manner (similarly to the initial positive and the first negative subsequent strokes) at the same time as it develops further the horizontal positive end of the channel.

(l): The negative end of the recoil leader reaches ground and produces the second negative stroke, behaving as a regular dart leader. After the first negative return stroke, no intense recoil activity was presented on that branch, and each new recoil leader was responsible for another negative return stroke. The new channel behaves like a regular negative flash, but at a smaller scale. Recoil leaders will continue to produce additional negative strokes as long as charges are still available around the positive leader and while the channel length remains stable.

2.6. Multicomponent Flashes

A term multiplicity is often used to denote the number of strokes per flash. The average number of strokes per flash is typically 3 to 5, with the geometric mean interstroke interval being about 60 ms. Research done by Rakov confirmed that 80% of cloud – to – ground discharges contain more than one stroke per flash with up to eighteen strokes per flash as observed in Russia and Florida. The largest number of strokes per flash observed in New Mexico (Kitagawa et al, 1962) is 26. The average numbers of strokes per flash observed in different locations are summarized in table 2.6.1.

Table 2.6.1. Average number of strokes per negative flash

Place	Average number of strokes per negative flash
New Mexico	6.4
Florida	4.6
Sweden	3.4
Sri Lanka	4.5
Brazil	4.6
Arizona	3.9
Malaysia	4.0

Although positive lightning discharges account for 10% or less of global cloud-to-ground lightning activity, there are several situations, including, for example, winter storms, that appear to be conducive to more frequent occurrence of positive lightning. The highest directly measured lightning currents (near 300 kA) and the largest charge transfers (hundreds of coulombs or more) are thought to be associated with positive lightning. Positive flashes are usually composed of a single stroke, although up to four strokes per flash were observed.

Subsequent strokes in positive and negative flashes can occur both in a new and in the previously-formed channel. It is very common that first stroke have larger currents than subsequent strokes, but it is not always true.

Chapter 3.

LINE SURGE ARRESTERS

3.1. Introduction

Surge arresters are devices that appeared on the market at the end of the 1970s. Surge arresters installed on a transmission line are termed line surge arresters (LSA). There are many line surge arrester applications, such as: line lightning performance improvement, extended protection of substations, switching surge control, compact lines, line voltage uprating, touch and step voltage reduction, etc.

There are several methods used for the transmission line lightning performance improvement, such as: tower footing resistance reduction, increase of line insulation level, installation of additional ground and guy wires, addition of under-built ground wires, etc. Some of them have limited effect, while others are very often related to very high costs and the corresponding difficulties. Thanks to the development of line surge arresters it is possible to maintain complete control on the line lightning performance. Line surge arresters are mainly used for line lightning performance improvement. For purposes of this thesis line surge arresters are used for transmission line lightning performance improvement.

Line surge arrester (LSA) is defined as:

A protective device for limiting surge voltages on transmission line insulation by discharging or bypassing surge current; it prevents continued flow of follow – current to ground and is capable of repeating these functions.

Many line surge arresters are in service today. Line surge arrester may fail in service if it is not correctly selected. In the selection of the line surge arrester for the line lightning performance improvement it is very important to determine arrester energy duty. Expected arrester energy duty is of extreme importance for the selection of the arrester class (arrester block size). Line surge arrester energy duty is mainly related to the lightning stroke parameters, line surge arrester installation configuration, line design, tower footing resistance and stroke location. Advanced measurement systems and lightning location systems can provide data such as: lightning current shape, number of components in flash, etc. The main idea of this work is analysis of line surge arrester energy duty due to bipolar flashes and multicomponent flashes for different transmission line designs. The facts regarding modelling and simulation cases will be described in next sections. This chapter describes basic principles regarding line surge arresters and provides explanation of the line surge arrester type which will be considered in this thesis.

3.2. Types of Line Surge Arresters

There are many ways to group line surge arresters, according to system voltage, the major problem on the line, housing types, etc. But the most important is the difference between line surge arrester without gap (gapless line arresters, NEGLAs) and externally gapped line arresters, the EGLAs.

3.2.1. Externally Gapped Line Arresters (EGLAs)

In general, an externally gapped line arrester (EGLA) consists of two parts: an active part represented by a polymer or porcelain Metal-Oxide (MO) surge arrester and an externally arc gap connected in series to the active part (see figure 3.2.1).

In normal service conditions, the active part is disconnected from the overhead power line through the series gap and thus it is not permanently stressed with the operating voltage. In case of overvoltage generated by a lightning stroke, which is terminating either on the power line directly or on the ground system the EGLA operates and the gap sparks over.

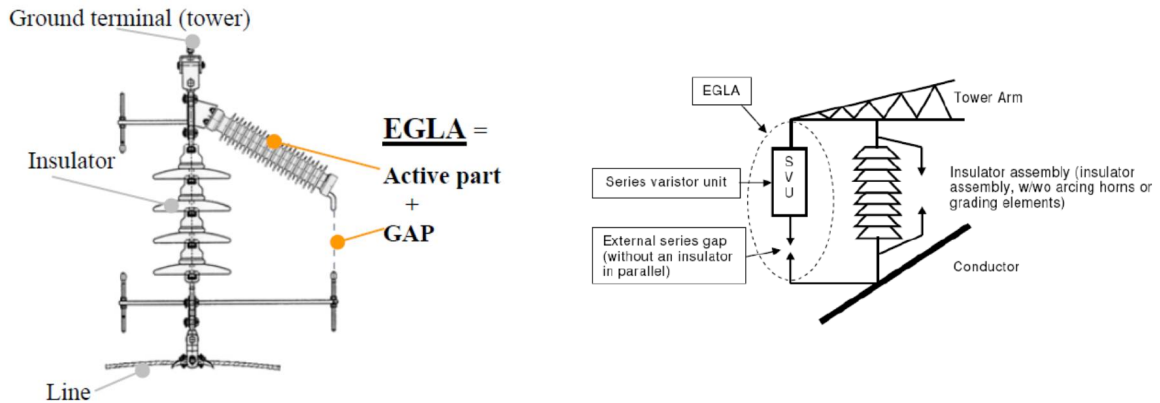


Figure 3.2.1. Design concept and standard configuration of an EGLA [28,32]

The new IEC 60099-8 defines the EGLA as an active part called series varistor unit (SVU) and an external series gap, see figure 3.2.1.

3.2.2. Gapless Line Arresters (NEGLAs)

Unlike the Gap-Type arrester, Gapless-Type arrester with Metal-oxide (ZnO) blocks is physically connected directly to the phase conductor. The ZnO blocks shall suppress the over voltage across the insulator string. In case of arrester failure, the disconnecting device operates and shatters in order to isolate the live conductor from the faulty arrester. Non-gapped line surge arresters offer a high degree of mounting flexibility and operational reliability. Depending on the tower design and the arrangement of insulators and lines, these arresters can either be installed directly on the insulators or on the tower (see figure 3.2.2).

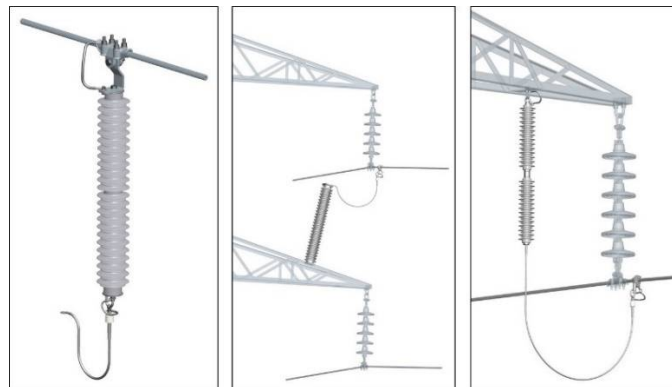


Figure 3.2.2. Installations of an NEGLA [35]

3.3. Metal Oxide Block and Housing

Metal oxide block (ZnO block) is without doubt the most important element of any surge arrester, which consists of 90 % of zinc oxide and of about 10 % additives. Figure 3.3.1 represents typical ZnO block design. Metal oxide blocks have extremely good non – linear characteristic.

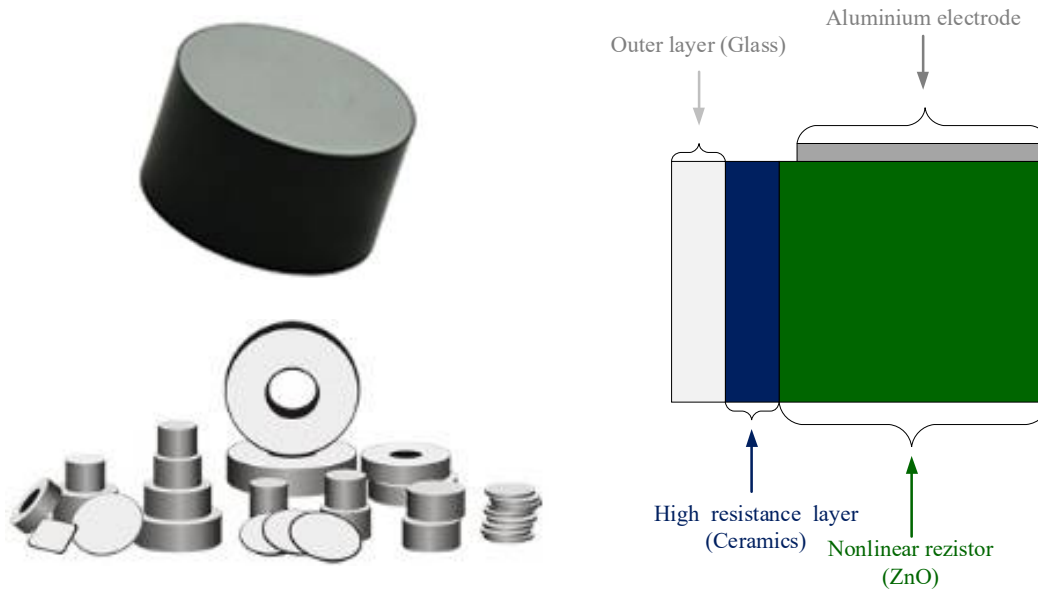


Figure 3.3.1. Typical ZnO block [35, 40]

The basic steps of the manufacturing process of Metal oxide blocks, which usually have cylindrical shape, are:

1. Mixing of the metal-oxide powders;
2. Spray drying of the powder mixture;
3. Pressing of the MO resistors;
4. Sintering;
5. Metallization of the contact areas;
6. Coating of the surface;
7. Final tests of the MO resistors;
8. MO resistors ready to be installed in the arrester.

To provide corresponding contacts between blocks, aluminium is applied on the both side. To prevent external flashover and chemical influence, an insulation layer is applied on the external surface. ZnO blocks may have different thickness and different diameters. Block thickness is related to the block rated voltage, while block diameter defines so called energy capability. Their diameter decisively determines the energy absorption and the current carrying capability. It is within range of about 30 mm up to 100 mm or more for high and extra – high voltage systems and special applications, for which high energy absorption capabilities are required. For especially high demands, active parts are also realized in a multi – column technique, that is, two or more columns are connected. To obtain the desired high voltage arrester rated voltage, several modules have to be used. With this design it is necessary to have additional interfaces because of the modules interconnections. In so-called parallel - series arrester modular design, arrester modules are connected in parallel to get the desired energy capability, while the number of the series stages is defined by the requested rated voltage. This design introduces very large number of the interfaces. In addition, if one of the arrester modules fails, then the complete device will have completely different characteristic than the new one. Table 3.3.1 represents example of correlation between block diameter and energy capability.

Table 3.3.1. Example of correlation between block diameter and energy capability

Characteristics	Block Type				
	40 mm	48 mm	63 mm	73 mm	100 mm
Block Diameter	40 mm	48 mm	63 mm	73 mm	100 mm
Class	1	2	3	4	5
Energy Capability	2.5 kJ/kV	5 kJ/kV	8 kJ/kV	12 kJ/kV	16 kJ/kV

Line surge arresters can be porcelain and polymer housed. If polymer housed surge arresters are compared with the porcelain housed arresters, the main advantages of polymer housed surge arresters are:

- Better pollution performance (especially with silicone rubber);
- Lower weight (less than half of the weight of an equivalent porcelain arrester);
- Compact design: easy to install and to transport;
- Reduced space requirements;
- Some designs are air free: no water penetration;
- Better seismic performance;
- Able to withstand dynamic mechanical stresses;
- Better thermal performance;
- Explosion proof;
- Maintenance free design;
- Can be installed in horizontal, angled and suspended position.

Polymer housed surge arrester overall performance depends mainly on: arrester design, housing material, ZnO blocks quality and manufacturing process.

3.4. U – I Characteristics

The voltage – current characteristic of its varistor is without doubt one of the most important parameters of any line surge arrester. Therefore it is necessary to discuss varistor U-I curve. The U-I characteristic shows the conductivity or resistance of a varistor/arrester. For any given voltage or current, there is a corresponding current or voltage. The varistor derives its name from the fact that it acts as a variable resistor whose resistance depends mainly on applied voltage, i.e. higher the voltage, lower the resistance.

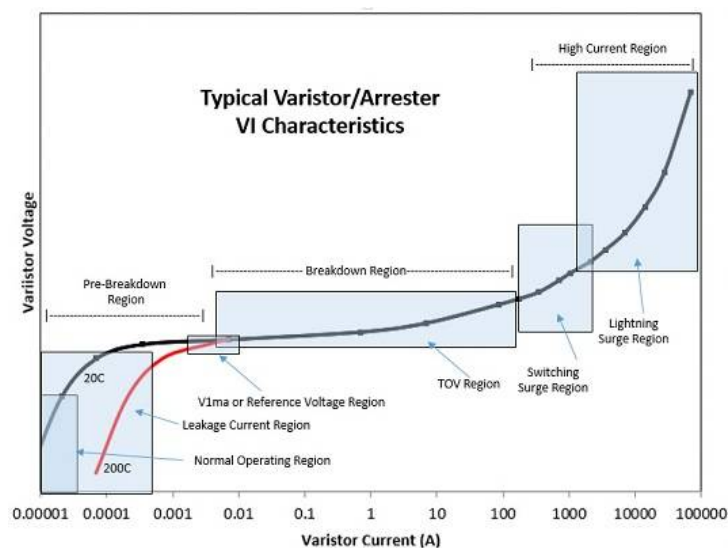


Figure. 3.4.1. Typical varistor/arrester U-I characteristics [44]

Three separate regions of varistor operation are:

- pre – breakdown,
- breakdown,
- and high current.

The pre – breakdown region is where a varistor is not in severe conduction mode and there are only microamperes flowing through the semiconductor. This region is known as the operating region or the leakage current region. This area of the U-I curve accounts for the vast majority of varistor typical life and, since very little heat is typically generated; the varistor can operate almost indefinitely. However, the resistance or conductivity of the varistor in this range of the curve is highly sensitive to temperature. If the varistor body temperature increases for any reason resistance decreases, moving the U-I curve to the right into a higher leakage current range.

A very important region of the U-I curve is the “knee” or $U_{I_{ma}}$ region – also known as the reference or characteristic voltage region. The reason it is so important is that it is not temperature sensitive and therefore, at current levels of 1 – 10 mA, the rest of the U-I curve can be accurately predicted.

In the breakdown region of the curve, resistance is controlled by varistor junctions, which are present throughout the semiconductor material. Conductivity in this region is usually caused by power frequency overvoltages that can lead to a significant temperature increase of the disks. As long as temperature remains between 100°C and 300°C, there is no long – term impact on the varistor. Note that conductivity in this region cannot last more than a few seconds or it will cause temperature to rise above the capability of the device.

The higher current region is where the varistor is performing its surge clamping function. Here, the varistor is conducting significant levels of current per square centimetre and the conductivity interval in this region is milliseconds down to microseconds. Moreover, the higher is the current, the shorter is the surge length. Also, in this region the zinc oxide grains are controlling the resistance of the varistor. The lower end of the high current region is where switching surges are found while above 2000 amps we find lightning currents. This is the region that gives us the discharge voltage or residual voltage data we find in most specification charts for arresters.

As can be seen, each region of the curve is important and together they provide for the varistor action associated with surge protection. Of course, other varistor characteristics are also important but this one is certainly near the top for any varistor/arrester designer.

3.5. Energy Handling Capability, Temperature and Degradation

High voltage systems are often subject to transient overvoltages of internal or external origin. The resultant surges travel along the transmission line and can cause damage to equipment. Thanks to the development of line surge arresters it is possible to maintain complete control of the transmission line lightning performance. Line surge arresters are mainly used for line lightning performance improvement. The performance of surge arresters in power systems is determined on the one hand by the electrical and thermal properties of the varistors, and on the other by the design and installation of the arrester.

CIGRE Brochure 544 (2013) reports a short summary of the different aspects of energy handling, basically divided into "thermal" and "impulse" energy stress.

Energy handling capability of metal-oxide (MO) arresters has many different aspects, which are only partly or not at all reflected in the actual standards. At least, though this list may not be complete, they have to be divided into:

- "thermal" energy handling capability,
- "impulse" energy handling capability,

- "single" impulse stress,
 - withstand values (deterministic approach),
 - values related to a certain failure probability (statistical approach),
- "multiple" impulse stress, i.e. impulses in time intervals too short to obtain an approximately uniform temperature distribution in the MO resistors,
- "repeated" impulse stress, where the time interval between impulses is sufficiently long to obtain cooling of the MO resistors close to their initial temperature (this includes durability and degradation aspects).

Metal-oxide varistor materials temperature and factors affecting rate of ZnO degradation are mentioned below. ZnO degradation due to surge absorption and multiple impulses is described in sections below.

3.5.1. Thermal Energy Handling Capability

Thermal energy handling capability can only be considered for complete arresters, as, besides the MO material properties, it is mainly affected by the heat dissipation capability of the overall arrester design. The situation is schematically illustrated in figure 3.5.1.

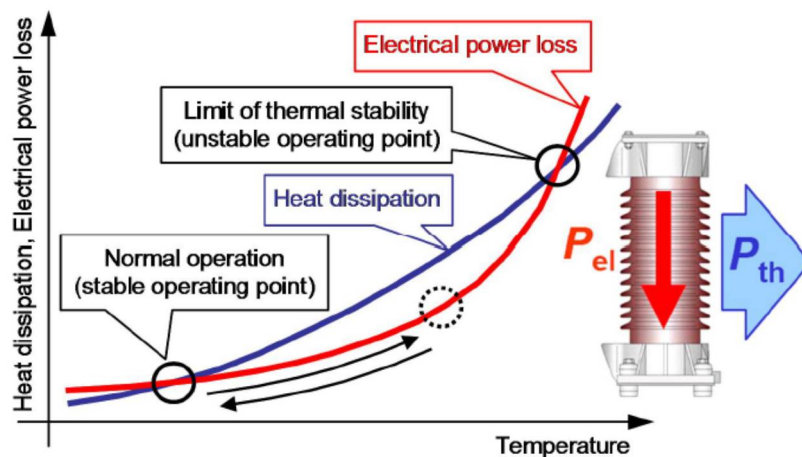


Figure 3.5.1. Heat loss – input diagram for steady state operation of a ZnO surge arrester [41, 46]

An arrester's heat dissipation capability (heat flow; measured in Watts) is determined by thermal conduction, convection and radiation. In the interesting temperature range (operating temperature below 250 °C) it increases non-linearly but moderately with the temperature difference to ambience. Electrical power losses under normal operating conditions are usually very small, in the range of tens of milliwatts per kilovolt of rated voltage for distribution arresters up to several hundreds of milliwatts per kilovolt for line discharge class five (LD 5) arresters. However, due to their temperature dependence, the power losses are much higher at higher temperatures, e.g. by a factor of ten to twenty at 150 °C compared with 20 °C. This power loss characteristic is specific to a particular MO material and make.

Under continuous operating conditions, an arrester will adopt an operating temperature slightly above ambient temperature, and the generated heat can easily be dissipated to the ambience: the arrester adjusts itself to a stable operating point (left intersection of the two curves in figure 3.5.1). However, once a high amount of energy is injected into the arrester under overvoltage conditions, the arrester temperature will be increased in form of a step function, with typical values of temperature increase under nominal energy stress up to 100 K or even more. The operating point will instantaneously jump to the right on the electrical power loss curve. As long as it remains left of the second intersection

point of the two curves, the generated heat can still be dissipated to the ambience, and the arrester will cool back to its normal operating temperature within five of its thermal time constants. But if the right intersection point – the limit of thermal stability – is reached or even exceeded, the arrester will generate more heat than can be dissipated and electrical power losses will further increase and finally destroy the MO material by excessive heat (puncture at several hundred degrees Celsius).

It is evident that, on one hand, the thermal stability limit depends on the overall arrester design. Arresters with MO resistors directly covered by a polymeric housing, for instance, will have a thermal stability limit at higher temperatures than conventional porcelain housed arresters, since they can better transfer heat from the MO resistors to ambience. On the other hand, also the MO material properties (electrical power losses and their temperature dependence) have an effect, because the more pronounced the increase of power losses with temperature is, the more will the right intersection point of the two curves be shifted to the left, i.e. to lower temperatures. As well, the curve of electrical power losses versus temperature is affected by possible impulse degradation, i.e. it will be shifted upwards (Hei 2001), which again changes the limit of thermal stability to lower temperatures.

However, definition and verification of the thermal energy handling capability is a comparatively easy task. Injected energy per volume and temperature increase is simply linked by the heat capacitance, which has a non-linear dependence of temperature, and can, according to Lat (1983), be calculated as:

$$\frac{W}{V} = \vartheta \cdot 2,59 \frac{J}{cm^3 \cdot K} + 0,0044 \frac{J}{cm^3 \cdot K^2} \cdot \vartheta^2$$

Where W is the contained energy in J, V is the MO volume in cm^3 and ϑ is the MO temperature in $^{\circ}C$. This dependence is shown in figure 3.5.2.

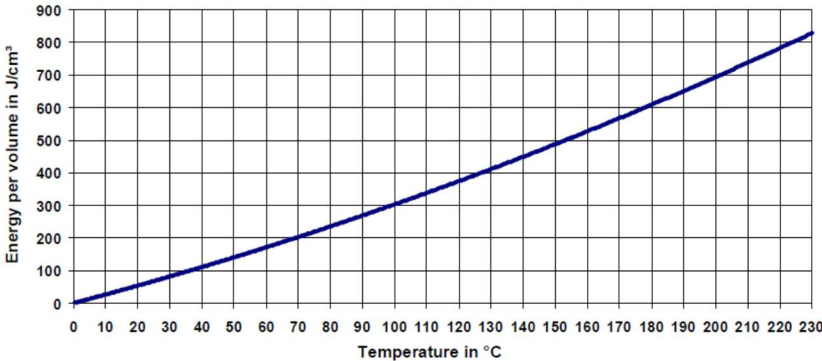


Figure 3.5.2. Metal-oxide resistor energy per volume vs. temperature [46]

In order to verify thermal energy handling capability, energy may thus be injected into the arrester by any suited method that will rise its temperature to a value related to the specified energy, because the only purpose of this verification is to demonstrate that the arrester is able to cool back afterwards. Of course, the operating conditions (applied power-frequency voltage) must be specified, and possible electrical aging of the MO material, e.g. by current impulse stress, must be considered by appropriate conditioning procedures.

3.5.2. Temperature of MO Varistor Materials

MO varistor materials have a temperature dependence that is significant only at low current densities. Temperature dependence does not need to be represented in simulations for typical overvoltage studies where the arrester currents exceed 1 A; it is of concern when selecting arrester ratings for steady state

and TOVs. The temperature-dependent U–I characteristic is important only for the evaluation of energy absorbed by the surge arrester, and should not influence the insulation protective margins [51].

When an MO surge arrester is connected to an electric power system, a very small resistive leakage current will flow through the arrester. When large surge energy is absorbed, the temperature of ZnO elements increases, causing the resistance value to decrease. As a result, the leakage current becomes greater and the heat generation increases. But, even if the heat generation increases, the temperature of ZnO elements may be below a limit intrinsic to the surge arrester. This occurs when the amount of heat generation is smaller than that of heat dissipation; in such case the temperature of the ZnO elements gradually drops and returns to that prior to the absorption of surge energy. However, when the temperature rise exceeds the temperature limit, the amount of heat generation becomes greater than the heat dissipation, and a thermal runaway occurs. Therefore, this temperature limit is a very important factor.

The term thermal runaway as defined by existing IEC 600 99 – 4 – 2014 [53] is used to describe a situation culminating in failure if the ZnO arrester is operated above the upper stability point. However, there are a number of factors which influence the position of this point (for more information see [52]).

3.5.3. Factors Affecting Rate of Degradation

A number of factors have been identified to affect the rate of ZnO degradation: composition and fabrication process, homogeneity, ambient temperature, working voltage, design and physical arrangements of ZnO surge arresters, pollution of surge arresters, environment, and surge absorption capability. In this section ZnO degradation due to surge absorption and multiple impulses is mentioned, while more information about ZnO degradation due to other previously mentioned parameters can be found in [52].

Surge absorption capability

In general, just after the application of a surge, there is a measurable degradation of ZnO electrical properties. Three types of overvoltages are of interest: switching surges, temporary overvoltages and lightning surges:

- a) *Switching surges*: Following the absorption of a high energy surge, the cooling conditions of the arrester have very little effect [52]. Experiments [54, 55, 56] showed that degradation is more severe under high current surge than high energy surge. Degradation resulting from energy surge absorption is therefore negligible in practice and has almost no effect on the life of the elements. However, high energy surge applied to ZnO elements exhibiting localized spots of conduction could melt the material [52, 55]. Switching surge degradation is pronounced under unidirectional surges but can be reduced to some extent by applying surges of opposite polarity [57]. Only 1 percent degradation was observed [56] on the direct voltage which produces 1 mA (U_{1mA}), after the discharge of positive and negative switching surges. After absorbing two rectangular surges of 600 A and 2 ms duration followed by power frequency, less than – 4 percent maximum variation in voltage, V_{1mA} , was observed [54], and the ZnO element could return to its initial working conditions of voltage and temperature after just one hour. V_{1mA} undergoes as little as 5 percent change when the arrester is subjected to 1000 switching surges of 600 A magnitude and 2 ms duration [54].
- b) *Temporary overvoltage (TOV)*: No change is measured after TOV absorption [56]. Durability of MOV against TOV depends mainly on global structural uniformity [52]. Temperature effects, however, may lead to thermal runaway if the surge parameters are higher than specific allowable values given in manufacturers' specifications [58].
- c) *Lightning discharge*: Degradation due to discharge of the surge energy largely depends on the peak value of the discharge current rather than the discharge energy. The presence of AC stress does not enhance nor restore the surge degradation. A few high current surges degrade ZnO arresters more than many high energy surges of lower current; two (8/20 μ s) surges of 65

kA amplitude caused the leakage current to increase by 50 percent [56]. The allowable number of surges decreases when the amplitude of the surge increases; e.g. a life of 50 years allows 130 surges of 50 kA or only 30 surges of 100 kA [59].

Multiple impulse response

Between 60 and 70 percent of all lightning ground flashes contain more than one stroke. A typical flash will consist of three or four strokes with time intervals between strokes of 20 to 200 ms. In addition, induced lightning surges on transmission lines are known to produce a transient overvoltage with two peaks of reverse polarity. A rapid series of transients may also occur during certain switching transients.

Extensive laboratory tests have shown that the cumulative nature of multiple impulses forms a significant part of the ZnO material degradation process, especially the insulating walls of the ZnO elements [52, 60]. Such deterioration was related to energy dissipation constraints. However, the V – I characteristic of the arrester is not significantly affected by multiple impulses of low energy [52].

3.6. Illustration of LSA Cooling and Energy Absorption

Figure 3.6.1 illustrates the case when line surge arrester absorbs energy due to bipolar or multicomponent lightning flash as well as LSA’s cooling process.

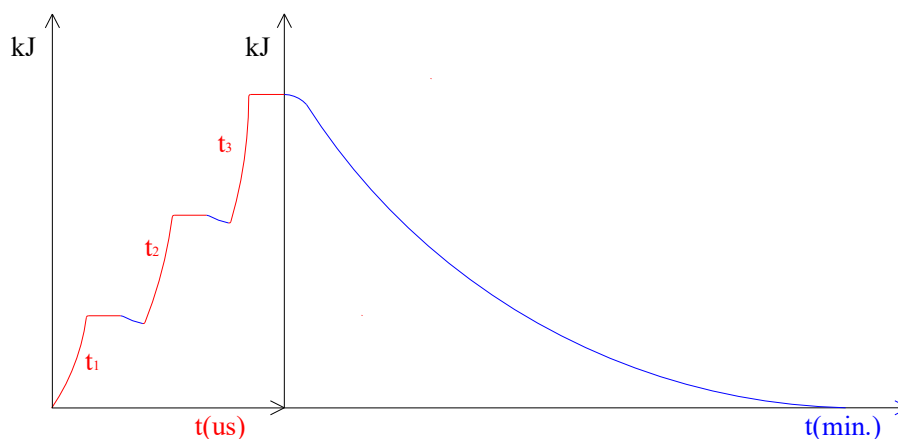


Figure 3.6.1. Illustration of case when line surge arrester absorbs energy due to bipolar or multicomponent lightning flash as well as LSA’s cooling process

As it can be seen from figure 3.6.1 first stroke causes operation of line surge arrester and energy absorption (red curve). During the interstroke time interval, line surge arrester starts cooling process (blue curve). The same situation happens for each following stroke. If there are no more strokes, line surge arrester cooling process begins. The cooling process lasts in accordance with environmental conditions and line surge arrester material.

3.7. Discussion NEGLA vs EGLA

Both, NEGLA and EGLA have their advantages and disadvantages. Table 3.7.1 represents EGLA's advantages and disadvantages while table 3.7.2 represents NEGLA's advantages and disadvantages.

Table 3.7.1. EGLA advantages and disadvantages

EGLA advantages	EGLA disadvantages
<ul style="list-style-type: none"> ⊕ Low risk of damage during transport. ⊕ No disconnection needed. ⊕ Lower arrester rated voltage needed (because arrester is not energized all the time). ⊕ It is believed that there is no contamination, but that is not always true. 	<ul style="list-style-type: none"> ∅ They might be difficult to install. ∅ They do not share the energy except in case of lightning. ∅ It may be technically difficult to locate an EGLA with a failed metal oxide resistor. ∅ Difficult insulation coordination. ∅ Subsequent operations of an EGLA with a failed metal oxide resistor may increase the possibility of solid material ejection. ∅ No control of switching overvoltages (no ignition of a gap, except only at lightning impulses). ∅ Specified design for each situation needed, i.e. for different tower / conductor designs. ∅ Arrester operation depends of environmental conditions.

Table 3.7.2. NEGLA advantages and disadvantages

NEGLA advantages	NEGLA disadvantages
<ul style="list-style-type: none"> ⊕ They may be easily installed, in some cases with live-line work methods. ⊕ They may control slow front overvoltages. ⊕ Failed NEGLA can be detected by helicopter or long-range visual inspection when the disconnect link falls away from the arrester. ⊕ All NEGLAs participate in energy sharing. ⊕ Arrester operates independently of environmental conditions. 	<ul style="list-style-type: none"> ∅ The disconnect and flexible lead which removes the arrester from service in case of arrester failure is often a weak point. It often fails mechanically from vibration, galloping, conductor restraint, corrosion or other stress. ∅ The disconnect may not operate if there is insufficient short circuit current on the line. ∅ The disconnect may also have an internal explosive device which can be an issue for transportation in some countries. ∅ Metal oxide blocks are permanently stressed by power frequency voltage, occasional temporary overvoltages and slow front overvoltages. ∅ Contamination may be an issue in heavy polluted area. ∅ Snow or ice accretion may be an issue in cold climates.

Definitely, there are good reasons for installing both EGLA and NEGLA type. However, it is not possible to generally decide which type is better. It is left to users to choose EGLA or NEGLA based on system characteristic, lightning incidence and environmental conditions of region.

For purposes of this thesis gapless-type arresters will be considered. The main reason for that is fact that all NEGLA participate in energy sharing. It is very interesting to consider energy sharing of line surge arresters installed along a transmission line, as well as energy duty of those arresters due to bipolar flashes and multicomponent flashes.

3.8. The NEGLA Selection Process

The IEEE and IEC application guides give versions of how to select a standard arrester, but neither one specifically covers the NGLA type. Selecting an arrester for any application starts by determining the characteristics of the power system in question as well as the location where the arrester is to be installed. Figure 3.8.1 represents selection of the NEGLA in six steps, such procedure is proposed in Standard IEC 60099 – 9 [61]. For each step, system parameters have to be determined first and only then are the corresponding arrester parameters selected.

First step – selecting arrester type

The selection process begins with choosing the type of arrester that best meets the overall needs of the application. Even though this is fundamentally the most important step, it is routinely left out of those procedures reviewed in the standards.

For example, when the goal is to select a suitable arrester for a 20 kV line, there is no need to consider Class 5 arresters ordinarily installed on 400-800 kV lines. The initial choice can then easily be subsequently modified if any unexpected problems arise. The main actions as part of this first step include:

- Identifying the approximate location of the arrester in the system;
- Reviewing available arresters and their characteristics;
- Making a selection of arrester type from among the different styles.

Another important consideration when selecting an arrester for a transmission line is to consider the ideal type of external housing. Whenever possible, the first priority should be given to polymer-housed types, since they are lighter and more easily mounted than porcelain-housed units.

Second step – selecting AC rating

Since most such arresters are energized with an AC voltage throughout their life, this step is critical. An incorrect AC rating can result in premature arrester failure and a resulting system outage. Rated voltage U_c of an arrester according to IEC 60099 designated maximum permissible r.m.s. value of power – frequency voltage between its terminals at which it is designated to operate correctly. This voltage may be applied to the arrester continuously without changing its characteristics. In the case of NGLAs, this voltage must be checked for temporary overvoltage (*TOV*) withstand capability and, if necessary, could be adjusted upward to meet these requirements. The initially selected AC rating is therefore generally a minimum value to be increased to meet other constraints as the selection process continues. Significant considerations in this regard are:

- Determining maximum steady state system line-ground voltage;
- Selecting an arrester U_c that is equal or greater than this voltage;
- Determining the maximum amplitude and duration of potential overvoltages;
- Checking that the arrester selected earlier can withstand the overvoltages determined above using the arrester *TOV* curve.

Third step – check margin of protection

The fundamental purpose of a transmission line arrester is to reduce the risk of insulator flashover due to either switching or lightning surges. The margin of protection is a standard means of evaluating the level of risk of a flashover. If the arrester clamps the voltage at a fraction of the Critical Flashover Voltage (*CFO*) of an insulator, then this risk is quite low. Neither IEC nor IEEE standards make a recommendation as to what constitutes an adequate margin of protection for line insulators but instead recommend that the arrester residual voltage should not be more than 80-85% of insulator *BIL* at stations. The fundamental aspects to the margin of protection selection process are:

- Determining insulation withstand characteristics;
- Determining arrester protective characteristics;
- Determining if there is any lead length effect;
- Calculating margin of protection.

Fourth step - check energy handling capabilities

This is another important part of the selection procedure of an NGLA and requires proper understanding of a purpose behind the specific arrester application. Considerations that need to be taken into account in this regard include:

- Systems with shield wire;
- Systems without shield wire;
- Switching surge energy considerations;
- Lightning impulse discharge capability test.

If the arrester is to be used on a system equipped with a shield wire, the energy requirements of the arrester are much lower than otherwise. If the footing resistance of the tower is high, more current will be diverted through the arrester and into the phase but even here most will still flow to earth instead of to the conductor. If the NGLA application is on a system without a shield wire, the full lightning stroke is likely to pass through the arrester. If the NGLA application is to control surges generated during switching operations, the potential switching surge energy of the system needs to be calculated and compared to the energy handling capabilities of the arrester. For arresters applied to systems up to 52 kV, high current impulse is the only means of classifying the lightning impulse capability. For arresters applied to systems of 52 kV and above, a special test requirement and withstand capability is available. Since 2006, all line surge arresters applied to systems above this level must be tested according to the lightning impulse discharge capability test outlined in IEC 60099-4 Annex N.

Fifth step – check failure modes

This is another important factor for selecting an NGLA, particularly if it is to be located near highways or public buildings. If the arrester is overloaded, it often becomes a short circuit to the system to which it is applied. If this happens, the power system will supply all potential fault current to the circuit, including the arrester. When a shorted arrester experiences more power-frequency fault current than it was designed to handle, it could eject very hot components at high velocity and over a significant distance. Such a fragmenting overload is clearly undesirable. To ensure that this type of overload response does not occur, the short circuit current withstand capability of the NGLA needs to be higher than the available fault current of the system. This short circuit rating for all arresters is found on the nameplate as well as in the manufacturing literature. Basically, users need to know the available fault current on the system to which any arrester is to be installed and this data is readily available from the relay or from system analysis personnel.

Sixth step - mounting considerations

Line surge arresters are stressed physically more than any other type of arrester since they are mounted on or near towers and exposed to the lightning events. For this reason, selection of mounting components is important and often one of the most difficult parts of NGLA selection. Also, since there are so many possible tower configurations, the mounting requirement for each installation is unique.

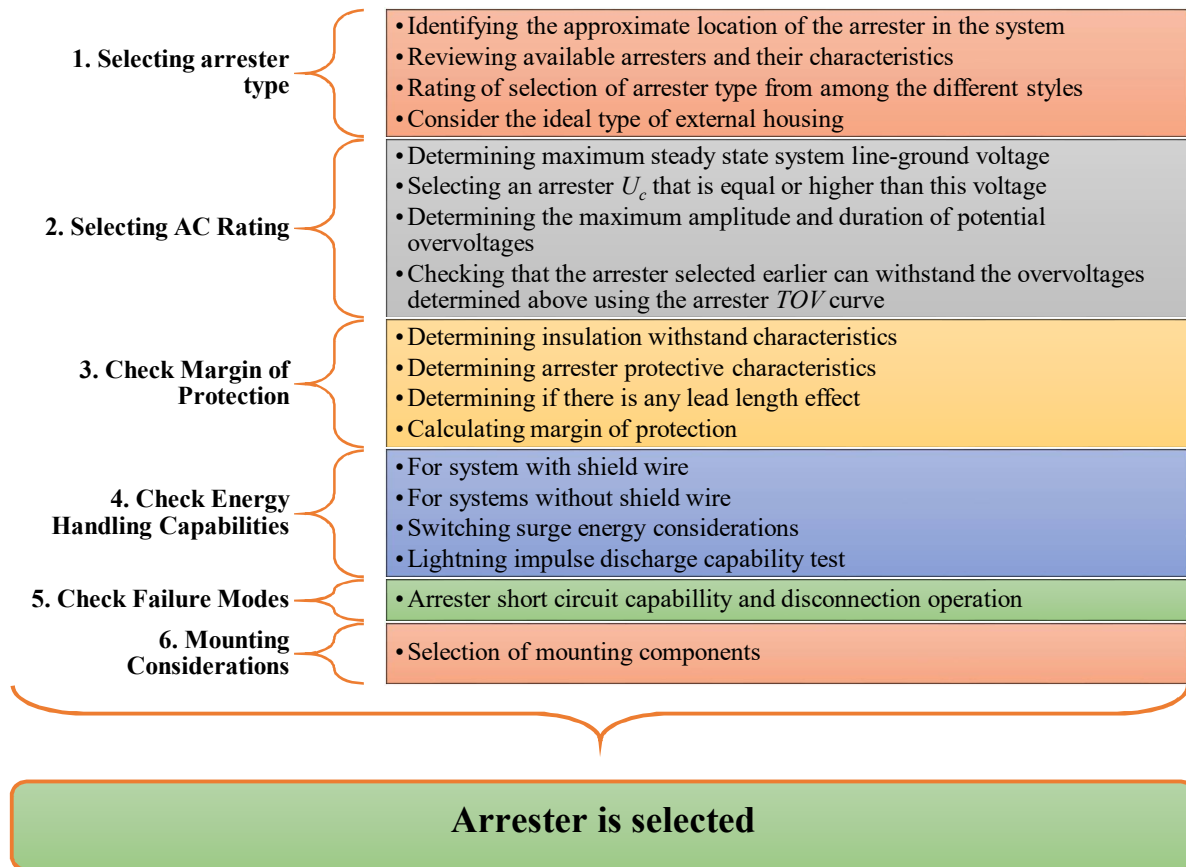


Figure 3.8.1. Selection of an NEGLA in six steps [61]

Chapter 4.

RECORDED BIPOLAR AND MULTICOMPONENT FLASHES ANALYSIS

4.1. Introduction

Lightning is a main cause of transmission line outages. It is a very severe problem for transmission lines, especially for those lines located in the regions of high lightning incidence and in regions with high tower footing resistance. Based on the development of line surge arresters it is possible to maintain complete control of the line lightning performance. Line surge arresters are mainly used for line lightning performance improvement. Any new equipment that needs to be installed into a power system is usually subjected to standard lightning impulse tests so as to be assured of its reliability and energy capability when exposed to lightning surge. Lightning natural characteristics are entirely different from testing procedures which focus only on a single impulse with specified impulse wave shape. Therefore, energy duty of line surge arrester should be considered under specific natural lightning impulses. Quantification of lightning parameters helps the scientific and engineering community to assess lightning effects and to design effective protection systems. The knowledge of lightning current parameters is of primary importance for an effective protection design of transmission lines. Advanced technologies are able to provide more data about lightning characteristics.

Three approaches can be used to obtain lightning data:

- Direct measurements using instrumented towers;
- Direct measurements using the technique of artificial initiation of lightning;
- Lightning location systems.

Data from lightning current measurement system installed on Corsica and data from lightning location system (LINET) are used for purposes of this work. The most important details about lightning measurement system and LINET are given in this chapter.

Also, the aim of this chapter is to analyse data obtained from measurements using instrumented tower on Corsica and lightning location system (LINET) for purposes of transient analysis.

In this chapter presentation of the bipolar lightning current shape is given, as well as an analysis of current parameters for bipolar impulse. In the second part of the chapter a special attention is given to description and analysis of the multicomponent flashes.

Bipolar flash and multicomponent flashes used in simulations conducted in this thesis are presented in this chapter. More examples of mentioned flashes as well as more data about these flashes can be found in Appendix A.3.

4.2. Lightning Activity Monitoring System and Lightning Location System

Block diagram of lightning monitoring system installed on Corsica (at the telecom base station Miluccia) is presented in figure 4.2.1. The monitoring system is based on an industrial computer (see figure 4.2.2). It records data from a 500 kA maximum input range current transformer (Pearson model 2093) installed on the tower top with its acquisition unit and offers different alternatives to transfer data to a remote server in real-time.

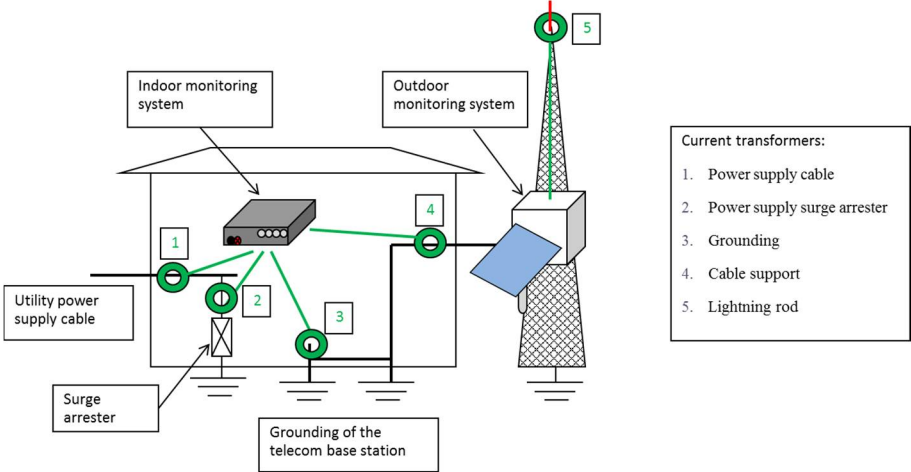


Figure 4.2.1. Block diagram of lightning monitoring system installed on Corsica [62]

The acquisition unit can be selected according to the specificities of the application. For measurements used in this work, a 4 channels card is used with an acquisition speed of 50 MSamples per second per channel and a 12 bits vertical resolution. The communication with the remote server is based on mobile (EDGE) and wireless networks (WiFi). The monitoring system transfers data to the remote server with mobile Internet with effective data rates of 56 kbits/s. Using an integrated GPS receiver, an accurate timing is performed regardless of the system location. Finally the low power consumption of the monitoring system (about 10 watts) permits its energization even by solar panels. Two solar panels of 130 watts each are permitting its continuous operation. Current transformer installed on the lightning rod of the telecom base station at Miluccia and monitoring system are presented in figure 4.2.2.

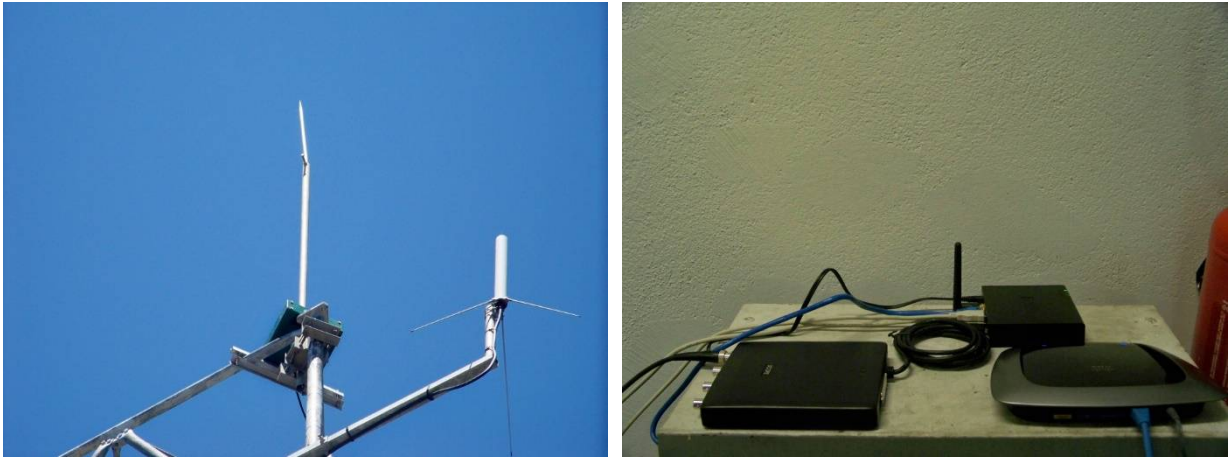


Figure 4.2.2. Current transformer installed on the Lightning rod of the telecom base station at Miluccia and monitoring system [62]

Lightning location system named LINET is developed in Germany and nowadays counts over 150 sensors installed across Europe. Each lightning detection sensor consists of the following three parts [63]:

- LINET field antenna (LFA);
- GPS antenna;
- LINET field processor (LFP).

Installation of LINET sensor on University of Sarajevo is illustrated in figure 4.2.3. LINET field antenna and GPS antenna are installed on roof, while LINET field processor is placed inside of building on distance of 30 meters.



Figure 4.2.3. LINET sensor installation

The LINET sensors measure the density of magnetic flux directly into the dependence of time. This feature is useful for the treatment of small signals. Magnetic flux component of detected signals are measured using orthogonal loop (antenna) in real time. Amplified value is induced current, not voltage, and as a result, the time dependence of the magnetic induction in the range 0.1 to 130 nT is obtained. The system LINET uses time of arrival method for determining the location of lightning impact assisted with method for determining the direction. Primarily time of arrival method is used for determining the location, where minimum four detection sensors are required. By combining time of arrival and direction finding methods the discharge can be detected by two or three sensors, but in this case, the location determine error is increased. In LINET system important components are optimized to determinate all lightning discharge, including those whose amplitude is less than 5 kA, where sensors should not be too far away. LINET uses the same very low frequency/low frequency method for detection of CG and IC lightning discharges. Special consideration should be taken into account to distinct these two types of lightning. For this reason, a new three-dimensional (3D) geometric algorithm for very low frequency/low frequency networks was developed. The procedure relies on the well-known fact that CG strikes broadcast very low frequency/low frequency discharge dominant in ionized channel near the ground level, while IC discharge occur in the ionized channel between clouds, high above the ground. This 3D technology is very reliable, especially if it is possible that the minimum distance between the sensors does not exceed 200 to 250 km. Particular efforts were made to achieve high location accuracy in monitored area. Today, it is achieved that the mean location accuracy is approximately 100 m [63].

LINET provides the following information for lightning strokes [63]:

- Date;
- GPS Time (100 nanoseconds resolution);
- GPS coordinates of the lightning stroke (latitude and longitude);
- Peak current and polarity of the stroke;
- Discharge type: CG – Cloud-to-Ground or IC – In-Cloud (and Cloud-to-Cloud);
- Location error.

4.3. Bipolar Lightning Current Shape

In this section measured bipolar lightning current shape is analysed. During observation period of one and a half year, thirteen bipolar events have been recorded by SADOVIC measurement system. Date and time of bipolar events occurrences are represented in the table 4.3.1.

Table 4.3.1. Bipolar events recorded on Corsica

No.	Place	Date	Time
1	Corsica	08.06.2011.	03:17:15.196 GMT
2	Corsica	08.06.2011.	03:21:36.281 GMT
3	Corsica	08.06.2011.	03:23:23.000 GMT
4	Corsica	08.06.2011.	03:24:22.441 GMT
5	Corsica	08.06.2011.	03:24:22.488 GMT
6	Corsica	08.06.2011.	03:28:21.713 GMT
7	Corsica	18.09.2011.	16:09:20.064 GMT
8	Corsica	14.10.2011.	12:58:31.371 GMT
9	Corsica	14.10.2011.	13:16:11.744 GMT
10	Corsica	14.10.2011.	13:18:32.603 GMT
11	Corsica	05.11.2011.	18:24:41.357 GMT
12	Corsica	11.12.2011.	16:08:15.855 GMT
13	Corsica	11.12.2011.	16:13:13.898 GMT

According to its parameters, the most interesting bipolar lightning event (shown in figure 4.3.1.), is event recorded on the 11th of December 2011 at 16:08:15.855 GMT. Therefore, this event is analysed in this chapter and it is used for purposes of simulations and line surge arrester energy duty calculations.

Current shapes of the other twelve bipolar lightning events recorded on Corsica (at the telecom base station Miluccia) are presented in Appendix A.2. Analysis of all thirteen bipolar lightning flashes is also given in Appendix A.2.

Bipolar lightning event – recorded on the 11th of December 2011 at 16:08:15.855 GMT

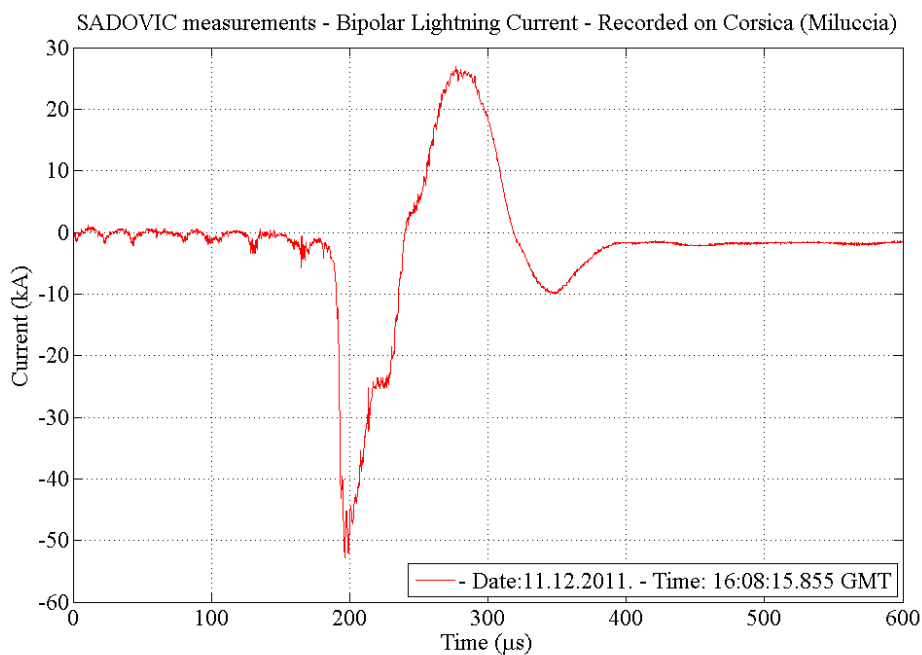


Figure 4.3.1. Shape of bipolar current for event recorded on the 11th of December 2011 at 16:08:15.855 GMT

For measured bipolar lightning current analysis developed software was used. Basic flowchart of this software is given in Appendix A.4. The following parameters of bipolar lightning current are determined:

- Current peaks (kA):
 - o Peak of positive part of bipolar stroke I_{max+}
 - o Peak of negative part of bipolar stroke I_{max-}
- Charge transfer (As):
 - o Positive charge transfer Q_+
 - o Negative charge transfer Q_-
 - o Total charge transfer $Q = Q_+ + Q_-$
- Front time (μ s):
 - o Front time for positive part of bipolar stroke t_{f+}
 - o Front time for negative part of bipolar stroke t_{f-}
- Tail time (μ s):
 - o Tail time for positive part of bipolar stroke t_{h+}
 - o Tail time for negative part of bipolar stroke t_{h-}
- Stroke duration (μ s):
 - o Duration of positive part T_+
 - o Duration of negative part T_-

The negative charge transfer is determined by integrating the absolute value of the current over the negative current component duration. The positive charge transfer is determined by integrating the current over the positive current component duration. For the integration the trapezoidal rule is used. The total transfer is summary of the negative and the positive charge transfers.

Front and tail times are determined according to CIGRE, IEEE and IEC recommendations [8, 64-68]. More details can be found in Appendix A.1. Determined parameters of bipolar stroke from figure 4.3.1 are given in table 4.3.2.

Table 4.3.2. Parameters of bipolar stroke from figure 4.3.1

Parameter	Value
I_{max+} (kA)	26.9000
I_{max-} (kA)	52.8600
Q_+ (As)	1.2487
Q_- (As)	2.4062
$Q = Q_+ + Q_-$ (As)	3.6549
t_{f+} (μ s)	28.0000
t_{f-} (μ s)	6.3333
t_{h+} (μ s)	65.5000
t_{h-} (μ s)	31.4000
T_+ (μ s)	78.9000
T_- (μ s)	55.0000

4.4. Multicomponent Flashes Data

This section considers LINET data from two locations on mountain Lovćen in Montenegro. The first location is a place called Njegoš's Mausoleum and the second one is broadcasting centre of Montenegro (LINET data in radius of 1000 m from mentioned places were analysed). Usual clustering criterion is used for grouping strokes into flashes. This criterion groups strokes into flashes using a spatial and temporal clustering algorithm. Strokes are added to any active flash for a specified time period (usually 1 second) after a first stroke, as long as the additional strokes are within a specified clustering radius (usually 10 km) of the first stroke and the time interval from the previous stroke is less than a maximum interstroke interval (usually 500 ms). Table 4.4.1 represents average number of strokes per flash for previously mentioned locations.

Table 4.4.1. Average number of strokes per flash for two locations in Montenegro

Place	Year	Number of strokes	Number of flashes	Average number of strokes per flash
Njegoš's Mausoleum	2012	103	59	1.75
Njegoš's Mausoleum	2013	85	48	1.77
Broadcasting centre	2012	2766	445	6.22
Broadcasting centre	2013	1395	291	4.79

Some specific (cloud – to – ground) lightning flashes are presented in this section such as:

- flashes that involve return strokes of opposite polarity – in literature known as bipolar lightning discharges of third type. It is very important to emphasize that lightning location systems can only detect bipolar flashes of the type 3, and
- flashes with currents of subsequent strokes larger than a current of the first stroke. Larger than first, subsequent strokes may represent an additional threat to transmission lines, line surge arresters and other systems.

Previously mentioned types of multicomponent flashes are used for simulation purposes and line surge arrester energy duty calculations. Examples of such flashes are given below.

Flash 1 – recorded on the 19th of April 2012 (flash number 241 in 2012)

Flash 1 is recorded at the location of the broadcasting centre of Montenegro. LINET data for flash 1 are represented in table 4.4.2.

Table 4.4.2. LINET data for flash 1

NO.	Date	Time	Latitude	Longitude	Type	Peak (kA)
1	20120419	21:30:29.4333488	42.3928	18.8159	CG	36.7
2	20120419	21:30:29.4384397	42.3935	18.8229	CG	-7.3
3	20120419	21:30:29.4524737	42.3948	18.8162	CG	-7.1

Flash 1 belongs to bipolar lightning type 3. It consists of three strokes where the first is positive and the others are negative. The positive stroke current peak is 36.7 kA and the negative stroke current peaks are -7.3 kA and -7.1 kA, respectively. The time interval between first and second stroke is 5.0909 ms and between second and third stroke it is 14.0340 ms. The mean value of interstroke time interval is 9.5624 ms.

Flash 2 – recorded on the 25th of May 2013 (flash number 222 in 2013)

Bipolar flash 2 is recorded at the location of broadcasting centre of Montenegro. LINET data for flash 2 are represented in table 4.4.3. Flash 2 consists of 5 strokes, two negative, one positive and two negative, respectively. Current peaks for each component are given in table 4.4.3. The interstroke time intervals are represented in table 4.4.4.

Table 4.4.3. LINET data for flash 2

NO.	Date	Time	Latitude	Longitude	Type	Peak (kA)
1	20130525	23:47:35.982	42.3919	18.8164	CG	-29.8
2	20130525	23:47:35.994	42.3922	18.8157	CG	-15.9
3	20130525	23:47:35.996	42.3974	18.8166	CG	9.6
4	20130525	23:47:36.295	42.3921	18.8158	CG	-20
5	20130525	23:47:36.321	42.392	18.8158	CG	-15.5

Table 4.4.4. Interstroke time interval for flash 2

Time interval between components	Interval duration (ms)
1 and 2	12.0000
2 and 3	2.0000
3 and 4	299.0000
4 and 5	26.0000

Flash 2 duration is 339 ms. Minimum and maximum time duration between components are 2 ms and 299 ms, respectively. Mean value of interstroke time intervals is 84.75 ms and standard deviation is 143.1721 ms.

Flash 3 – recorded on the 13th of September 2012 (flash number 33 in 2012)

Flash 3 is recorded at the location of Njegoš's Mausoleum in Montenegro. LINET data for flash 3 are represented in table 4.4.5.

Table 4.4.5. LINET data for flash 3

NO.	Date	Time	Latitude	Longitude	Type	Peak (kA)
1	20120913	06:02:28.796	42.3946	18.8389	CG	-27
2	20120913	06:02:28.885	42.3938	18.8423	CG	-39.8
3	20120913	06:02:28.976	42.3936	18.8394	CG	-42.7
4	20120913	06:02:29.049	42.3933	18.8399	CG	-15.9
5	20120913	06:02:29.178	42.3936	18.8396	CG	-30.6
6	20120913	06:02:29.249	42.3947	18.8396	CG	-14.2
7	20120913	06:02:29.361	42.3940	18.8395	CG	-14.2
8	20120913	06:02:29.436	42.3939	18.8422	CG	-7.5
9	20120913	06:02:29.517	42.3942	18.8394	CG	-15.1

All components in flash 3 are negative and current peaks for each component are given in table 4.4.5. The interstroke time intervals are represented in table 4.4.6. Table 4.4.7 represents a summary of basic data for flash 3.

Table 4.4.6. Interstroke time interval for flash 3

Time interval between components	Interval duration (ms)
1 and 2	89.0000
2 and 3	91.0000
3 and 4	73.0000
4 and 5	129.0000
5 and 6	71.0000
6 and 7	112.0000
7 and 8	75.0000
8 and 9	81.0000

Table 4.4.7. Summary of basic data for flash 3

Number of components in flash	9
Type	CG
Polarity	all negative
Peak (kA)	-39.8
Flash duration (ms)	721
Minimum duration between components (ms)	71
Maximum duration between components (ms)	129
Mean value of interstroke time interval (ms)	90.1250
Standard deviation of interstroke time interval (ms)	20.5735

Display and histogram of interstroke time interval data are shown in figure 4.4.1.

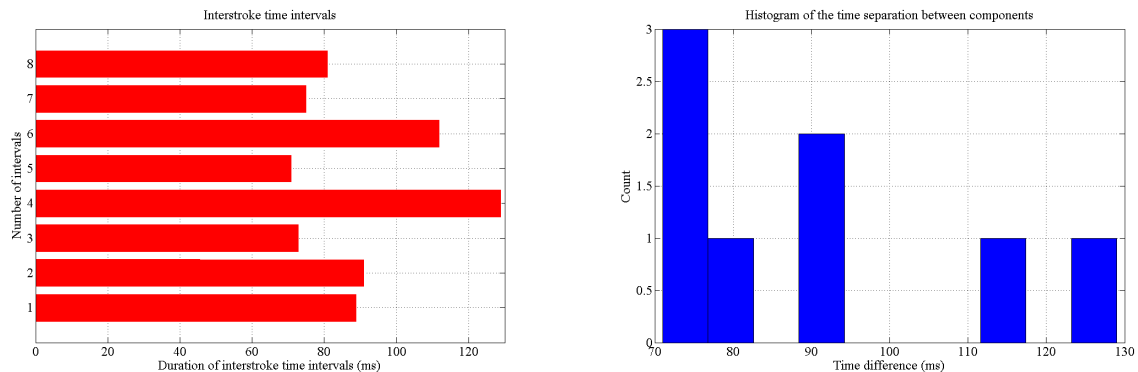


Figure 4.4.1. Display and histogram of interstroke time interval data for flash 3

In the histogram of the interstroke time interval most of the strokes are separated by a time interval between 60 ms and 90 ms. Two interstroke time intervals are greater than 110 ms.

It is very common that first stroke have larger currents than subsequent strokes, but it is not always the case. Flash 3 is a good example of this fact. In table 4.4.5 it is possible to see that first stroke has current peak of -27 kA, but second and third stroke have current peaks of -39.8 kA and -42.7 kA, respectively.

Following data of interest can be obtained from lightning location systems database:

- Lightning stroke current peak
- Lightning stroke polarity (positive or negative)
- Lightning stroke type (cloud to ground (CG) or cloud to cloud (CC))
- Date and time
- Latitude and longitude

Using data obtained from lightning location systems and using usual clustering criterion for grouping strokes into flashes, it is possible to determine:

- number of components in flash, and
- interstroke intervals.

In order to select the appropriate lightning protection system, it is necessary to identify lightning current parameters:

- Shape of the lightning current (peak value, front time, tail time and duration)
- Polarity
- Multiplicity – number of components in flash

Front time, tail time and duration time can be determined only from direct measurements (if lightning current shape is recorded). These parameters are needed in making of simulations of lightning performance of overhead power lines. Therefore, these parameters were selected according to CIGRE, IEEE and IEC recommendations [8, 64-68]. Parameters of log – normal distributions of current waveform parameters (for both negative and positive as well as for first and subsequent strokes) are given in CIGRE Brochure 63 (1991) and IEEE Std. 1410 – 2010.

Data obtained in mentioned literature are based on small sample of measured data published by Berger, Anderson and Ericson [69-70]. Nevertheless last CIGRE Brochure 549 (2013) and last IEEE review of parameters of lightning strokes (2005) recommends usage of these data until more data are available.

More facts about lightning current parameters can be found in [8, 64-68] and in chapter 6 of this work. More examples of multicomponent flashes can be found in Appendix A.3.

4.5. Lightning parameters comparison

CIGRE Brochure number 63 named „*Guide to procedures for estimating the lightning performance of transmission lines*“ reports lightning parameters for lightning performance studies. In this brochure lightning flashes are grouped in four categories: downward negative lightning discharges, upward positive lightning discharges, downward positive lightning discharges and upward negative lightning discharges. This brochure does not provide classification of lightning flashes that include bipolar lightning flashes. This report concentrates mainly on parameters for downward negative flashes and positive flashes. Each lightning stroke is considered as an ideal current source of infinite source impedance and the parameters contained within the incident impulse current wave shape determine the transmission network response. These wave shape parameters include the peak current amplitude (crest value), time to crest, steepness and duration. Also of importance are the polarity, time interval and number of incident strokes within each lightning stroke.

Previously mentioned classification of lightning flashes is extended in CIGRE Brochure 549 named „*Lightning performances for engineering applications*“, to additionally include bipolar lightning flashes that transport both negative and positive charges to ground. But parameters of bipolar lightning flashes are not considered. Furthermore, this brochure reports the largest number of strokes per flash observed in New Mexico (Kitagawa et al, 1962) is 26.

During researching for this thesis it has been concluded that bipolar and multicomponent lightning flashes are very destructive. Also it is shown that, when compared to unipolar negative lightning flashes, bipolar and multicomponent lightning flashes rarely occur, but they do occur often, especially in very high regions and from tall objects. Therefore, multicomponent lightning flashes that consist of more than 30 components are recorded and analysed. To include bipolar lightning flashes in a dimensioning process of equipment, the following parameters should be consider:

- two current peaks (for positive and negative part),
- two front and two tail times (for positive and negative part) and
- duration of positive and negative part of bipolar stroke.

Chapter 5.

MODELLING PROCEDURES

5.1. Introduction

A system model is similar but much simpler than a system it represents. One purpose of a model is to enable the analyst to predict the effects of changes made to the system. On the one hand, a model should be a close approximation to the real system and incorporate most of its salient features. And on the other hand, it should not be so complex that it is impossible to understand it and to experiment with it. A good model is a judicious trade – off between realism and simplicity.

When calculating line surge arrester energy duty, numerical tools are very important for the calculation of the transient stresses, well known software EMTP – RV (ElectroMagnetic Transient Program – Restructured Version) is used for calculation purposes of this thesis.

The quality of the results is mainly based on a proper modelling of all transmission line components and lightning current source. To have a proper modelling of the configuration to be studied, following information is required: tower type, tower geometry, span length, grounding resistance and grounding configuration, shield wire(s), air gaps and arresters. Figure 5.1.1 illustrates information required for modelling the system.

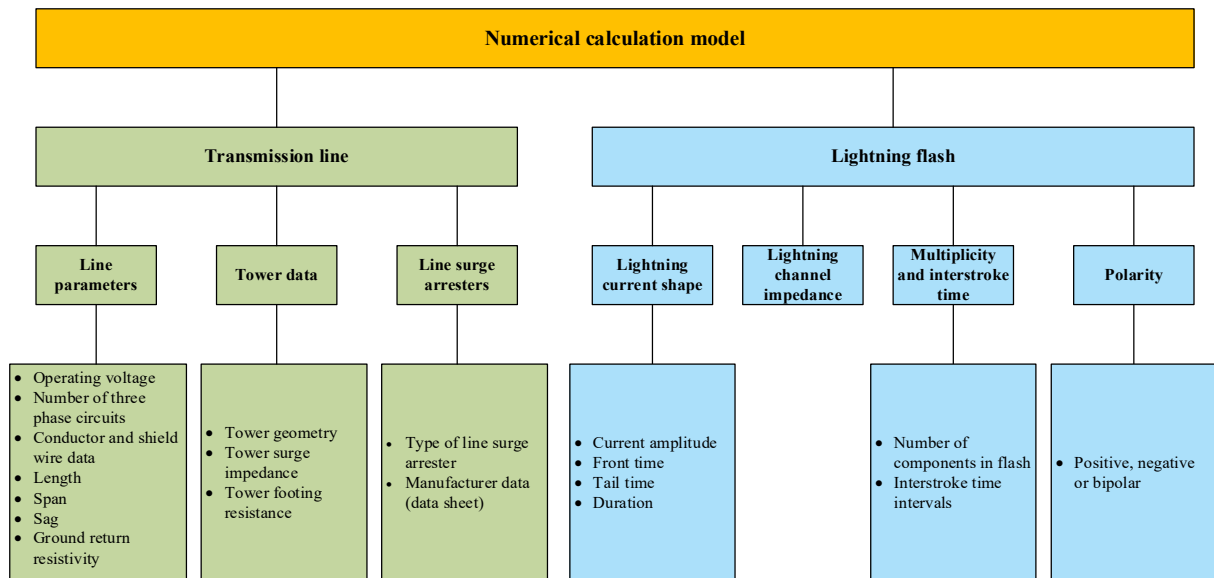


Figure 5.1.1. Information required for system modelling

Line surge arrester energy duty calculation/consideration due to bipolar and multicomponent lightning flashes is classified as transient analyses. Modelling of transmission lines for transient studies will be described in this chapter. Firstly, basic mathematical models and circuit representation for transmission line components will be described. Then, developed EMTP – RV models of transmission line components, used for purposes of this thesis, will be described. After that modelling of a complete transmission line will be described. Importance of modelling a complete transmission line will be explained.

5.2. Fundamental Mathematical Models

This section presents fundamental mathematical models for all components needed for appropriate line surge arrester energy duty calculations. Fundamental mathematical models for transmission line components such as: phase conductors and shield wires (if shielded line design is modelled), transmission line towers, tower footing resistance and line surge arresters are given. Substation model as well as lightning flash model are described.

5.2.1. Phase Conductors and Shield Wire Model

A simulation of transient phenomena may require representation of network components valid for a frequency range that varies from DC to several MHz. Although an accurate and wideband representation of transmission line is not impossible, it is more advisable to use and develop models appropriate for a specific range of frequencies. Each range of frequencies will correspond to a particular transient phenomenon. Two types of time domain models have been developed for overhead lines: lumped and distributed parameter model. The most accurate models for transient calculations are those that take into account the distributed nature of the line parameters. Two categories of parameters can be distinguished for these models: constant and frequency dependent parameters.

To model shield wires and phase conductors, the Constant Parameter (CP) line is used, which is classified as a frequency independent transmission line model. Its main advantage is computational speed. It is less precise than frequency dependent line and cable models, but it can be successfully used in analysis of problems with limited frequency dispersion. The CP line parameters are calculated at a given frequency and that is why it is labelled as a frequency independent line. The CP line is a distributed parameter model. Figure 5.2.1 shows equivalent circuit of a differential section of a single phase overhead line [74, 75].

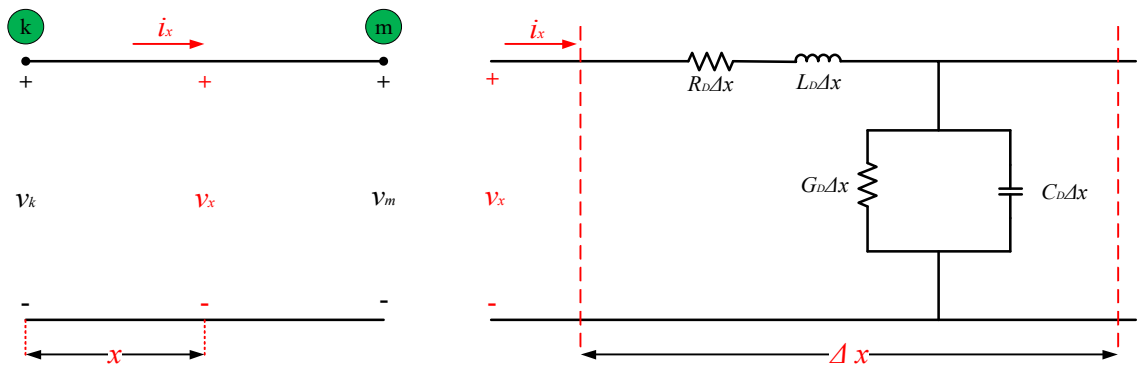


Figure 5.2.1. Distributed parameter line model [2].

The basic time domain equations of the single phase distributed parameter line, shown in figure 5.2.1, are [75]:

$$\frac{dv(x,t)}{dx} = -R_D i(x,t) - L_D \frac{di(x,t)}{dt} \quad (5.1)$$

$$\frac{di(x,t)}{dx} = -G_D v(x,t) - C_D \frac{dv(x,t)}{dt} \quad (5.2)$$

where

$v(x,t)$ and $i(x,t)$ are respectively the voltage and the current, R_D , L_D , C_D are the line parameters expressed in per unit length.

Time domain equations of a multiphase line can be expressed as follows below [75].

$$\frac{d \mathbf{v}(x,t)}{dx} = -\mathbf{R}_D \mathbf{i}(x,t) - \mathbf{L}_D \frac{d \mathbf{i}(x,t)}{dt} \quad (5.3)$$

$$\frac{d \mathbf{i}(x,t)}{dx} = -\mathbf{G}_D \mathbf{v}(x,t) - \mathbf{C}_D \frac{d \mathbf{v}(x,t)}{dt} \quad (5.4)$$

where

$\mathbf{v}(x,t)$ and $\mathbf{i}(x,t)$ are respectively the voltage and the current vectors, \mathbf{R}_D , \mathbf{L}_D , \mathbf{C}_D are the line parameter matrices expressed in per unit length.

5.2.2. Transmission Line Tower Model

Although the lightning response of a transmission line tower is an electromagnetic phenomenon, the representation of a tower is usually made in circuit terms, that is, the tower is represented by means of several line sections and circuit elements that are assembled taking into account the tower structure. There are some reasons to use this approach: such representation can be implemented in general purpose simulation tools (e.g., EMTP – RV), and it is easy to understand by practical engineers. Transmission line tower model, used in simulation is presented in figure 5.2.2.

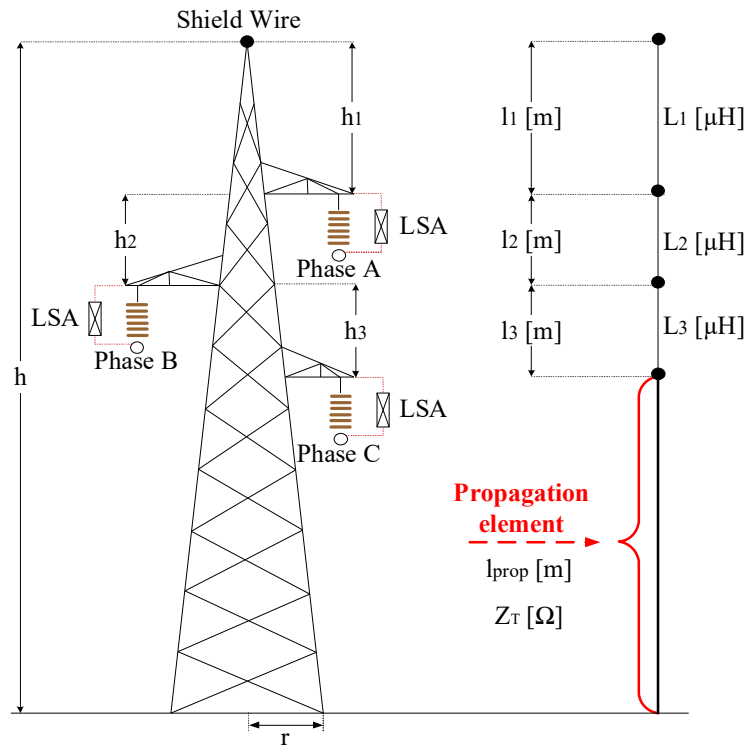


Figure 5.2.2. Tower representation

Each tower is divided in four parts. First part is section of the tower from bottom crossarm to the ground and it is represented as the propagation element, which is defined by the surge impedance and the propagation length. Second part is section between tower top and top crossarm. Third and fourth parts are sections between crossarms. Sections on the tower top (between tower top and top crossarm and between crossarms) are modelled as inductance branches. On this way it was possible to calculate transient on tower top [76, 86, 87]. Tower surge impedance is calculated according tower shape theory. The most common tower shapes are shown in figure 5.2.3.

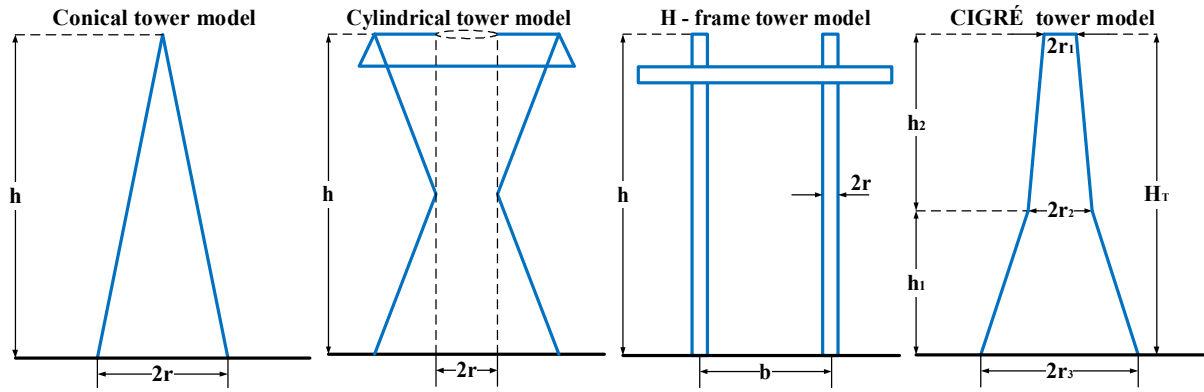


Figure 5.2.3. Tower shapes [77]

The surge impedance for the most common tower shapes can be calculated according to the expressions given in table 5.2.1.

Table 5.2.1. Tower surge impedance formulas [64, 78]

Tower shape	Tower surge impedance formula	Description
Conical	$Z_T = 30 \ln \frac{2(h^2 + r^2)}{r^2}$	h is tower height (m) r is tower base radius (m)
Cylindrical	$Z_T = 60 \left[\ln \left(\sqrt{2} \frac{2h}{r} \right) - 1 \right]$	h is tower height (m) r is tower base radius (m)
H - frame	$Z_T = \frac{Z_s + Z_m}{2}$ $Z_s = 60 \ln \frac{h}{r} + 90 \frac{r}{h} - 60$ $Z_m = 60 \ln \frac{h}{b} + 90 \frac{b}{h} - 60$	h is tower height (m) r is cylinder radius (m) b is distance (m) Z_s is self impedance (Ω) Z_m is mutual impedance (Ω)
CIGRÉ	$Z_T = 60 \ln \cot \left[\frac{1}{2} \tan^{-1} \left(\frac{r_{avg}}{H_T} \right) \right]$ $r_{avg} = \frac{r_1 h_2 + r_2 (h_1 + h_2) + r_3 h_1}{h_1 + h_2}$ $H_T = h_1 + h_2$	h_1 is the height from base to waist (m) h_2 is the height from waist to top (m) r_1 is the tower top radius (m) r_2 is the tower radius at waist (m) r_3 is the tower base radius (m) r_{avg} is weighted average of the tower radius (m)

Branch inductance L_n is determined according to the section length l_n , tower surge impedance Z_T and propagation velocity v [76].

$$L_n = \frac{Z_T}{v} l_n (H), \quad n = \overline{1, 3}.$$

IEC document named “Computational guide to insulation co – ordination and modelling of electrical networks” and IEEE document named “Modelling guidelines for fast front transients” recommend that the velocity of propagation can be assumed to be equal to the speed of light ($v = 300 \text{ m}/\mu\text{s}$). Thus, for purposes of this work wave propagation speed on the tower was taken to be equal to the velocity of light. Tower surge impedance is calculated according conical tower shape.

5.2.3. Tower Footing Resistance Model

Tower footing resistance can be represented with fixed resistance value model or with nonlinear soil ionization model.

The resistance of a ground electrode may decrease due to ionization of the soil. When a current is injected to the electrode, an ionization process will occur in regions around the electrode if a critical field gradient is exceeded. In those regions, low ohmic discharge channels are formed, being the resistance of the ionized zone reduced to a negligible value. The ground resistance of an electrode remains at the value determined by the electrode geometry and the soil resistivity until ionization breakdown is reached; after breakdown, the resistance varies. This soil breakdown can be viewed as an increase of the geometry of the electrode. Large increase in conductor diameter mathematically increases the per – unit length conductance of the conductor, so that the ground conductor can effectively dissipate more lightning current into the soil, and therefore reduces the potential rise at the injection point and the grounding impedance.

The value of the soil ionization gradient may be set equal to that suggested by Mousa, $E_g=300$ kV/m, or that recommended by CIGRE, $E_g=400$ kV/m, or that recommended by IEEE standard, $E_g=350$ kV/m [64, 79].

The grounding model may be represented by means of nonlinear resistance whose value is approximated as follows [64, 79, 81]

$$R_i = \begin{cases} R_0, & I < I_g \\ \frac{R_0}{\sqrt{1 + \frac{I}{I_g}}}, & I \geq I_g \end{cases} \quad (5.5)$$

where:

- R_i (Ω) – tower footing impulse resistance;
- R_0 (Ω) – footing resistance at low current and low frequency;
- I (kA) – stroke current through the resistance;
- I_g (Ω) – limiting current to initiate sufficient soil ionization.

The limiting current is given by:

$$I_g = \frac{E_g \rho}{2\pi R_0^2} \quad (5.6)$$

where:

- ρ (Ωm) – soil resistivity;
- E_g (kV/m) – soil ionisation critical electric field.

5.2.4. Line Surge Arrester Model

Literature describes few different line surge arrester models. But, the basic arrester model equation is given by [78]:

$$i_a = kv_a^\alpha . \quad (5.7)$$

Where i_a is the arrester current and v_a is the arrester voltage. The parameter k depends upon the dimensions of the valve block, while α , which describes the nonlinear characteristic, depends upon the valve – block material. For SiC arresters the value of α is between 2 to 6. For MO arresters $10 \leq \alpha \leq 60$. The SiC α is almost constant, in contrast the MO varies within the operating region, it reaches a maximum of around 60 in the TOV region and decreases to about 10 in the lightning region. It means that a single exponential can be used for most SiC, but several exponential segments are needed for MO. The k parameter is the constant used in fitting the arrester characteristic.

5.2.5. Line Surge Arrester Energy Duty Calculation

The lightning energy E (in Joules) absorbed by an arrester can be determined according to relation [81, 82]:

$$E = \int_{t_0}^t u(t)i(t)dt , \quad (5.8)$$

where

$u(t)$ is the residual voltage of arrester in kV and $i(t)$ is the value of discharge current through arrester in kA.

When the absorbed energy by the arrester exceeds their maximum acceptable level of energy, than they will fail (damage).

Integral from relation (5.8) can be solved using trapezoidal rule. This method approximates the integration over an interval by breaking the area down into trapezoids with more easily computable areas. For an integration with $N+1$ evenly spaced points, the approximation is [83, 84]:

$$\int_a^b f(x)dx \approx \frac{b-a}{2N} \sum_{n=1}^N (f(x_n) + f(x_{n+1})) = \frac{b-a}{2N} [f(x_1) + 2f(x_2) + \dots + 2f(x_N) + f(x_{N+1})] , \quad (5.9)$$

where the spacing between each point is equal to the scalar value $(b-a)/N$.

If the spacing between the points is not constant, then the formula generalizes to

$$\int_a^b f(x)dx \approx \frac{1}{2} \sum_{n=1}^N (f(x_n) + f(x_{n+1}))(x_{n+1} - x_n) , \quad (5.10)$$

where $(x_{n+1}-x_n)$ is the spacing between each consecutive pair of points [83, 84].

In next section comparison between EMTP – RV line surge arrester energy calculation and calculation using numerical trapezoidal integration held in MATLAB will be shown.

5.2.6. Lightning Current Model

The lightning current produced by a lightning stroke to an overhead transmission line could be model using a variable current source in parallel to resistance. To describe lightning current shape, usually manufacturers use ramp or double exponential function which are easier to implement in test equipment. In 1991, based on statistical analysis of recorded lightning strokes around world CIGRE proposed a more complex formulation of lightning current. Recently, in literature the Heidler lightning current function is used for the study transients on transmission lines.

The main idea of this work is to calculate and analyse line surge arrester energy duty due to impulses that are very similar to natural lightning strokes. Therefore, in this work for bipolar lightning flashes measured current shape is used, while multicomponent flashes were modelled using lightning location system data and CIGRE recommendations (more data can be found in Chapter 4 and Chapter 6 of this work).

Equation (5.11) describes CIGRE lightning current shape model [64]:

$$I_{CIGRE}(t) = \begin{cases} A_1 t + A_2 t^n, & t \leq t_n \\ B_1 \exp(-\frac{t-t_n}{t_1}) - B_2 \exp(-\frac{t-t_n}{t_2}), & t > t_n \end{cases} \quad (5.11)$$

The basic assumption is that the current shape reaches the instant of maximum steepness (90% amplitude) at a time t_n dependent on the exponent n . In equation (5.11), t_1 and t_2 are time constants, while A_1 , A_2 , B_1 and B_2 are constants which describe front and tail part of lightning current shape. More information about CIGRE lightning current shape can be found in [64].

Lightning channel impedance is an important parameter that can influence the current injected into the strike object. As it is mentioned in previous sections, arrester energy duty depends on lightning current parameters. Because of these facts lightning channel impedance should be included in procedures that consider arrester energy duty. The equivalent impedance of the lightning channel is needed for specifying the source in circuit models used in direct strike studies. Many scientists and engineers attempt to estimate the equivalent impedance of the lightning channel. Some of attempts are mentioned below.

It is possible to estimate the equivalent impedance of the lightning channel from measurements of lightning current waveforms at a very tall object, if the characteristic impedance of the object and the grounding impedance are known or can be reasonably assumed. Such measurements were performed at the 540 m high Ostankino tower in Moscow by Gorin and Shkilev. The estimates based on these measurements varied from 600 Ω to 2.5 k Ω , when the characteristic impedance of the tower was assumed to be 300 Ω and the grounding resistance was assumed to be zero. Also, it has been observed, for rocket-triggered lightning, that the average return stroke peak current is not much influenced by the impedance “seen” at the strike point, ranging from as low as 0.1 Ω (Rakov et al., 1998) to 200 Ω or so (Schoene et al., 2009), which implies that the equivalent lightning channel impedance is of the order of kilohms, consistent with the findings of Gorin and Shkilev. Further, Wagner and Hileman (1961), from theoretical considerations, suggested that, what they referred to as the surge impedance of the stroke should vary from 900 Ω to 2 k Ω , with larger values corresponding to lower current strokes. Finally, Rakov (1998), from lossy transmission line modelling, estimated the characteristic impedance of the channel created by the dart leader, which is “seen” by frequency components between 100 kHz and 1 MHz of the return stroke wave, to be about 0.5 – 1 k Ω . Thus, it appears that the equivalent impedance of the lightning channel should be appreciably higher than the surge impedance, of an overhead wire, which is about 400 Ω . CIGRE Brochure 549 named “*Lightning Parameters for Engineering Applications*” provide concluding remarks as follows:

- The estimates of this impedance from limited experimental data suggest values ranging from several hundred ohms to a few kilo ohms. In many practical situations the impedance “seen” by lightning at the strike point is some tens of ohms or less, which allows one to assume

infinitely large equivalent impedance of the lightning channel. In other words, lightning in these situations can be viewed as an ideal current source.

- Representation of lightning by a current source with internal impedance of 400 Ω , similar to that of an overhead wire, is probably not justified.

The main problem is in fact that it is unknown which value should be taken for lightning channel impedance for proper interpretation of lightning stroke. Lightning channel impedance cannot be exactly determined. It varies from stroke to the stroke. Predictions of lightning channel impedance is very difficult even for negative lightning strokes that are much more studied than bipolar and positive lightning strokes. Some authors use ideal current source, some of them use Norton equivalent circuit with impedance value of 400 Ω , etc.

In the model lightning stroke hitting a tower or a phase conductor can be replaced by a surge current generator and a resistor (Norton equivalent circuit) as it is shown in figure 5.2.4.

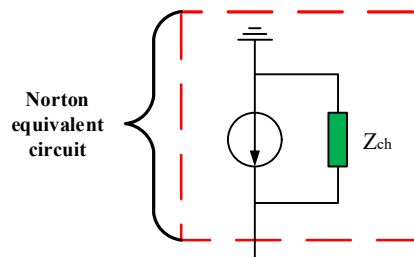


Figure 5.2.4. Lightning stroke representation with Norton equivalent circuit

5.2.7. Substation Model

The overall substation models are derived from the substation layout drawings. The views from all three ordinal directions are very beneficial to locate the exact position of substation equipment. When performing lightning transient study it is very important to correctly model substation elements. Overvoltage shapes and peak values at different substations points depend on the selected models for different substation elements and on the selected data. Best is to take substation element data from the equipment manufacturer data sheets or from the measurements (if available). References [85], [86] and [87] suggest substation element models for transient studies. Modelling of crucial substation elements in transient studies is described below.

The phase conductors inside substations and connections between the substation equipment are explicitly represented by line sections. These line sections are modelled by constant parameter lines. Impedance of phase conductor in substation may be computed by the following formula [93]:

$$Z = 60 \ln \frac{2h_c}{r_c} \quad (5.12)$$

where:

- h_c – conductor average height (m);
- r_c – conductor radius (m).

The substation equipment, such as circuit breakers, substation transformers, and instrument transformers, are represented below.

Power transformer is usually represented as surge capacitance to ground. Power transformer representation is given in figure 5.2.5.

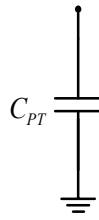


Figure 5.2.5. Power transformer representation [87]

Power transformer surge capacitance to ground of the highest voltage winding can be calculated using the power law equation [93]:

$$C_{PT} = A(S_{PT})^B \quad (5.13)$$

where:

- C_{PT} - power transformer surge impedance to ground (nF)
- S_{PT} - power transformer rating per phase (MVA)
- A, B - constants given in table 5.2.2.
- BIL - winding Basic Impulse Level (kV)

Table 5.2.2. Constants used for the computation of the power transformers surge capacitance

<i>BIL</i> (kV)	<i>A</i>	<i>B</i>
110	1.5	0.62
150	1.5	0.58
200	1.4	0.58
250	1.2	0.56
350	1.1	0.52
450	1.0	0.46
550	0.8	0.51
650	0.6	0.52

Power transformer surge capacitance to ground as a function of BIL only is given in table 5.2.3.

Table 5.2.3. Power transformer surge capacitance to ground (nF)

<i>BIL</i> (kV)	<i>C_{PT}</i> (nF)
550	2.4 to 3.4
825	2.2 to 3.0
1050	2.0 to 2.7
1300	1.7 to 2.3
1550	1.5 to 2.0
1800	1.4 to 1.8

Circuit breakers representations, dead tank and live tank, are shown in figure 5.2.6.

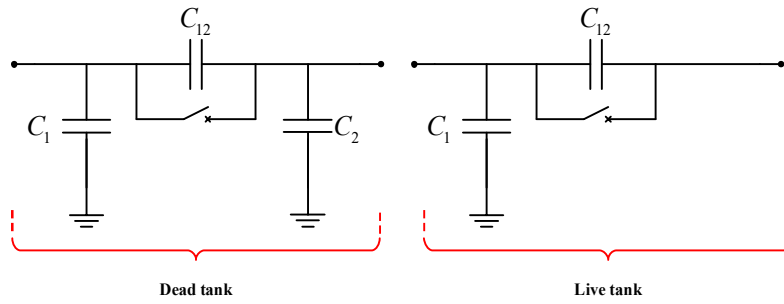


Figure 5.2.6. Circuit breaker representation [87]

For dead tank it is:

$C_{12}=0.006$ to 0.01 nF - for some breaker designs C_{12} may be between 0.650 to 1 nF per break.

$$C_1=C_2=C_B/2$$

C_B - Breaker total surge capacitance to ground (table 5.2.4)

Table 5.2.4. Dead tank breaker total surge capacitance to ground

U_s (kV)	C_B (nF)
115	0.10
400	0.15
765	0.60

U_s is nominal system voltage (kV)

For live tank it is:

$$C_{12} = 0.006 \text{ to } 0.01 \text{ nF}$$

$$C_1 = 0.005 \text{ nF}$$

$$C_2 = 0 \text{ nF}$$

Measuring transformers are represented as surge capacitance to ground (figure 5.2.7). Measuring transformer surge capacitance to ground depends on the transformer design and system voltage. Measuring transformer surge capacitance to ground is given in table 5.2.5.

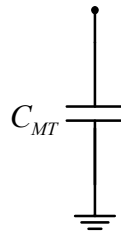


Figure 5.2.7. Measuring transformer representation [87]

Table 5.2.5. Measuring transformer surge capacitance to ground C_{MT} (nF)

U_s (kV)	Capacitive Potential (nF)	Magnetic Potential (nF)	Current (nF)
115	8	0.50	0.25
400	5	0.55	0.68
765	4	0.60	0.80

Other substation equipment such as disconnector switches and bus support insulators are modelled as surge capacitance to ground. Typical values are given in table 5.2.6.

Table 5.2.6. Disconnector switches and bus support insulators surge capacitance to ground C_E (nF)

U_s (kV)	Disconnector switch (nF)	Bus support insulator (nF)
115	0.10	0.08
400	0.20	0.12
765	0.16	0.15

5.3. EMTP – RV Models

Simulations for a transient analysis of the transmission lines are commonly based on a model that consists of only few towers on the both sides from the point of the lightning impact. In this work the complete transmission line is created and solved in the EMTP – RV for the purpose of the transient analyses. The transmission line is modelled from several parts: towers, insulators, phase conductors, shield wire, line surge arresters and tower footing resistance. The substations are modelled on the both ends of the transmission line as it is illustrated in figure 5.3.1. EMTP – RV model of each transmission line element is described below.

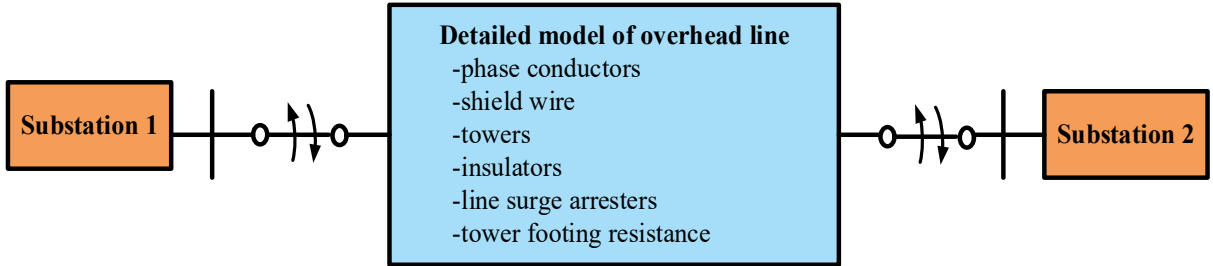


Figure 5.3.1. Transmission line model.

5.3.1. Model for Phase Conductors and Shield Wire in EMTP – RV

Available versions for constant parameter line model in EMTP – RV are:

- CP 1 – phase (only for a 1-phase line);
- CP 3 – phase (only for a 3-phase line);
- CP double (double-circuit transmission line);
- CP m – phase.

Although CP m – phase can be used in all cases, the above versions are provided for convenience and simplicity of usage.

For modelling shielded transmission line, CP line multiphase model shown in figure 5.3.2 was used, while for modelling unshielded line, CP line three phase model from figure 5.3.3 was used.

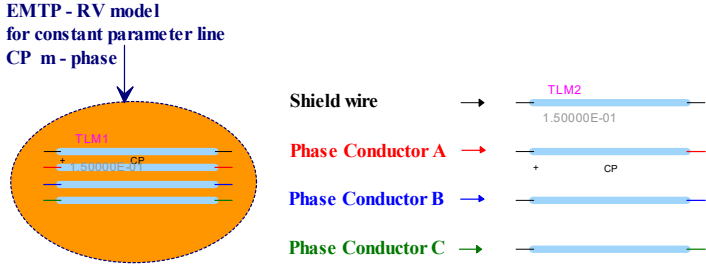


Figure 5.3.2. EMTP – RV CP line multiphase

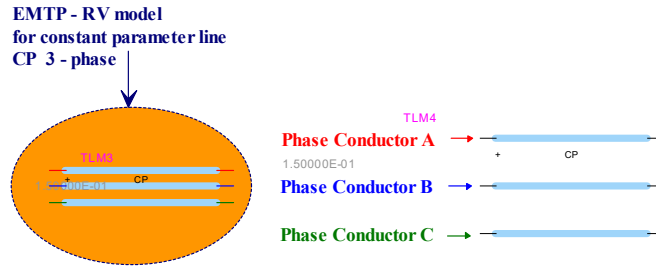


Figure 5.3.3. EMTP – RV CP line three phase

To develop line models for transient simulations, the following data must be available:

- Physical dimensions of each conductor and shield wire;
- DC resistance of each conductor and shield wire;
- (x,y) coordinates for each conductor and shield wire;
- Vertical height at midspan of the conductor above the ground at the middle of the span;
- Ground return resistivity;
- Line length.

All above mentioned data are input for EMTP – RV element “Line Data”, that is shown in figure 5.3.4. For purposes of this work input data for “Line Data” element are as in [90]. For shielded line conductor data are given in table 5.3.1. For unshielded line conductor data are same as in table 5.3.1 only without shielded wire.

Table 5.3.1. Shielded line conductor data [90]

	DC resistance [Ω /km]	Outside diameter [cm]	x [m]	y[m]	y at midspan [m]
Shield Wire	0.4555	0.900	0	28.9	21.3
Phase A	0.1444	1.708	2.5	22.7	14.1
Phase B	0.1444	1.708	-3	20.5	11.9
Phase C	0.1444	1.708	3.5	18.3	9.7

Data needed to develop line models for transient simulations are loaded into line data device. The line data device is used to generate the model data needed for the EMTP – RV CP line multiphase or three phase. CP line multiphase model is used to simulate shielded line, while CP line three phase is used to simulate unshielded line. Modelling procedure of phase conductors and shield wire is shown in figures 5.3.4 and 5.3.5 for shielded and unshielded line, respectively.

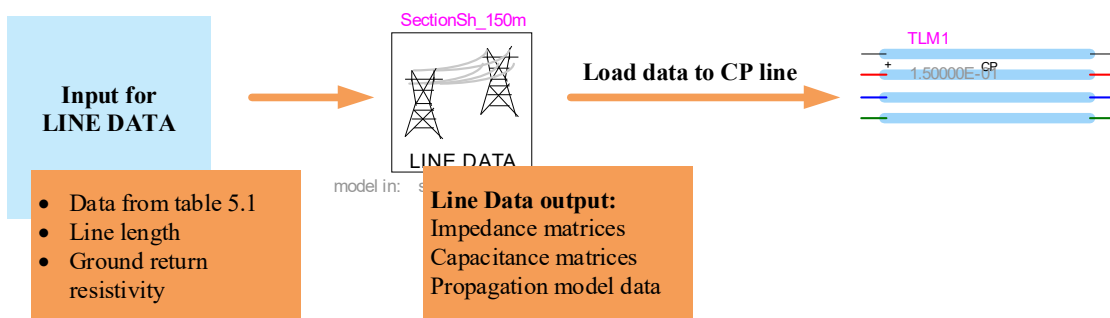


Figure 5.3.4. Input data for EMTP – RV CP line multiphase – Shielded line model

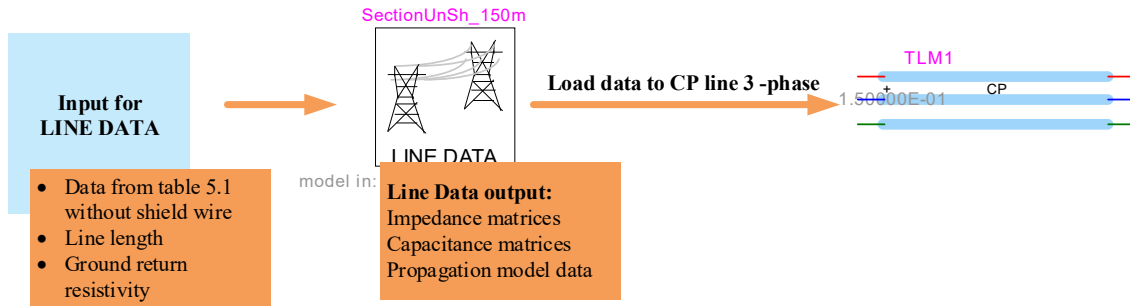


Figure 5.3.5. Input data for EMTP – RV CP line 3 – phase – Unshielded line model

5.3.2. Transmission Line Tower Model in EMTP – RV

As it is previously mentioned each tower is divided in four parts. First part is section of the tower from bottom crossarm to the ground and it is represented as the propagation element, which is defined by the surge impedance and the propagation length. In EMTP – RV software this part is modelled as constant parameter (CP) line model (1 – phase version). Second part are sections between tower top and top crossarm. Third and fourth parts are sections between crossarms. In EMTP – RV sections on the tower top (between tower top and top crossarm and between crossarms) are modelled as inductance branches. Tower surge impedance is calculated according tower shape theory.

Tower surge impedance calculator developed in C# was used to prepare data for tower modelling in EMTP – RV. Application is shown in figure 5.3.6.

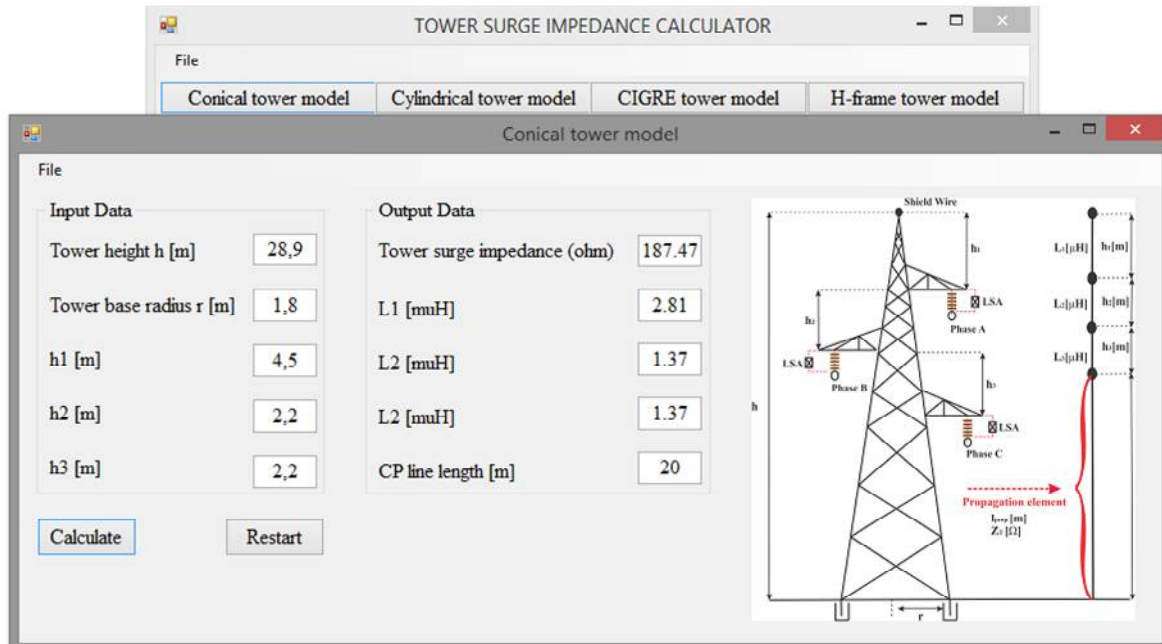


Figure 5.3.6. Tower surge impedance calculator – C#

Input data are: tower height, tower base radius, length of section from tower top to the top crossarm, and length of sections between crossarms. All lengths are given in meters. Output data, that are needed for EMTP – RV modelling, are: tower surge impedance (Ω), branch inductance (μH), and length of propagation element (m).

Figure 5.3.7 shows described tower model in EMTP – RV with all elements and connections with other elements. This way it is possible to connect line surge arresters in parallel, connect tower footing resistance, and inject lightning current to the tower top.

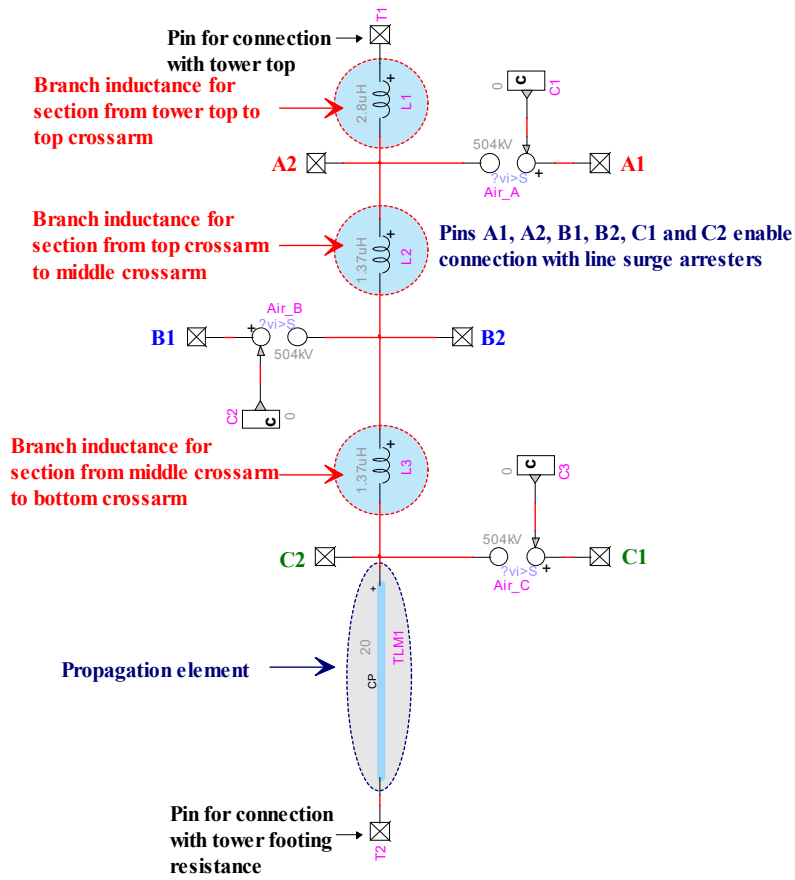


Figure 5.3.7. Tower model in EMTP – RV

All elements shown in figure 5.3.7 are grouped in subcircuit. This subcircuit is illustrated in figure 5.3.8 and can be use many times for modelling complete transmission line.

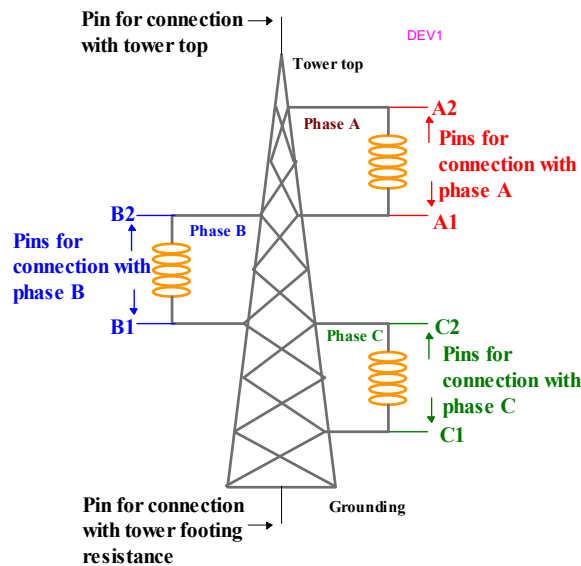


Figure 5.3.8. EMTP – RV symbol for tower subcircuit

5.3.3. Tower Footing Resistance Model in EMTP – RV

In EMTP – RV it is easy to model tower footing resistance as fixed resistance value by using simple resistance element. But, for modelling nonlinear soil ionization, more complex solution is needed. In this case the tower grounding is represented as EMTP – RV non – linear resistor device that is used to model a nonlinear resistance using controlled resistance and admittance. Control device function, input selector and constants are EMTP – RV blocks that are used for resistance control. EMTP – RV symbol and model for tower footing resistance are shown in figure 5.3.9.

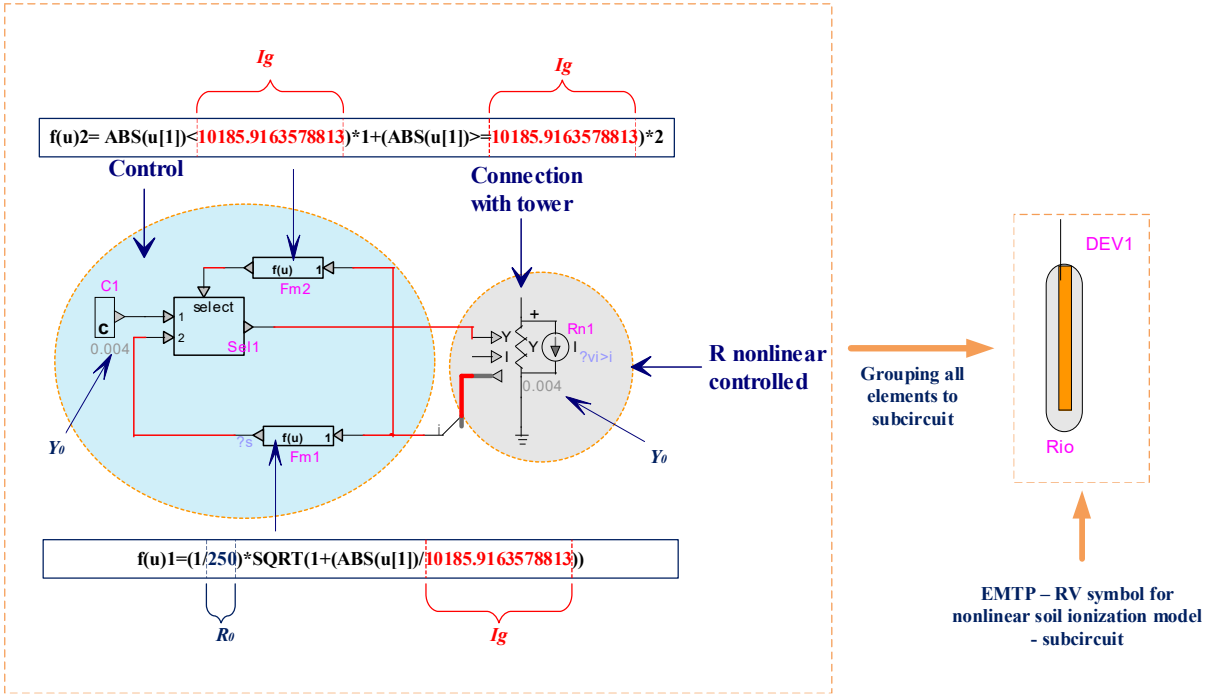


Figure 5.3.9. EMTP – RV tower footing resistance representation for nonlinear soil ionization model

As it is recommended in CIGRE brochure number 63: in transient studies tower footing resistance with fixed value can be used. Therefore, for simulation purposes of this work tower footing resistance fixed value is used.

5.3.4. Line Surge Arrester Model in EMTP – RV

In EMTP – RV there are two types of arresters: Metal Oxide (MO or ZnO) and Silicon Carbide SiC. A comparison between MO and SiC arrester data indicates that MO has a much flatter characteristic than SiC. It is contrary for SiC, since its steady-state current would fail the arrester, and thus gaps are required in series with the material. This explains why SiC devices are less popular. Figure 5.3.10 shows the three basic MO arrester types. For purposes of this work gapless ZnO surge arrester was used. Explanation for this choice is given in Chapter 3.

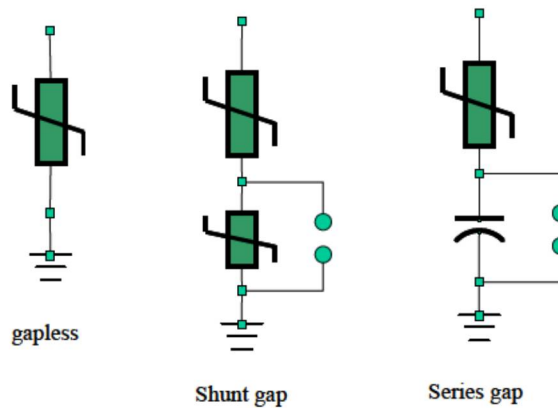


Figure 5.3.10. Three basic metal oxide arrester types

The fitting function allowing to convert manufacturer data to the ZnO model data is available through the “ZnO data function” device. Modelling procedure of an arrester in EMTP – RV is illustrated in figure 5.3.11.

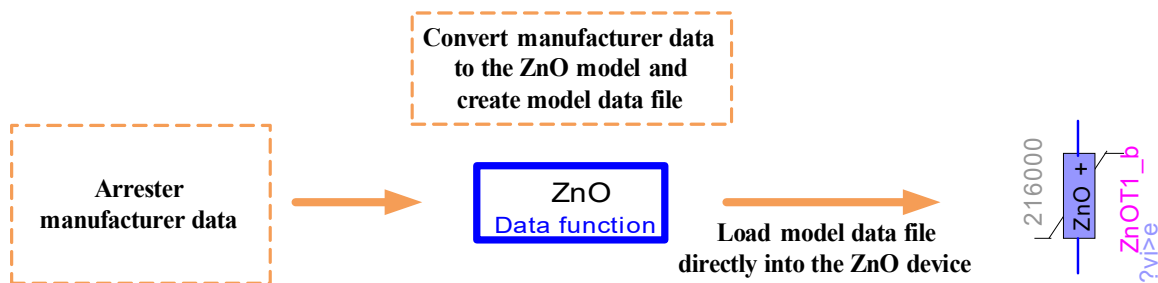


Figure 5.3.11. Modelling procedure of arrester in EMTP – RV

Arrester device accepts both 1 – phase and 3 – phase signals. The 3 – phase version is the equivalent of 3 decoupled branches (one for each phase). The ZnO arrester data function device is used to generate the model data needed for the EMTP – RV arrester model (ZnO device). The model data is generated from the actual current-voltage characteristic of the arrester available from manufacturer tests.

In the time-domain solution this device is a nonlinear function. It is solved through the iterative process of EMTP – RV until convergence according to the relative tolerance option given in the convergence data tab.

Used arrester has the following characteristics [90]:

Rated voltage:	108 (kV _{rms})
MCOV:	86 (kV)
IEC class:	II
Nominal discharge current:	10 (kA)

The non – linear behaviour of line surge arrester is represented by the $U – I$ characteristic (8/20 μ s) shown in figure 5.3.12.

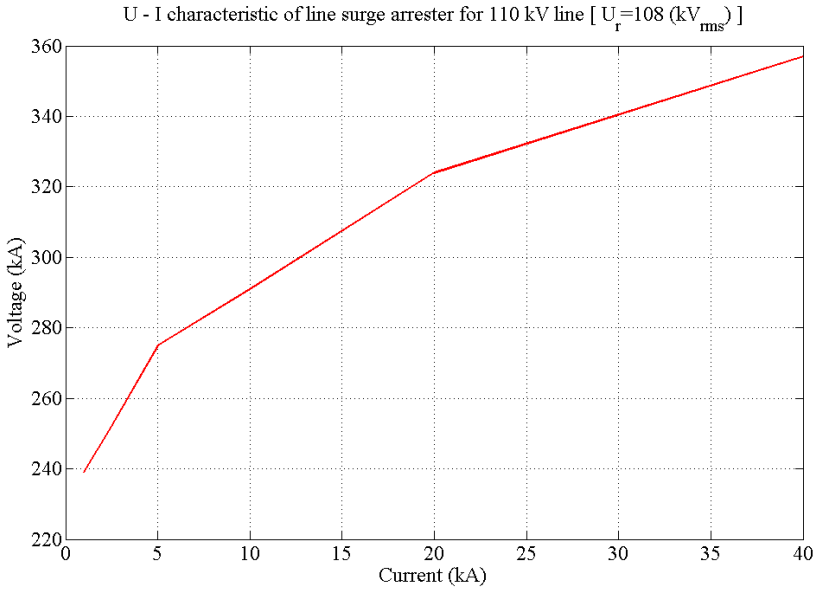


Figure 5.3.12. Arrester $U – I$ characteristic (8/20 μ s)

CIGRE brochure 39, from 1990, provides very useful guidelines to represent metal – oxide surge arresters, which are summated in table 5.3.2. Fifth column in the table 5.3.2 is the most important for transient studies due to lightning discharges.

Table 5.3.2. Guidelines to represent metal oxide surge arresters

Model Characteristics	Low Frequency Transients	Slow front Transients	Fast front transients	Very fast front transients
Temperature dependent $U – I$ characteristic	Important	Negligible	Negligible	Negligible
Frequency dependent $U – I$ characteristic	Negligible	Negligible	Important	Very important
MVO block inductance	Negligible	Negligible	Important	Very important
Ground lead inductance	Negligible	Negligible	Important	Very important

5.3.5. Analogy between Calculation of Line Surge Arrester Energy Duty in MATLAB and EMTP – RV

Comparison between line surge arrester energy duty calculation in EMTP – RV and MATLAB is presented in this section. Line surge arrester current is presented in figure 5.3.13 (green curve).

Arrester voltage determined in MATLAB is calculated using cubic spline interpolation method. Input data for cubic spline interpolation method are arrester $U – I$ characteristic (that is given by manufacturers) and arrester current.

Let U_i be interpolated voltage vector. Then, U_i containing elements corresponding to the elements I_{ar} (I_{ar} is arrester current). Interpolated voltage vector is determined by interpolation within vectors u_k and

i_k (u_k and i_k are voltage and current vectors determined from line surge arrester $U - I$ characteristic). The vector u_k specifies the points at which data i_k is given.

Interpolated arrester voltage is represented by red curve in figure 5.3.13, while arrester voltage calculated using EMTP – RV is represented by blue curve. Interpolated arrester voltage is voltage calculated using cubic spline interpolation method and arrester $U - I$ characteristic and arrester current.

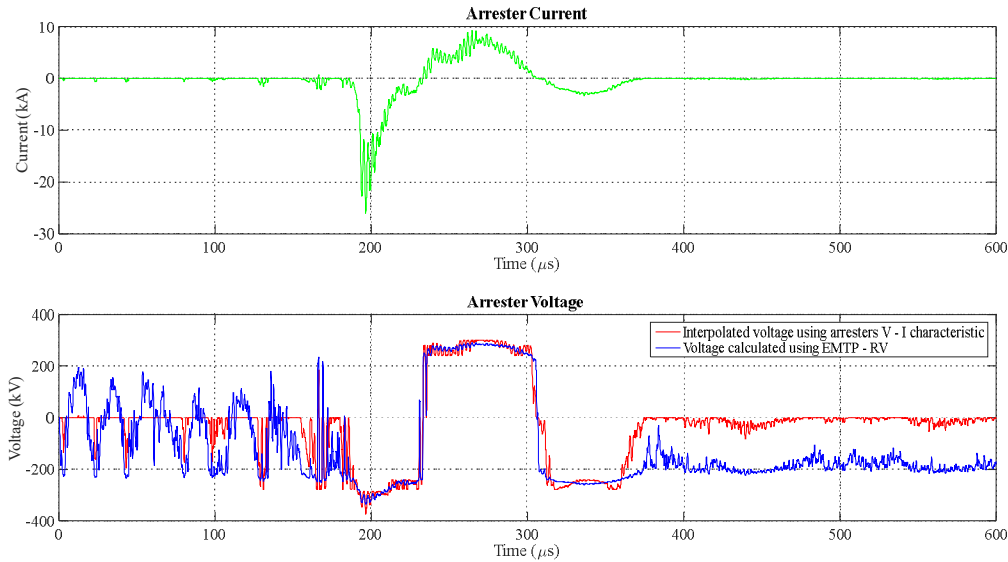


Figure 5.3.13. Arrester current and voltage (interpolated in MATLAB and calculated in EMTP – RV)

For energy duty calculation in MATLAB relation (5.8) is used. Integral from relation (5.8) is solved using trapezoidal rule that is described in section 5.2.5.

Comparison between line surge arrester energy duty calculation in EMTP – RV and MATLAB is shown in figure 5.3.14.

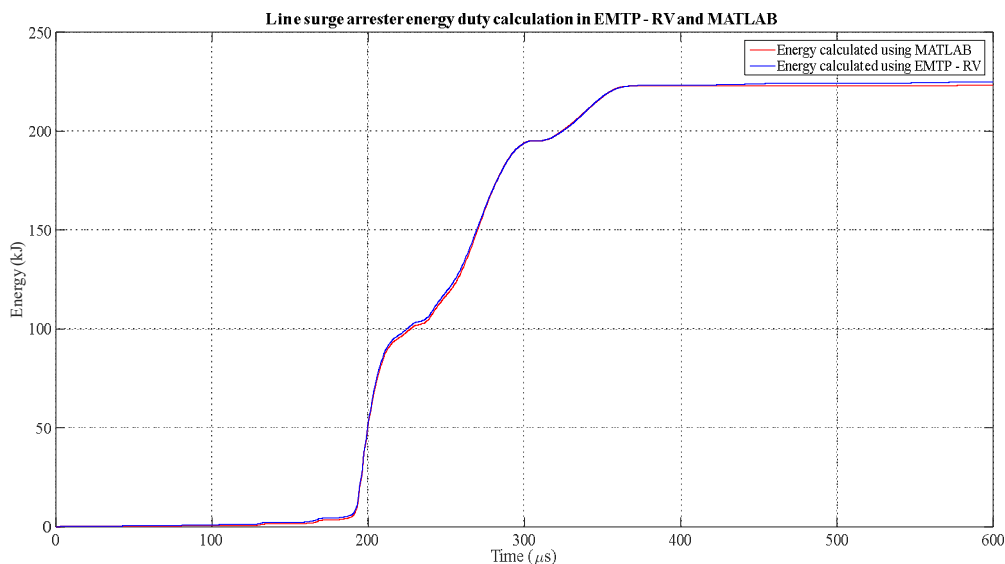


Figure 5.3.14. Analogy between calculation of line surge arrester energy duty in MATLAB and EMTP – RV

From figure 5.3.14 it is possible to conclude that difference in energy calculated in EMTP – RV and MATLAB is very small and hardly noticeable. Line surge arrester energy calculated in few interesting time points in EMTP – RV and MATLAB is presented in table 5.3.3.

Table 5.3.3. Line surge arrester energy calculated in EMTP – RV and MATLAB

Time point (μs)	EMTP – RV Energy (kJ)	MATLAB Energy (kJ)
$t_1 = 230$	103.39	101.93
$t_2 = 300$	194.94	195.09
$t_3 = 600$	224.87	223.09

For each time point from 0 μs to 600 μs (with simulation/calculation step $\Delta t=10 \text{ ns}$) comparison in energy calculation between EMTP –RV and MATLAB has been held. Maximum energy difference is 2.2148 kJ or 0.9849% (percentage is calculated with respect to energy calculated in EMTP –RV).

5.3.6. Lightning Current Model in EMTP – RV

The lightning flash is modelled as a current source (so called 'I – point by point source') because it is possible to import measured data point by point. The current shapes and values can be changed in order to study different lightning flashes. The lightning current (bipolar) used in the simulation was measured in Corsica and it is analysed in Chapter 4 and shown in figure 4.2.1. For multicomponent flashes current shapes are generated in MATLAB and loaded into I – point by point EMTP – RV block.

I – point by point source from EMTP – RV (ideal current source) is show in figure 5.3.15 as well as its modelling procedure.

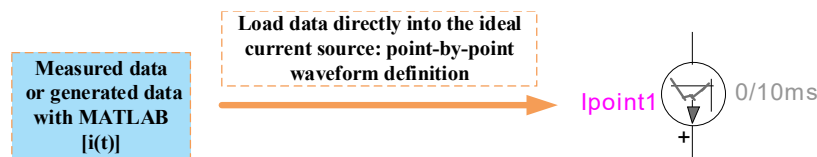


Figure 5.3.15. Modelling procedure of ideal current source in EMTP – RV

EMTP – RV representation of lightning flash, in case when lightning channel impedance is taken into account, is presented in figure 5.3.16. Measured or generated data are loaded into ideal current source which is in parallel with resistance that represents lightning channel impedance. Lightning current shape can be changed as well as lightning channel impedance to model different lightning flashes.

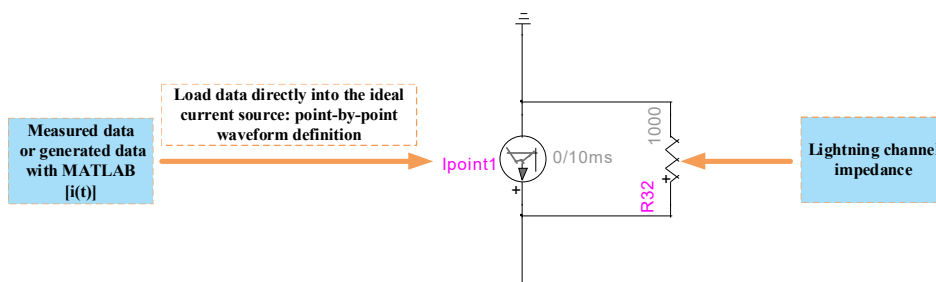


Figure 5.3.16. Lightning stroke representation with Norton equivalent circuit in EMTP – RV

5.3.7. Substation Model in EMTP – RV

Figure 5.3.17 illustrates a substation modelled in EMTP – RV. All elements are modelled according to recommendations from CIGRE brochures, IEEE and IEC modelling guides. Also drawings for substation helps a lot in substation modelling.

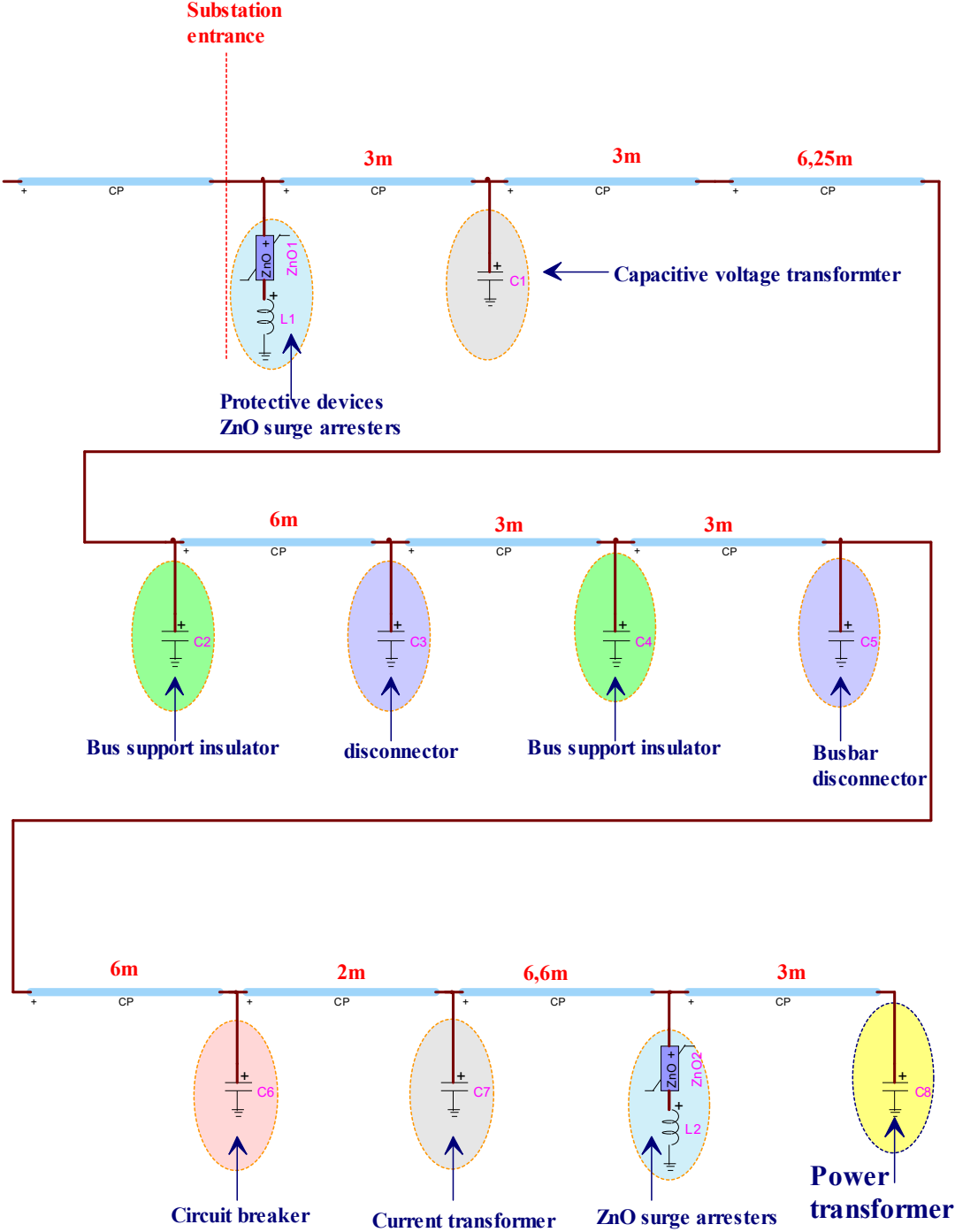


Figure 5.3.17. Substation model in EMTP –RV

Phase conductors in substation are modelled as 3 – phase CP line EMTP – RV element. Impedance of phase conductor in substation is determined according to the conductor average height and conductor radius. Protective devices that can be used for protection of the substation equipment are: protective gaps, silicon carbide surge arresters with series gap and gapless metal – oxide arresters. In this case, gapless metal – oxide (ZnO) arresters were used as protective devices. These arresters were modelled using EMTP – RV elements ZnO arrester data and ZnO device. A lumped inductance of about 1 μ H/m for the ground leads also have to be included in models for high frequencies. Other crucial substation elements such as: power transformer, measuring transformers, circuit breaker, disconnectors and busbar support insulators are represented as surge capacitance to ground. Also another elements could be modelled by means of surge capacitance. If some of the substation equipment are close to each other, such as closer than 3m their capacitances can be grouped together for simplification.

All elements shown in figure 5.3.17 can be grouped in subcircuit. This way new subcircuit element named Substation is created. This subcircuit element is illustrated in figure 5.3.18 and can be use many times for modelling substations (in case that all substations are the same). For modelling different substations it is very easy to make changes in subcircuit element.

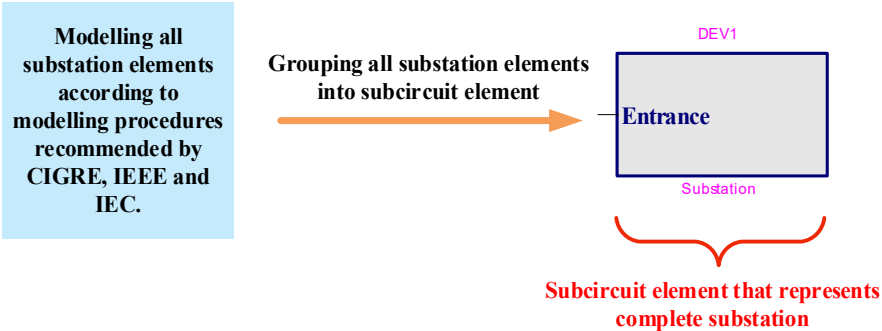


Figure 5.3.18. EMTP – RV symbol for substation subcircuit

Substation model when it is modelled as the voltage source with a Thevenin impedance is shown in figure 5.3.19. Input parameters for this EMTP – RV block can be calculated according theory given in section 5.2.7.



Figure 5.3.19. EMTP – RV block for substation modelled as the voltage sources with a Thevenin impedance

5.4. Modelling of Complete Transmission Line and EMTP – RV’s Grouping Elements into Subcircuits

EMTP – RV software has a very important and useful possibility. It is possible of grouping basic electrical elements into higher structures, so called subcircuits. Subcircuit elements such as transmission line tower, tower footing resistance (nonlinear ionization model) and substation are described in previous sections. Furthermore, subcircuits can be grouped in to more complex subcircuits. Figure 5.4.1 illustrates the main idea of the EMTP – RV modelling in this work. The idea consists of grouping subcircuits inside the other (more complex) subcircuits with the possible connections between all elements in the model.

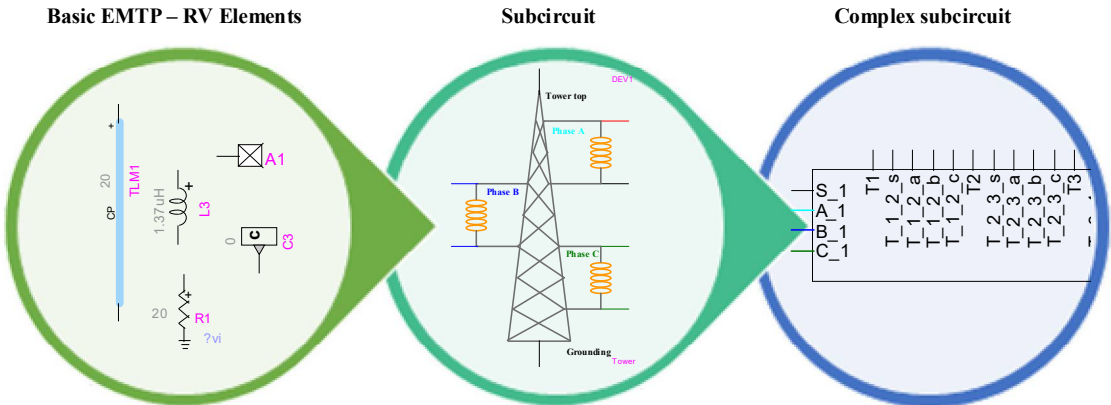


Figure 5.4.1. Main idea of the EMTP – RV modelling

To explain subcircuit term, transmission line tower will be used as example. Basic EMTP – RV elements such as inductances, CP line single phase version, insulators and EMTP – RV pins are grouped into subcircuit (transmission line tower). Pins are EMTP – RV devices that are needed for electrical connections between elements that are closed into subcircuit and other elements in model.

In this model the shield wires and the phase conductors are subdivided into number of segments. Each segment is presented with a constant parameter (CP) line model (multiphase). Each span of 300 m is divided in two segments to enable connection between the current source and the middle of the span for the shield wire and the phase conductors (see figure 5.4.2).

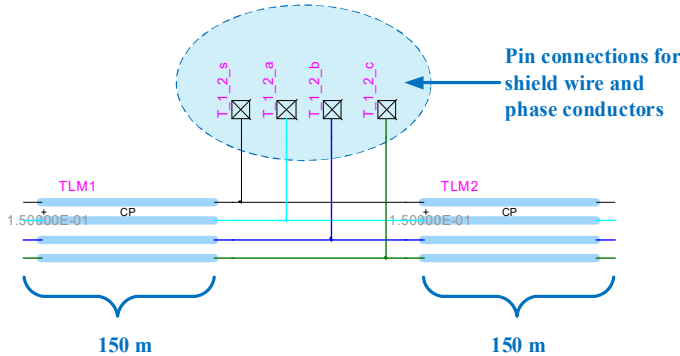


Figure 5.4.2. Span division in two segments

A certain number of the tower subcircuit elements, spans, line surge arresters, grounding footing resistances and the corresponding pins (for connection with other elements) are all grouped into the complex subcircuit element that represents the transmission line section. Elements of a complex subcircuit are illustrated in figure 5.4.3.

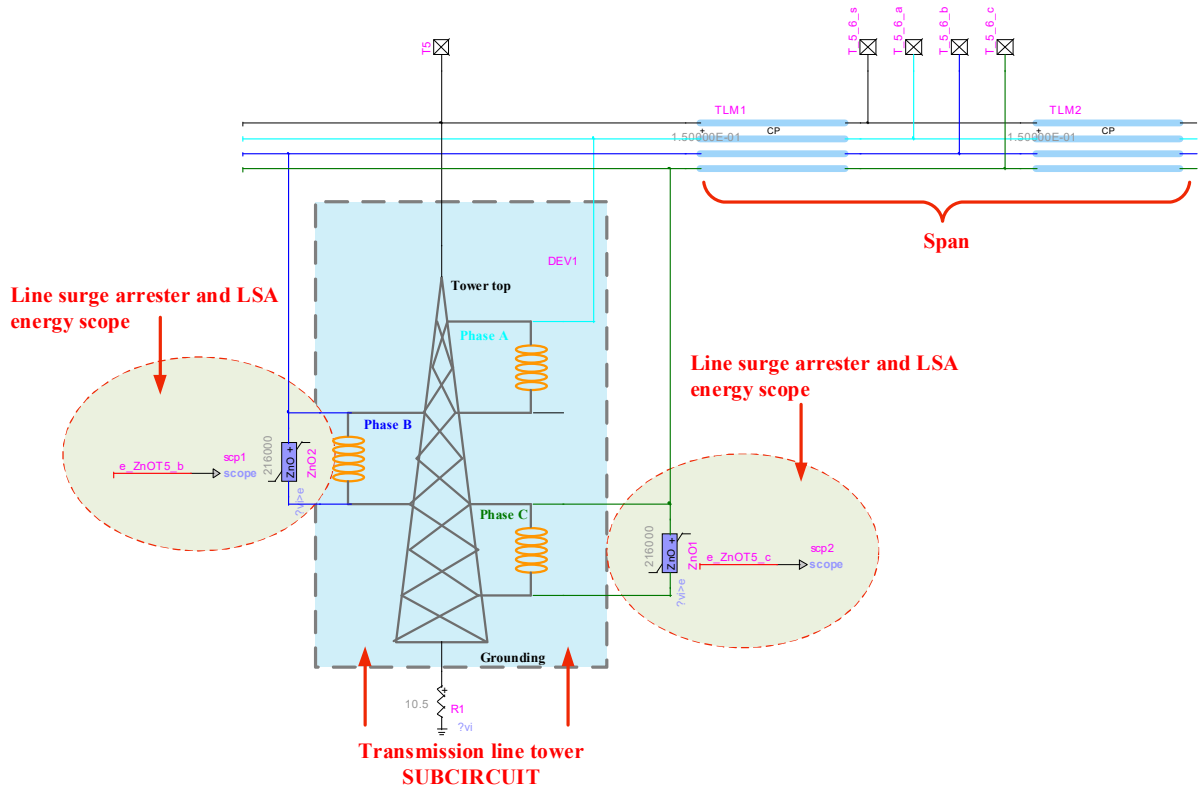


Figure 5.4.3. Elements needed for modelling complex subcircuit (line section)

Example for the transmission line section that consists of 10 towers is given in figure 5.4.4. On the both ends of the section shown in figure 5.4.4 are the pin connections for the shield wire and the phase conductors. This means that it is possible to make connection between two or more section subcircuit elements to get complete transmission line. On the top of the section subcircuit elements shown in figure 5.4.4 are the pins for the lightning current source connection with the tower top and the middle of the span. Lightning stroke can hit the shield wire or the phase conductor at the middle of the span or directly at the tower top.

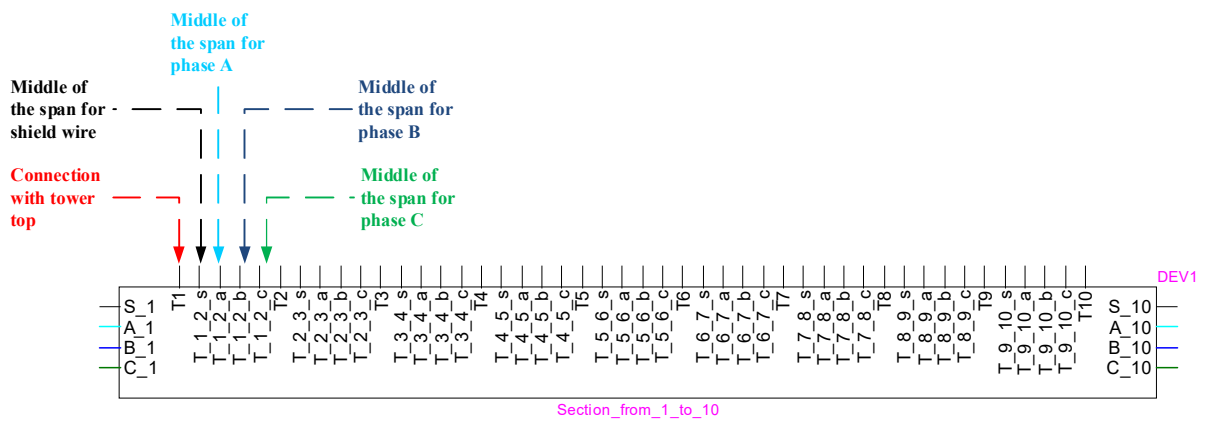


Figure 5.4.4. EMTP – RV section of transmission line

It is possible to model sections with 50 or more towers. In this work some sections consist of 50 towers and some of them of 10 towers. Figure 5.4.5 illustrates complete transmission line model in EMTP – RV. That include: substations, all towers, shield wire, phase conductors, insulators, grounding and line surge arresters.

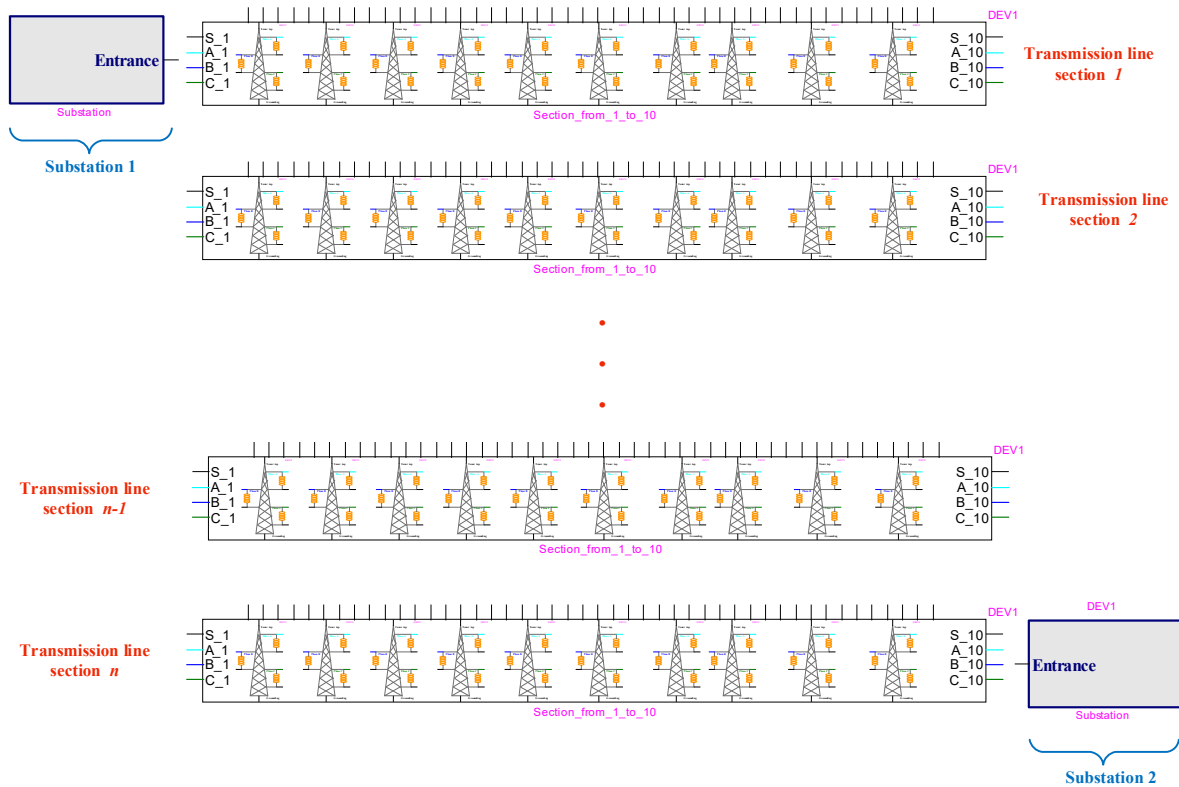


Figure 5.4.5. Illustration of complete transmission line model in EMTP – RV

Complete transmission line is modelled thanks to EMTP – RV possibility of grouping elements. As it is shown in figure 5.4.5 transmission line consists of complex subcircuit elements (substations on both ends of transmission line and n transmission line sections). It is very important to emphasise that connection between all elements in model is possible and all input data can be changed according to user's needs. For example, change of span length can be made "manually" in model or using developed code (in MATLAB or Visual Basic or so) to make change for you in EMTP – RV net file.

This model consists of large number of input and output data. Voltages and currents can be calculated in each circuit node as well as arrester energy duty. Arrester current, voltage and energy duty calculations are the most important calculations for purposes of this thesis.

Review of so many output data (current and voltage shapes, energy duties, etc.) is not difficult thanks to good organization inside complex subcircuit elements. Each subcircuit has its own name and number, so for example output data for transmission line section 1 are grouped according its name. It is the same for each subcircuit.

CPU time is the amount of time for which a central processing unit (CPU) was used for processing instructions of a computer program. Amount of input and output data is large, so it is important to show CPU timers.

For example, for one simulation case: time was 600 (μ s) and time – step was 50 (ns). Simulation statistics are: total number of network nodes 1742, size of the main system equations 2175, total number of solution points in time-domain 15441, total number of iterations 47972 and number of iterations per time-point 3.11. Total simulation time was 27.18750 s. CPU timings are based on a Quad – core i7 processor (logical processors: 8 and 2.2 GHz) with 8 GB of RAM. There are no parallel computation in this simulation. It has been shown that is possible to model complete transmission line and provide plenty of output data. Despite of fact that there is a plenty of input and output data CPU time is not long.

5.5. Summary of Modelling and Calculation Procedure for Transient Studies

Simulations for transient analysis of transmission lines are commonly based on model that consists of only few towers on both sides from point of the lightning impact. Complete transmission line is created and solved in EMTP – RV for purposes of this work.

The quality of the results of lightning transient calculations of transmission lines is mainly based on a proper modelling procedure and proper calculation procedure.

Modelling and calculation procedure in general is as follows:

- 1) Collecting data about transmission line and collecting data about lightning flash;
- 2) Selection of appropriate mathematical models for transmission line components and lightning flash (in case when lightning current shape is unknown);
- 3) Selection of appropriate software package for modelling and simulation and selection of additional software (for example, software for preparing input data for main software);
- 4) Modelling in selected software;
- 5) Calculation;
- 6) Data display and analyses.

Steps for lightning transient calculation procedure are presented on flowchart in figure 5.5.1.

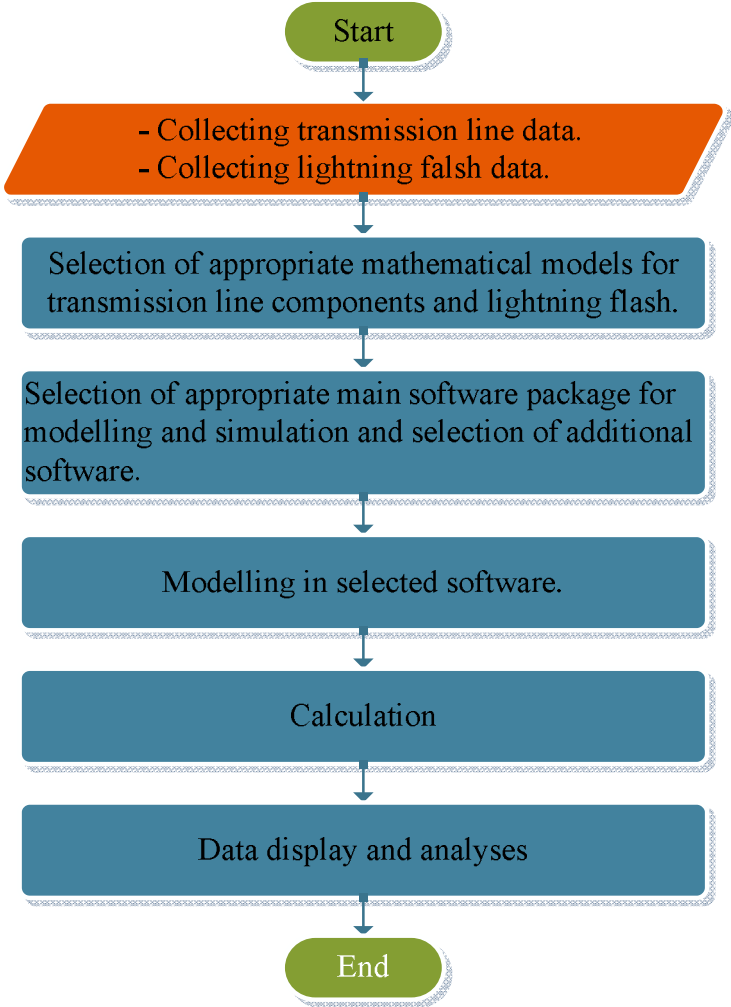


Figure 5.5.1. Flowchart of procedure for transient studies of transmission lines

Step 1 – Data collecting

Transmission line data are:

- Line parameters:
 - o Operating voltage
 - o Number of three phase circuits
 - o Conductor and shield wire data:
 - Physical dimensions for each conductor and shield wire;
 - DC resistance of each conductor and shield wire;
 - (x,y) coordinates for each conductor and shield wire;
 - Vertical height at midspan of the conductor above ground at the middle of the span.
 - o Line length
 - o Span
 - o Ground return resistivity
- Tower data:
 - o Tower geometry
 - o Tower surge impedance
 - o Tower footing resistance
- Line surge arresters
 - o Type of line surge arrester
 - o Manufacturer data (data sheet):
 - Rated voltage;
 - MCOV – maximum continuous operating voltage;
 - IEC Class;
 - Nominal discharge current;
 - U – I characteristic.
- Substation data:
 - o Substation layout drawings (views from all three ordinal directions)
 - o Substation element data from the equipment manufacturer data sheets or from the measurements (if available)

Lightning flash data are:

- Lightning current shape (peak value, front time, tail time and duration)
- Polarity (positive, negative or bipolar)
- Multiplicity – number of components in flash
- Lightning channel impedance

Step 2 – Selection of appropriate mathematical models

As it is mentioned, a simulation of transient phenomena may require representation of network components valid for a frequency range that varies from DC to several MHz. Although an accurate and wideband representation of transmission line is not impossible, it is more advisable to use and develop models appropriate for a specific range of frequencies. Each range of frequencies will correspond to a particular transient phenomenon. Therefore, for more accurate calculations it is important to select appropriate mathematical model for each component (phase conductors and shield wire, transmission line tower, tower footing resistance, etc.). Fundamental mathematical models are given in section 5.2.

Step 3 – Selection of appropriate software package

Transmission line surge arrester energy duty calculation due to bipolar and multicomponent flashes is not easy task. As it is previously presented there are many input parameters as well as output parameters. For static energy duty calculation and consideration longer simulation times are needed, but also for more accurate calculation smaller simulation step is needed. Therefore, powerful software is needed for such calculations. In this work EMTP – RV was used as main software package. EMTP – RV is a full – featured and technically advanced simulation and analyses professional software for power systems transients. The package is a sophisticated computer program for the simulation of electromagnetic, electromechanical and control systems transients in multiphase electric power systems. EMTP – RV is used worldwide as a reference tool by the main actors in power system industry. It is suited for a wide variety of power system studies whether they relate to project, design, and engineering, or to solving problems and unexplained failures. EMTP – RV’s standard library provides a comprehensive and well – documented list of components and function blocks that allow the user to realise easily complete and complex power system studies. EMTP – RV software has a very important and useful possibility. It is possible of grouping basic electrical elements into higher structures, so called subcircuits. On that way complete transmission line can be solved in very short time (around 2 minutes). MATLAB and C# were used for preparation of input data for EMTP –RV, while fro output data analyses MATLAB was used.

Step 4 – Modelling in selected software

It is very important correctly implement mathematical models in software package. Section 5.3 describes EMTP – RV models for each component.

Step 5 – Calculation

Transmission line surge arrester energy duty calculation due to bipolar and multicomponent flashes is complex task. Transmission line with all its components is large and complex system. Therefore, numerical calculations are needed. In this work EMTP – RV’s numerical solution has been held.

Step 6 – Data display and analyses

In order to analyse and compare results it is important to have efficient data display. In this work Scope View was used for data visualisation and export in MATLAB. Scope View provides waveform visualization and mathematical post – processing capabilities. Also, data from Scope View can be export in different formats. Connection with MATLAB is very important because some functions such as cubic spline interpolation, plotting etc. can be easier implemented in MATLAB. Simulation cases, results and data display are given in Chapter 6.

Chapter 6.

SIMULATIONS AND RESULTS

6.1. Introduction

Studies and analyses of electrical power systems and their components can be very expensive or even impossible in some conditions, so simulation is very powerful tool for such studies. Simulation is a tool used to evaluate the performance of a system, existing or proposed, under different configurations of interest and over long periods of a real time. Simulation is used before an existing system is altered or a new system built, to reduce the chances of failure, to meet specifications, to eliminate unforeseen bottlenecks, to prevent under or over-utilization of resources, and to optimize system performance. A simulation experiment is a test or a series of tests in which meaningful changes are made to the input variables of a simulation model so that we may observe and identify the reasons for changes in the performance measures. According to practitioners, simulation modelling and analysis is one of the most frequently used operations research techniques. When used judiciously, simulation modelling and analysis makes it possible to:

- Obtain a better understanding of the system by developing a mathematical model of a system of interest, and observing the system's operation in detail over long periods of time;
- Test hypotheses about the system for feasibility;
- Compress time to observe certain phenomena over long periods or expand time to observe a complex phenomenon in detail;
- Experiment with new or unknown situations about which only weak information is available.

Bipolar lightning does not occur very often. It is still a poorly understood and often unrecognized phenomenon. The bipolar lightning is studied by the meteorological institutions and companies operating lightning location system. To the author's best knowledge the influence of the bipolar lightning on the transmission lines and their components is not studied (except author's papers that are written as part of this thesis). The computer modelling and the simulations represent significant beginning in research of the influence of a bipolar lightning on a transmission lines, especially on line surge arresters and line surge arrester energy duty.

All simulations were performed in EMTP – RV. Needed input data were prepared in MATLAB, such as tower footing resistance randomly determined using Monte Carlo method. Also output data were export from EMTP – RV into MATLAB and were analysed in MATLAB.

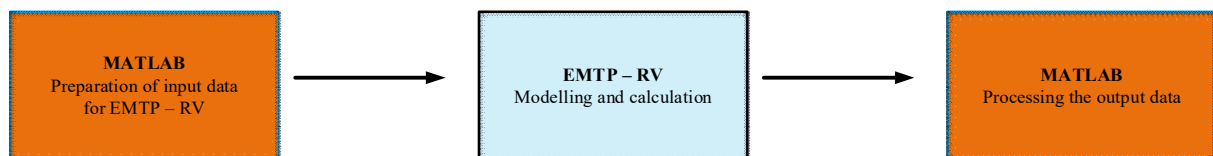


Figure 6.1.1. EMTP – RV and MATLAB in simulation process

This chapter presents line surge arrester energy duty considerations. Shielded and unshielded lines are considered. Also, line surge arrester current shapes are computed and presented for both line designs. Energy duties for the bipolar lightning flashes and for multicomponent lightning flashes are presented. Parametric analysis was carried out to select the appropriate arrester, considering different parameters that affect its energy calculation. Using these studies, it is possible to determine an optimum application of surge arresters, and make a more accurate selection of arrester rating in terms of protective level and energy stress.

6.2. Line Surge Arresters Energy Duty Calculations – Conducted Simulations

This section represents line surge arrester energy duty consideration for unshielded and shielded line design due to bipolar and multicomponent flashes. In this section unshielded and shielded transmission line design is described and impact of lightning flashes on both line designs. Simulation cases are presented in this section. Results are also represented and analysed.

6.2.1. Unshielded and Shielded Transmission Line Designs – Description

The transmission line is modelled from several parts: towers, insulators, phase conductors, shield wire (for shielded line design), line surge arresters and tower footing resistance. Modelling of complete line is described in chapter 5. Studied 110 kV transmission line is 42.9 km long, and consists of 144 towers. A span or a line length between two towers is considered as a mean value of 300 meters. The soil resistivity is 1200 Ωm . The energy capability of the considered line surge arrester is 450 kJ.

Unshielded line design

In a case of the unshielded line bipolar lightning stroke or multicomponent flash is injected to the middle of the span of top phase conductor (see figure 6.2.1.).

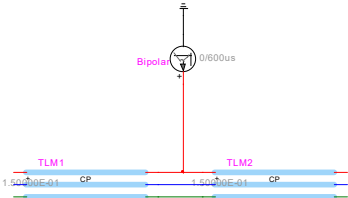


Figure 6.2.1. Lightning flash is injected to the middle of the span of top phase conductor

Shielded line design

Transmission lines are usually shielded. However, shielding failures cannot be totally prevented, but when the lightning stroke hits phase conductor in the case of the shielded line (shielding failure), duration of the LSA current is similar to the duration of the LSA currents in the case of the unshielded lines, but current peaks are lower (shielding failures happen for the low amplitude lightning strokes). Therefore, in this work shielding failure is not considered.

In a case of the shielded line bipolar lightning stroke or multicomponent flash is applied to the tower top (see figure 6.2.2.).

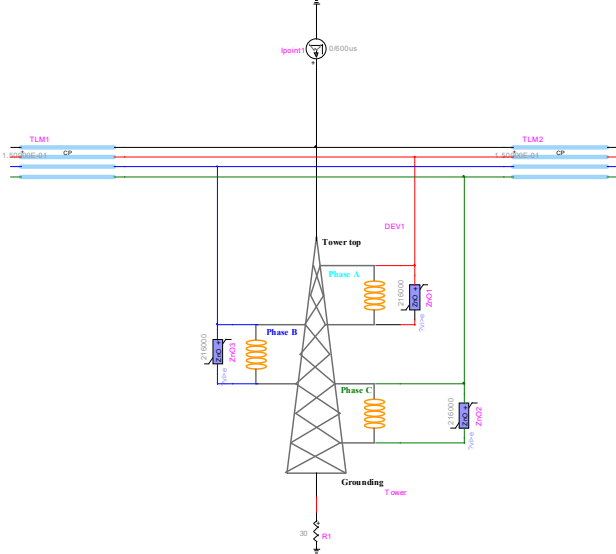


Figure 6.2.2. Lightning flash is applied to the tower top

6.2.2. Effect of Bipolar Lightning Stroke on Arrester Energy Duty – Unshielded Line Design

Effect of the bipolar lightning stroke is emphasized in figure 6.2.3. For better explanation, lightning current, arrester current and arrester energy duty are shown on same figure (see figure 6.2.3.). The energy duty is shown for the duration time of the bipolar lightning stroke.

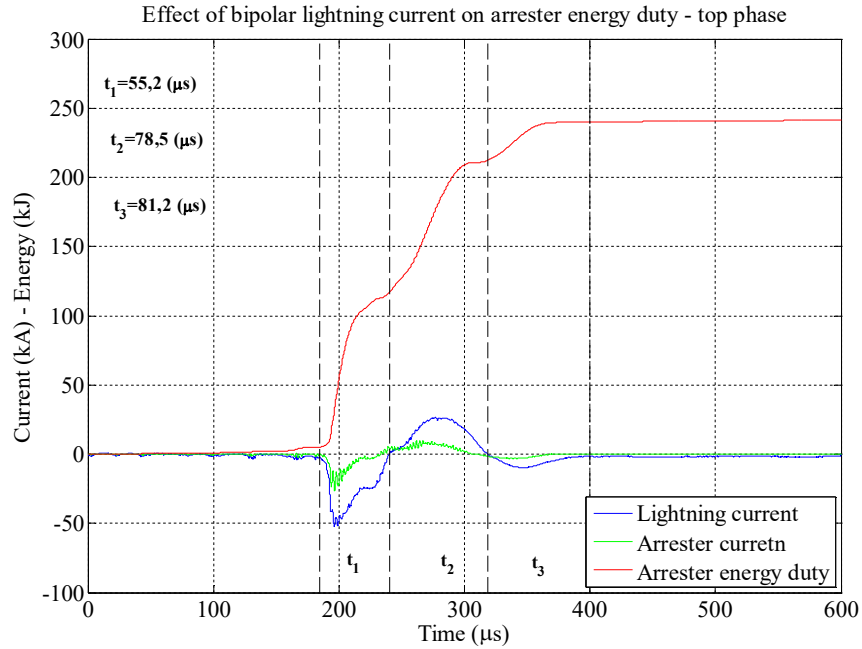


Figure 6.2.3. Illustration of bipolar lightning effect on arrester energy duty – unshielded line design

Table 6.2.1. Maximum values of lightning current, arrester current and arrester energy

Max lightning current (part 1) (kA)	Max lightning current (part 2) (kA)	Max lightning current (part 3) (kA)
-52.86	26.9	-10
Max arrester current (part 1) (kA)	Max arrester current (part 2) (kA)	Max arrester current (part 3) (kA)
-26.77	10	3.5
Max arrester energy (part 1) E_1 (kJ)	Max arrester energy (part 2) E_2 (kJ)	Max arrester energy (part 3) E_3 (kJ)
116.68	212.29	240
Increase of energy (kJ) $\Delta E_{31} = E_3 - E_1$	Increase of energy (kJ) $\Delta E_{21} = E_2 - E_1$	Increase of energy (kJ) $\Delta E_{32} = E_3 - E_2$
123.32	95.61	27.71

Maximum values of lightning current, arrester current, arrester energy and change of arrester energy are given in Table 6.2.1. From the consideration of the energy duty it is possible to conclude that the arrester energy rises up as the bipolar lightning current arrives at the arrester. Surge arrester current peaks are high, not as original lightning stroke, but very high. Durations of arrester currents are very close to the durations of the original stroke. Figures 6.2.4 and 6.2.5 represent arrester currents and energy duties for arresters installed on the middle and bottom phases, respectively.

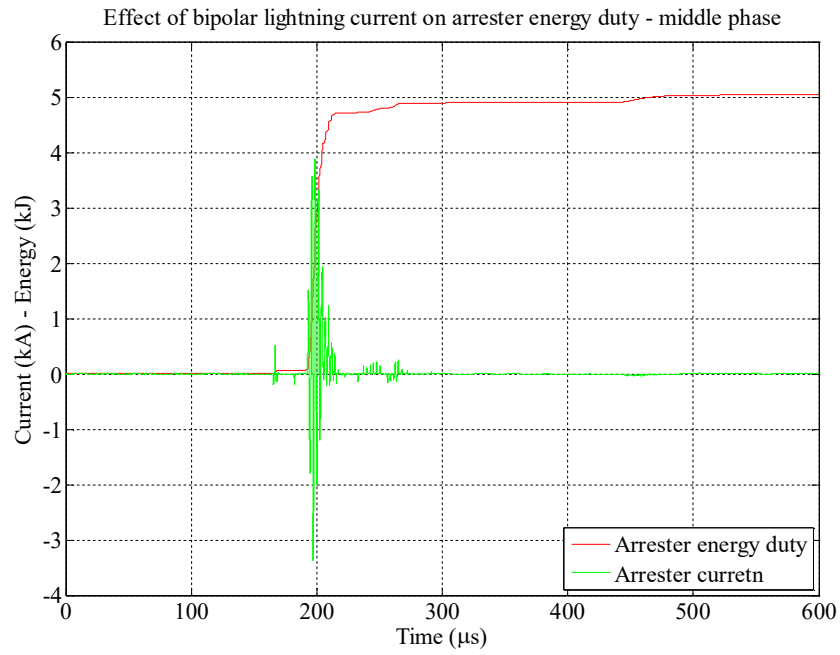


Figure 6.2.4. Arrester current and energy duty calculated for arrester installed on the middle phase conductor – unshielded line design

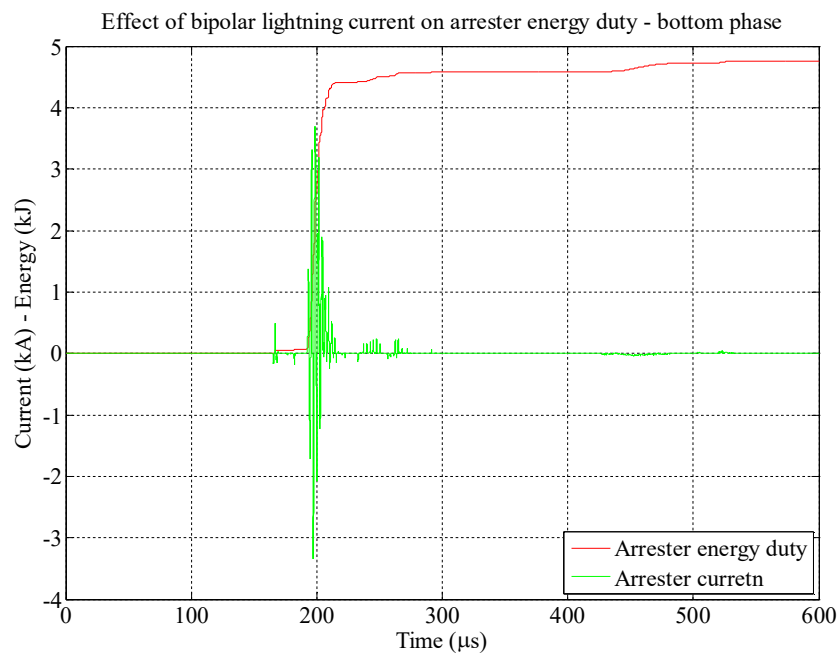


Figure 6.2.5. Arrester current and energy duty calculated for arrester installed on the bottom phase conductor – unshielded line design

6.2.3. Effect of Bipolar Lightning Stroke on Arrester Energy Duty – Shielded Line Design

Effect of the bipolar lightning stroke is emphasize in figure 6.2.6. For better explanation, lightning current, arrester current and arrester energy duty are shown on the same figure (see figure 6.2.7). The energy duty is shown for the duration time of the bipolar lightning stroke.

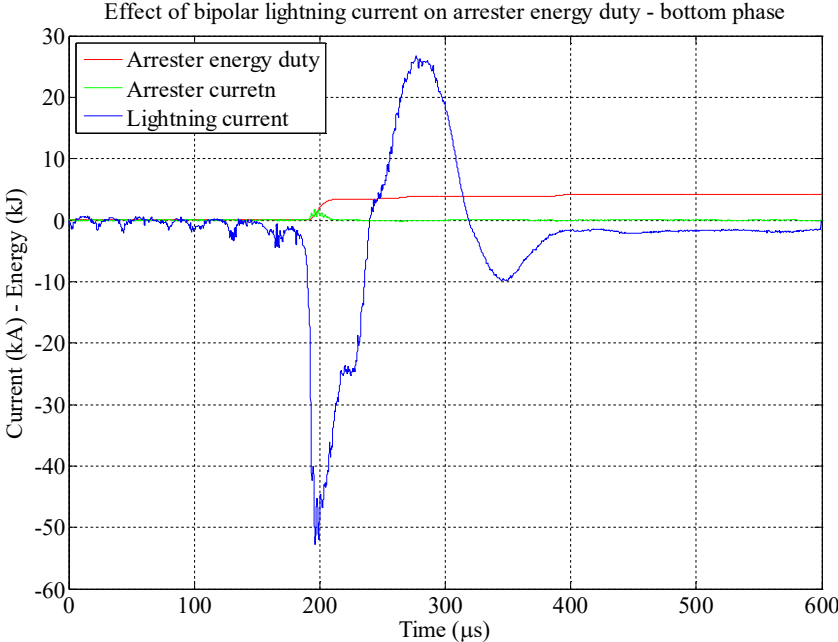


Figure 6.2.6. Illustration of bipolar lightning effect on arrester energy duty – shielded line design

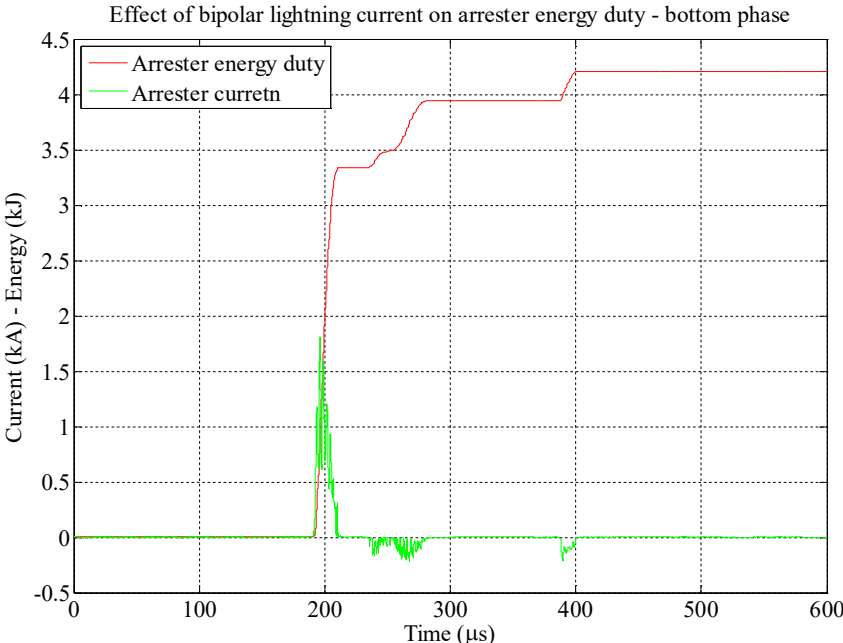


Figure 6.2.7. Arrester current and energy duty from figure 6.2.6 – shielded line design

From the consideration of the energy duty it is possible to conclude that the arrester energy rises up as the bipolar lightning current arrives at the arrester. From arrester current and energy duty we can see

that the arrester current peaks are not so high, compared to the peaks of the original lightning stroke or compared to arrester current for unshielded line design. It is also important to note that the durations of the arrester current are much shorter than the durations of the original lightning strokes.

Figures 6.2.8 and 6.2.9 represent arrester currents and energy duties for arresters installed on the top and middle phases, respectively.

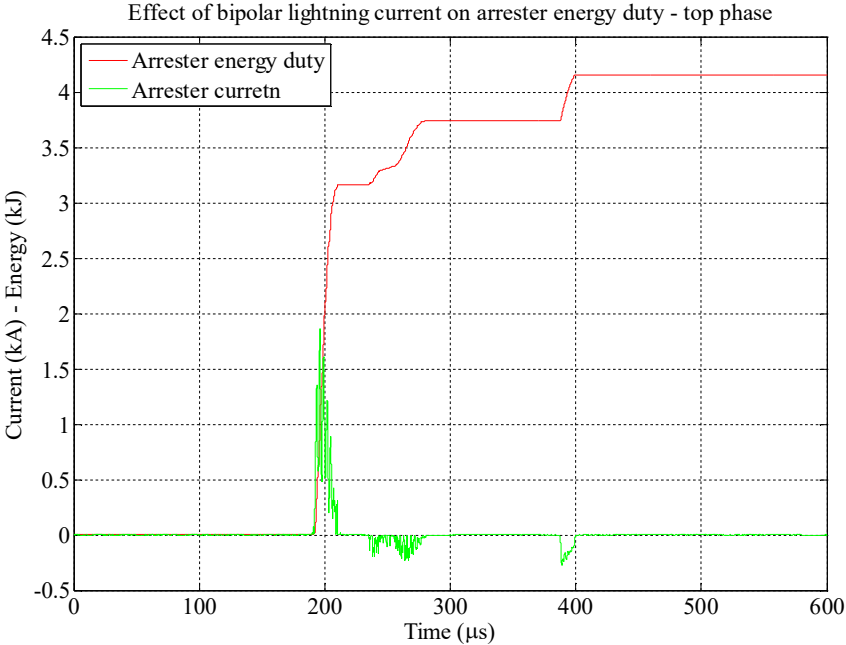


Figure 6.2.8. Arrester current and energy duty calculated for arrester installed on the top phase conductor – shielded line design

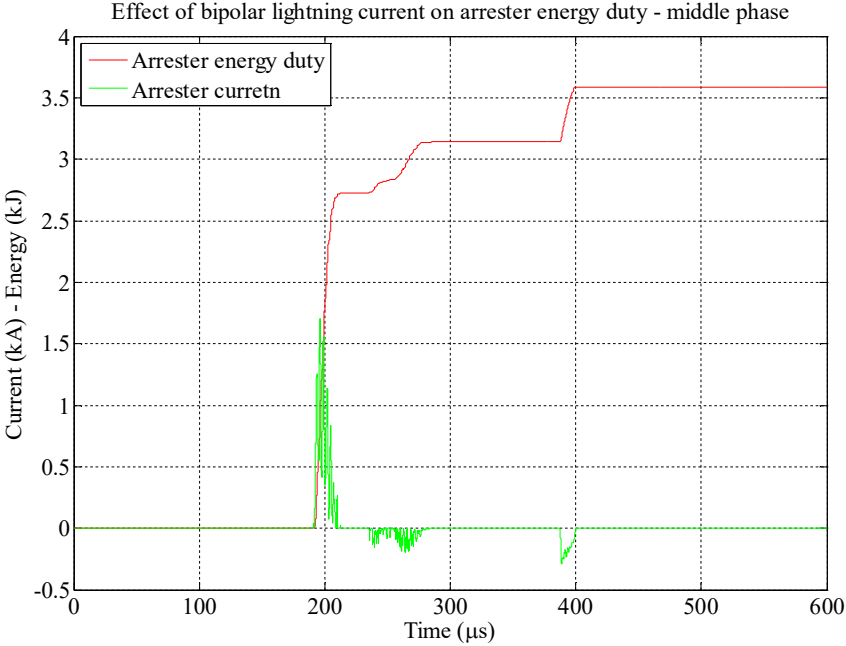


Figure 6.2.9. Arrester current and energy duty calculated for arrester installed on the middle phase conductor – shielded line design

6.2.4. Multicomponent Flashes

Multicomponent lightning flashes simulated in EMTP – RV were based on data for flash 1,2 and 3 from chapter 4. It was implemented in EMTP – RV using ideal current source (I – point by point source). An accurate knowledge of the parameters of lightning strokes is essential for the prediction of the severity of the transients generated in power systems by a direct stroke to the power line. However, no two lightning strokes are the same. LINET data (from Chapter 4) were used to determine:

- lightning stroke current peak,
- lightning stroke polarity,
- number of components in flash and
- interstroke intervals.

Front time and tail time were selected according CIGRE, IEEE and IEC recommendations. According to [64] data for front and tail time are given below.

- Positive first stroke 22/230 μs , with 5% probability of being exceeded;
- Negative first stroke 18/200 μs , with 5% probability of being exceeded;
- Negative first stroke 5.5/77.5 μs , with 50% probability of being exceeded;
- Negative subsequent stroke 4.5/140 μs , with 5% probability of being exceeded;
- Negative subsequent stroke 1.1/32 μs , with 50% probability of being exceeded;

Using LINET data and recommended data it was possible to model recorded flashes from chapter 4. Multicomponent flashes were generated in MATLAB and loaded into mentioned EMTP – RV block.

Line surge arresters energy duties, due to multicomponent flashes, for the shielded and for unshielded lines are considered. Multicomponent flashes applied on transmission line are shown in figures from 6.2.10 to 6.2.12. Front and tail times are varied to show their influence on line surge arrester energy duty.

According [64] and LINET, data for multicomponent flash #1 are:

- first stroke 36.7 kA, 22/230 μs ,
- subsequent stroke #1 -7.3 kA, 4.5/140 μs and
- subsequent stroke #2 -7.2 kA, 4.5/140 μs .

Interstroke intervals for all three flashes are given in Chapter 4.

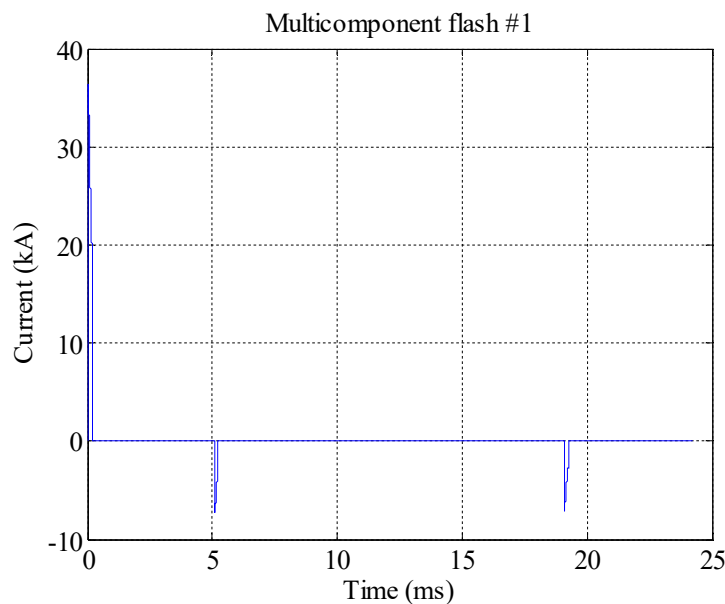


Figure 6.2.10. Multicomponent flash #1 from chapter 4

Data for multicomponent flash #2 are:

- first stroke -29.8 kA, 18/200 μ s,
- subsequent stroke #1 -15.9 kA, 4.5/140 μ s,
- subsequent stroke #2 9.6 kA, 15/200 μ s,
- subsequent stroke #3 -20 kA, 4.5/140 μ s and
- subsequent stroke #4 -15.5 kA, 4.5/140 μ s.

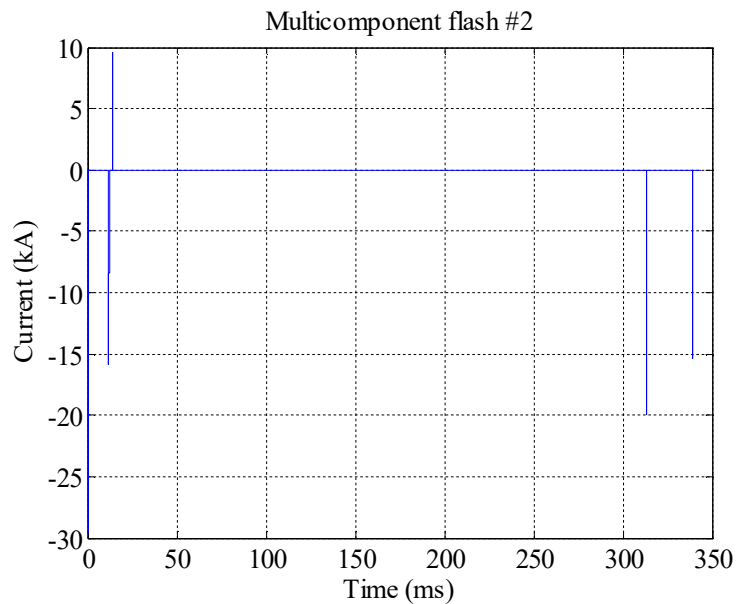


Figure 6.2.11. Multicomponent flash #2 from chapter 4

All components in flash #3 are negative (current peaks and interstroke intervals are given in chapter 4). First stroke data are 18/200 μ s and following strokes data are 4.5/140 μ s.

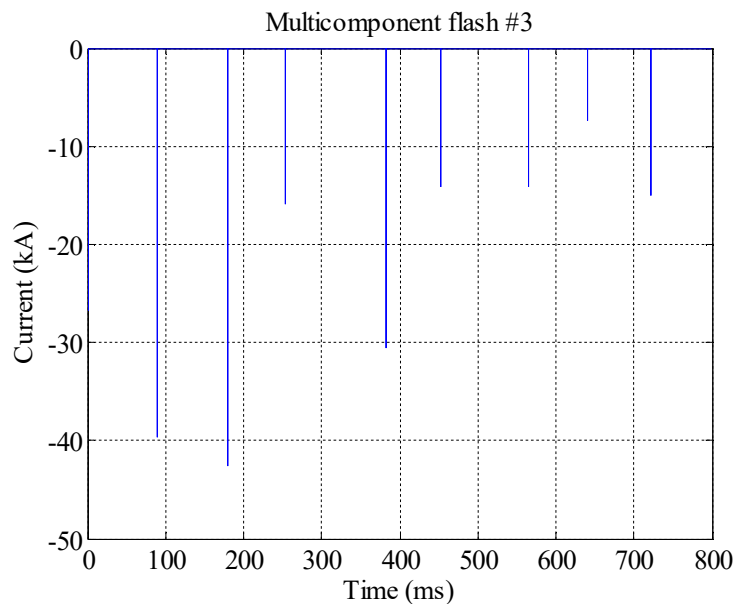


Figure 6.2.12. Multicomponent flash #3 from chapter 4

6.2.5. Effect of Multicomponent Lightning Flashes on Arrester Energy Duty – Unshielded Line Design

For unshielded line lightning flash hit middle of the span of the top phase. Arrester current and energy duty due to impact of flashes from section 6.2.4 are represented in figures below. Arrester current and energy duty are considered for arrester installed on the top phase conductor (this arrester is the most stressed).

Multicomponent flash # 1

Arrester current due to flash #1 is shown in figure 6.2.13. All three components can be noted and arrester current has same duration as original lightning flash. Arrester current peaks are not high as peaks of original lightning flash (about two times lower compared to the original lightning flash). Comparison of arrester current and original lightning flash current is shown on zoomed – in diagram in figure 6.2.14.

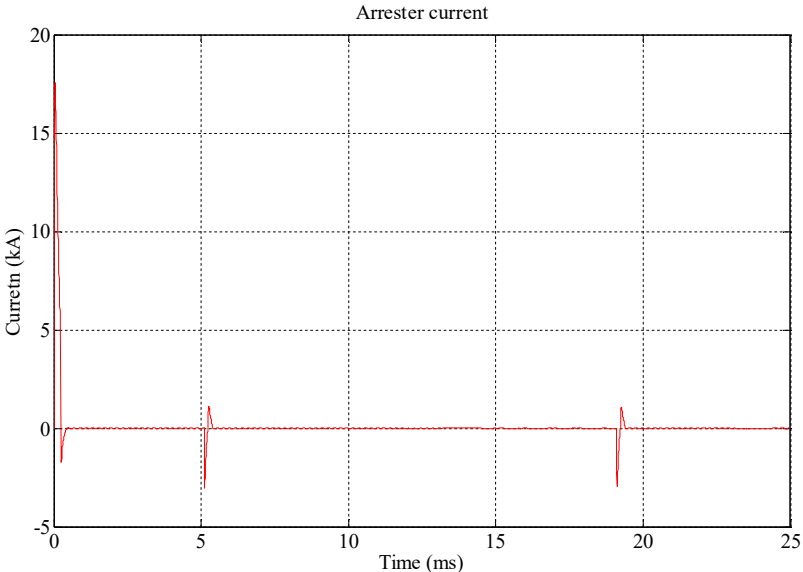


Figure 6.2.13. Arrester current due to flash # 1 – unshielded line design

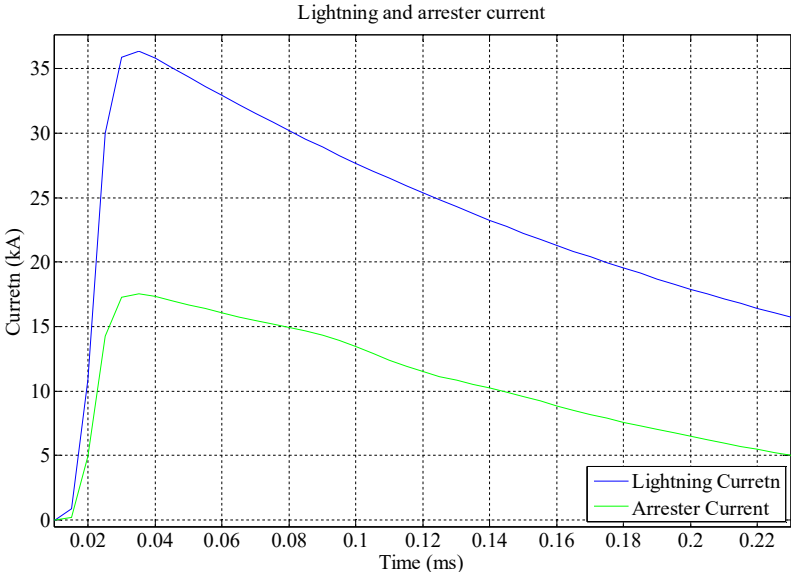


Figure 6.2.14. Arrester current due to flash # 1, and flash #1 current comparison – unshielded line design

Effect of the flash # 1 is emphasized in figure 6.2.15. The energy duty is shown for the duration time of the multicomponent lightning flash #1.

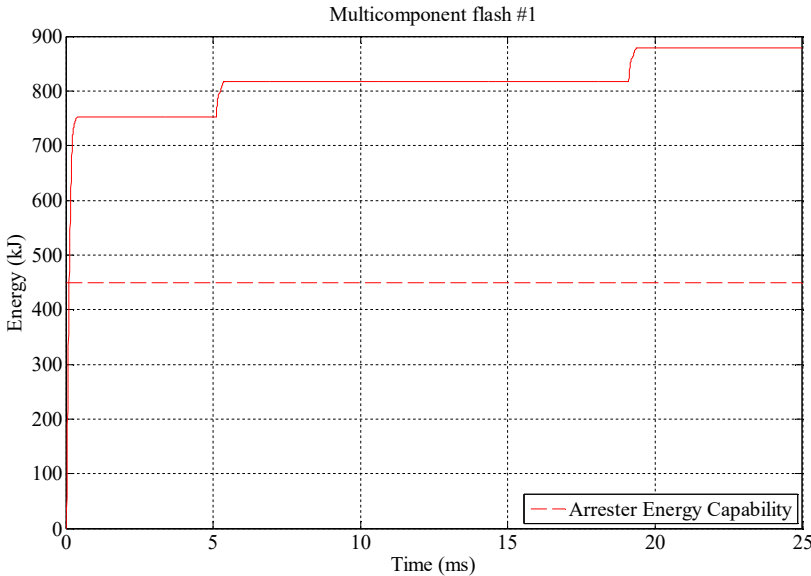


Figure 6.2.15. Arrester energy duty due to flash # 1 – unshielded line design

From the consideration of the energy duty it is possible to conclude that the arrester energy rises up as the current of flash arrives at the arrester. Then, it is possible to conclude that energy increase depends on current peak. Energy of arrester increases with increasing current peaks.

From figure 6.2.15 change of energy seems to be instant (energy change at the moment). So, for better presentation of energy change a zoomed – in diagram is shown in figure 6.2.16.

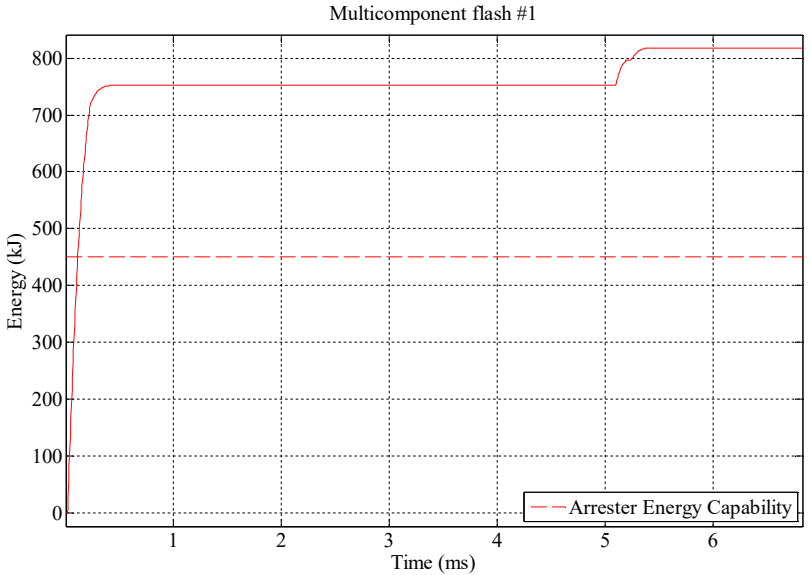


Figure 6.2.16. Arrester energy duty due to flash # 1 zoomed – in

Multicomponent flash # 2

Arrester current due to flash #2 is shown in figure 6.2.17. All five components can be noted and arrester current has same duration as original lightning flash. Arrester current peaks are not high as peaks of original lightning flash (about two times lower compared to the original lightning flash).

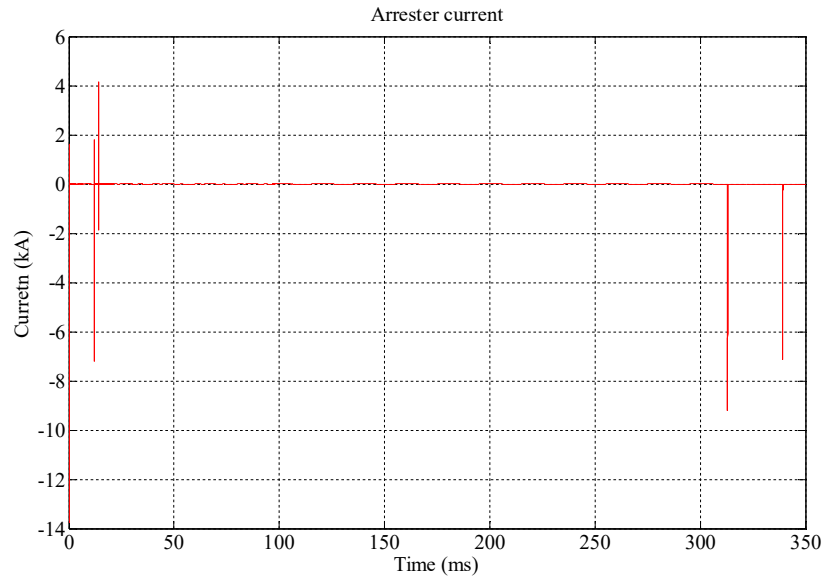


Figure 6.2.17. Arrester current due to flash # 2 – unshielded line design

Effect of the flash # 2 is emphasized in figure 6.2.18. The energy duty is shown for the duration time of the multicomponent lightning flash #2.

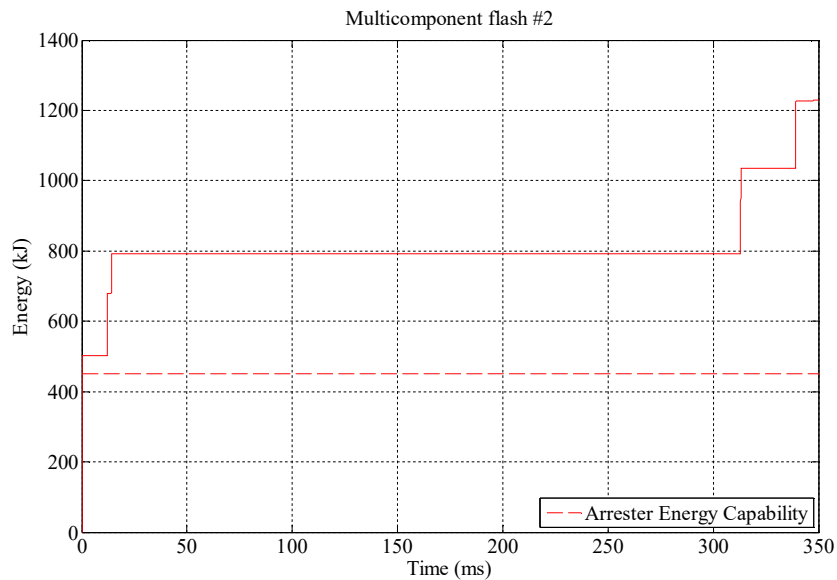


Figure 6.2.18. Arrester energy duty due to flash # 2 – unshielded line design

Multicomponent flash # 3

Arrester current due to flash #3 is shown in figure 6.2.19. All nine components can be noted and arrester current has same duration as original lightning flash. Arrester current peaks are not high as peaks of original lightning flash (about two times lower compared to the original lightning flash). Flash # 3 is very interesting for consideration, because it is a flashes with currents of subsequent strokes larger than a current of the first stroke.

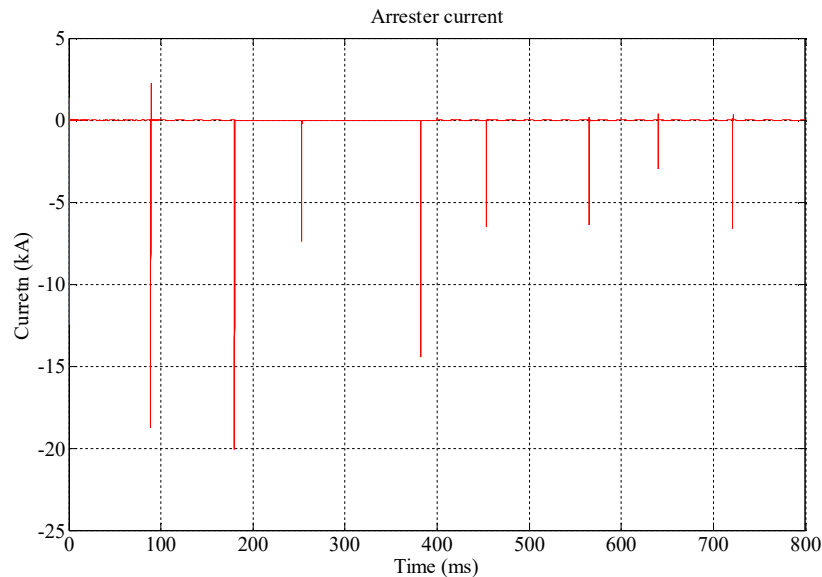


Figure 6.2.19. Arrester current due to flash # 3 – unshielded line design

Effect of the flash # 3 is emphasized in figure 6.2.20. The energy duty is shown for the duration time of the multicomponent lightning flash #3.

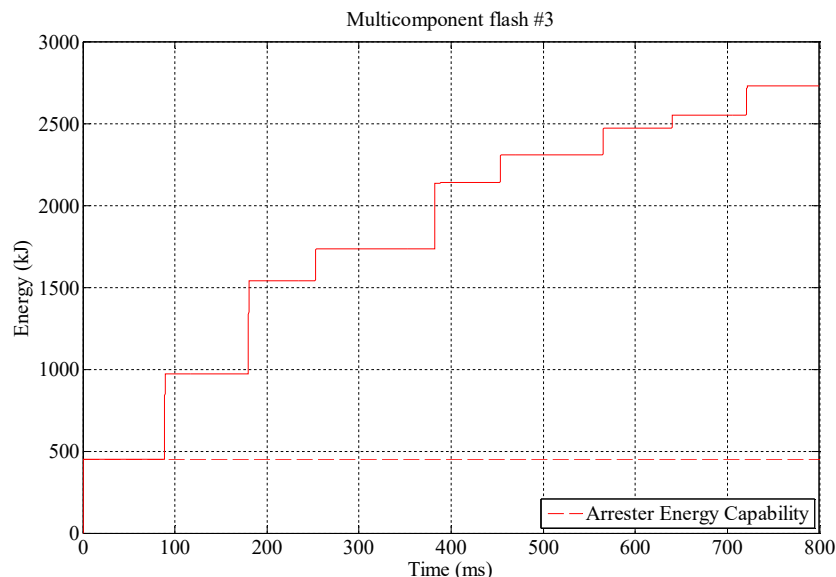


Figure 6.2.20. Arrester energy duty due to flash # 3 – unshielded line design

Multicomponent flashes have significant influence on arrester energy duty. They can provide a large amount of energy that exceeds arrester energy capability (in some cases for many times).

6.2.6. Effect of Multicomponent Lightning Flashes on Arrester Energy Duty – Shielded Line Design

For shielded line lightning flash hit tower top. Arrester current and energy duty due to impact of flashes from section 6.2.4 are represented in figures below. Arrester current and energy duty are considered for arrester installed on the bottom phase conductor (this arrester is the most stressed).

Multicomponent flash # 1

Arrester current due to flash #1 is shown in figure 6.2.21. For shielded line small fraction of current is diverted through arrester. Only first stroke in flash #1 has influence on arrester energy duty. Second and third stroke have not so high current peak and they have not influence on line surge arrester energy duty. Arrester current peak is not high (compared to original first stroke). Duration of arrester current is much shorter than the original lightning stroke.

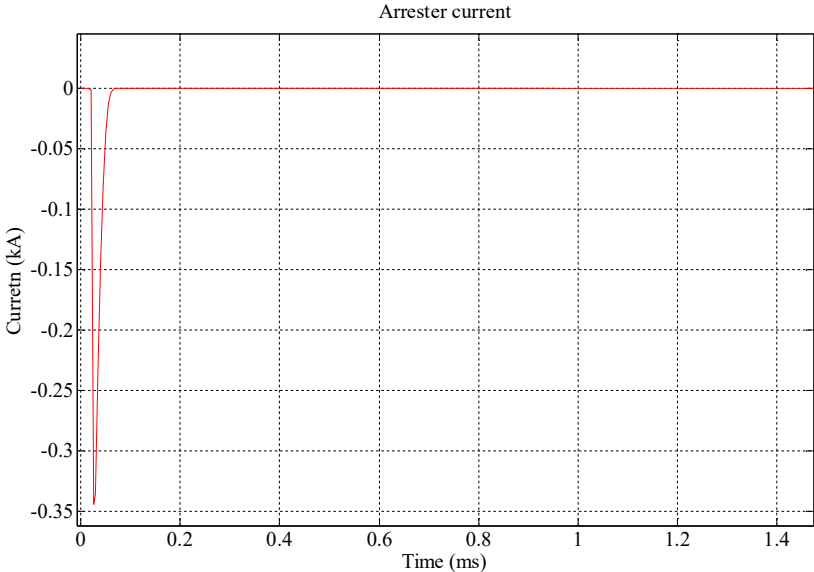


Figure 6.2.21. Arrester current due to flash # 1 – shielded line design

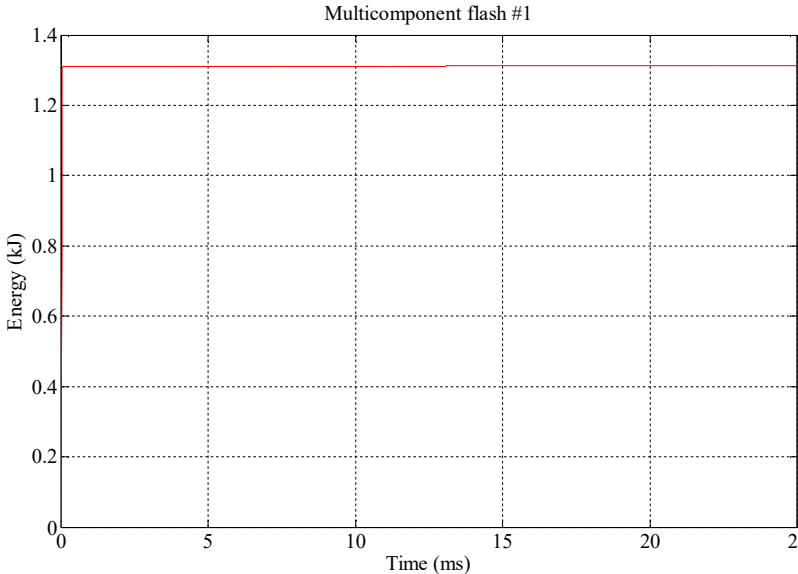


Figure 6.2.22. Arrester energy duty due to flash # 1 – shielded line design

Effect of the flash # 1 is emphasized in figure 6.2.22. The energy duty is shown for the duration time of the multicomponent lightning flash #1. From the consideration of the energy duty it is possible to conclude that the arrester energy for shielded line consideration is not high.

Multicomponent flash # 2

Arrester current due to flash #2 is shown in figure 6.2.23. Three of five components has influence on line surge arrester energy duty. Arrester energy duty due to flash #2 is shown in figure 6.2.24.

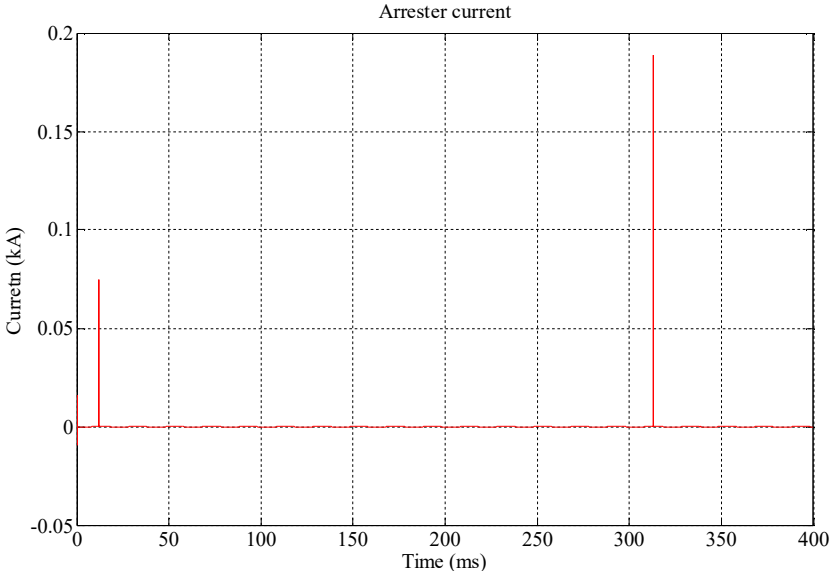


Figure 6.2.23. Arrester current due to flash # 2 – shielded line design

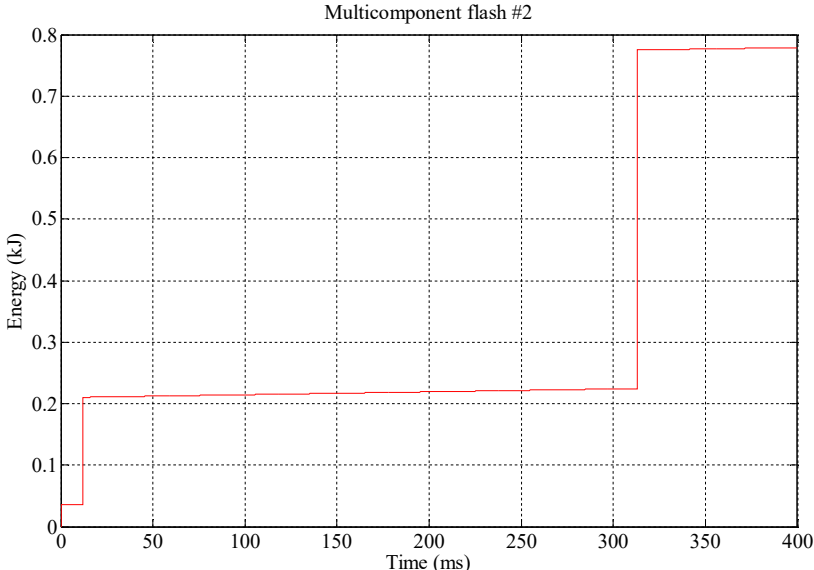


Figure 6.2.24. Arrester energy duty due to flash # 2 – shielded line design

Multicomponent flash # 3

Arrester current due to flash #3 is shown in figure 6.2.25. Seven of nine components has influence on line surge arrester energy duty. Arrester energy duty due to flash #3 is shown in figure 6.2.26.

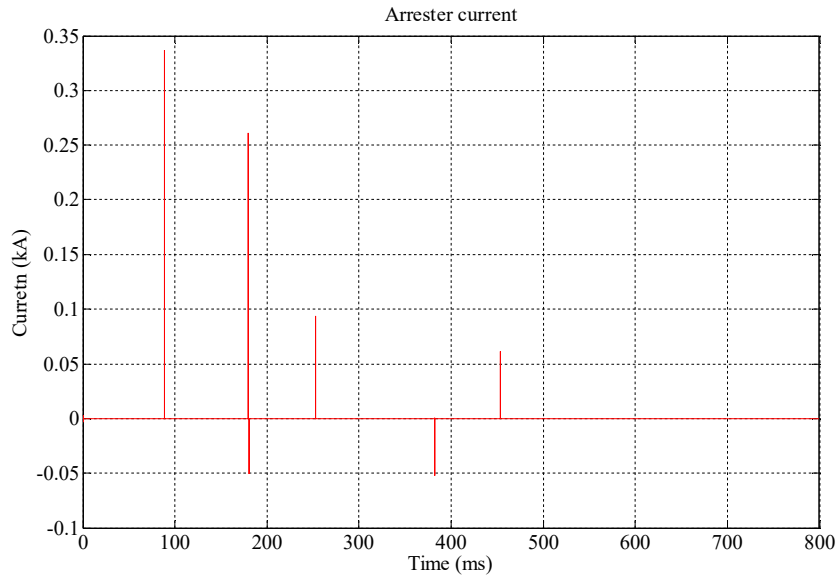


Figure 6.2.25. Arrester current due to flash # 3 – shielded line design

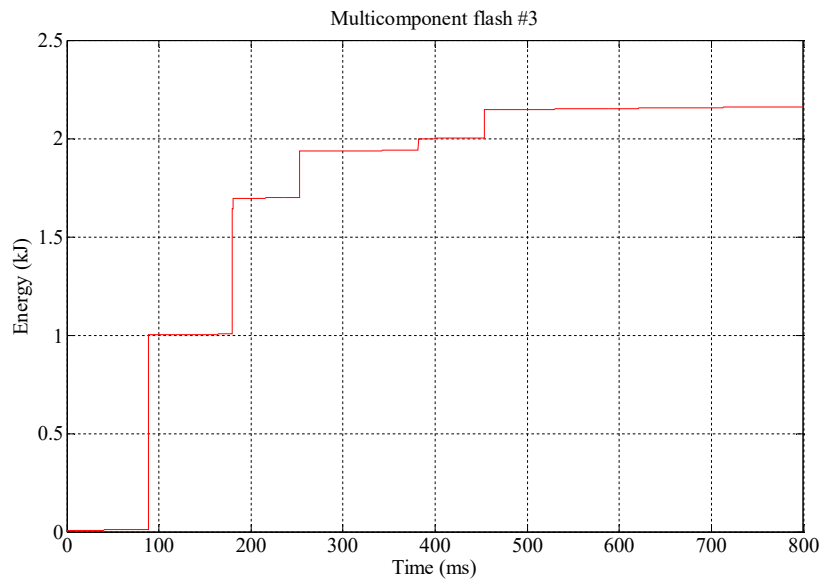


Figure 6.2.26. Arrester energy duty due to flash # 3 – shielded line design

From the consideration of the energy duties (for all three considered flashes) it is possible to conclude that the arrester energy rises up as the current of flash arrives at the arrester. Then, it is possible to conclude that energy increase depends on current peak. It has to be noted that in case of shielded line configuration all components in flash have not influence at line surge arrester energy duty.

6.3. Arrester Energy Sharing and Importance of Complete Transmission Line Modelling

It is indicated that lightning stroke hitting transmission line usually produce operation of more than one line surge arrester. In previous section it is shown that there is a big difference in the energy duties for the line surge arresters installed on the shielded and on the unshielded lines. Line surge arresters installed on the unshielded line are much more stressed than line surge arresters on the shielded line. Therefore, for arrester energy sharing calculations unshielded line design was considered.

As it is previously mentioned modelling of complete transmission line, in line surge arrester energy duty studies, is very important for more accurate arrester energy sharing calculation. Figures below represent line surge arresters energy sharing in two cases and for few different tower footing resistance values. In first case five towers were modelled on the both sides from the point of the lightning impact. While in second case fifteen towers were modelled on the both sides from the point of the lightning impact. Examples of five and fifteen towers were taken for better visualization and understanding. It is important to emphasize possibility to monitor energy for all arresters along the complete transmission line. Lightning hits middle of the span of the top phase (Phase A). So, arresters on the top phase are the most stressed and energy of arresters installed on the top phase conductor is considered.

Percentage (with respect to energy absorbed by arrester at tower first to the point of lightning impact) of energy shared by adjacent arresters at towers along the line – 10 towers case is shown in figure 6.3.1, while percentage (with respect to energy absorbed by arrester at tower first to the point of lightning impact) of energy shared by adjacent arresters at towers along the line – 30 towers case is shown in figure 6.3.2.

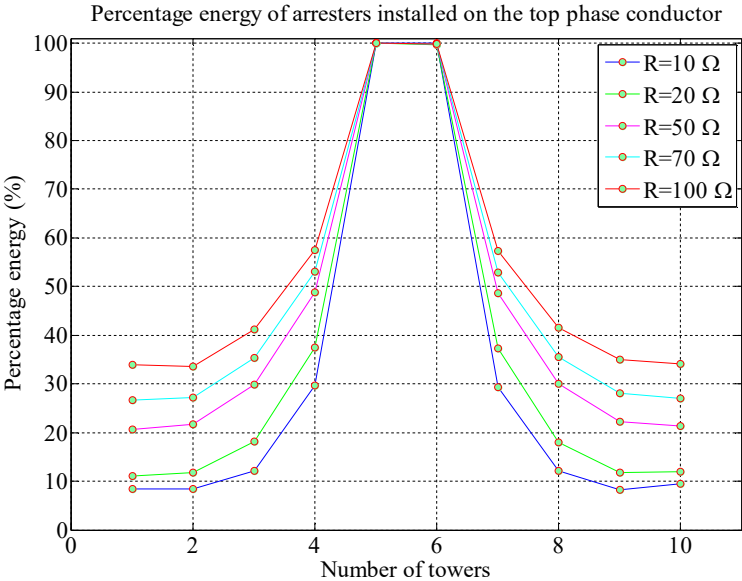


Figure 6.3.1. Percentage (with respect to energy absorbed by arrester at tower first to the point of lightning impact) of energy shared by adjacent arresters at towers along the line – 10 towers case

If curve with tower footing resistance of 50 Ω is considered, it can be said that the arrester on second tower from point of lightning impact absorb almost 50% of energy (with respect to energy absorbed by arrester at tower first to the point of lightning impact) in both cases.

Arrester on third tower absorbs about 30% of energy, on fourth about 22% of energy and on fifth about 20% of energy.

In second case arrester on third tower absorbs less than 30% of energy, on fourth about 15% of energy and on fifth less than 10% of energy. This value decreases to only 3% for the arresters at far end.

Details for better understanding are given in figure 6.3.3 and in table 6.3.1.

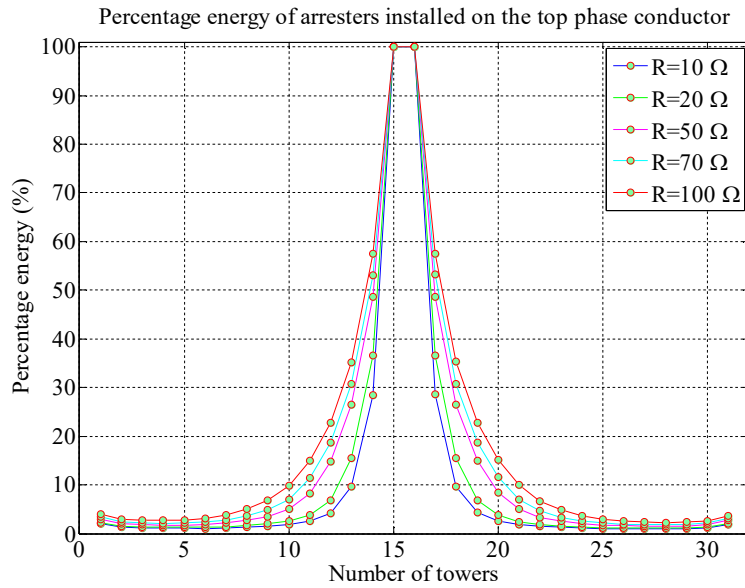


Figure 6.3.2. Percentage (with respect to energy absorbed by arrester at tower first to the point of lightning impact) of energy shared by adjacent arresters at towers along the line – 30 towers case

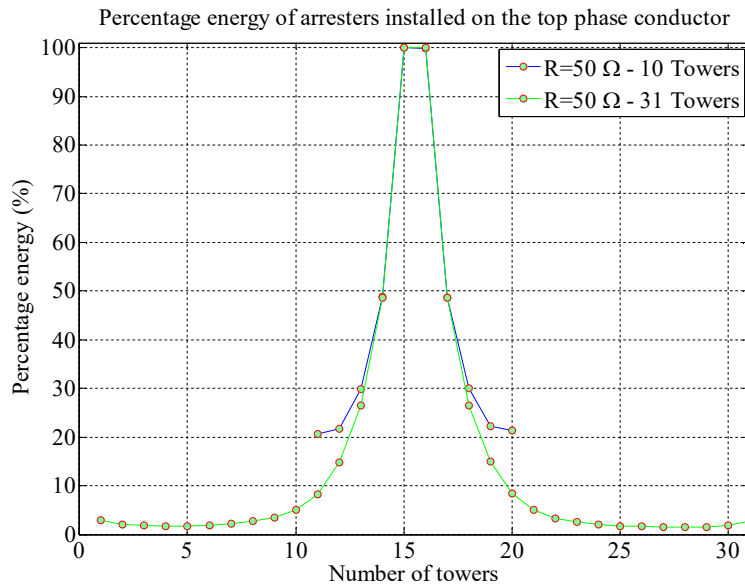


Figure 6.3.3. Percentage (with respect to energy absorbed by arrester at tower first to the point of lightning impact) of energy shared by adjacent arresters at towers along the line – comparison 10 and 30 towers

Table 6.3.1. Percentage of absorbed energy

Number of tower from point of lightning impact	1	2	3	4	5
Percentage of absorbed energy case 1 (%)	100	48.7676	29.9424	21.7053	20.6565
Percentage of absorbed energy case 2 (%)	100	48.6390	26.4839	14.8627	8.31890

6.4. Parametric Analysis

Previous section shows that line surge arrester energy duty depends on line design. Except transmission line design appropriate selection of an arrester as a function of its energy stress depends upon different parameters. These parameters can be classified as transmission line parameters and lightning flash parameters.

Parameters such as: tower footing resistance, different arrester installation configuration are considered as line parameters. Lightning flash parameters have significant influence on energy stress in line surge arresters. This can be considered as one of the key factor for selection of the arrester. Following lightning flash parameters were considered: lightning channel impedance, front time, tail time, multiplicity and current peak.

In next sections the following considerations are held:

- Influence of uniform, tower footing resistance distribution on line surge arrester energy duty;
- Influence of non – uniform tower footing resistance distribution on line surge arrester energy duty;
- Arrester energy duty consideration for different arrester installation configuration;
- Influence of lightning channel impedance on line surge arrester energy duty;
- Influence of front time on line surge arrester energy duty;
- Influence of tail time on line surge arrester energy duty;
- Influence of current peak on line surge arrester energy duty;

Influence of some parameters on line surge arrester energy duty is hardly noticeable for shielded line design. Therefore, that parameters are considered only for unshielded line design.

For example, in case of shielded line design, arrester installed on tower that is point of lightning impact absorbs the most energy, while arresters on adjacent towers are not significantly stressed. Also, in case of shielded transmission line design tower footing resistance for tower that is point of lightning impact is important parameter, while tower footing resistance for adjacent towers has not important influence on line surge arrester energy duty. In case of unshielded line design arrester that is nearest to the point of lightning impact is the most stressed, but arresters installed on adjacent towers are also stressed significantly. It depends on tower footing resistance of adjacent towers. Therefore, in case of unshielded line design influence of non – uniform tower footing resistance distribution on line surge arrester energy duty is considered, while for shielded line it is not considered.

6.4.1. Influence of Uniform Tower Footing Resistance Distribution on Line Surge Arrester Energy Duty – Unshielded Line Design

The value of tower footing resistance has significant influence on line surge arrester energy duty. Unshielded line was considered, in the conditions when lightning hits a middle of the span of the top conductor. Tower footing resistance was varied from 10 Ω to 100 Ω with step of 10 Ω.

Energy duties for arresters nearest to the point of the lightning impact (for different tower footing resistance values) are presented in figures below.

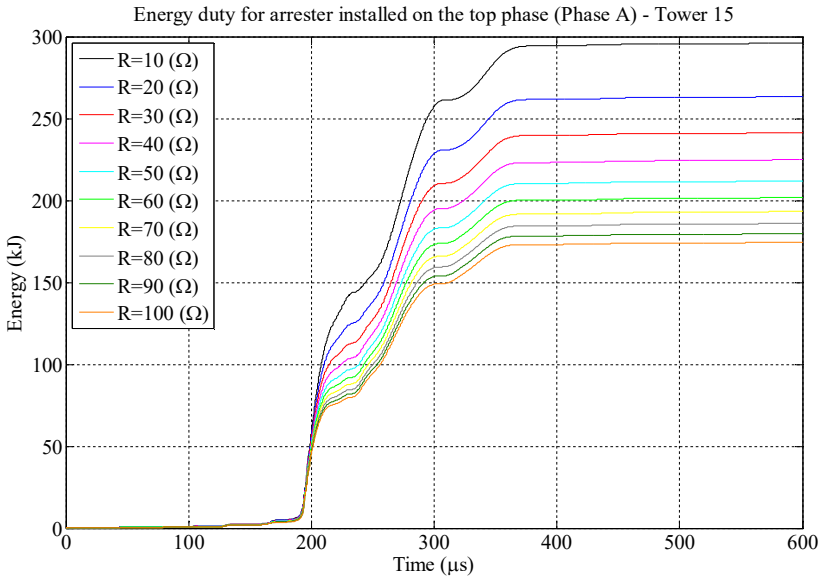


Figure 6.4.1. Arrester energy duty for different values of tower footing resistance – on the first tower to the point of lightning impact – unshielded line design

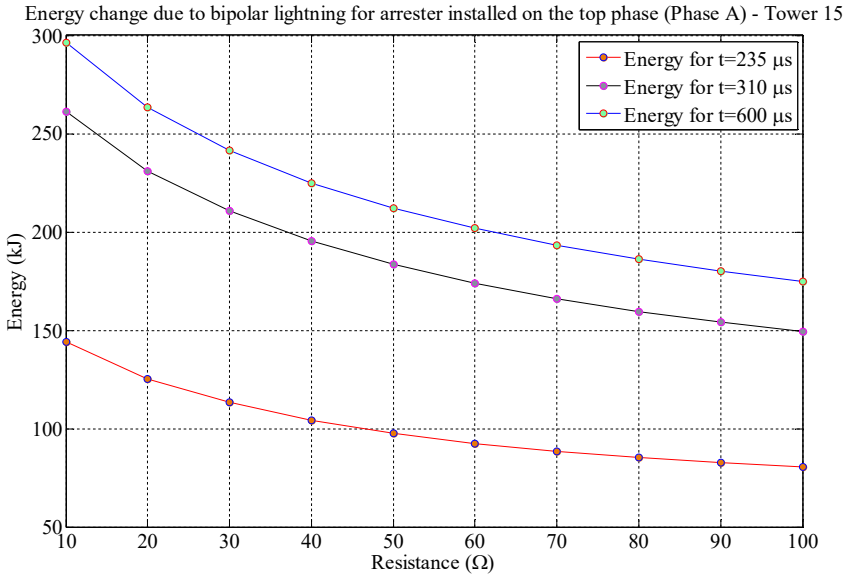


Figure 6.4.2. Arrester energy change due to bipolar lightning for different values of tower footing resistance – on the first tower to the point of lightning impact – unshielded line design

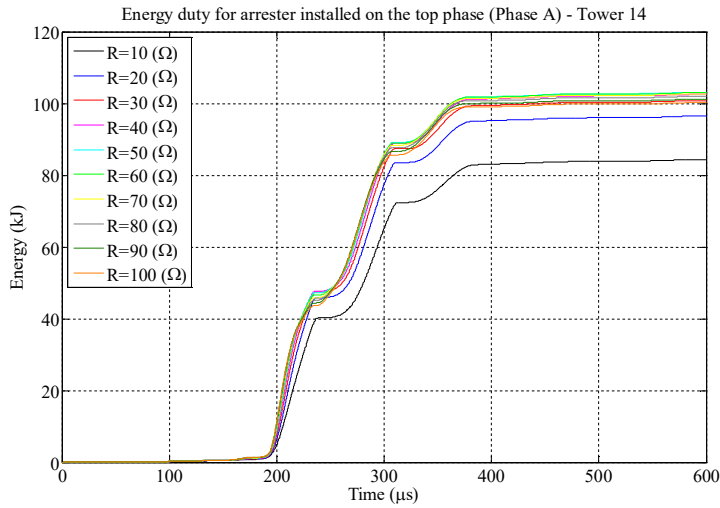


Figure 6.4.3. Arrester energy duty for different values of tower footing resistance – on the second tower to the point of lightning impact – unshielded line design

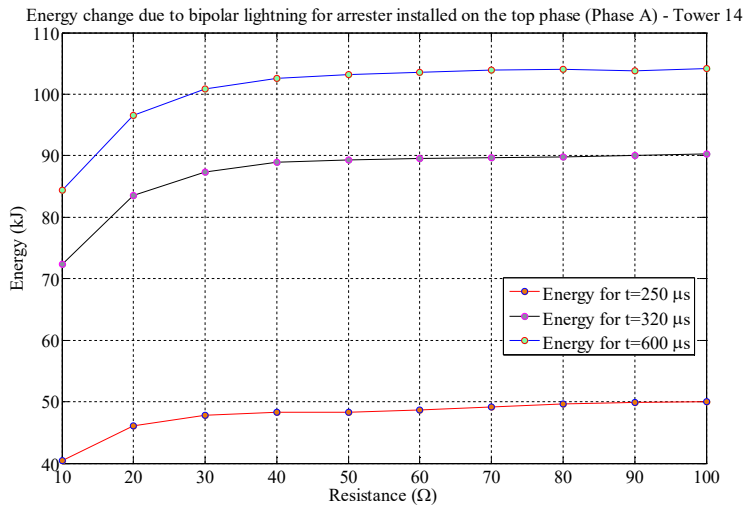


Figure 6.4.4. Arrester energy change due to bipolar lightning for different values of tower footing resistance – on the second tower to the point of lightning impact – unshielded line design

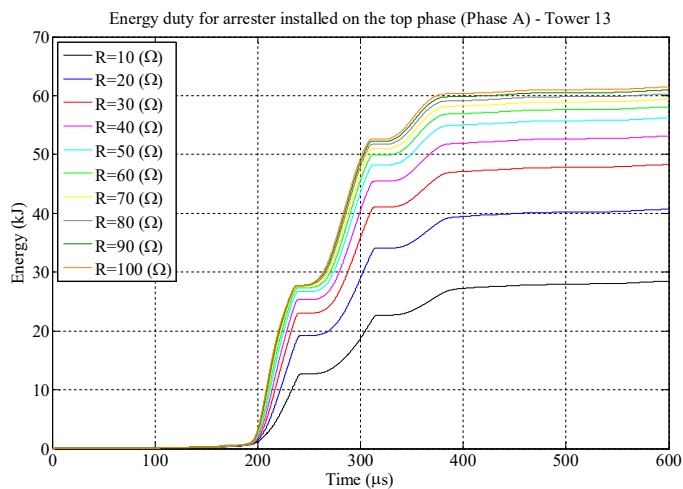


Figure 6.4.5. Arrester energy duty for different values of tower footing resistance – on the third tower to the point of lightning impact – unshielded line design

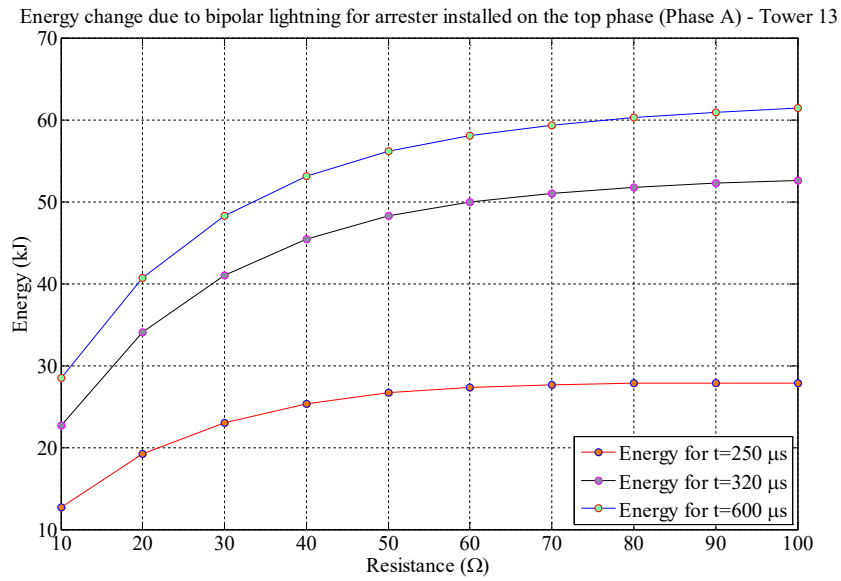


Figure 6.4.6. Arrester energy change due to bipolar lightning for different values of tower footing resistance – on the third tower to the point of lightning impact – unshielded line design

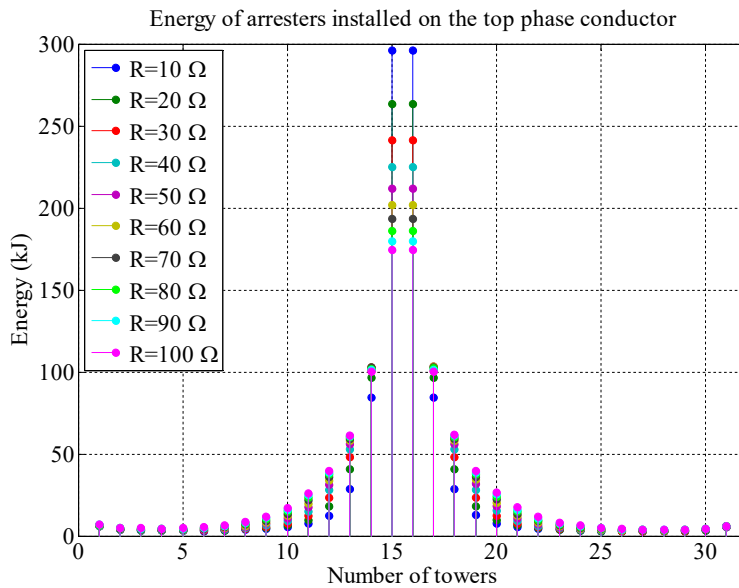


Figure 6.4.7. Maximum arrester energy for different values of tower footing resistance along unshielded transmission line

From previously presented figures it is possible to say that the energy absorbed by the nearest arrester decreases with increasing tower footing resistance. This means that with increase of the tower footing resistance less current is flowing through tower footing resistance and more current has to be diverted through line surge arrester. In case of higher tower footing resistance adjacent towers absorb more energy than in case of low tower footing resistance of the nearest tower.

Arresters on adjacent towers also absorb significant part of energy. Energy of those arresters increases with increasing tower footing resistance.

6.4.2. Influence of Uniform Tower Footing Resistance Distribution on Line Surge Arrester Energy Duty – Shielded Line Design

The value of tower footing resistance has significant influence on line surge arrester energy duty. Shielded line was considered, a lightning hits a tower top. Tower footing resistance was varied from 10 Ω to 100 Ω with step of 10 Ω. Energy duty for bottom phase arrester installed on hit tower (for different tower footing resistance values) is presented in figure 6.4.8.

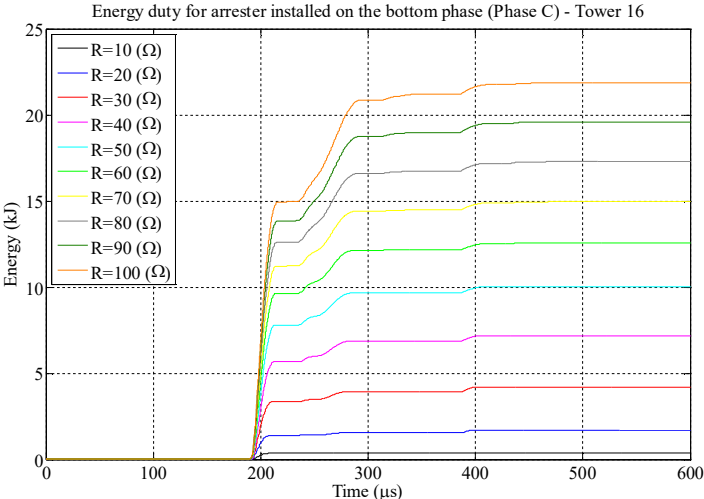


Figure 6.4.8. Arrester energy duty for different values of tower footing resistance – shielded line design

Figure 6.4.9 represents arrester energy change due to bipolar lightning for different values of tower footing resistance.

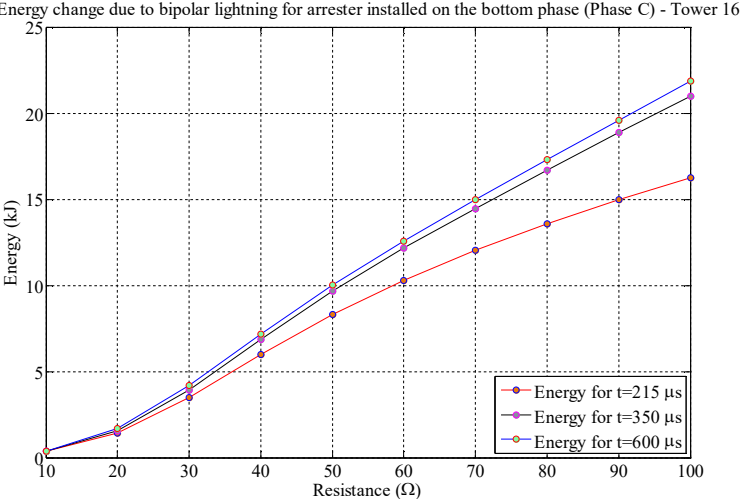


Figure 6.4.9. Arrester energy change due to bipolar lightning for different values of tower footing resistance – shielded line design

Figure 6.4.10 represents maximum arrester energy (bottom phase) for different values of tower footing resistance.

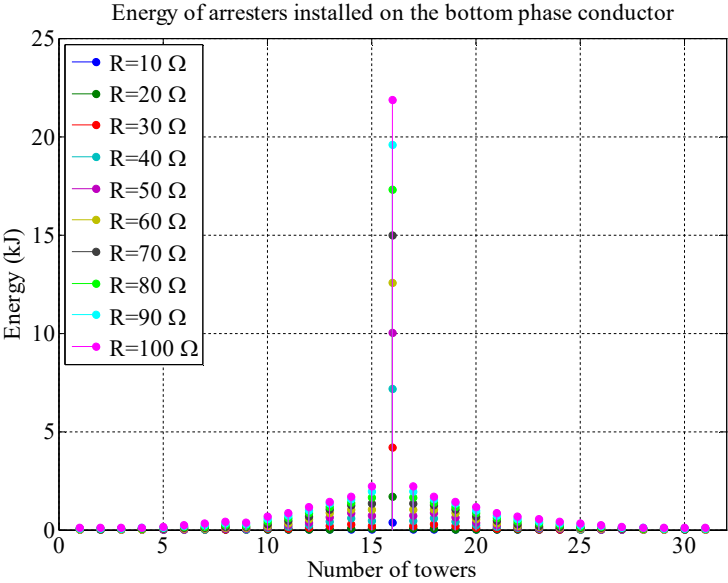


Figure 6.4.10. Bottom phase arrester energy for different values of tower footing resistance along shielded transmission line

From figures 6.4.8 and 6.4.10 it is possible to say that the arrester energy increases with increasing tower footing resistance. Also, this conclusion is valid for adjacent towers.

6.4.3. Arrester Energy Duty Consideration for Different Arrester Installation Configuration – Unshielded Line Design

When two or more arresters are installed, they are not equally stressed. For unshielded line two arrester configurations are considered:

- Line surge arresters are installed on three phase conductors and;
- Line surge arresters are installed on the top and on the middle phase conductors.

Figures 6.4.11 and 6.4.12 represents energy of arresters installed on all three phases for tower footing resistance of $10\ \Omega$ and $100\ \Omega$ respectively. Lightning hits middle of the span of the top conductor.

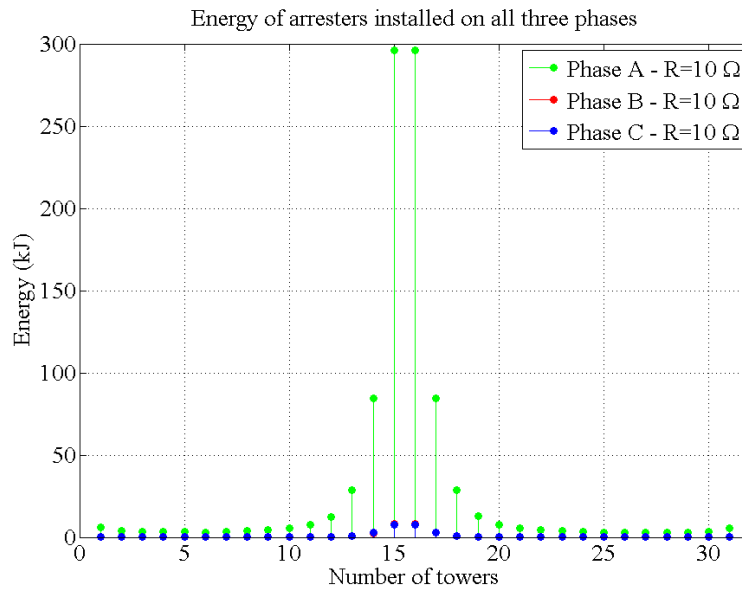


Figure 6.4.11. Energy of arrester installed on all three phases along unshielded transmission line – tower footing resistance $10\ \Omega$

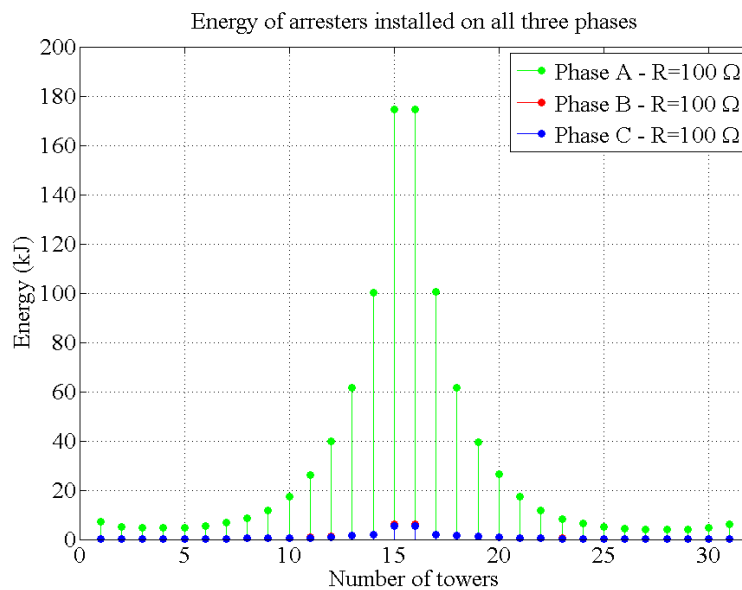


Figure 6.4.12. Energy of arrester installed on all three phases along unshielded transmission line – tower footing resistance $100\ \Omega$

Line surge arresters installed on top phase conductor are the most stressed and they absorb most of energy. Line surge arrester installed on the middle and bottom phase absorb a small portion of energy and have almost the same value of energy. The nearest arresters to the point of the lightning impact, that are installed on the middle and bottom phase conductors, absorbed only 3 % of energy (in respect to the most stressed arrester installed on the top phase conductor) for both resistance values. Line surge arresters installed on the middle and bottom phase at the far end does not absorb any energy.

Figures 6.4.13 and 6.4.14 represents energy of arresters installed on the top and middle phase conductor for tower footing resistance of 10 Ω and 100Ω respectively. Lightning hits middle of the span of the top conductor.

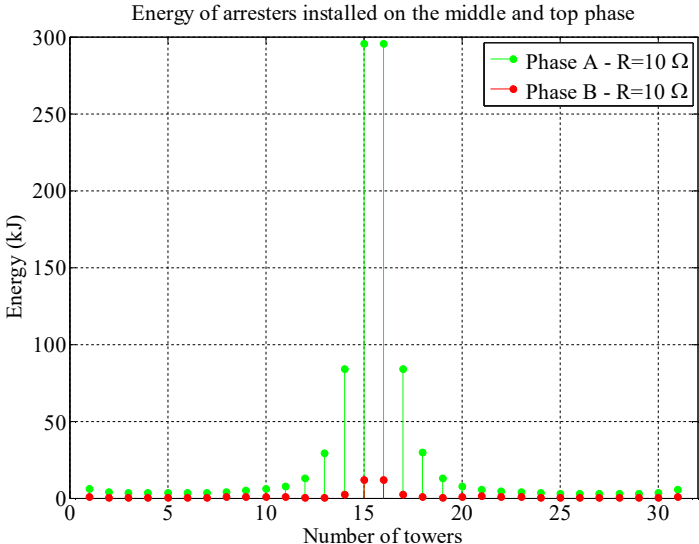


Figure 6.4.13. Energy of arrester installed on the top and middle phases along unshielded transmission line – tower footing resistance 10 Ω

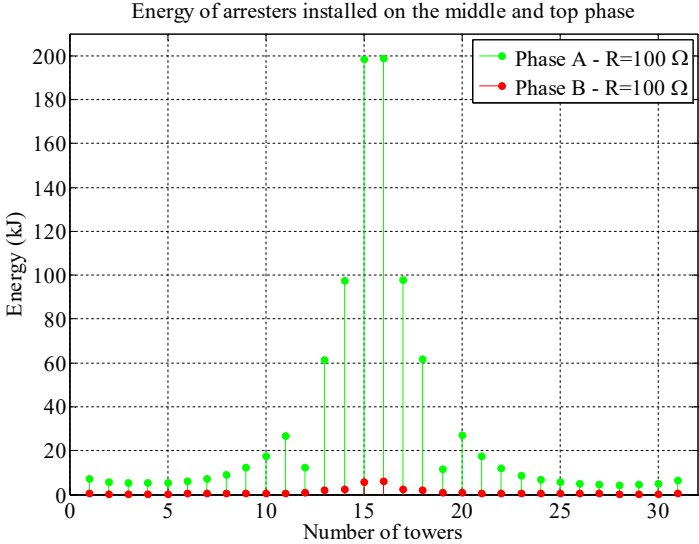


Figure 6.4.14. Energy of arrester installed on the top and middle phases along unshielded transmission line – tower footing resistance 100 Ω

Also in this case, the nearest arresters to the point of the lightning impact, which are installed on the middle phase conductor, absorbed only 3 % of energy (in respect to the most stressed arrester installed on the top phase conductor) for both resistance values. Top phase line surge arresters (for two arresters installation configuration) that are nearest (on first tower) to the point of lightning impact absorb about 15% more energy than nearest arresters for three arresters installation configuration.

6.4.4. Arrester Energy Duty Consideration for Different Arrester Installation Configuration – Shielded Line Design

When two or more arresters are installed, they are not equally stressed. For shielded line, three arrester configurations are considered:

- Line surge arresters are installed on all three phase conductors;
- Line surge arresters are installed on the middle and on the bottom phase conductors;
- Line surge arresters are installed on the bottom phase conductor.

Figures 6.4.15 and 6.4.16 represent energy of arresters installed on all three phases for tower footing resistance of 10 Ω and 100Ω, respectively. A lightning hits a tower top.

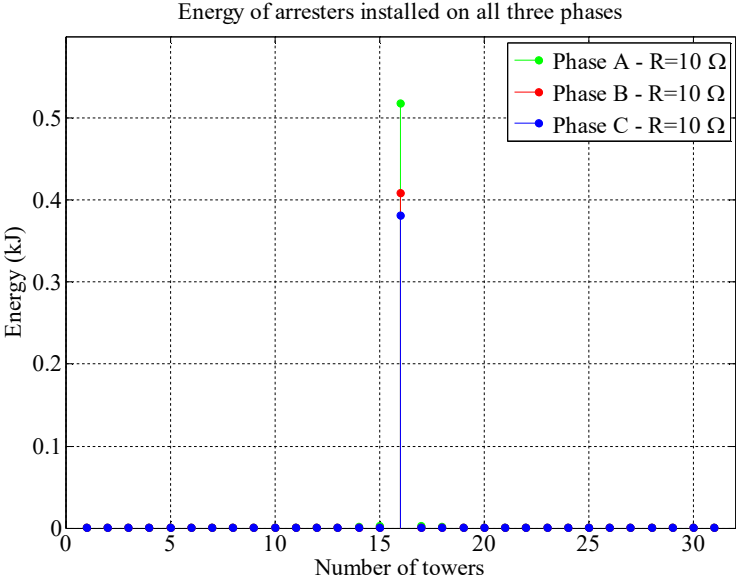


Figure 6.4.15. Energy of arrester installed on all three phases along shielded transmission line – tower footing resistance 10 Ω

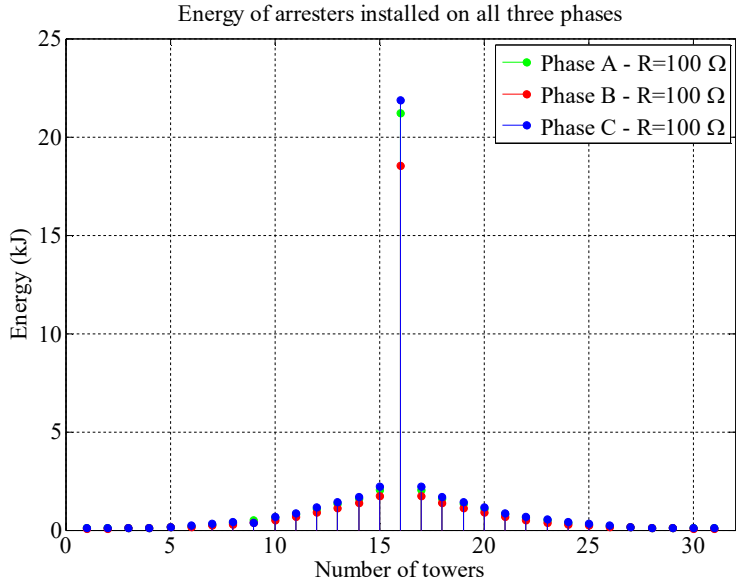


Figure 6.4.16. Energy of arrester installed on all three phases along shielded transmission line – tower footing resistance 100 Ω

When lightning hits shielded line, lightning stroke current is diverted along shield wire, tower construction and tower footing resistance. For low tower footing resistance values (case of shielded line) more current is flowing through tower footing resistance and less has to be diverted through line surge arrester. So, that small portion of energy is absorbed by arresters installed on hit tower, while adjacent towers do not absorb significant energy. The arrester installed on the top phase is the most stressed.

For higher tower footing resistance values, less current is flowing through tower footing resistance and more current has to be diverted through line surge arrester. Arresters installed on hit tower absorb more energy as well as adjacent towers. Arrester installed on the bottom phase is the most stressed, reason for that is effect of reflection.

Figures 6.4.17 and 6.4.18 represent energy of arresters installed on the middle and bottom phase conductor for tower footing resistance of 10 Ω and 100Ω respectively. Figures 6.4.19 and 6.4.20 represent energy of arresters installed on the bottom phase conductor for tower footing resistance of 10 Ω and 100Ω, respectively. A lightning hits a tower top.

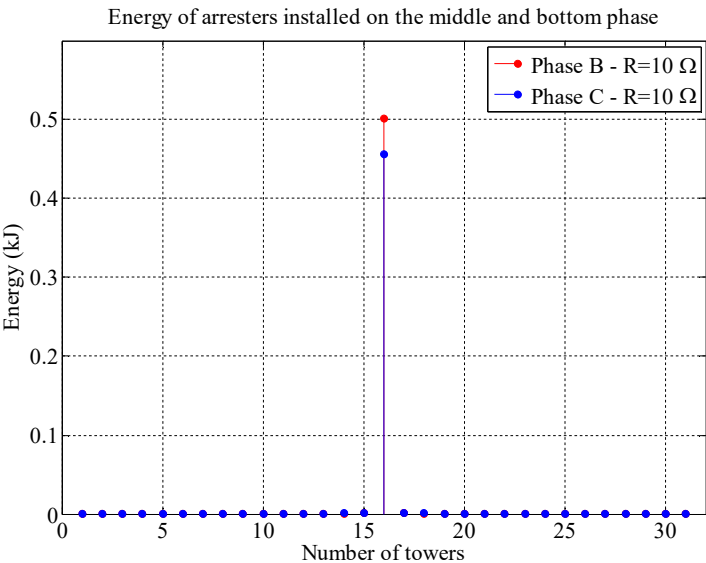


Figure 6.4.17. Energy of arresters installed on the middle and bottom phase conductors along shielded transmission line – tower footing resistance 10 Ω

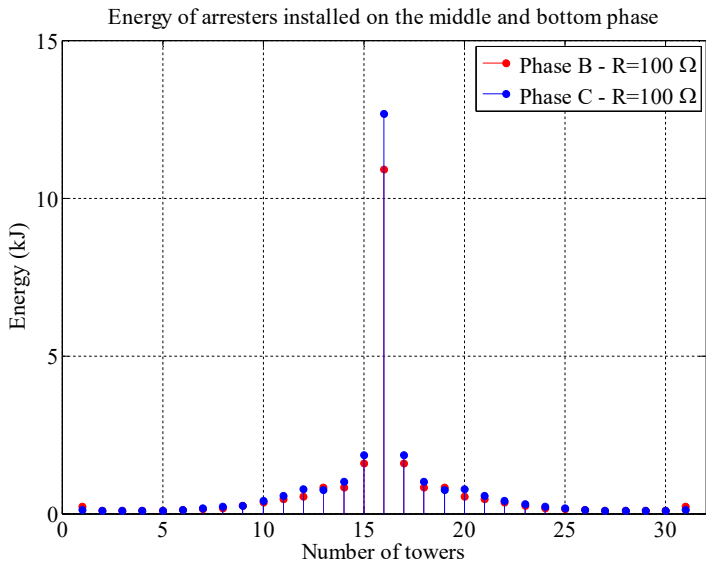


Figure 6.4.18. Energy of arresters installed on the middle and bottom phase conductors along shielded transmission line – Tower footing resistance 100 Ω

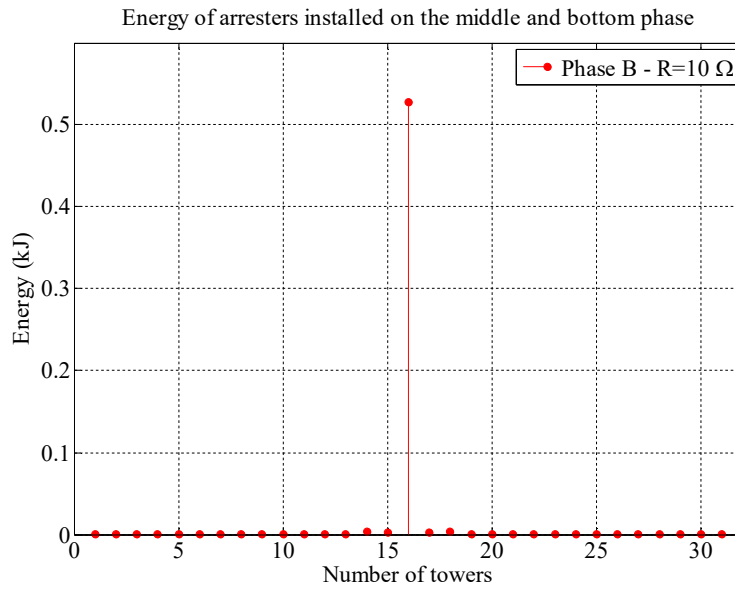


Figure 6.4.19. Energy of arresters installed on the bottom phase conductor along shielded transmission line –resistance 10 Ω

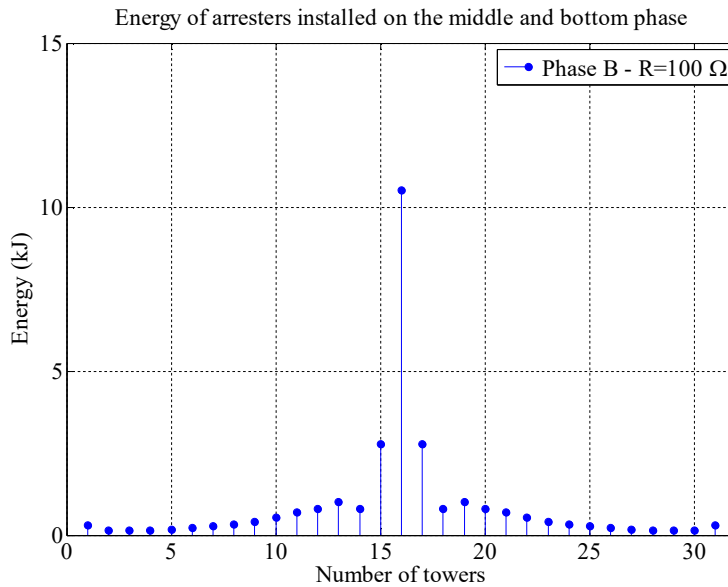


Figure 6.4.20. Energy of arresters installed on the bottom phase conductor along shielded transmission line – tower footing resistance 100 Ω

Comparison of arresters energies for different arrester installation configuration is represented in Tables 6.4.1. – 6.4.4.

Table 6.4.1. Middle phase arrester energy for different LSA installation configuration (resistance 10 Ω)

Tower footing resistance = 10 Ω	Tower 14	Tower T15	Tower T16	Tower T17	Tower 18
Arrester energy phase B 3 LSA installation configuration	0.0003 (kJ)	0.0007 (kJ)	0.4091 (kJ)	0.0007 (kJ)	0.0003 (kJ)
Arrester energy phase B 2 LSA installation configuration	0.0010 (kJ)	0.0013 (kJ)	0.5019 (kJ)	0.0013 (kJ)	0.0010 (kJ)

Table 6.4.2. Bottom phase arrester energy for different LSA installation configuration (resistance 10 Ω)

Tower footing resistance = 10 Ω	Tower 14	Tower T15	Tower T16	Tower T17	Tower 18
Arrester energy phase C 3 LSA installation configuration	0.0005 (kJ)	0.0008 (kJ)	0.3811 (kJ)	0.0008 (kJ)	0.0005 (kJ)
Arrester energy phase C 2 LSA installation configuration	0.0011 (kJ)	0.0014 (kJ)	0.4564 (kJ)	0.0014 (kJ)	0.0011 (kJ)
Arrester energy phase C 1 LSA installation configuration	0.0036 (kJ)	0.0022 (kJ)	0.5281 (kJ)	0.0022 (kJ)	0.0036 (kJ)

For low tower footing resistance middle phase arrester absorb more energy for 2 LSA installation configuration compared to 3 LSA installation configuration. While, bottom phase arrester absorb the most energy in case of 1 LSA installation configuration.

Table 6.4.3. Middle phase arrester energy for different LSA installation configuration (resistance 100 Ω)

Tower footing resistance = 100 Ω	Tower 14	Tower T15	Tower T16	Tower T17	Tower 18
Arrester energy phase B 3 LSA installation configuration	1.3964 (kJ)	1.7178 (kJ)	18.5525 (kJ)	1.7178 (kJ)	1.3964 (kJ)
Arrester energy phase B 2 LSA installation configuration	0.8244 (kJ)	1.5848 (kJ)	10.8973 (kJ)	1.5848 (kJ)	0.8244 (kJ)

Table 6.4.4. Bottom phase arrester energy for different LSA installation configuration (resistance 100 Ω)

Tower footing resistance = 100 Ω	Tower 14	Tower T15	Tower T16	Tower T17	Tower 18
Arrester energy phase C 3 LSA installation configuration	1.6894 (kJ)	2.2215 (kJ)	21.8836 (kJ)	2.2215 (kJ)	1.6894 (kJ)
Arrester energy phase C 2 LSA installation configuration	1.0100 (kJ)	1.8641 (kJ)	12.6651 (kJ)	1.8641 (kJ)	1.0100 (kJ)
Arrester energy phase C 1 LSA installation configuration	0.8046 (kJ)	2.7781 (kJ)	10.5102 (kJ)	2.7781 (kJ)	0.8046 (kJ)

For high tower footing resistance middle phase arrester absorb more energy for 3 LSA installation configuration compared to 2 LSA installation configuration. While, bottom phase arrester absorbs the most energy in case of 3 LSA installation configuration. In case of high tower footing resistance value arresters installed on adjacent towers are more involved in energy absorption.

6.4.5. Influence of Lightning Channel Impedance on Line Surge Arrester Energy Duty – Unshielded Line Design

Unshielded line model is described in previous sections. In this case, lightning stroke hits upper phase in the middle of the span between two towers. Tower footing resistance for few neighbouring towers is 20 Ω . Lightning current is bipolar lightning flash from figure 4.2.1 and lightning channel impedance is varied from 100 Ω to 3000 Ω . Simulations are performed for different values of lightning channel impedance, while other parameters stay the same in all simulation cases. Arresters installed on towers that are nearest to the point of the lightning impact will be the most stressed, especially arrester on upper phase. Thus, energy change for arrester installed on upper phase is considered. In case when lightning stroke is modelled as ideal current source arrester energy has value of 263.4874 kJ. Table 6.4.5 represents maximum arrester energy for different values of lightning channel impedance and percentage of energy decrease in regard to case when ideal current source is used.

Table 6.4.5. Maximum line surge arrester energy for different values of lightning channel impedance and percentage of energy decrease – unshielded line design

Z_{ch} (Ω)	Arrester Energy (kJ)	Percentage of energy decrease (%)	Z_{ch} (Ω)	Arrester Energy (kJ)	Percentage of energy decrease (%)
100	191.1350	27.4595	1600	254.9358	3.2456
200	221.2250	16.0396	1700	255.3634	3.0833
300	232.4873	11.7653	1800	255.7502	2.9365
400	238.4399	9.5061	1900	256.1019	2.8030
500	242.1924	8.0820	2000	256.4220	2.6815
600	244.8759	7.0635	2100	256.7174	2.5694
700	246.9192	6.2881	2200	256.9897	2.4661
800	248.5270	5.6778	2300	257.2417	2.3704
900	249.8324	5.1824	2400	257.4740	2.2822
1000	250.9181	4.7704	2500	257.6902	2.2002
1100	251.8395	4.4207	2600	257.8899	2.1244
1200	252.6288	4.1211	2700	258.0777	2.0531
1300	253.3162	3.8602	2800	258.2522	1.9869
1400	253.9218	3.6304	2900	258.4145	1.9253
1500	254.4580	3.4269	3000	258.5693	1.8665

When lightning channel impedance is 100 Ω arrester energy is 191.1350 kJ that means decrease of energy of 27.4595 % in regard to ideal current source. Energy decrease for impedance of 400 Ω that is very often used is 9.5061 %. Changes of energy for different lightning channel impedances are significant. For resistance from 100 Ω to 1000 Ω changes of energy are higher, for resistance values higher than 1000 Ω arrester energy changes are lower. Also, for resistance values higher of 1000 Ω changes of arrester energy are lower than 5%.

Arrester energy for different values of lightning channel impedance and in time points when bipolar lightning flash changes polarity is given in figure 6.4.21. Figure 6.4.22 illustrates percentage of energy decrease in regard to case when ideal current source is used.

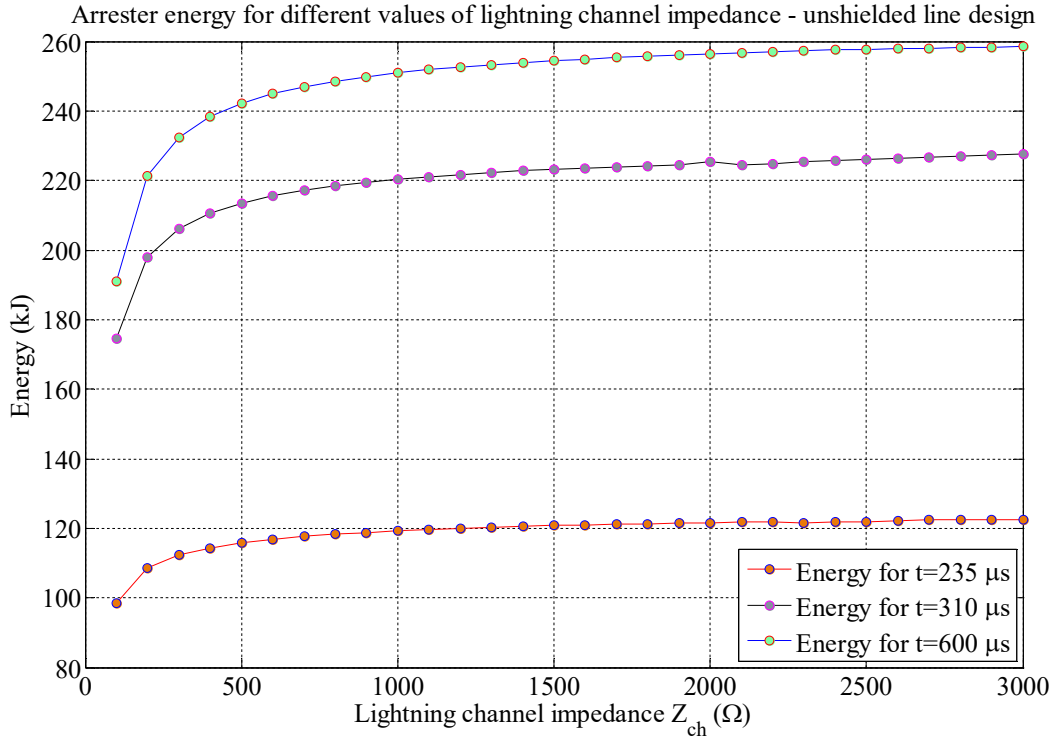


Figure 6.4.21. Arrester energy for different values of lightning channel impedance – unshielded line design

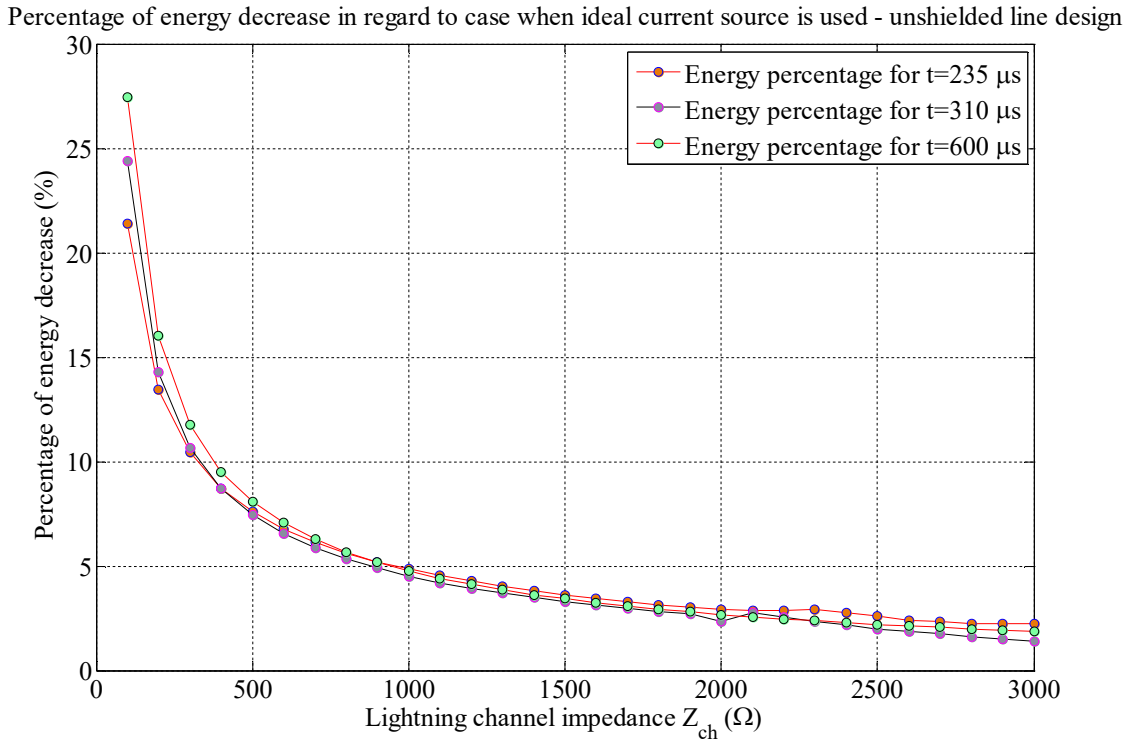


Figure 6.4.22. Percentage of energy decrease for different time points in regard to case when ideal current source is used – unshielded line design

6.4.6. Influence of Lightning Channel Impedance on Line Surge Arrester Energy Duty – Shielded Line Design

Shielded line model is described in previous sections. In this case lightning stroke hits tower top. Tower footing resistance is 20 Ω . Lightning current is bipolar lightning from figure 4.2.1 and lightning channel impedance is varied from 100 Ω to 3000 Ω . Simulations are performed for different values of lightning channel impedance, while other parameters stay the same in all simulation cases. Arresters installed on bottom phase will be the most stressed. Thus, energy change for arrester installed on bottom phase is considered. In case when lightning stroke is modelled as ideal current source arrester energy has value of 10.4589 kJ. Table 6.4.6 presents arrester energy for different values of lightning channel impedance and percentage of energy decrease in regard to case when ideal current source is used.

Table 6.4.6. . Maximum line surge arrester energy for different values of lightning channel impedance and percentage of energy decrease – shielded line design

Z_{ch} (Ω)	Arrester Energy (kJ)	Percentage of energy decrease (%)	Z_{ch} (Ω)	Arrester Energy (kJ)	Percentage of energy decrease (%)
100	5.9639	42.9773	1600	10.1150	3.2876
200	7.9479	24.0083	1700	10.1350	3.0966
300	8.7240	16.5877	1800	10.1528	2.9266
400	9.1351	12.6572	1900	10.1687	2.7744
500	9.3889	10.2300	2000	10.1830	2.6375
600	9.5613	8.5824	2100	10.1960	2.5134
700	9.6858	7.3913	2200	10.2078	2.4006
800	9.7800	6.4908	2300	10.2187	2.2968
900	9.8537	5.7862	2400	10.2286	2.2018
1000	9.9129	5.2198	2500	10.2377	2.1146
1100	9.9616	4.7550	2600	10.2461	2.0341
1200	10.0023	4.3658	2700	10.2539	1.9599
1300	10.0368	4.0354	2800	10.2612	1.8901
1400	10.0667	3.7497	2900	10.2679	1.8256
1500	10.0924	3.5037	3000	10.2743	1.7653

When lightning channel impedance is 100 Ω arrester energy is 5.9639 kJ - that means decrease of energy of 42.9773 % in regard to ideal current source. Energy decrease for impedance of 400 Ω (that is very often used) is 12.6572 %. Changes of energy for different lightning channel impedances are significant. For resistance from 100 Ω to 1000 Ω changes of energy are higher, for resistance values higher than 1000 Ω arrester energy changes are lower. Also, for resistance values higher of 1000 Ω changes of arrester energy are lower than 5%. Energy of line surge arrester for shielded line is much lower than energy capability of line surge arrester. Thus, these energy changes caused by variation of lightning channel impedance are not so important for shielded line design. This means that selection of lightning channel impedance is not so important for case of shielded line design.

Arrester energy for different values of lightning channel impedance and in time points when bipolar lightning flash changes polarity is given in figure 6.4.23. Figure 6.4.24 illustrates percentage of energy decrease in regard to case when ideal current source is used.

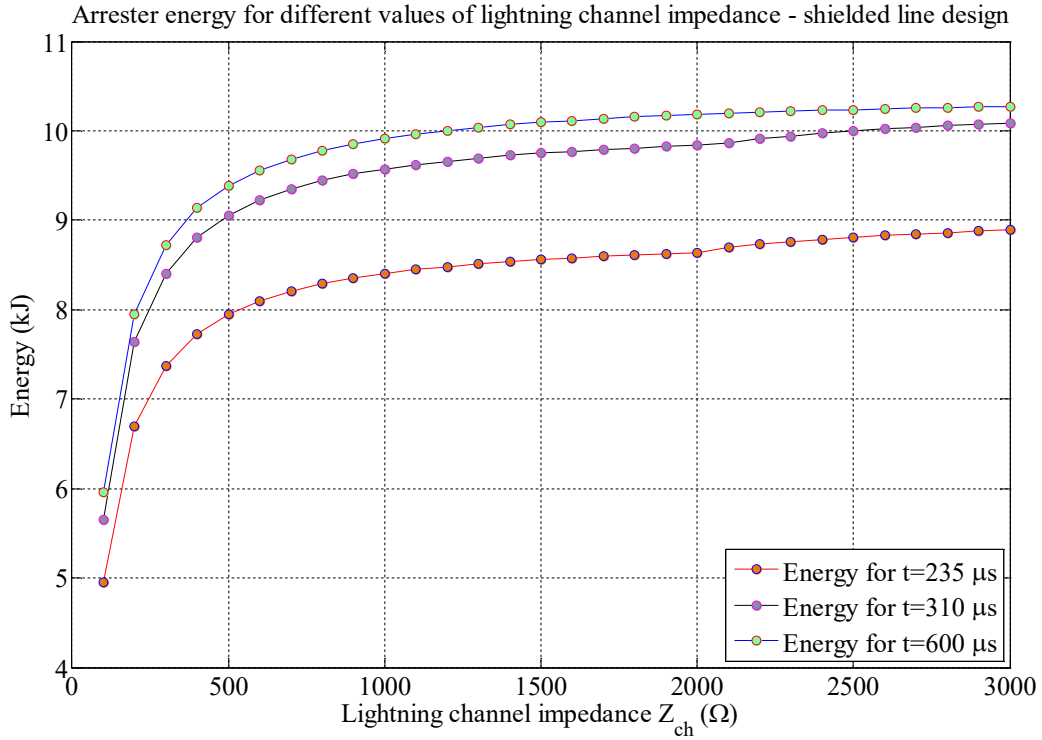


Figure 6.4.23. Arrester energy for different values of lightning channel impedance – shielded line design

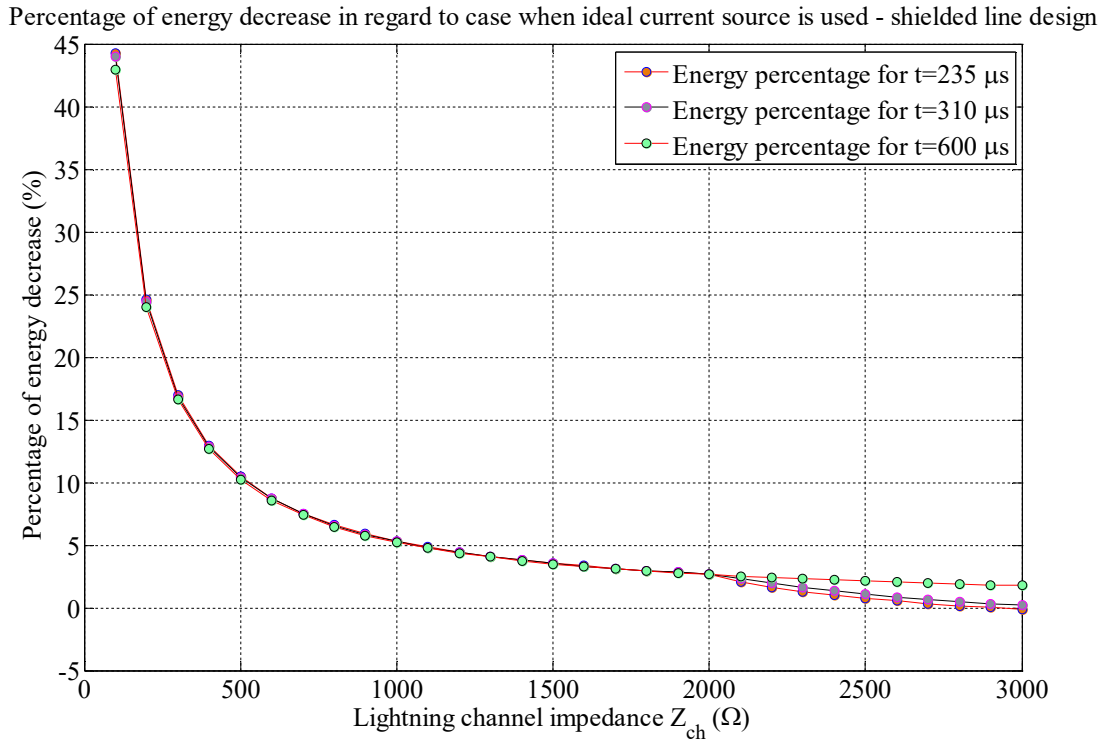


Figure 6.4.24. Percentage of energy decrease for different time points in regard to case when ideal current source is used – shielded line design

6.4.7. Influence of Non – Uniform Tower Footing Resistance Distribution on Line Surge Arrester Energy Duty – Unshielded Line Design

Previous considerations show the energy profile for the case when all towers have the same footing resistance. It is well known that transmission line has a different footing resistance along the line route.

Figure 6.4.25 represents arrester energy and distance of corresponding towers from the point of lightning impact for case when all towers have the same footing resistance. If we consider only 15 towers from both sides of the point of the lightning impact and if span or a line length between two towers is considered as a mean value of 300 meters, in fact we consider part of the transmission line with length of about 10 km. Definitely, it is not possible that all towers in range of 10 km have the same tower footing resistance.

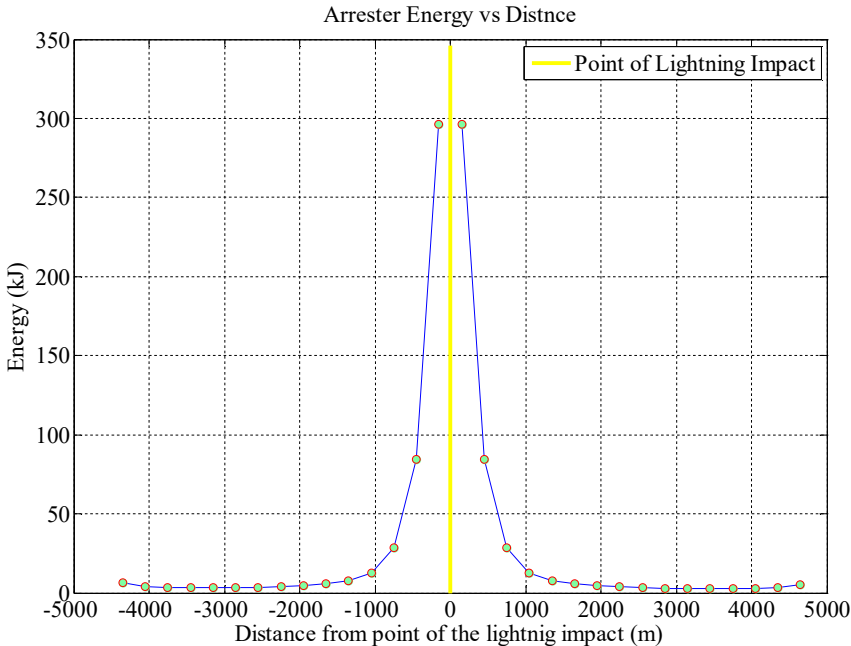


Figure 6.4.25 Arrester energy vs. distance from the point of lightning impact – towers have same footing resistance

Transmission line usually passes through different terrain configurations. That means changes of tower footing resistance. Usually tower footing resistance has lower value on transmission line ends near substations, while for transmission line passing through rocky terrain tower footing resistance has greater value, but that is not always case. This depends on soil and on what has been done by utility. However, transmission line can be considered for low tower footing resistance regions and for high tower footing resistance regions, as it is illustrated in figure 6.4.26.

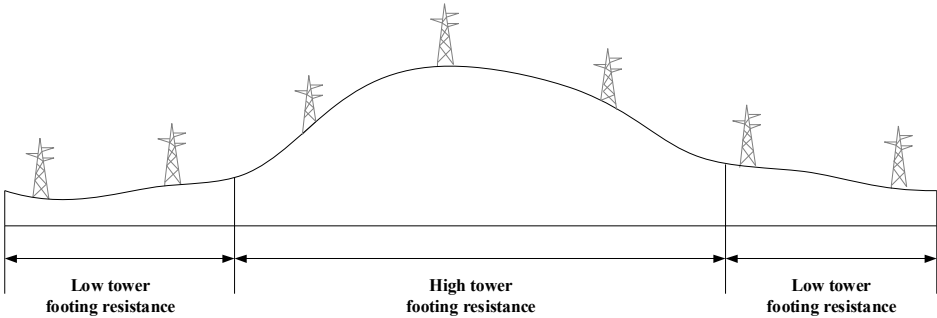


Figure 6.4.26. Illustration of low and high tower footing resistance regions

Using Monte Carlo method tower footing resistance value is varied along the line route. Two cases are considered:

- region of low tower footing resistance and
- region of high tower footing resistance.

A large number of Monte Carlo simulations is performed. Figure 6.4.27 represents arrester energy change for 50 Monte Carlo simulations.

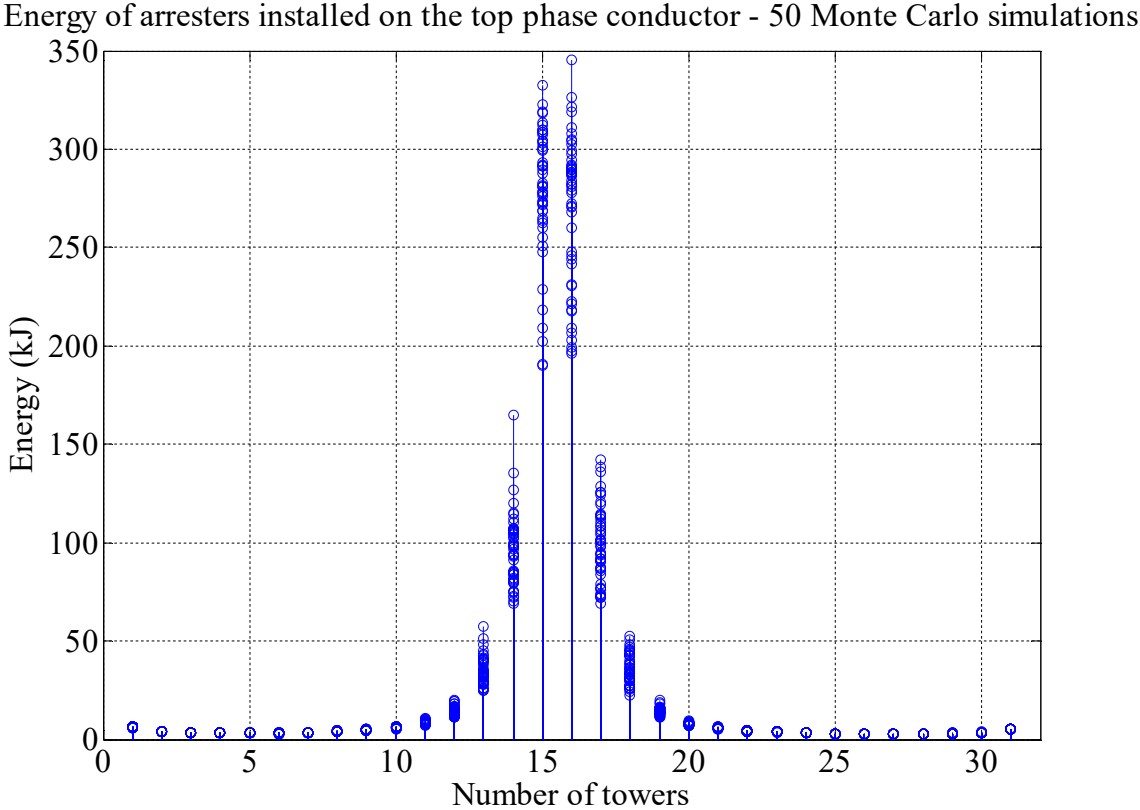


Figure 6.4.27. Energy of arresters for 50 Monte Carlo simulations

From figure 6.4.27 it can be seen that change of tower footing resistance has influence on five towers from point of lightning impact. As a tower footing resistance changes, arrester energy also changes in significant interval. It should be noted that modelling of the far towers is important for knowing how much energy arresters, installed on those towers, will absorb and also for more accurate calculation of energy duty for nearest arresters.

Region of low tower footing resistance

Figure 6.4.28 represents tower footing resistance sample of 5 simulation cases. Tower footing resistance for each tower was randomly determined using Monte Carlo method. For low tower footing resistance region, tower footing resistance was randomly varied from 5 Ω to 35 Ω.

Energies of line surge arresters installed on the top phase conductor for five corresponding simulations from figure 6.4.28 are shown in figure 6.4.29.

Figure 6.4.30 represents (for better visualization and understanding) tower footing resistance (non – uniform distribution) and corresponding arrester energies along transmission line.

Examples of uniform and non-uniform tower footing resistance distributions are shown in figure 6.4.31. Arresters energies for uniform and non-uniform tower footing resistance distributions from figure 6.4.31 are presented in figure 6.4.32.

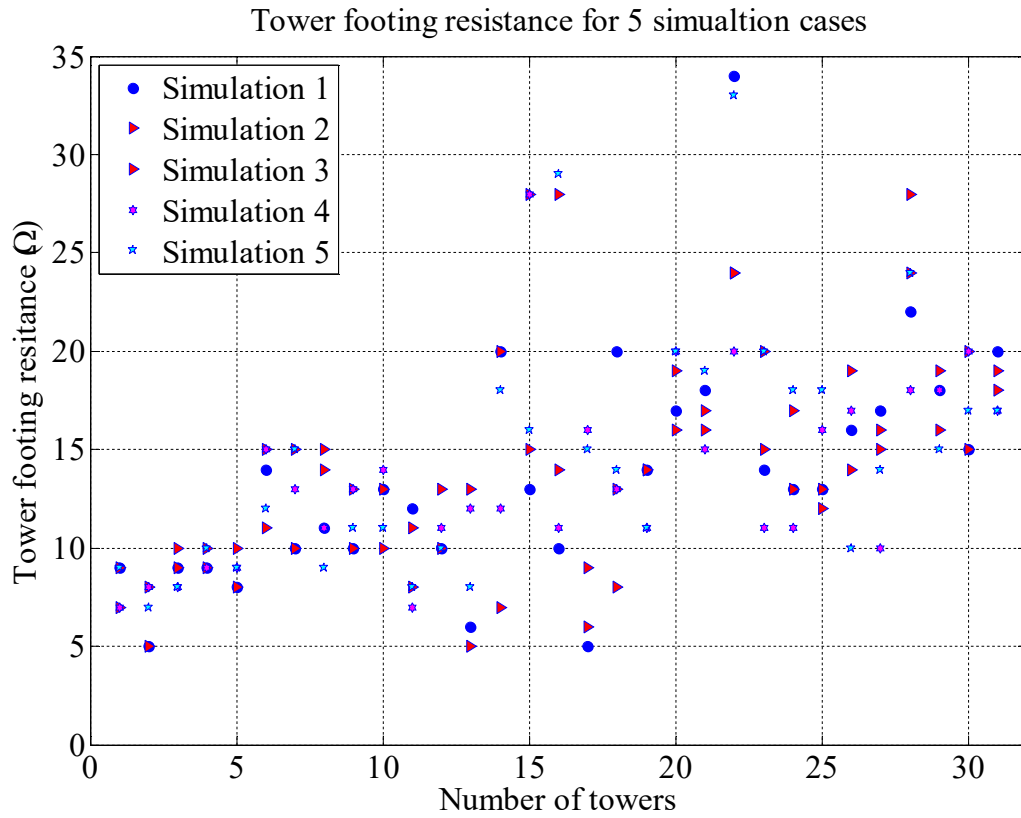


Figure 6.4.28. Tower footing resistance for 5 simulation cases

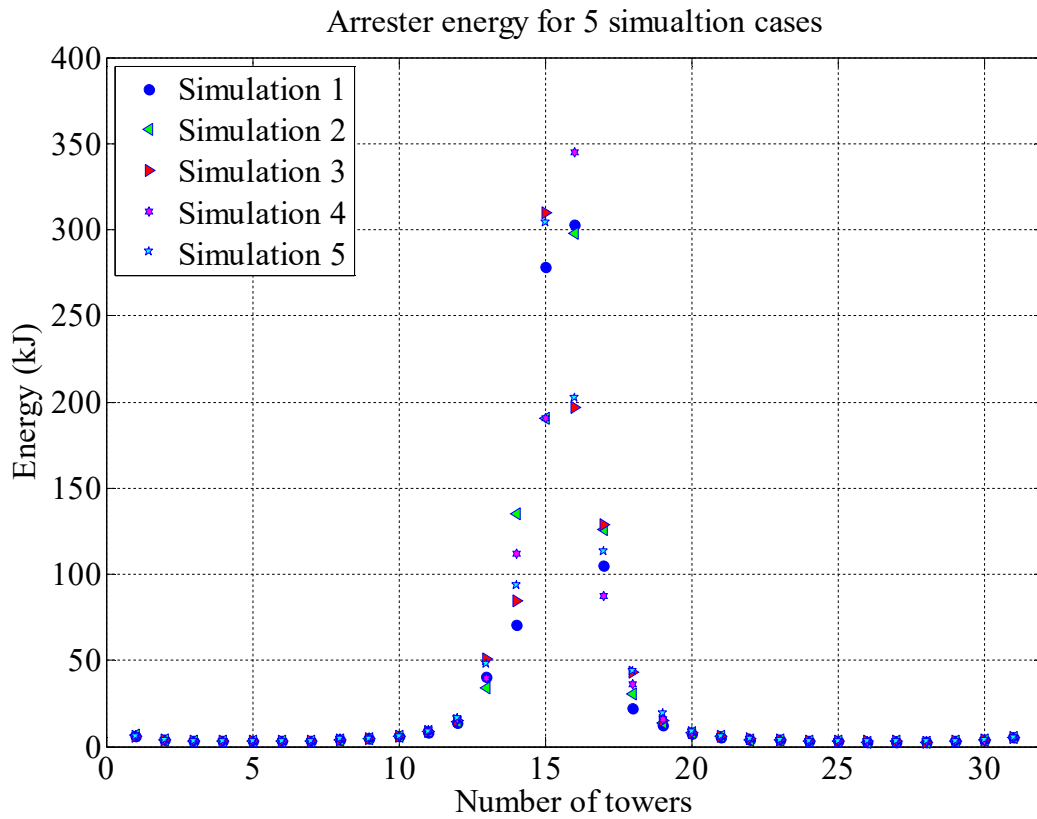


Figure 6.4.29. Arrester energy for 5 simulation cases

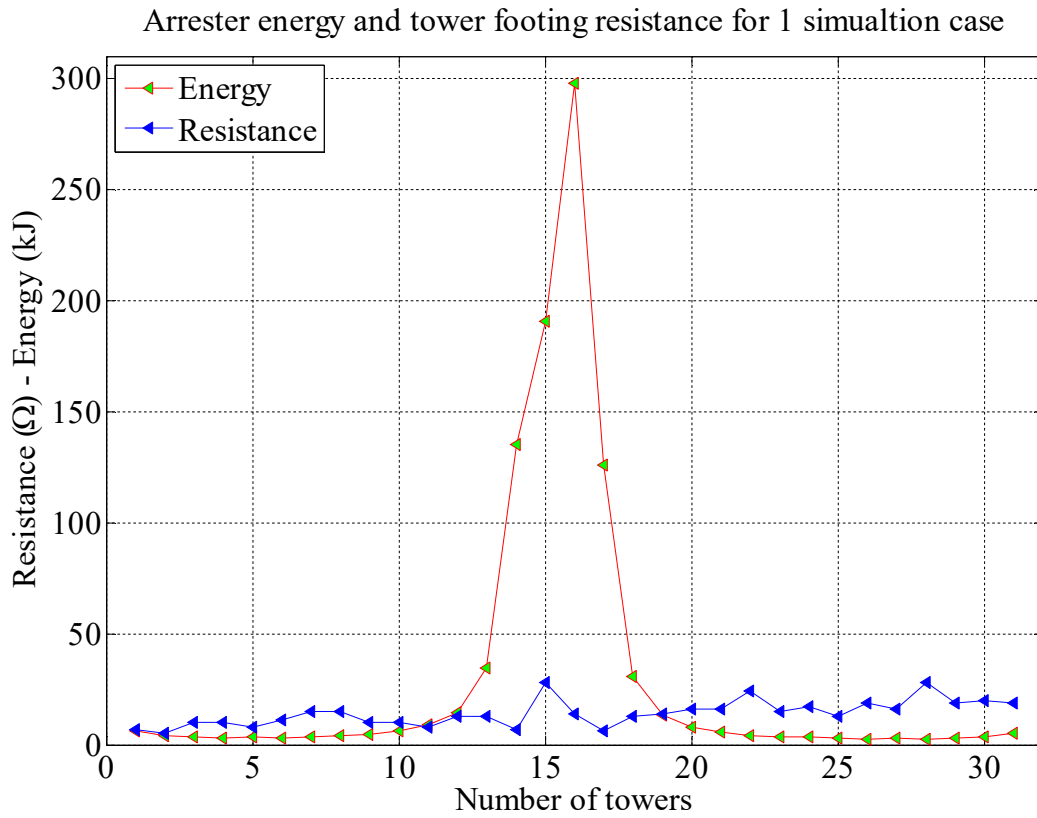


Figure 6.4.30. Arrester energy and tower footing resistance for 1 simulation case

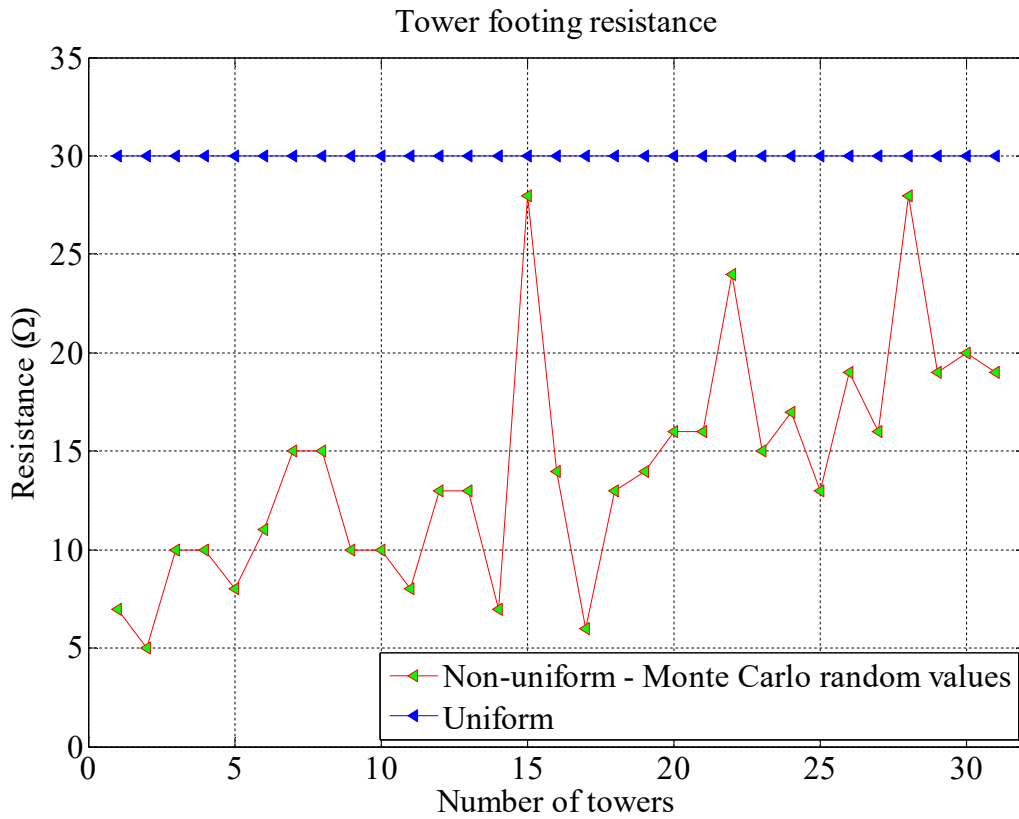


Figure 6.4.31. Examples of uniform and non-uniform tower footing resistance distributions

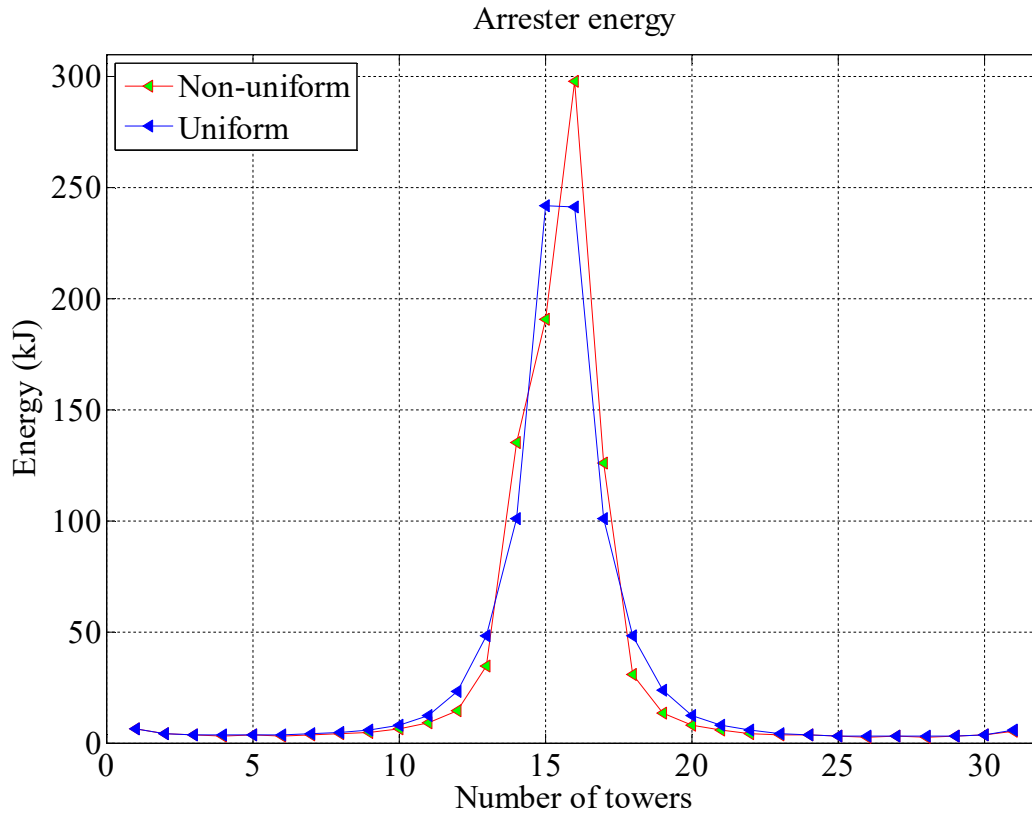


Figure 6.4.32. Arresters energies for uniform and non-uniform tower footing resistance distributions from figure 6.4.31

From previously presented figures it is possible to conclude that change of tower footing resistance has influence on arresters installed on eight towers on the both sides from the point of the lightning impact. In low tower footing resistance region the energy absorbed by the nearest arrester decreases with increasing tower footing resistance.

Region of high tower footing resistance

Figure 6.4.33 represents tower footing resistance sample of 5 simulation cases. Tower footing resistance for each tower was randomly determined using Monte Carlo method. For high tower footing resistance region, tower footing resistance was randomly varied from 35 Ω to 100 Ω .

Energies of line surge arresters installed on the top phase conductor for five corresponding simulations from figure 6.4.33 are shown in figure 6.4.34.

Figure 6.4.35 represents (for better visualization and understanding) tower footing resistance (non – uniform distribution) and corresponding arrester energies along transmission line.

Examples of uniform and non-uniform tower footing resistance distributions are shown in figure 6.4.36. Arresters energies for uniform and non-uniform tower footing resistance distributions from figure 6.4.36 are presented in figure 6.4.37.

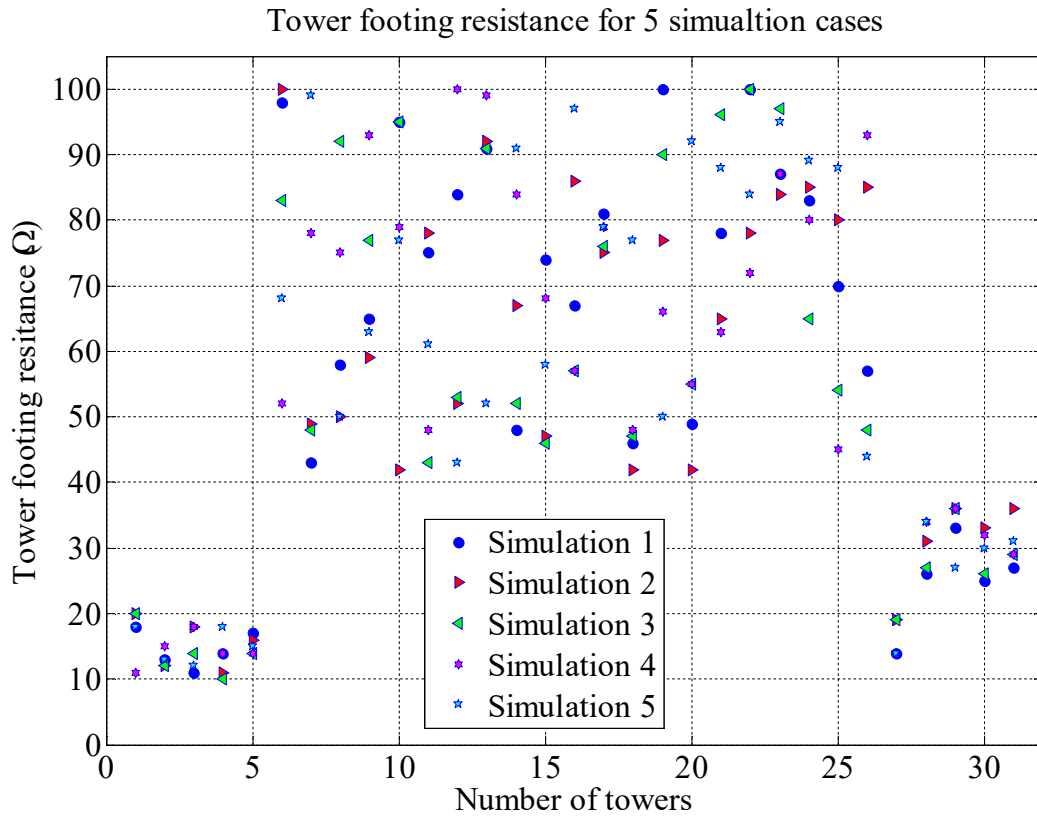


Figure 6.4.33. Tower footing resistance for 5 simulation cases

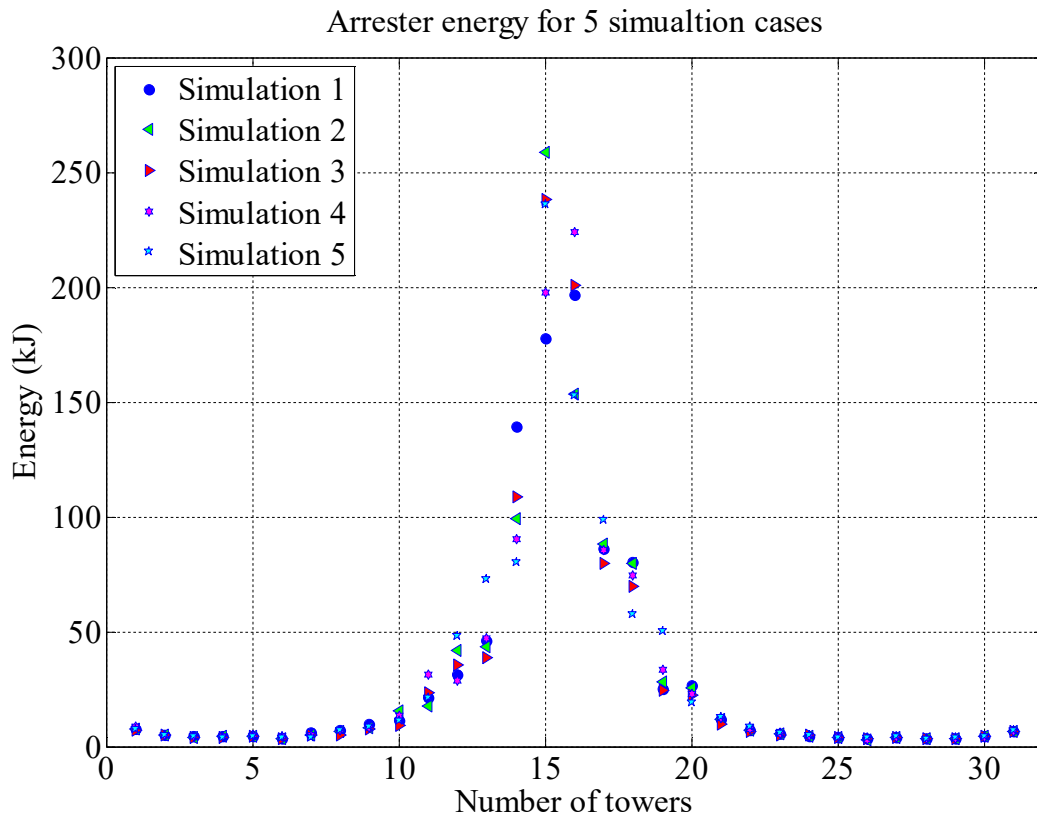


Figure 6.4.34. Arrester energy for 5 simulation cases

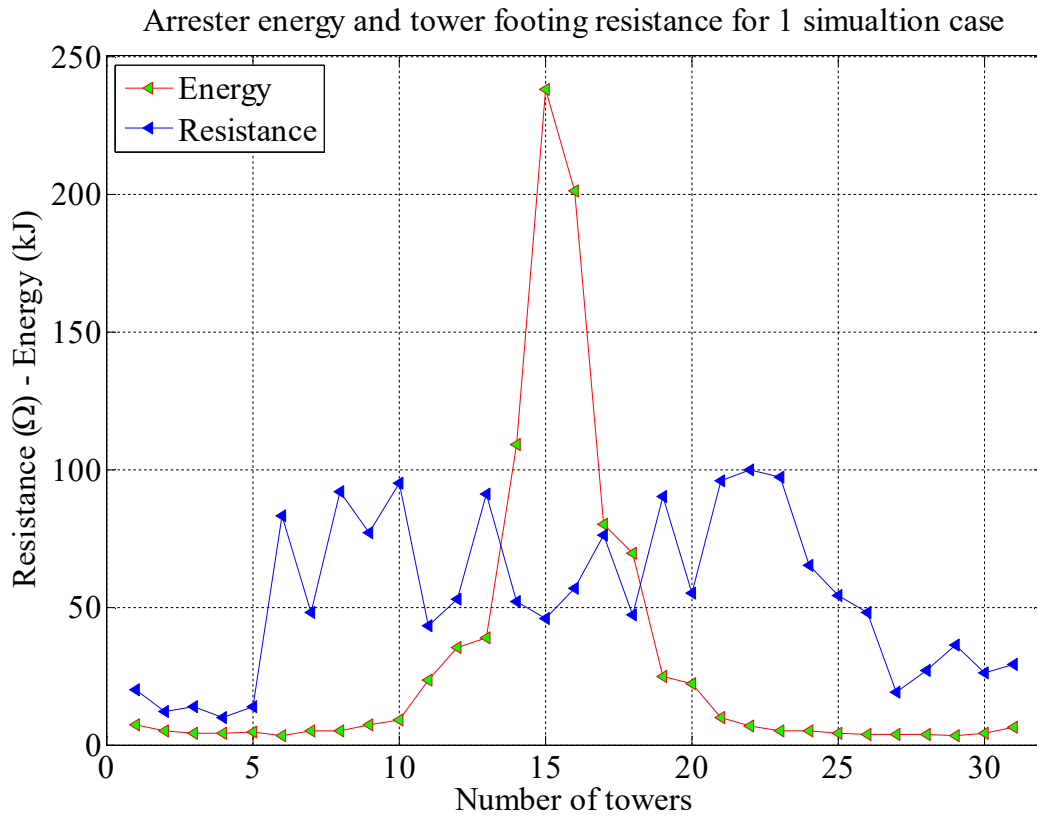


Figure 6.4.35. Arrester energy and tower footing resistance for 1 simulation case

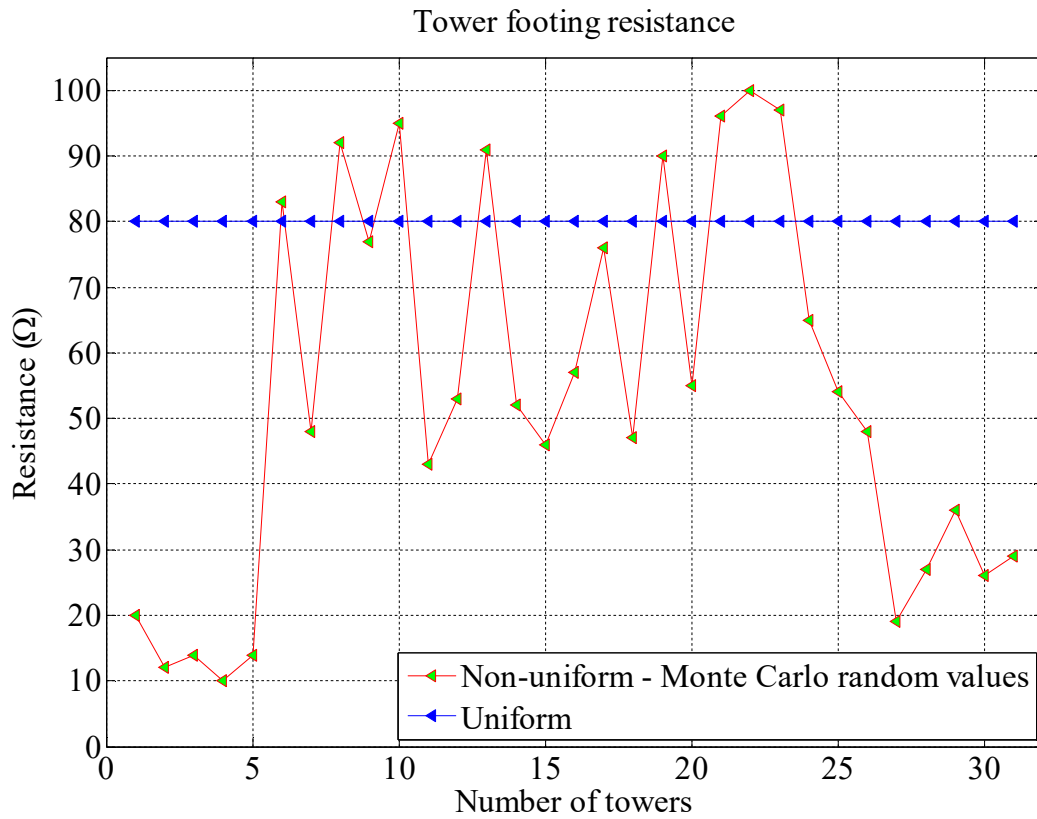


Figure 6.4.36. Examples of uniform and non-uniform tower footing resistance distributions

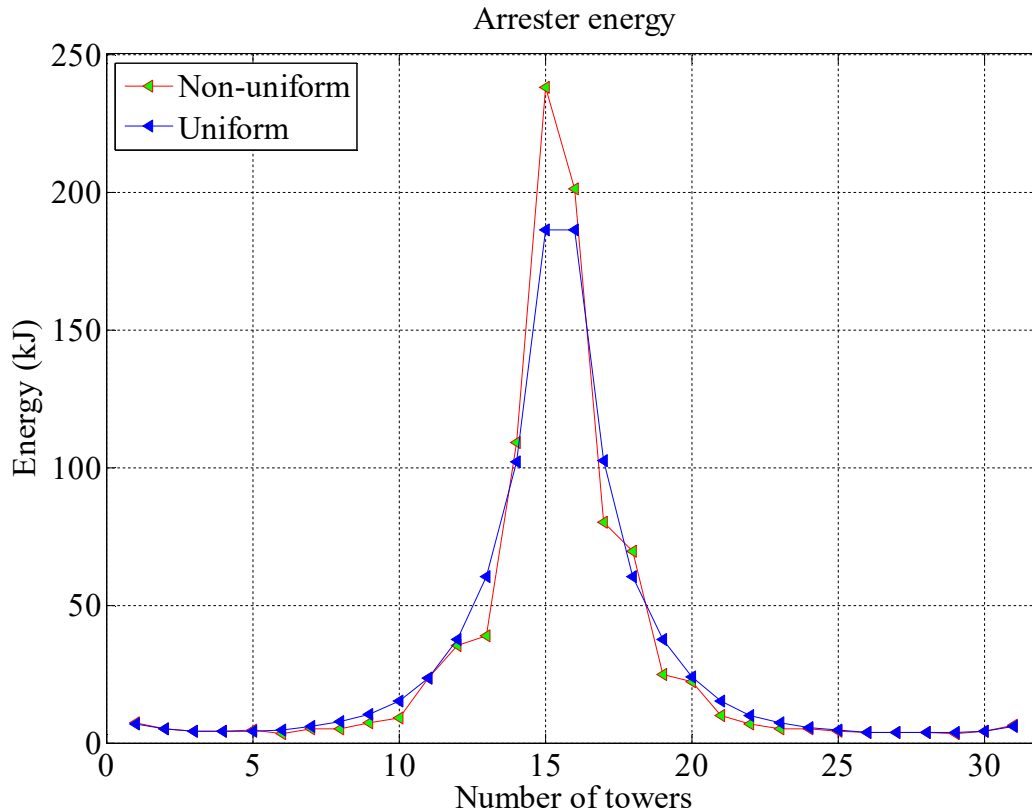


Figure 6.4.37. Arresters energies for uniform and non-uniform tower footing resistance distributions from figure 6.30

From previously presented figures it is possible to conclude that change of tower footing resistance has influence on arresters installed on eight towers on the both sides from the point of the lightning impact. In case of higher tower footing resistance adjacent towers absorb more energy than in case of low tower footing resistance region.

6.4.8. Influence of Non – Uniform Distributed Tower Footing Resistance on Line Surge Arrester Energy Duty for Nearest and Farthest Tower

Nearest tower

Monte Carlo variation of tower footing resistance for tower nearest to the point of lightning impact is represented in figure 6.4.38, while change of energy is represented in figure 6.4.39. Histograms of tower footing resistance and arrester energy are shown in figures 6.4.40 and 6.4.41, respectively. From energy histogram it is possible to conclude that significant changes of energy exist.

Maximum and minimum tower footing resistance values are 29 Ω and 10 Ω , respectively. Mean value of tower footing resistance is 15.1 Ω . While, variance and standard deviation are 30.5 Ω and 5,522 Ω .

Maximum and minimum arrester energy values are 332.5403 kJ and 190.2190 kJ, respectively. Mean value of arrester energy is 278.5491 kJ. While, variance and standard deviation are 1127.7960 kJ and 33.5827 kJ.

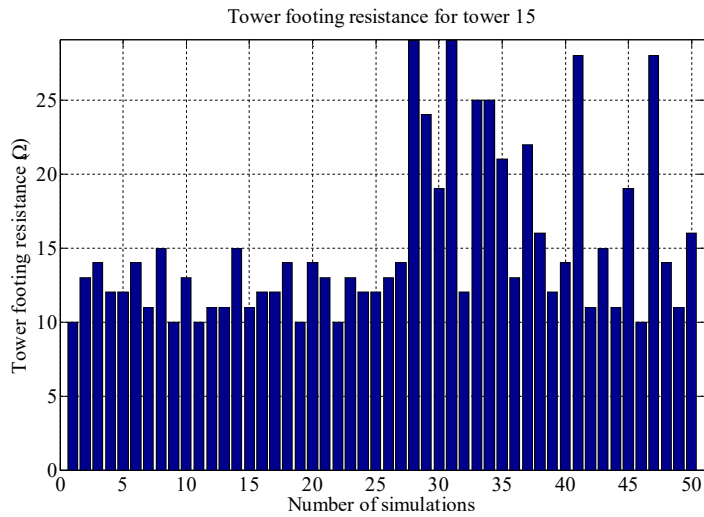


Figure 6.4.38. Change of tower footing resistance for tower nearest to the point of lightning impact

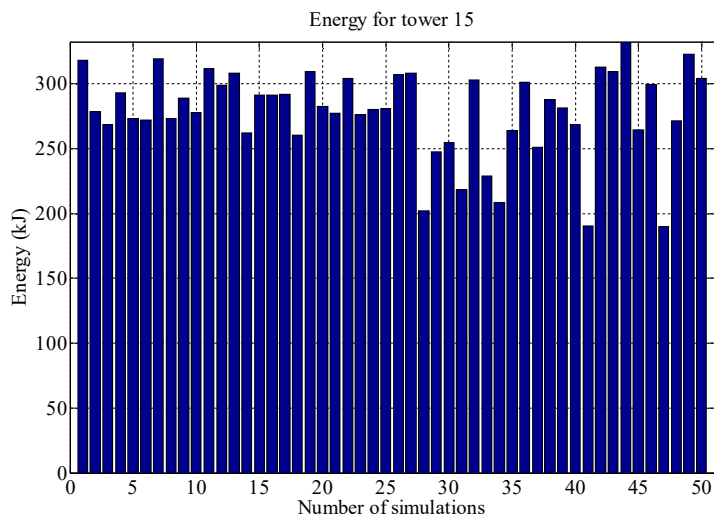


Figure 6.4.39. Change of energy of arrester installed on tower nearest to the point of lightning impact

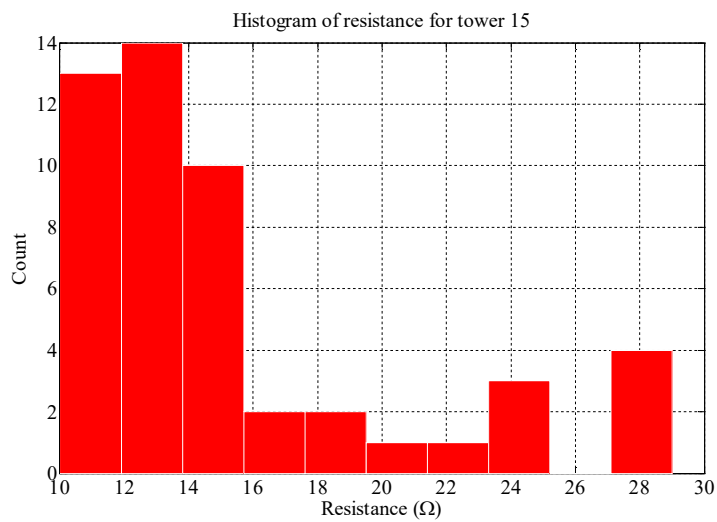


Figure 6.4.40. Histogram of tower footing resistance for tower nearest to the point of lightning impact

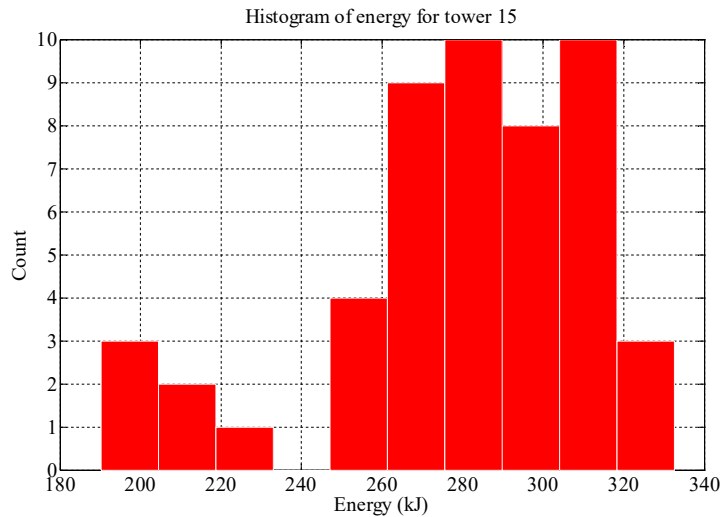


Figure 6.4.41. Histogram of energy for arrester installed on tower nearest to the point of lightning impact

Farthest tower

Monte Carlo variation of tower footing resistance for tower farthest to the point of lightning impact is represented in figure 6.4.42, while change of energy is represented in figure 6.4.43. Histograms of tower footing resistance and arrester energy are shown in figures 6.4.44 and 6.4.45, respectively. From energy histogram it is possible to conclude that there is no significant energy change, in ranges from 6 kJ to 6.5kJ.

Maximum and minimum tower footing resistance values are 10 Ω and 5 Ω , respectively. Mean value of tower footing resistance is 7.42 Ω . While, variance and standard deviation are 3.1873 Ω and 1.7853 Ω .

Maximum and minimum arrester energy values are 6.5238 kJ and 6.2190 kJ, respectively. Mean value of arrester energy is 6.2638 kJ. While, variance and standard deviation are 0.0116 kJ and 0.1078 kJ.

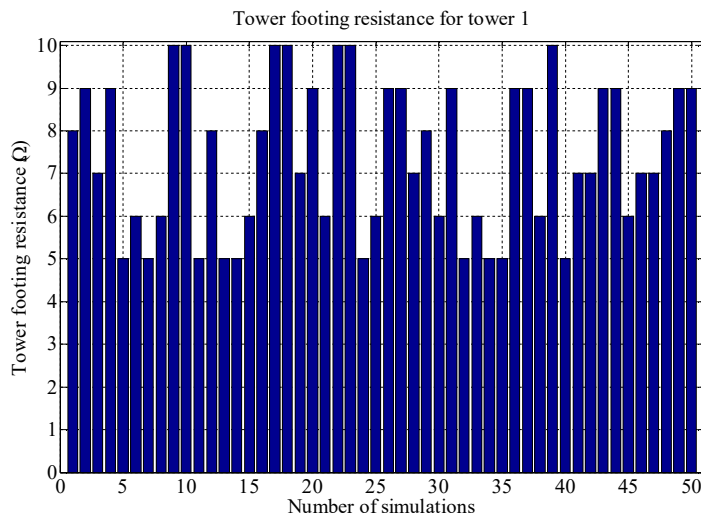


Figure 6.4.42. Change of tower footing resistance for tower farthest of the point of lightning impact

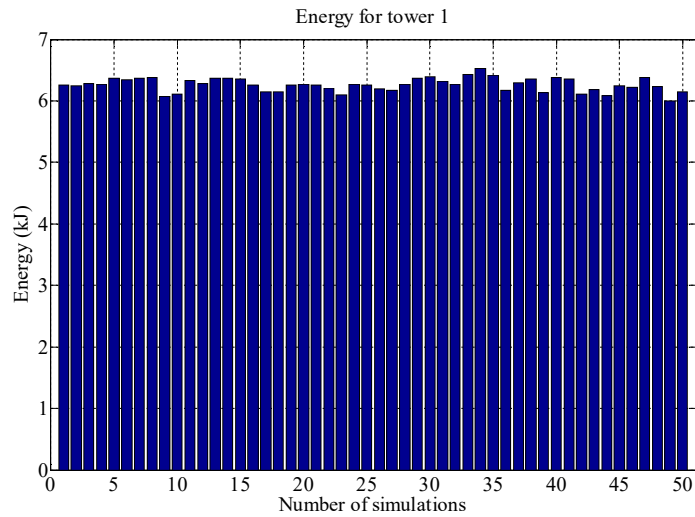


Figure 6.4.43. Change of energy of arrester installed on tower farthest to the point of lightning impact

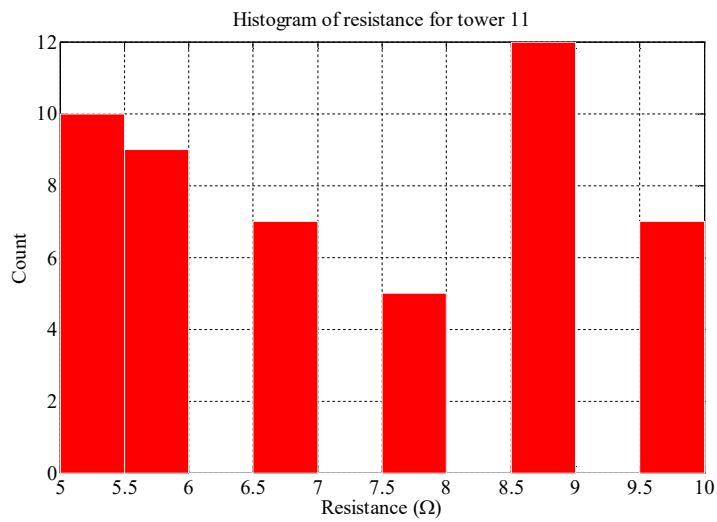


Figure 6.4.44. Histogram of tower footing resistance for tower farthest to the point of lightning impact

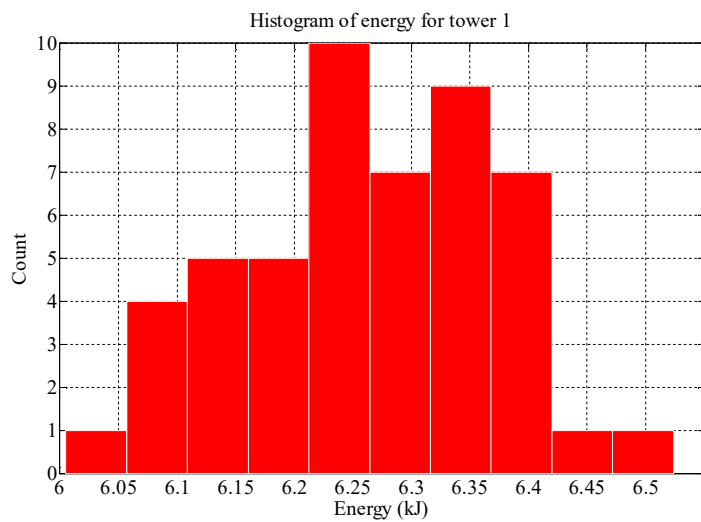


Figure 6.4.45. Histogram of energy for arrester installed on tower farthest to the point of lightning impact

6.4.9. Influence of Front Time, Tail Time and Current Peak on Arrester Energy Duty

In order to analyse influence of front and tail time on line surge arrester energy duty multicomponent flash #1 was used in simulations. To show influence of lightning current peak on line surge arrester energy duty multicomponent flash #3 was used.

Case 1 – Simulations for different front time were conducted, while tail time and current peak were the same.

Input data for lightning flash were: current peak, tail time and front time, while output data is line surge arrester energy. These data are presented in table from 6.4.7 to 6.4.10 and illustrated in figure 6.4.46.

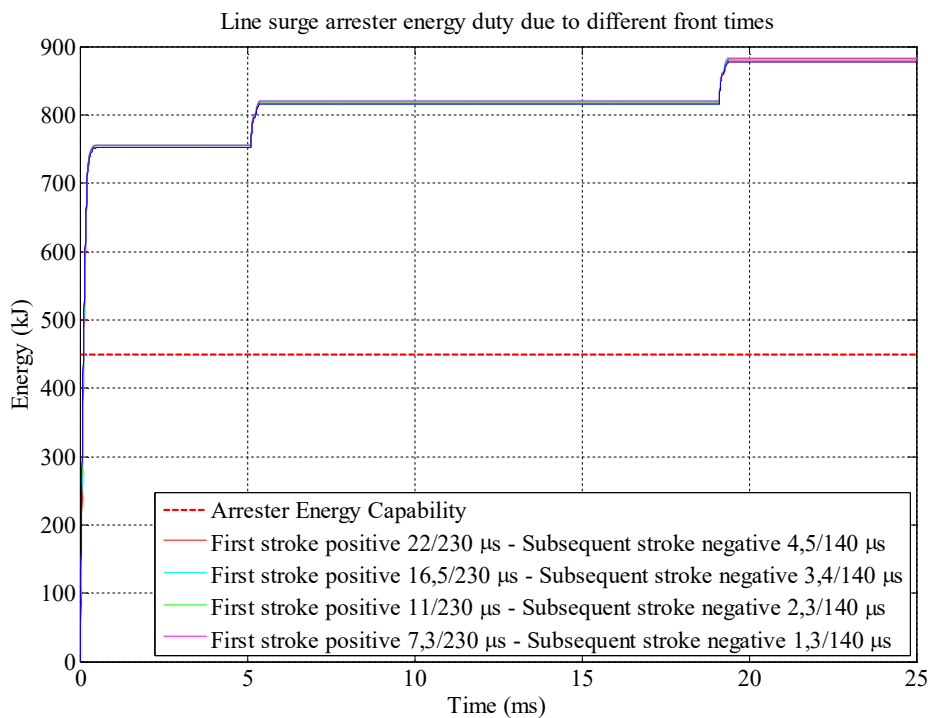


Figure 6.4.46. Arrester energy duty due to different front times – unshielded line design

Table 6.4.7. Input and output data for simulation 1 – different front time

Stroke	Peak (kA)	Tail time(μs)	Front time (μs)	Arrester energy (kJ)
First	36.7	230	22	752.32
Subsequent #1	-7.3	140	4.5	816.99
Subsequent #2	-7.1	140	4.5	879.11

Table 6.4.8. Input and output data for simulation 2 – different front time

Stroke	Peak (kA)	Tail time(μs)	Front time (μs)	Arrester energy (kJ)
First	36.7	230	16.5	755.17
Subsequent #1	-7.3	140	3.4	820.80
Subsequent #2	-7.1	140	3.4	883.88

Table 6.4.9. Input and output data for simulation 3 – different front time

Stroke	Peak (kA)	Tail time(μ s)	Front time (μ s)	Arrester energy (kJ)
First	36.7	230	11	754.88
Subsequent #1	-7.3	140	2.3	819.29
Subsequent #2	-7.1	140	2.3	881.20

Table 6.4.10. Input and output data for simulation 4 – different front time

Stroke	Peak (kA)	Tail time(μ s)	Front time (μ s)	Arrester energy (kJ)
First	36.7	230	7.3	755.27
Subsequent #1	-7.3	140	1.3	819.52
Subsequent #2	-7.1	140	1.3	881.24

From previously presented data it can be concluded that front time has not significant influence on line surge arrester energy duty calculation. For example, for front time of 22 μ s arrester energy has value of 752.32 kJ, while for front time of 7.3 μ s arrester energy has value of 755.27 kJ. Difference of 2.95 kJ (or 0.4%) is negligible.

Case 2 – Simulations for different tail time were conducted, while front time and current peak were the same. Input data for lightning flash were: current peak, tail time and front time, while output data is line surge arrester energy. These data are presented in table from 6.4.11 to 6.4.14 and illustrated in figure 6.4.47.

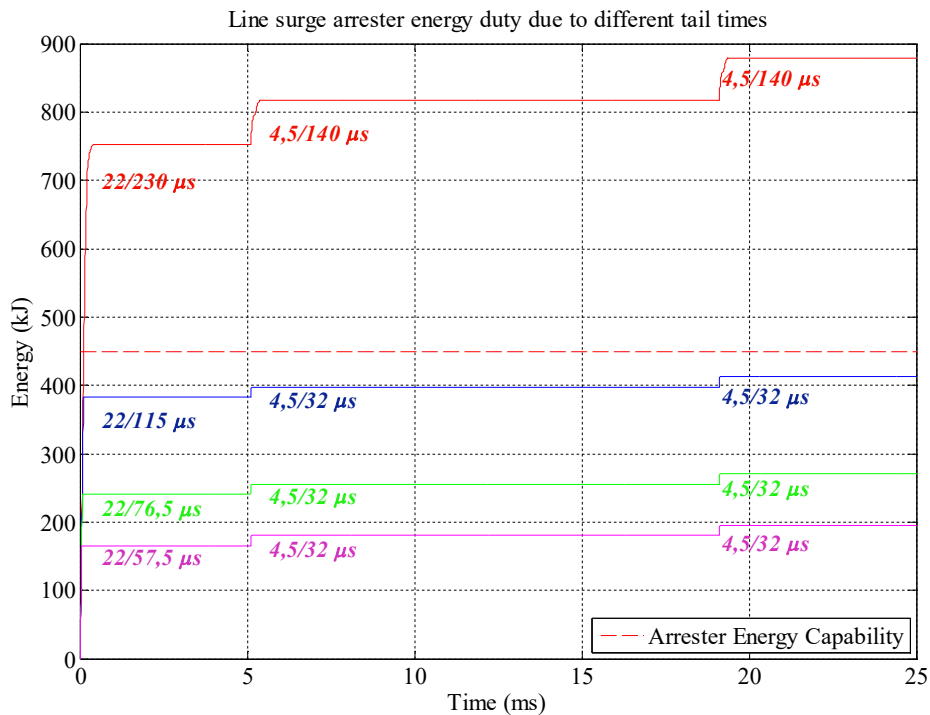


Figure 6.4.47. Arrester energy duty due to different tail times – unshielded line design

Table 6.4.11. Input and output data for simulation 1 – different tail time

Stroke	Peak (kA)	Front time (μs)	Tail time(μs)	Arrester energy (kJ)
First	36.7	22	230	752.32
Subsequent #1	-7.3	4.5	140	816.99
Subsequent #2	-7.1	4.5	140	879.11

Table 6.4.12. Input and output data for simulation 2 – different tail time

Stroke	Peak (kA)	Front time (μs)	Tail time(μs))	Arrester energy (kJ)
First	36.7	22	115	382.63
Subsequent #1	-7.3	4.5	32	397.78
Subsequent #2	-7.1	4.5	32	412.33

Table 6.4.13. Input and output data for simulation 3 – different tail time

Stroke	Peak (kA)	Front time (μs)	Tail time(μs)	Arrester energy (kJ)
First	36.7	22	76.5	240.19
Subsequent #1	-7.3	4.5	32	255.64
Subsequent #2	-7.1	4.5	32	270.19

Table 6.4.14. Input and output data for simulation 4 – different tail time

Stroke	Peak (kA)	Front time (μs)	Tail time(μs)	Arrester energy (kJ)
First	36.7	22	57.5	165.60
Subsequent #1	-7.3	4.5	32	180.75
Subsequent #2	-7.1	4.5	32	195.55

Amount of arrester discharge energy depends on number of components in flash, but also it strongly depends on time to half of the stroke current.

Case 3 – Simulations for different tail time due to flash #3 were conducted. Arrester energy duty due to different tail times is shown in figure 6.4.48.

Simulation case with first stroke 18/200 μs and subsequent strokes 4.5/140 μs should be considered to emphasis current peak effect. Flash #3 current peaks and line surge arrester energy values due to flash #3 are given in table 6.4.15.

Table 6.4.15. Input and output data for simulation 4 – different tail time

Stroke	Peak (kA)	Front time (μs)	Tail time(μs)	Arrester energy (kJ)
First	-27	18	200	488.7
Subsequent #1	-39.8	4.5	140	973.3
Subsequent #2	-42.7	4.5	140	1537.0
Subsequent #3	-15.9	4.5	140	1736.3
Subsequent #4	-30.6	4.5	140	2137.3
Subsequent #5	-14.2	4.5	140	2305.3
Subsequent #6	-14.2	4.5	140	2468.8
Subsequent #7	-7.5	4.5	140	2549.0
Subsequent #8	-15.1	4.5	140	2727.7

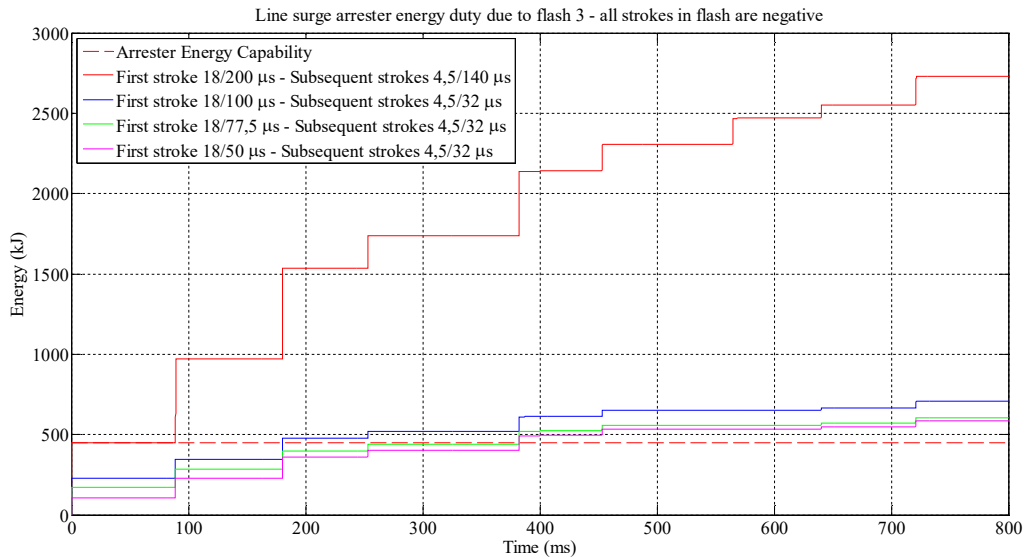


Figure 6.4.48. Arrester energy duty due to different tail times – unshielded line design

In case of higher current peaks (but front and tail times are same) arrester energy increase is greater. For example, for current peak of -42.7 kA energy increase is 563.7 kJ, while for current peak of -7.5 kA energy increase is 80.2 kJ.

It has to be mentioned that during simulations and considerations all towers are equipped with line surge arresters. In real systems usually line surge arrester are not installed on all phase conductors and on all towers.

In this chapter it is shown that line surge arrester energy duty due to bipolar and multicomponent lightning flashes has very high values, especially for unshielded line design. Therefore, due to dimensioning these facts should be taken into account. Some results are summarized in tables below. It is important to emphasise that energy capability of the considered line surge arrester is 450 kJ.

Table 6.4.16. Energy duty values due to bipolar lightning flash for unshielded and shielded line design

	Unshielded line E (kJ)	Shielded line E (kJ)
Negative part of bipolar (-52.86 kA)	116.68	3.4
Positive part of bipolar (26.9 kA)	212.29	3.9

Table 6.4.17. Energy duty values due to multicomponent lightning flash for unshielded and shielded line design

	Unshielded line E (kJ)	Shielded line E (kJ)
First stroke (36.7 kA, 22/230 μ s)	752.5	1.31
Second stroke (-7.3 kA, 4.5/140 μ s)	817.0	1.31
Third stroke (-7.2 kA, 4.5/140 μ s)	879.1	1.31

Chapter 7.

SUMMARY OF RESULTS, CONCLUSIONS AND RECOMMENDATIONS

The aim of this thesis was transmission lines surge arrester energy duty calculation and consideration due to bipolar and multicomponent lightning flashes. Motivation for this thesis was described in chapter 1. In this chapter, summary of results, conclusions and recommendations for future work are given.

Chapter 2 presents phenomenology and classification of lightning discharges. Bipolar lightning is poorly understood and often unrecognized phenomenon. To date, the knowledge of the physics of bipolar lightning is not as sufficient as that of negative or positive lightning. However, bipolar events were recorded all over the world. Most of bipolar lightning flashes were recorded on tall objects. Measurements of lightning currents on tall towers provide a useful way to investigate the occurrence of bipolar flashes. In Chapter 2, bipolar lightning is defined, as well as its parameters. An overview of different types of bipolar lightning discharges is also given. Furthermore, a term multiplicity is explained and basic facts regarding multicomponent lightning flashes are presented. During literature review it has been concluded that bipolar and multicomponent lightning flashes are very destructive. Also it is shown that, when compared to unipolar negative lightning flashes, bipolar and multicomponent lightning flashes rarely occur, but they do occur often, especially in very high regions and from tall objects. A large number of electrical power system objects, especially transmission lines are located on mountains and in the regions of high lightning incidence and with high tower footing resistance. Therefore, it is concluded that there is a need for a line surge arrester energy duty considerations due to bipolar and multicomponent flashes.

Line surge arrester is very important protective device for limiting surge voltages on transmission line insulation by discharging or bypassing surge current. It is well known that the energy, stressing line arresters, depends on several factors such as: line design (shielded or unshielded), lightning activity characteristics, number of multiple strokes, lightning polarity and resulting charge levels in first stroke, protective level, shape of the current flowing through the arrester, arrester design (gapless - NEGLA or with a gap - EGLA), considered tower footing resistance (especially for unshielded lines) and tower footing resistance of the neighbouring towers, and in the end, on arrester installation configuration. Chapter 3 describes basic principles regarding transmission line surge arresters and provides explanation of the line surge arrester type considered in this thesis. Considering standards, technical brochures and manufacturer datasheets, it is concluded that there are good reasons for installing both EGLA and NEGLA types. However, it is not possible to generally decide which type is better. The decision to choose EGLA or NEGLA is left to users, based on system characteristic, lightning incidence and environmental conditions of region. For purposes of this thesis, gapless type arrester was considered. The main reason for choosing this type was the fact that all NEGLAs participate in energy sharing. It is very useful to consider energy sharing of line surge arresters installed along a transmission line, as well as energy duty of those arresters due to bipolar flashes and multicomponent flashes. There are differences regarding energy duty for the arrester, depending on

whether or not the line is protected by shield wires. When the line is efficiently protected with shield wires, the high peak lightning strokes will impact the shield wire and it will be partly diverted to ground. Only a fraction of the total lightning current will circulate through the arresters. The shape of the line arrester current will be different than the shape of the original stroke. Thus, the line arrester current tail will be shorter and less energy will be injected in the arrester. In a case of unshielded line, a phase conductor can be hit directly by high peak current lightning strokes. This may produce line surge arrester to be severely stressed. The shape of the line arrester current will be similar to the shape of the original lightning stroke. The energy absorbed by the arrester will be essentially proportional to the charge transfer. Absorbed energy due to negative flashes may have a reasonable value, while for bipolar and multicomponent lightning flashes it may exceed. Therefore, it was decided to consider line surge arrester energy duty for both line designs.

The knowledge about lightning parameters and characteristics for different regions is very useful for transient studies in electrical power systems. Current shape parameters are very important for modelling and simulations. In order to select the appropriate lightning protection system, it is necessary to identify lightning current parameters:

- shape of the lightning current (peak value, front time, tail time and duration)
- polarity and
- multiplicity – number of components of the flash.

For a better protection design, true data recorded from direct measurements at towers and lightning location systems are especially important. Direct measurements at towers provide the most accurate data about lightning current parameters. Therefore, the aim of Chapter 4 was to analyse data obtained from measurements using instrumented tower (at the telecom base station Miluccia in Corsica) and lightning location systems (LINET). It has been shown that bipolar lightning current is characterized with:

- positive and negative charge transfer,
- two current peaks (for positive and negative part),
- two front and two tail times (for positive and negative part) and
- duration of positive and negative part of bipolar stroke.

Data obtained from lightning location systems are also very useful for lightning protection design. Lightning location systems provide the following data:

- lightning stroke current peak,
- lightning stroke polarity,
- number of components in flash and
- interstroke time intervals.

Lightning location systems do not provide data about front and tail time. The front time and tail time can be determined only from direct measurements (if the lightning current shape is recorded). These parameters are needed in making of overhead power lines lightning performance simulations. Therefore, these parameters were selected according to CIGRE and IEEE recommendations.

Line surge arrester energy duty depends on transmission line and lightning flash parameters. Therefore, the quality of the simulation results is mainly based on a proper modelling of all transmission line components and lightning current source. Modelling of transmission lines for transient studies is described in Chapter 5. Firstly, basic mathematical models and circuit representation for transmission line components are described. Afterwards in this chapter, models for transmission line components are developed in EMTP – RV. Transmission line model includes modelling of: phase conductors, shield wire (for shielded line design), transmission line tower, tower footing resistance, line surge arresters, lightning current source and substation.

An analogy has been made between calculation of line surge arrester energy duty in EMTP – RV and MATLAB. It can be concluded from figure 7.1.1 that difference in energy calculated in EMTP – RV

and MATLAB is very small and hardly noticeable. For each time point from 0 μs to 600 μs (with simulation/calculation step of $\Delta t = 10 \text{ ns}$) comparison in energy calculation between EMTP –RV and MATLAB has been made. Maximum energy difference is 2.2148 kJ or 0.9849% (percentage is calculated with respect to energy calculated in EMTP –RV).

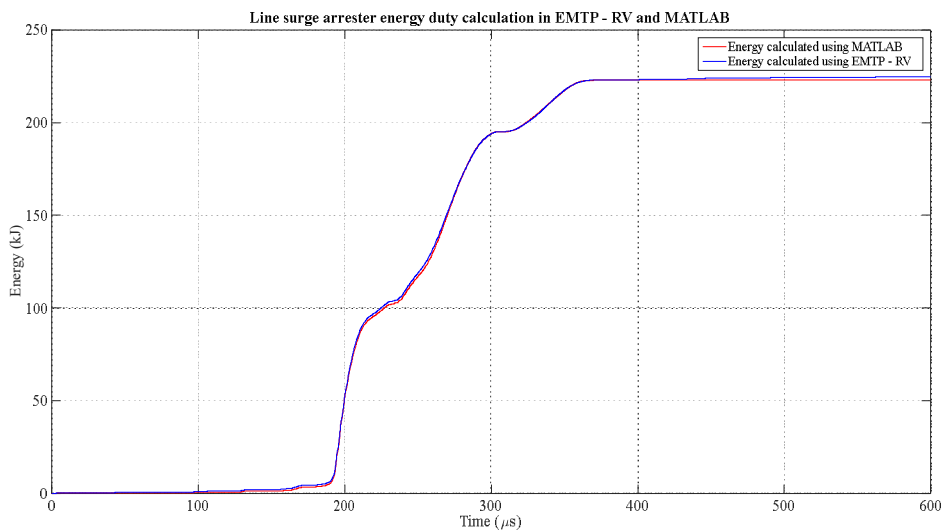


Figure 7.1.1. Analogy between calculation of line surge arrester energy duty in EMTP – RV and MATLAB

Simulations for a transient analysis of the transmission lines are commonly based on a model that consists of only few towers on the both sides from the point of the lightning impact. In this thesis the complete transmission line is created and solved in the EMTP – RV for the first time.

EMTP – RV software has a very important and useful feature. It has possibility of grouping basic electrical elements into higher structures, commonly named subcircuits. Furthermore, subcircuits can be grouped into more complex subcircuits. The main idea of the EMTP – RV modelling in this work consists of grouping subcircuits inside the other (more complex) subcircuits with the possible connections between all elements in the model. For example, basic EMTP – RV elements such as inductances, CP line single phase version, insulators and EMTP – RV pins are grouped into subcircuit that represents transmission line tower. A certain number of the tower subcircuit elements, spans, line surge arresters, grounding footing resistances and the corresponding pins (for connection with other elements) are all grouped into the complex subcircuit element that represents the transmission line section.

Therefore, complete transmission line is modelled based on EMTP – RV possibility of grouping elements. Transmission line consists of complex subcircuit elements (substations on both ends of transmission line and n transmission line sections). It is very important to emphasise that connection between all elements in a model is possible and all input data can be changed according to user's needs. This model consists of large number of input and output data. Energy duty for all arresters can be calculated as well as voltages and currents in each circuit node. Arrester current, voltage and energy duty calculations are the most important calculations for purposes of this thesis.

Review of so many output data (current and voltage shapes, energy duties, etc.) is not difficult thanks to good organization inside complex subcircuit elements. Each subcircuit has its own name and number, so for example output data for transmission line section l are grouped according to its name. It is the same for each subcircuit. Despite of fact that there is a plenty of input and output data, CPU time is not too long.

It is indicated that lightning stroke, hitting transmission line, usually produces operation of more than one line surge arrester. As it is previously mentioned, modelling of complete transmission line, in line surge arrester energy duty studies, is very important for more accurate arrester energy sharing calculation. Two cases of line surge arresters energy sharing were considered. In first case, five towers

were modelled on both sides from the point of the lightning impact. While in second case fifteen towers were modelled on the both sides from the point of the lightning impact. Examples of five and fifteen towers were taken for better visualization and understanding. It is important to emphasize possibility to monitor energy for all arresters along the complete transmission line.

In both cases, lightning flash hits top phase conductor at the middle of the span. Therefore, arresters on the top phase are the most stressed and because of that their energy is calculated and considered.

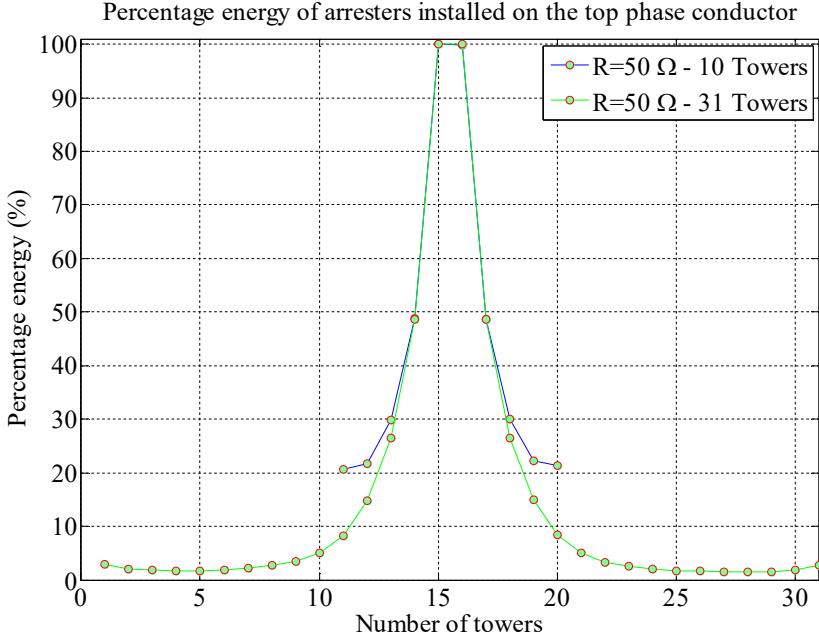


Figure 7.1.2. Percentage of energy (with respect to energy absorbed by arrester at tower placed first to the point of lightning impact) shared by adjacent arresters at towers along the line – comparison 10 and 30 towers

Based on results, it can be seen that in the first simulation case arrester on fifth tower absorbs 20% of energy, while in the second simulation case arrester on fifth tower absorbs less than 10% of energy. This effect is especially important for unshielded line design studies, when arrester energy capability can be easily exceeded. It is shown that for different number of modelled towers energy absorption of arresters installed on adjacent towers is also different.

The lightning flash is modelled as a current source (so called 'I – point by point source') because it is possible to import measured data point by point. The current shapes and values can be changed in order to study different lightning flashes. The lightning current (bipolar) used in the simulation was measured in Corsica and it is analysed in Chapter 4 and shown in figure 4.2.1. Multicomponent flashes current shapes are generated in MATLAB and loaded into I – point by point EMTP – RV block. In case when lightning channel impedance is taken into account, EMTP – RV representation of lightning flash is also presented. Measured or generated data are loaded into ideal current source which is in parallel with resistance that represents lightning channel impedance. Lightning current shape can be changed as well as lightning channel impedance to model different lightning flashes.

A summary of modelling and calculation procedure is given in Chapter 5. The quality of the results of lightning transient calculations of transmission lines is mainly based on proper modelling and calculation procedures. Modelling and calculation procedures in general are as follows:

- 1) Collecting data about transmission line and collecting data about lightning flash;
- 2) Selection of appropriate mathematical models for transmission line components and lightning flash (in case when lightning current shape is unknown);
- 3) Selection of appropriate software package for modelling and simulation, and selection of additional software (for example, software for preparing input data for main software);

- 4) Modelling in selected software;
- 5) Calculation;
- 6) Data display and analyses.

In Chapter 6 line surge arrester energy duty due to bipolar and multicomponent flashes is calculated and analysed. Also, shielded and unshielded line designs are considered. Line surge arrester current shapes are computed and presented for both line designs. Parametric analysis was carried out.

Energy stresses of transmission line surge arresters are commonly analysed due to unipolar flashes that transport charge of one polarity to ground. Also, it is very important to analyse energy stresses on transmission line surge arresters due to bipolar and multicomponent lightning flashes that can cause serious problems in electrical power systems. This thesis represents the first analysis of energy stresses of transmission line surge arresters due to bipolar and multicomponent flashes.

Effect of the bipolar lightning stroke is emphasized in figure 7.1.3. For better explanation, lightning current, arrester current and arrester energy duty are shown on same figure. The energy duty for both line designs (unshielded and shielded) is shown for the time duration of the bipolar lightning stroke.

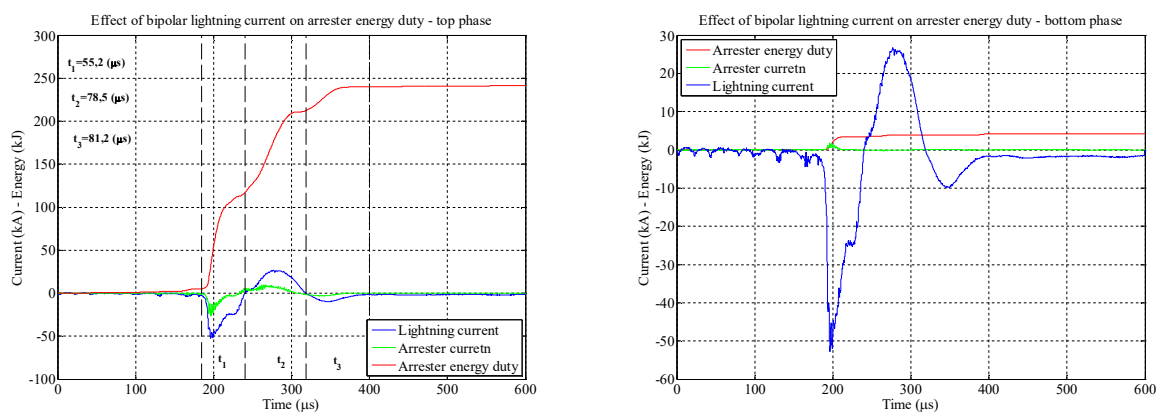


Figure 7.1.3. Illustration of bipolar lightning effect on arrester energy duty – unshielded and shielded line designs respectively

From the consideration of the energy duty it is possible to conclude that the arrester energy rises up as the bipolar lightning current arrives at the arrester. It is shown that in very short time period two portions of energy (positive and negative part of bipolar lightning impulse) have to be absorbed by line surge arrester, almost instantly. Time needed for arrester cooling is about 20 minutes or more and it is incomparable with microsecond scale of bipolar lightning. Because of that, line surge arrester has no time for cooling. Bipolar lightning flashes are very dangerous and destructive for line surge arrester as well as for complete transmission line.

Line surge arresters installed on the unshielded and shielded lines are differently stressed. Line surge arresters on the unshielded lines are more stressed than arresters on the shielded lines. The main reason for this is in the difference in the arresters current shapes. For example, most stressed arresters energy duties are 246 kJ for unshielded line and 4.5 kJ for shielded line. Mentioned values are calculated for tower footing resistance of 30 Ω .

In the design and the selection of the line surge arresters, it is very important to know the shapes of the current flowing through the arresters. For unshielded line design surge arrester current peaks are much higher than in the case of the shielded line (with the same original lightning stroke). The duration of the arresters current is also much longer than shielded line case.

In the case of unshielded line design the arrester current peaks are not as high as peaks of the original lightning flash (about two times lower compared to the original lightning flash). The comparison of arrester current and original lightning flash current is shown in the diagram in figure 7.1.3. In shielded line design the duration of the arrester current is much shorter than the original lightning stroke.

Multicomponent flashes also have interesting influence on arrester energy duty. In the case of unshielded line lightning flash hits top phase conductor at the middle of the span. The arrester current

due to multicomponent lightning flash (multicomponent lightning flash from figure 6.2.10 – flash #1) is shown in figure 7.1.4. Arrester current has the same duration as the original lightning flash and all three components can be noted. The arrester current peaks are about two times lower compared to the original lightning flash. The comparison of arrester current and original lightning flash current is shown in the diagram also in figure 7.1.4 (zoomed in).

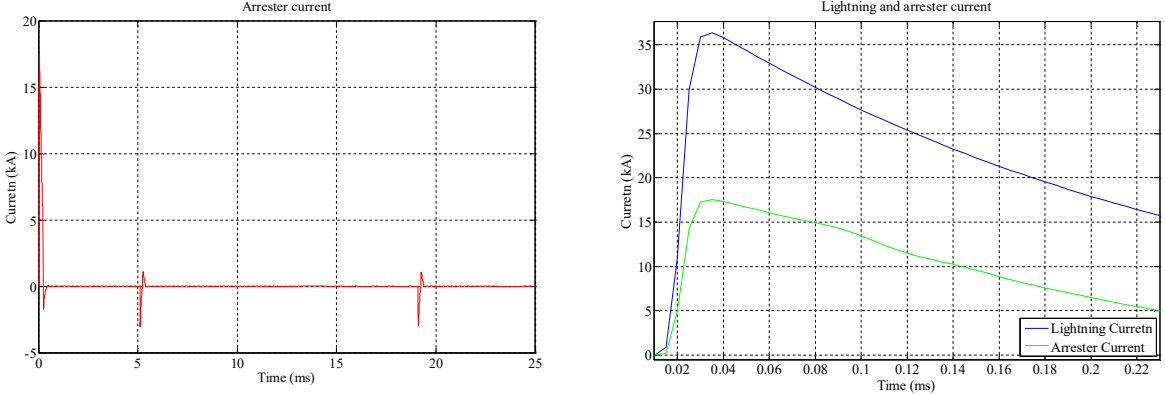


Figure 7.1.4. Arrester current due to flash #1 and zoomed in diagram of comparison between arrester current due to flash #1 and flash #1 current – unshielded line design

The effect of flash #1 on the line surge arrester energy duty is emphasized in figure 7.1.5. The energy duty is shown for the time duration of the multicomponent lightning flash #1. So, for a better presentation of the energy change a zoomed in part of the diagram is shown also in figure 7.1.5.

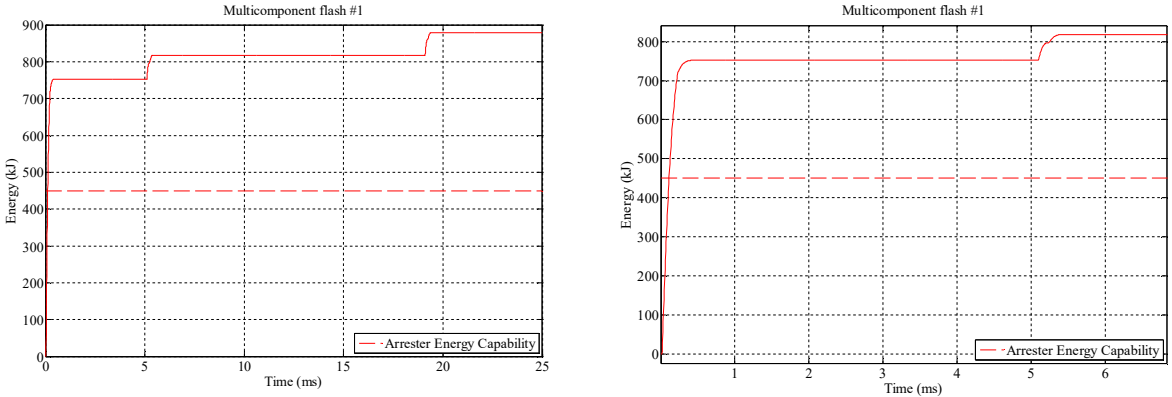


Figure 7.1.5. Arrester energy duty due to flash #1 and zoomed in diagram of arrester energy duty due to flash #1

From the consideration of the energy duty it is possible to conclude that the arrester energy rises up as the current of flash arrives at the arrester.

In the case of shielded line, lightning flash hits top of the tower. The arrester current and the energy duty for the multicomponent lightning flash #1 are represented in figure 7.1.6. The arrester current and energy duty are considered for arresters installed on the bottom phase conductor (this arrester is the most stressed).

The arrester current due to flash #1 is shown in figure 7.1.6. For shielded line, a small fraction of current is diverted through the arrester. Only the first stroke in flash #1 has an influence on arrester energy duty. The second and third strokes do not have such high current peak and they have no influence on the line surge arrester energy duty. Compared to the original first stroke, arrester current peak is not high. The duration of the arrester current is much shorter than the original lightning stroke.

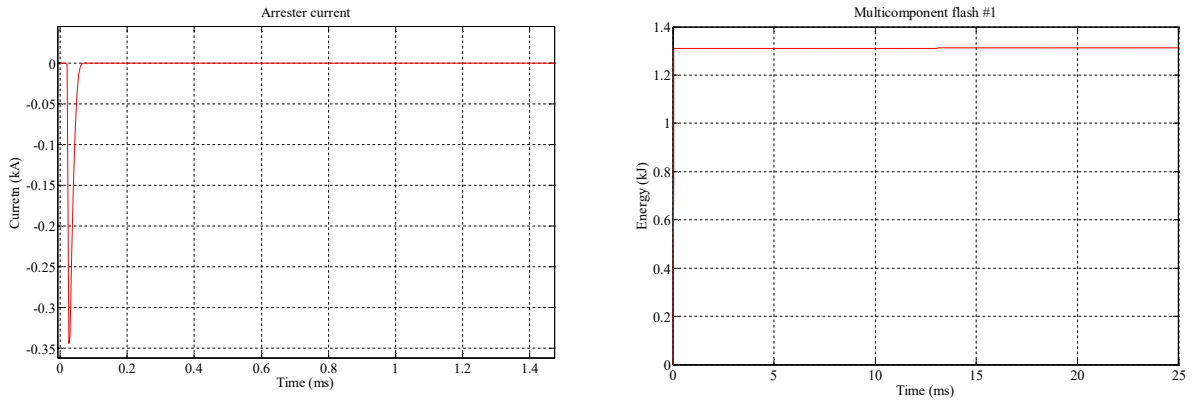


Figure 7.1.6. Arrester current and arrester energy duty due to flash #1 – shielded line design

The effect of flash #1 on the line surge arrester energy duty is emphasized in figure 7.1.6. The energy duty is shown for the time duration of the multicomponent lightning flash #1. From the consideration of the energy duty it is possible to conclude that the arrester energy for shielded line consideration is not high. For example, most stressed arresters energy duties are 879.11 kJ for unshielded line and 1.31 kJ for shielded line.

As it is mentioned in previous chapters, multicomponent lightning flashes interstroke time interval mean value is around 30 ms. Therefore line surge arrester has no time for cooling and the absorbed energy increases with every stroke and because of that line surge arrester can eventually blow up.

In order to select the appropriate arrester, parametric analysis was carried out, considering different parameters that affect arrester's energy calculation. Parameters such as: tower footing resistance, different arrester installation configuration are considered as line parameters. Lightning flash parameters have significant influence on energy stress in line surge arresters. Following lightning flash parameters were considered: lightning channel impedance, front time, tail time, polarity, multiplicity and current peak.

The value of tower footing resistance has significant influence on line surge arrester energy duty. For both line designs tower footing resistance was varied from 10 Ω to 100 Ω with step of 10 Ω . In the case of unshielded line design, lightning flash hits top phase conductor at the middle of the span, while in shielded line design, lightning flash hits top of the tower. In the case of unshielded line design energy absorbed by the nearest arrester from the point of lightning impact decreases with increasing tower footing resistance. This means that with the increase of tower footing resistance less current is flowing through it and more current has to be diverted through line surge arrester. In case of higher tower footing resistance adjacent towers absorb more energy than in case of low tower footing resistance of the nearest tower. Arresters on adjacent towers also absorb significant part of energy. Energy of those arresters increases with increasing tower footing resistance.

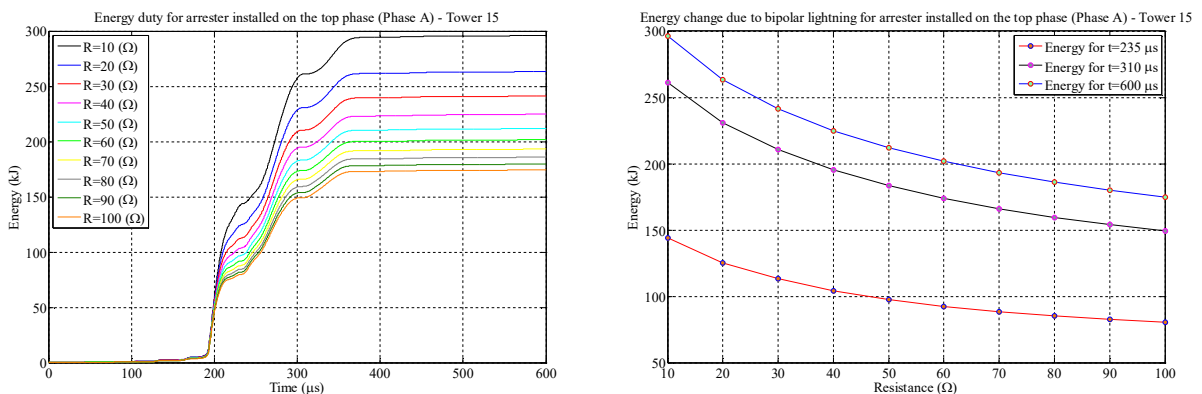


Figure 7.1.7. Arrester energy duty for different values of tower footing resistance (left) and arrester energy change due to bipolar lightning for different values of tower footing resistance (right) – for nearest arrester from the point of lightning impact – unshielded line design

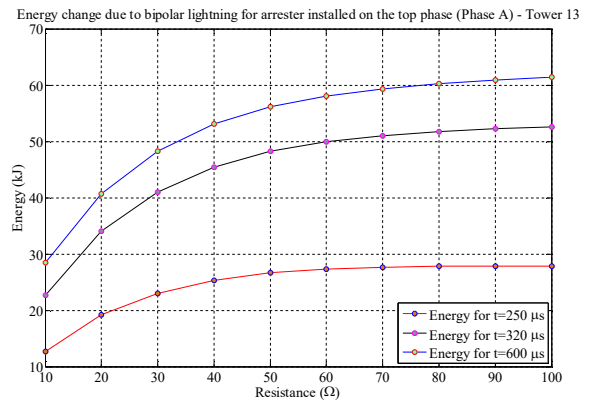
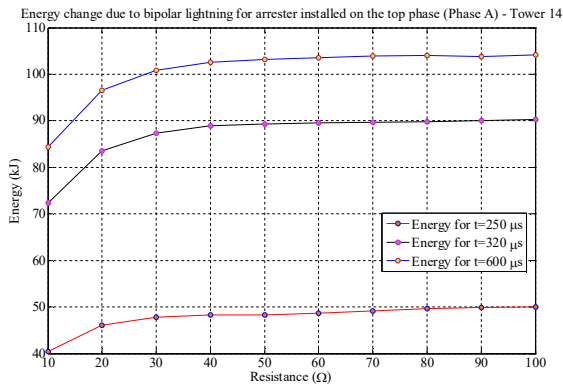


Figure 7.1.8. Arrester energy change due to bipolar lightning for different values of tower footing resistance – on the second tower from the point of lightning impact (left) and on the third tower from the point of lightning impact (right) – unshielded line design

In shielded line design it is possible to say that the arrester energy increases with increasing tower footing resistance. Also, this conclusion is valid for adjacent towers. The value of tower footing resistance has significant influence on line surge arrester energy duty. Energy duty for bottom phase arrester installed on tower that has been hit (for different tower footing resistance values) is presented in left graph in figure 7.1.9.

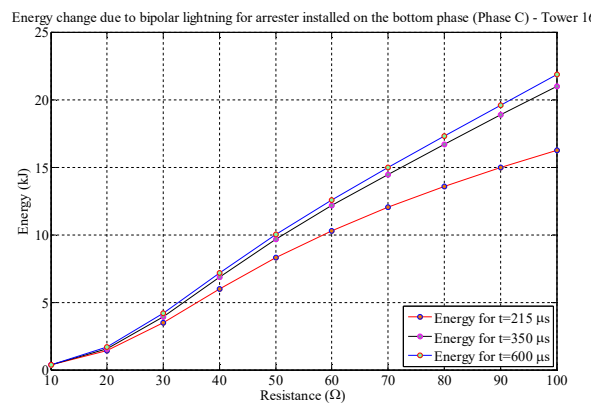
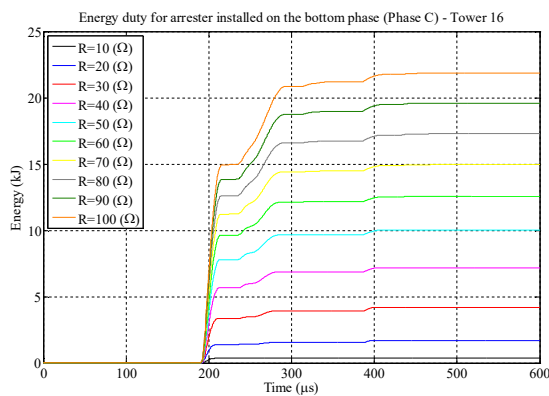


Figure 7.1.9. Arrester energy duty for different values of tower footing resistance and arrester energy change due to bipolar lightning for different values of tower footing resistance – for nearest arrester from the point of lightning impact – shielded line design

Right graph in figure 7.1.9 represents arrester energy change due to bipolar lightning for different values of tower footing resistance.

In addition to the line design (shielded or unshielded), line surge arrester installation configuration influences arrester energy duty. When two or more arresters are installed, they are not equally stressed.

In case of unshielded line, two arrester configurations are considered: line surge arresters are installed on three phase conductors and line surge arresters are installed on the top and on the middle phase conductors. Top phase line surge arresters (in two arresters installation configuration) that are nearest (on first tower) to the point of lightning impact absorb about 15% more energy than nearest arresters in three arresters installation configuration.

For shielded line design, three arrester configurations are considered: line surge arresters are installed on all three phase conductors, line surge arresters are installed on the middle and on the bottom phase conductors and line surge arresters are installed on the bottom phase conductor. In case of low tower footing resistance, compared to 3 LSA installation configuration, middle phase arrester absorbs more energy in 2 LSA installation configuration. While, bottom phase arrester absorbs the most energy in case of 1 LSA installation configuration. In case of high tower footing resistance, compared to 2 LSA installation configuration, middle phase arrester absorbs more energy in 3 LSA installation configuration. While, bottom phase arrester absorbs most of the energy in case of 3 LSA installation

configuration. In case of high tower footing resistance, value arresters installed on adjacent towers are more involved in energy absorption.

Previous considerations show the energy profile for the case when all towers have the same footing resistance. It is well known that transmission line has a different footing resistance along the line route. If we consider only 15 towers on each side from the point of the lightning impact and if a span or a line length between two towers is considered as a mean value of 300 meters, then we are considering part of the transmission line with length of about 10 km. Definitely, it is not possible that all towers in range of 10 km have the same tower footing resistance.

Transmission line usually passes through different terrain configurations and because of that there are changes of tower footing resistance. On transmission line ends near substations, tower footing resistance has lower value, while for transmission line passing through rocky terrain, tower footing resistance has higher value. Thus, transmission line can be considered for both low and high tower footing resistance regions.

In simulations, it was common practice to use uniform tower footing resistance distribution. Based on previously stated facts, the following question has emerged: what kind of influence on line surge arrester energy would have non – uniform tower footing resistance distribution?

For that purpose Monte Carlo method was used. Tower footing resistance value is varied along the line route. Two cases are considered:

- region of low tower footing resistance and
- region of high tower footing resistance.

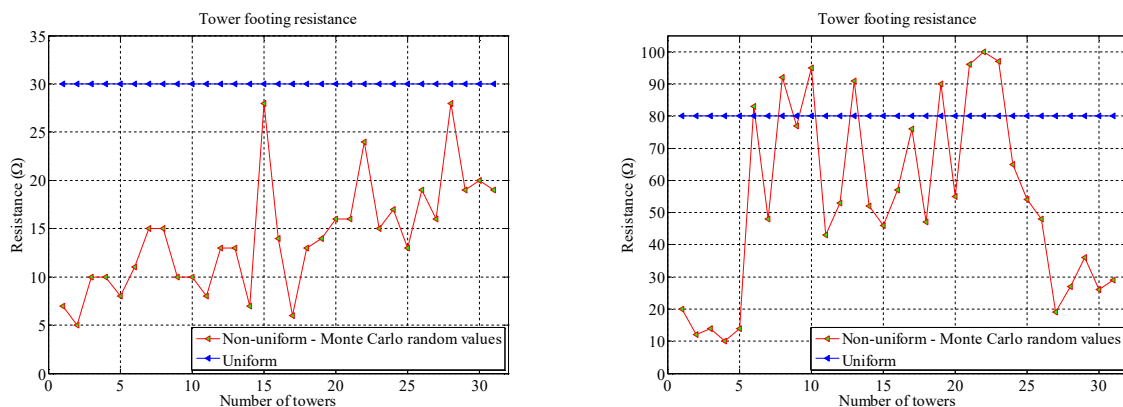


Figure 7.1.10. Examples of uniform and non-uniform tower footing resistance distributions – region of low tower footing resistance (left) and region of high tower footing resistance (right)

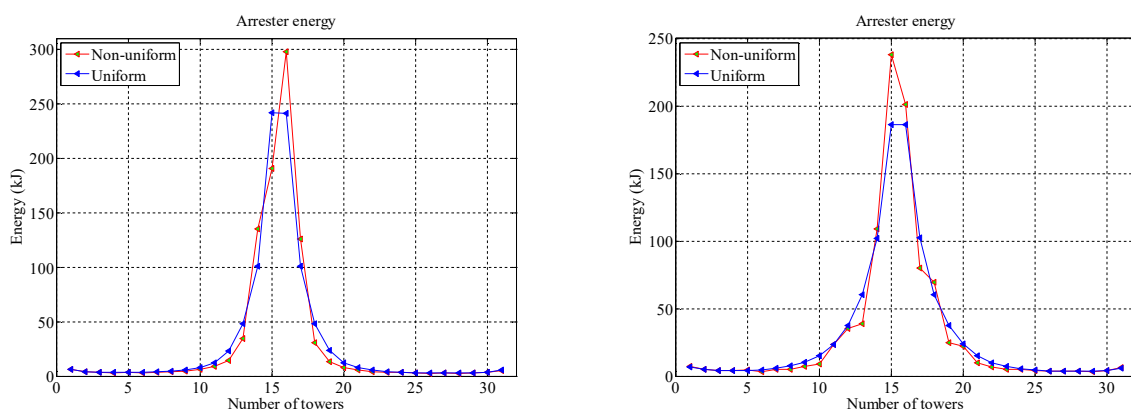


Figure 7.1.11. Arresters energies for uniform and non-uniform tower footing resistance distributions – region of low tower footing resistance (left) and region of high tower footing resistance (right)

Uniform and non – uniform tower footing resistance distribution have different influence on arresters installed on several adjacent towers on the both sides from the point of the lightning impact. For arresters on far ends there is no difference between uniform and non – uniform distribution.

Lightning channel impedance has influence on line surge arrester energy duty for both line designs. The main problem is that for proper interpretation of lightning stroke, it is unknown which value should be taken for lightning channel impedance. Lightning channel impedance cannot be exactly determined. It varies from stroke to stroke. Predictions of lightning channel impedance are very difficult even for negative lightning strokes which are much more studied than bipolar and multicomponent lightning flashes. Some authors use ideal current source, some of them use Norton equivalent circuit with impedance value of 400Ω , while some of them use impedance value of 1000Ω . In both line designs, energy difference between ideal current source and Norton equivalent circuit with impedance value of 400Ω (very often used in calculations) is about 10%. This 10% represents significant change of energy, especially for unshielded line design when line surge arrester energy capability can be easily exceeded. For lightning channel impedance from 100Ω to 1000Ω changes of energy are higher, and for resistance values higher than 1000Ω arrester energy changes are lower. Also, for resistance values higher of 1000Ω changes of arrester energy are lower than 5%. Arrester energy increases with increasing lightning channel impedance. Thus, calculations with lightning channel impedance of 1000Ω or with using ideal current source could be sufficient.

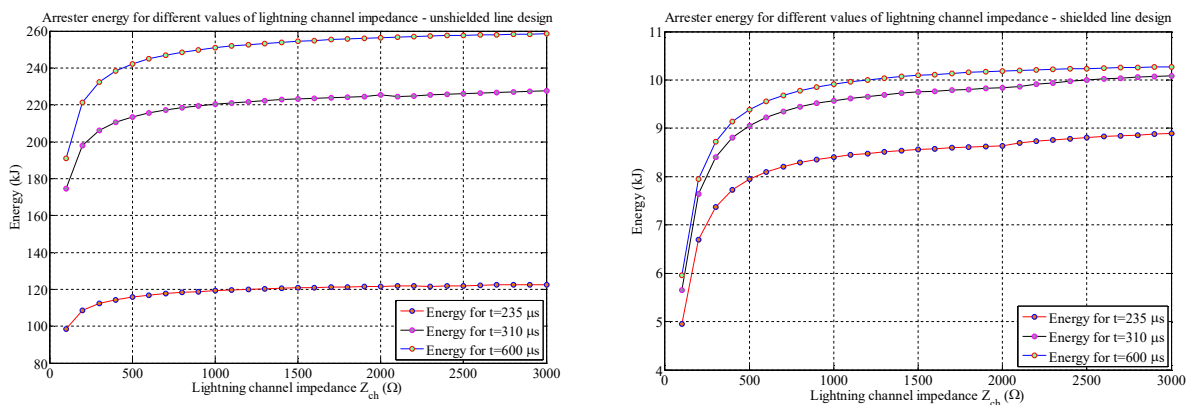


Figure 7.1.12. Arrester energy for different lightning channel impedance values – unshielded line design (left) and shielded line design (right)

In order to analyse influence of front time, tail time and current peak on line surge arrester energy duty multicomponent flash #1 was used in simulations. To show influence of lightning current peak on line surge arrester energy duty multicomponent flash #3 (multicomponent lightning flash #3 from figure 6.2.12) was used.

Simulations were conducted for different front and tail time. Results from conducted simulations are presented in figure 7.1.13. Line surge arrester energy duty depends on tail time, while influence of front time is hardly noticeable.

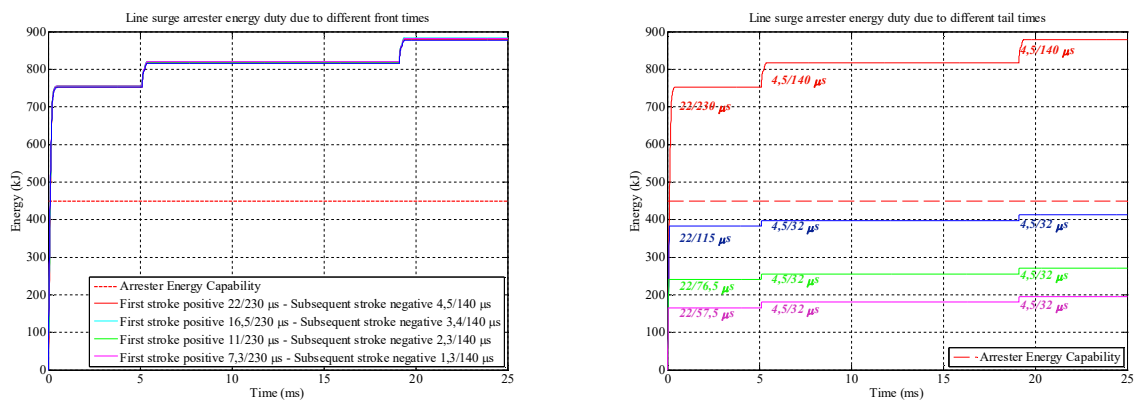


Figure 7.1.13. Arrester energy duty due to different front times (left) and arrester energy duty due to different tail times (right) – unshielded line design

Figure 7.1.14 illustrates change of energy due to different lightning stroke current peaks. In case of higher current peaks (front and tail times are the same) arrester energy increase is higher. For example, for current peak of -42.7 kA energy increase is 563.7 kJ, while for current peak of -7.5 kA energy increase is 80.2 kJ.

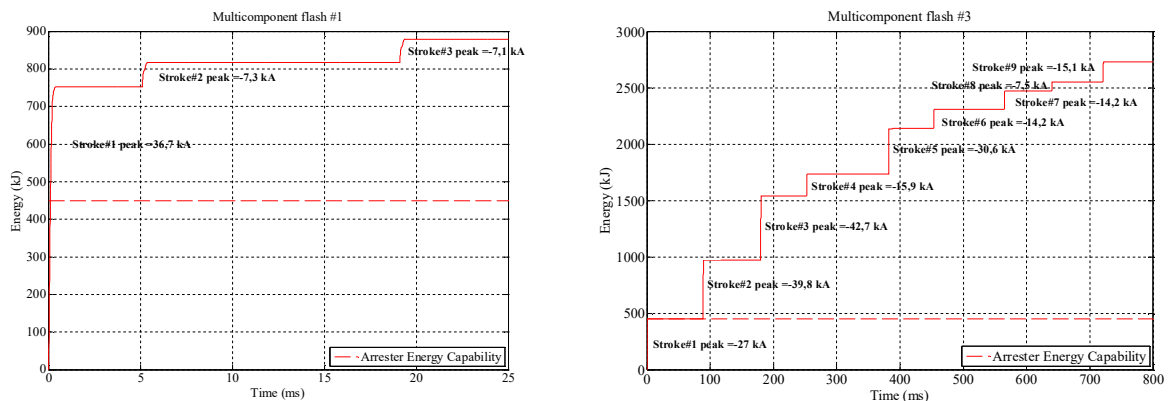


Figure 7.1.14. Arrester energy duty due to flash # 1 (left) and flash #3 (right) – unshielded line design

In general, we can make several conclusions.

From the consideration of the energy duty it is possible to conclude that the arrester energy rises up as the bipolar or multicomponent lightning current arrives at the arrester. It is shown that in very short time period two or more portions of energy have to be absorbed by line surge arrester. Therefore, bipolar and multicomponent lightning flashes are very dangerous and destructive for line surge arrester as well as for complete transmission line.

Line surge arresters installed on the unshielded and shielded lines are differently stressed. Line surge arresters on the unshielded line are more stressed than the ones on the shielded line. The main reason for this is in the difference in the arresters current shapes. In the design and the selection of the line surge arresters, it is very important to know the shapes of the current flowing through the arresters. For unshielded line design surge arrester current peaks are much higher than in the case of the shielded line (for the same original lightning stroke). The duration of the arresters current is also much longer than for the shielded line case.

Lightning stroke hitting transmission line usually produces operation of several line surge arresters. Modelling of complete transmission line, in line surge arrester energy duty studies, is very important for more accurate arrester energy sharing calculation. This effect is especially important for unshielded line design studies. In addition to the line design (unshielded or shielded) line surge arrester installation configuration influences arrester energy duty. When two or more arresters are installed, they are not equally stressed.

Tower footing resistance is very important parameter that has influence on arrester energy duty. In the case of unshielded line design energy absorbed by the nearest arrester from the point of lightning impact decreases with increasing tower footing resistance. In case of higher tower footing resistance adjacent towers absorb more energy than in case of low tower footing resistance of the nearest tower. Arresters on adjacent towers also absorb significant part of energy. Energy of those arresters increases with increasing tower footing resistance. In shielded line design it is possible to say that the arrester energy increases with increasing tower footing resistance. Also, this conclusion is valid for adjacent towers.

Uniform and non – uniform tower footing resistance distribution have different influence on arresters installed on several adjacent towers on the both sides from the point of the lightning impact. For arresters on far ends there is no difference between uniform and non – uniform distribution.

Lightning channel impedance has influence on line surge arrester energy duty for both line designs. In both line designs, energy difference between ideal current source and Norton equivalent circuit with impedance value of 400Ω (very often used in calculations) is about 10%. This 10% represents

significant change of energy, especially for unshielded line design when line surge arrester energy capability can be easily exceeded. Arrester energy increases with increasing lightning channel impedance.

Certainly, for both line designs (unshielded and shielded) the energy duty depends on the number of strokes of the flash, current peak and tail time, while the influence of front time is hardly noticeable.

CIGRE brochure 63 gives comment on the selection of lightning parameters. Downward negative flash is considered the most important discharge process that affects the lightning performance of transmission lines. It is therefore recommended that parameters describing the downward negative flash are used to calculate the lightning performance of lines, unless another lightning data are known. Thanks to development of lightning location and measurement systems on tall towers bipolar lightning flashes were recorded and lightning data for different regions are now more accurate. Based on result of this thesis it is possible to conclude that bipolar lightning flashes are very destructive and they should be taken into account when dimensioning line surge arresters.

As mentioned in Chapter 4, for an effective protection design of transmission line, the knowledge of lightning current parameters is of primary importance. Knowledge about lightning parameters and characteristics for different regions is also very useful for transient studies in electrical power systems. Therefore, for better quantification and characterisation of lightning current parameters, larger dataset is needed. So, data exchange between lightning activity monitoring stations all over the world should be encouraged. Direct measurements provide the most accurate data about lightning current parameters. Data obtained from lightning location systems are also very useful, but lightning location systems do not provide data about front and tail time. It would be very interesting to find correlation between current peak and front and tail time from large dataset using predictive methods. Adequate Neural Network tool can be used to find mentioned correlation, where lightning current peaks can present input data, while front and tail time can be used as targets.

As it is written in Chapter 3, energy handling capability of metal-oxide (MO) arresters has many different aspects, which are only partly or not at all reflected in the actual standards. At least, though this list may not be complete, they can be divided into:

- "thermal" energy handling capability and
- "impulse" energy handling capability.

Therefore, thermal stresses of metal – oxide blocks as well as complete surge arresters due to bipolar and multicomponent lightning flashes should be considered. Also, it would be very interesting to study what kind of effect has a change of polarity (bipolar lightning) on material in line surge arrester.

Even though calculation time for complete transmission line model is not so long, it can be optimized using parallel programming and parallel processing techniques.

There is no energy monitoring system developed or installed in the world. Energy monitoring system can be developed using advanced technologies. Such system can be used for energy sharing monitoring. The same system can be used for power quality monitoring in distribution lines.

References

- [1] V. A. Rakov, M. A. Uman, *Lightning Physics and Effects*, Cambridge University Press, 2003
- [2] V.A. Rakov, *Positive and Bipolar Lightning Discharges: A Review*, University of Florida
- [3] V. A. Rakov, *Lightning Phenomenology and Parameters Important for Lightning Protection*, IX International Symposium on Lightning Protection, Foz do Iguaçu, Brazil, November 2007
- [4] H. Zhou, G. Diendorfer, R. Thottappillil, H. Pichler, M. Mair, *Upward Bipolar Lightning Flashes Observed at the Gaisberg Tower*, International Conference of Lightning Protection, Italy, September 2010
- [5] A. C. V. Saraiva, L. Z. S. Campos, G. S. Zepka, J. Alves, E. R. Williams S, Heckman, J. C. Bailey, C. A. Morales, R. J. Blakeslee, *Optical Evidence of the Inception Mechanisms of Natural Bipolar Cloud-to-Ground Lightning*, 23rd International Lightning Detection Conference, Tucson, Arizona, USA, March, 2014
- [6] A. C. V. Saraiva, L. Z. S. Campos, E. R. Williams, G. S. Zepka, J. Alves, O. Pinto Jr, S. Heckman, T.S. Buzato, J. C. Bailey, C. A. Morales, R. J. Blakeslee, *High – speed video and electromagnetic analysis of two natural bipolar cloud – to – ground lightning flashes*, AGU Publications, Journal of Geophysical Research, 2014
- [7] W. Schulz, G. Diendorfer, *Bipolar Flashes Detected with Lightning Location Systems and measured on an instrumented tower*, OVE – ALDIS, Austria
- [8] *Lightning parameters for engineering applications*, CIGRE Brochure 549, August 2013
- [9] *Lightning Striking Characteristics to Very High Structures*, CIGRE Brochure 633, 2015
- [10] N. Honma, Y. Hongo, N. Suzuki, T. Konno, *Comparison of Tohoku LLS Data and Lightning Current Waveforms in Winter*, International Conference on Lightning Protection (ICLP), Shanghai, China, 2014
- [11] A. M. Hussein, M. Milewski, E. Burnazovic, W. Janischewskyj, *Current Waveform Characteristics of CN Tower Negative and Positive Lightning*, X International Symposium on Lightning Protection, Curitiba, Brazil, November 2009
- [12] T. Shindo, H. Shiraishi, S. Sekioka, M. Ishii, D. Natsuno, *Studies of lightning protection design for wind power generation systems in Japan*, CIGRE C4_306_2012, 2012
- [13] C. Romero, F. Rachidi, M. Rubinstein, M. Paolone, V. A. Rakov, D. Pavanello, *Positive lightning flashes recorded on the Säntis tower from May 2010 to January 2012*, JOURNAL OF GEOPHYSICAL RESEARCH: ATMOSPHERES, VOL. 118, 2013
- [14] D. Wang, N. Takagi, *Three Unusual Upward Positive Lightning Triggered by Other Nearby Lightning Discharge Activity*, 22nd International Lightning Detection Conference, Broomfield, Colorado, USA, April, 2012
- [15] G. Diendorfer, H. Zhou, H. Pichler, R. Thottappillil, *Review of Upward Positive and Bipolar Lightning Flashes at the Gaisberg Tower*, 7th Asia-Pacific International Conference on Lightning, Chengdu, China, November 2011

- [16] C. Romero, M. Rubinstein, F. Rachidi, M. Paolone, V. A. Rakov, D. Pavanello, *Some Characteristics of Positive and Bipolar Lightning Flashes Recorded on the Sântis Tower in 2010 and 2011*, International Conference on Lightning Protection (ICLP), Vienna, Austria, 2012
- [17] S. Xue, P. Yuan, J. Cen, J. Liu, Y Li, *Study on Physical Characteristics of a Bipolar Cloud-to-Ground Lightning Discharge Plasma*, IEEE Transactions on Plasma Science, VOL. 43, NO. 3, March 2015
- [18] C. Romero, M. Paolone, F. Rachidi, M. Rubinstein, V. A. Rakov, A. Rubinstein, C. A. Nucci, P. Zweiacker, *Current Waveforms Associated with Positive Flashes Recorded on the Sântis Tower in Summer 2010*, XI International Symposium on Lightning Protection, Fortaleza, Brazil, October 2011
- [19] C. Romero, F. Rachidi, M. Rubinstein, V. A. Rakov, M. Paolone, D. Pavanello, *Bursts of Fast Pulses in Positive Lightning Current Waveforms Recorded on the Sântis Tower*, XII International Symposium on Lightning Protection, Belo Horizonte, Brazil, October 2013
- [20] M. Azadifar, M. Paolone, D. Pavanello, F. Rachidi, V.A. Rakov, C. Romero, M. Rubinstein, *An Update on the Characteristics of Positive Flashes Recorded on the Sântis Tower*, International Conference on Lightning Protection (ICLP), Shanghai, China, 2014
- [21] D. Wang, N Takagi, *Characteristics of Upward Bipolar Lightning Derived from Simultaneous Recording of Electric Current and Electric Field Change*, University of Japan
- [22] P. Baranski, P. Bodzak, *Some observations of bipolar flashes during summer thunderstorms near Warsaw*, Acta Geophysica, VOL. 54, NO. 1, 2006
- [23] S. A. Fleenor, C. Biagi, C. Cummins, E. Krider, *Characteristics of Cloud to Ground Lightning in Warm Season Thunderstorms in the Great Plains*, International Lightning Detection Conference, Arizona, USA, April 2008
- [24] V.A. Rakov, *A Review of Positive and Bipolar Lightning Discharges*, American Meteorological Society, June 2003
- [25] M. Azadifar, F. Rachidi, M. Rubinstein, M. Paolone, V.A. Rakov, D. Pavanello, S. Metz, C. Romero, *Characteristics of Electric Fields of Upward Negative Stepped Leaders*, XIII International Symposium on Lightning Protection, Balneário Camboriú, Brazil, 28th Sept. – 2nd Oct. 2015.
- [26] J.J. Woodworth, *Externally Gapped Line Arrester A Comprehensive Review*, Transmission and Distribution Conference and Exposition IEEE PES, New Orleans, LA, USA, 2010.
- [27] M. T. Chen, S. J. Hsiao, *Lightning Transient Simulation and Analysis of EGLA under Single-Ended Circuit Breaker Open System*, 7th Asia-Pacific International Conference on Lightning, November 1-4, 2011, Chengdu, China, 2011.
- [28] P. Bunov, L. Klingbeil, D. Udovicic, D. Biswas, *Externally Gapped Line Arresters – First experience with the new IEC 60099-8 standard and Line study analysis*, Transmission and Distribution Conference and Exposition (T&D) IEEE PES, Orlando, FL, USA, 2012.
- [29] T. H. Pham, S. A. Boggs, H. Suzuki, T. Imai, *Effect of Externally Gapped Line Arrester Placement on Insulation Coordination of a Twin-Circuit 220 kV Line*, IEEE TRANSACTIONS ON POWER DELIVERY, VOL. 27, NO. 4, OCTOBER 2012.
- [30] J.J. Woodworth, *Externally Gapped Line Arresters A Critical Design Review*, T&D Conference and Exposition IEEE PES, Chichago, IL, USA, 2014.
- [31] I. M. Rawi, M. P. Yahaya, M. Z. A. Ab. Kadir, N. Azis, *Experience and long term performance of 132kV overhead lines gapless-type surge arrester*, International Conference on Lightning Protection (ICLP), Shanghai, China, 2014.

- [32] V. Hinrichsen, *Overview of IEC Standards' recommendations for lightning protection of electrical high-voltage power systems using surge arresters*, International Conference on Lightning Protection (ICLP), Shanghai, China, 2014.
- [33] *IEC Standard Surge arresters – Part 8: Metal – oxide surge arresters with external series gap (EGLA) for overhead transmission and distribution lines of a.c. systems above 1 kV*, IEC 60099 – 8 – 2011.
- [34] *IEC Standard Surge arresters – Part 5: Selection and application recommendations*, IEC 60099 – 5 – 2013.
- [35] *Product Guide High Voltage Surge Arresters*, SIEMENS AG Energy Sector, Germany, 2014.
- [36] *IEEE Standard for Metal – Oxide Surge Arresters for AC Power Circuits (> 1 kV)*, IEEE - C62.11, New York, NY, USA, 2005.
- [37] *IEEE Guide for the Application of Metal-Oxide Surge Arresters for Alternating-Current Systems*, IEEE - C62.22, New York, NY, USA, 2009.
- [38] *IEEE Standard for Insulation Coordination – Definition, Principles and Rules*, IEEE – 1313.1, New York, NY, USA, 2011.
- [39] *IEEE Guide for Application of Insulation Coordination*, IEEE – 1313.2, New York, NY, USA, 1999.
- [40] S. Sadovic, *Seminar on Surge Arrester Design, Application and Testing*, Abu Dhabi, 2003.
- [41] *MO Surge Arresters Stresses and Test Procedures*, CIGRE Brochure 544, August 2013.
- [42] *Use of Surge Arresters for Lightning Protection of Transmission Lines*, CIGRE Brochure 440, December 2010.
- [43] *Metal – Oxide Arresters in AC Systems*, CIGRE Brochure 60, April 1991.
- [44] *Helping Understand V – I Characteristic Curve*, INMR WEEKLY TECHNICAL REVIEW, April 2015.
- [45] *Selection Non – Gapped Line Arresters*, INMR WEEKLY TECHNICAL REVIEW, August 2015.
- [46] M.V. Lat, *Thermal Properties of Metal – Oxide Surge Arresters*, IEEE Transactions on Power Apparatus and Systems, Vol. PAS – 102, No.7, July 1983.
- [47] M.V. Lat, *Analytical Method for Performance Prediction of Metal – Oxide Surge Arresters*, IEEE Transactions on Power Apparatus and Systems, Vol. PAS – 104, No.10, October 1985.
- [48] A. Petit, X. Dai Do, G. St – Jean, *An Experimental Method to Determine the Electro – thermal model Parameters of Metal – Oxide surge arresters*, IEEE Transactions on Power Delivery Vol.6, No.2, April 1991.
- [49] G. St – Jean, A. Petit, *Metal – Oxide Surge Arrester Operating Limits Defined by Temperature Margin Concept*, IEEE Transactions on Power Delivery Vol.5, No.2, April 1990.
- [50] M. Bartkowiak, M.G. Comber, G.D. Mahan, *Failure Modes and Energy Absorption Capability of ZnO Varistors*, IEEE Transactions on Power Delivery Vol.14, No.1, January 1999.
- [51] J.A. Marzinez – Velasco, *Power System Transients – Parameter Determination*, CRC Press Taylor and Francis Group, October 2009.
- [52] A. Haddan, D. Warne, *Advances in High Voltage Engineering*, IET Power and Energy Series 40, 2004.
- [53] *IEC Standard Surge Arresters – Part 4: Metal – Oxide surge arresters without gaps for a.c. systems*, IEC 600 99 – 4 – 2014.

- [54] M. Kobayashi, M. Mizuno, T. Aizawa, M. Hayashi, K. Mitani, *Development of Zinc – Oxide Non – Liner Resistors and Their Applications to Gapless Surge Arresters*, IEEE Transactions on Power Apparatus and Systems, Vol. PAS – 97, No.4, July/August 1978.
- [55] M. Mizuno, M. Hayashi, K. Mitani, *Thermal stability and life of the gapless surge arrester*, IEEE Transactions on Power Apparatus and Systems, Vol. PAS – 100, No.5, May 1981.
- [56] M. Kan, S. Nishiwaki, T. Sato, S. Kojima, S. Yanabu, *Surge discharge capability and thermal stability of a metal oxide surge arrester*, IEEE Transactions on Power Apparatus and Systems, Vol. PAS – 102, No.2, February 1983.
- [57] Y. Fujiwara, Y. Shibuya, M. Imataki, T. Nitta, *Evaluation of surge degradation of metal oxide surge arresters*, IEEE Transactions on Power Apparatus and Systems, Vol. PAS – 101, No.4, April 1982.
- [58] H. Nishikawa, M. Sukehara, T. Yoshida, *Thyristor valve gapless arrester element lifetime performance and thermal stability*, IEEE Transactions on Power Apparatus and Systems, Vol. PAS – 104, No.7, July 1985.
- [59] M. Oyama, I. Ohshima, M. Honda, M. Yamashita, S. Kojima, *Life performance of zinc-oxide elements under DC voltage*, IEEE Transactions on Power Apparatus and Systems, Vol. PAS – 101, No.6, June 1992.
- [60] R.A. Sargent, G.L. Dunlop, M. Darveniza, *Effects of multiple impulse currents on the microstructure and electrical properties of metal oxide varistors*, IEEE Transactions on Electrical Insulation, Vol.27, No.3, June 1992.
- [61] *IEC Standard Surge Arresters – Part 9: Metal – Oxide Surge Arresters without Gaps for HVDC Converter Stations*, IEC 60099 – 9 – 2014.
- [62] S. Sadovic, T. Sadovic, H.-D. Betz, *Lightning Activity Monitoring on Telecom Towers*, International Colloquium on Lighting and Power Systems Lyon, France, 2014.
- [63] LINET Sensor Manual, 2015.
- [64] *Guide to Procedure for Estimating the Lightning Performance of Transmission Lines*, CIGRE Brochure 63, Oct. 1991.
- [65] *IEEE Guide for Improving the Lightning Performance of electric Power Overhead Distribution Lines*, IEEE Std. 1410 – 2010.
- [66] *Parameters of Lightning Strokes: A Review*, IEEE Trans. Power Delivery, vol.20, pp. 346 – 358, Jan.2005.
- [67] *IEC Standard Protection against lightning electromagnetic impulse*, IEC 61312-1-1995.
- [68] *IEC Standard Protection against lightning*, IEC 62305-1-2010.
- [69] K. Berger, R. B. Anderson, and H. Kroninger, *Parameters of lightning flashes*, *Electra*, no. 41, pp. 23–37, Jul. 1975.
- [70] R. B. Anderson and A. J. Eriksson, *A summary of lightning parameters for engineering applications*, in *Proc. CIGRE*, 1980, Paper no. 33-06.
- [71] T. Narita, T. Yamada, A. Mochizuki, E. Zaima, and M. Ishii, *Observation of current waveshapes of lightning strokes on transmission towers*, IEEE Trans. Power Delivery, vol. 15, pp. 429–435, Jan. 2000.
- [72] F. Heidler, J. Cvetic, *A Class of Analytical Functions to Study the Lightning Effects Associated With the Current Front*, ETEP Vol.12, No.2, March/April 2002.
- [73] F. Heidler, W. Zischank, Z. Flisowski, Ch. Bouquegneau, C. Mazzetti, *Parameters of Lightning Current Given in IEC 62305 – Background, Experience and Outlook*, 29th International Conference on Lightning Protection, 23rd – 26th, June, 2008, Uppsala, Sweden.

- [74] H. W. Dommel, *Digital Computer Solution of Electromagnetic Transients in Single and Multiphase Networks*, IEEE Transactions on Power Apparatus and Systems, Vol.88, No.4, April 1969.
- [75] *ElectroMagnetic Transient Program (EMTP) Theory Book*
- [76] Y.A. Wahab, Z.Z. Abidin, S. Sadovic, *Line Surge Arrester Application on the Quadruple Circuit Transmission Line*, IEEE Bologna PowerTech Conference, Bologna, Italy, 2003.
- [77] *Sigma slp Version 2.1 – Software for the determination of transmission and distribution line electrical performance – User manual*, Sadovic Consultant, Paris, France, 2009.
- [78] J.A. Marzinez – Velasco, *Power System Transients – Parameter Determination*, CRC Press Taylor and Francis Group, October 2009.
- [79] A. Geri, *Behaviour of Grounding Systems Excited by High Impulse Currents: the Model and its Validation*, IEEE TRANSACTIONS ON POWER DELIVERY, VOL.4. NO.3, July 1999.
- [80] I. Uglešić, V. Milardić, B. Filipović – Grčić, *Evaluation of energy stresses on line arresters*, Applications of Line Surge Arresters in Power Distribution and Transmission Systems Cigre Colloquium, Cavtat, Croatia, 2008.
- [81] C.A. Christodoulou, I.F. Gonos, I.A. Stathopoulos, *Lightning performance of high voltage transmission lines protected by surge arresters: a simulation for the hellenic transmission network*, International Conference on Lightning Protection (ICLP), Uppsala, Sweden, 2008.
- [82] B. Filipović – Grčić, I. Uglešić, V. Milardić, A. Xemard, A. Guerrier, *Energy Stress of Surge Arresters Due to Temporary Overvoltages*, International Power System Transient Conference, Delft, Netherlands, June 14-17, 2011.
- [83] E. Isaacson, H. B. Keller, *Analyses of Numerical Methods*, Dover Publications INC. New York, USA, 1994.
- [84] N.S. Bakhvalov, *Numerical Methods*, Moscow State University, Mir Publishers Moscow, 1977.
- [85] Task Force on Very Fast Transients in IEEE Working Group on Modelling and Analysis of System Transients Using Digital Programms, *Modelling and Analysis Guidelines for very Fast Transients*, IEEE Transactions on Power Delivery, Vol. 11, No. 4, October 1996.
- [86] Report Prepared by the Fast Front Transients Task Force of the IEEE Modeling and Analysis of System Transients Working Group, *Modelling Guidelines for very Fast Transients*, IEEE Transactions on Power Delivery, Vol. 11, No. 1, January 1996.
- [87] Report Prepared by the Fast Front Transients Task Force of the IEEE Modeling and Analysis of System Transients Working Group, *Modelling Guidelines for very Fast Transients*, December 1997.
- [88] B. Filipović – Grčić, I. Uglešić, A. Xemard, *Selection of station surge arresters for control of slow-front overvoltages on compact lines*, CIGRE C4 Colloquium on Lightning and Power System, Kuala Lumpur, 16 – 19 May, 2010.
- [89] T. Sadovic, S. Sadovic, *EMTP – RV modelling for the transmission line lightning performance computation*, User Group Meeting, 20 April 2009, Dubrovnik, 2009.
- [90] A. Xemard, M. Mesic, T. Sadovic, D. Marin, S. Sadovic, *Lightning current field measurement on a transmission line, comparison with electromagnetic transient calculations*, International Conference on Power Systems Transients (IPST2015) Cavtat, Croatia, June 15 - 18, 2015.
- [91] *IEC Computational guide to insulation coordination and modelling of electrical networks*, 2003.

- [92] S. Sadovic, M. Babuder, M. Hrast, D. Bokal, M. Marnisek and T. Sadovic, *Line Surge Arrester Application on 123 kV Double Circuit Line*, International Symposium on High Voltage Engineering, Johannesburg, South Africa, 2009.
- [93] S.Sadovic, R. Gacanovic, *Impulsne karakteristike uzemljivača*, Sarajevo, 2008.

Appendix A

LIGHTNING CURRENT SHAPE PARAMETERS BIPOLAR AND MULTICOMPONENT FLASHES

A.1. Lightning Current Shape Parameters

The first comprehensive analysis of lightning current impulse shape characteristics was carried in 1957 on Berger's measured data from San Salvatore – leading to a full summary of impulse parameters and their statistical distributions. Correlations amongst various parameters were also examined. The basic analysis, however, was carried out upon impulse records that has been manually evaluated and this involved certain restrictions. In addition, in this earlier analysis, the front characteristics were defined only in terms of the maximum rate of rise of current (i.e. steepest tangent) on the front of a stroke, together with the front duration, arbitrarily determined between the 2 kA point on the front and the first peak of the current. Accordingly, in view of the importance of an adequate knowledge of impulse front characteristics in many engineering applications, it was considered necessary that the available data (which had subsequently been digitized) should be analysed more rigorously and a computerized system of analysis has been adopted. Several additional front parameters were also introduced, in the belief that an examination of their distributions and possible correlations might lead to a better representation of stroke front shapes.

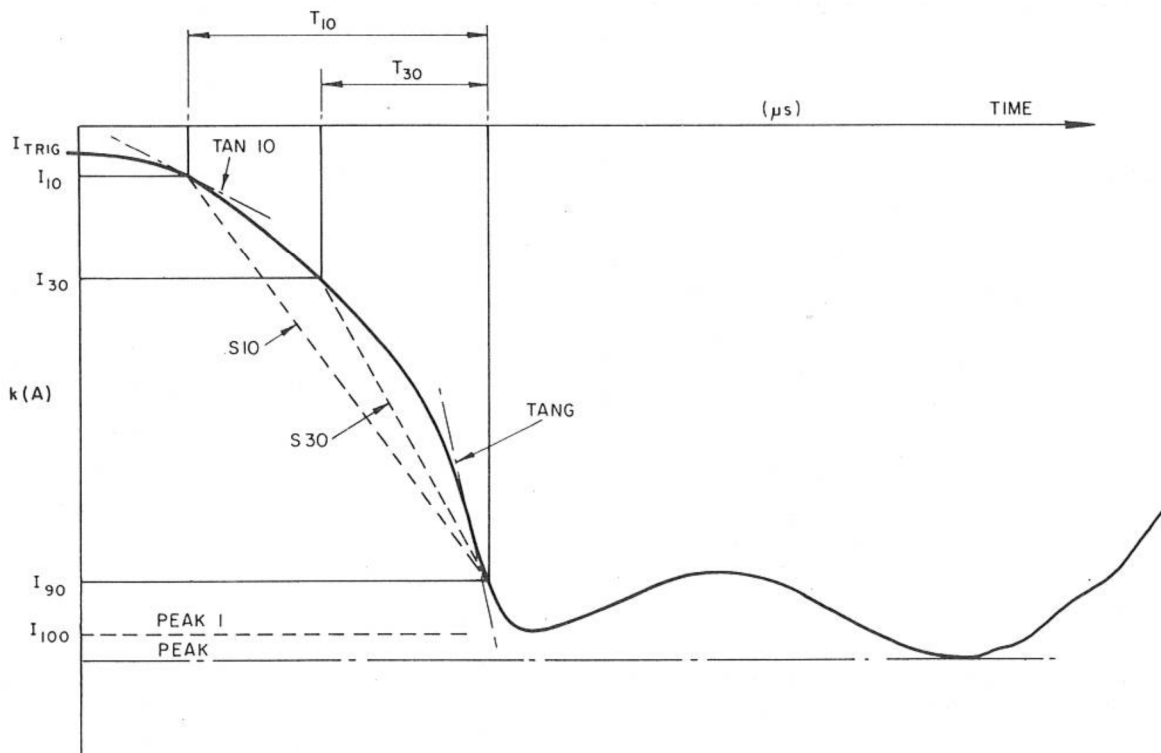


Figure A.1.1. Definition of current shape parameters (illustrated for a negative impulse)

These parameters are shown on an idealized form of negative stroke in figure A.1.1. As more rigorous approach, and in order to be more consistent with standardized concepts, the 90 percent amplitude on the front (with respect to the first peak amplitude), has been used as a basis for definition of most of the additional parameters. These are defined as follows:

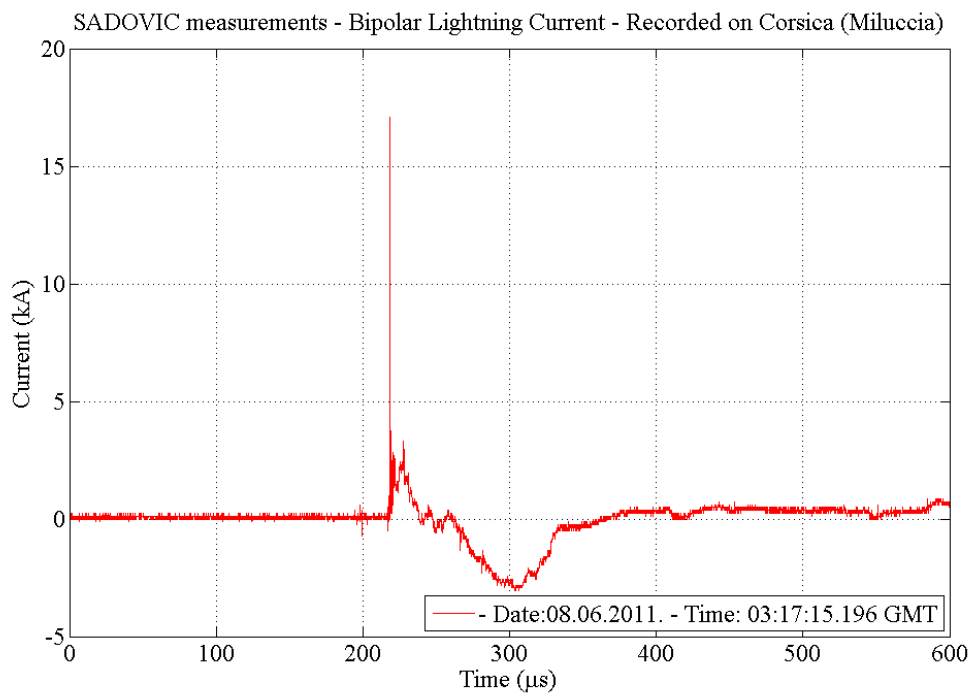
- $T_{10} = t_{90} - t_{10}$ – the front duration expressed as the interval between the 10 percent and 90 percent amplitude intercept of the front. (Note that the equivalent t_f is equal in this case $T_{10}/0,8$);
- $T_{30} = t_{90} - t_{30}$ – the front duration expressed as the interval between the 30 percent and 90 percent amplitude intercept of the front. (Note that the equivalent t_f is equal in this case $T_{30}/0,6$);
- TAN_{10} – the rate of rise of current, i.e. tangent to front shape of at the 10 percent amplitude intercepts. (This parameter was introduced in order to obtain an impression of the initial rates of rise of current (or line voltage) which surge arrester may experience);
- $S_{10} = \frac{(I_{90} - I_{10})}{T_{10}}$ – the average current steepness or rate of rise of current between 10 percent and 90 percent amplitude intercepts;
- $S_{30} = \frac{(I_{90} - I_{30})}{T_{30}}$ – the average current steepness or rate of rise of current between 30 percent and 90 percent amplitude intercepts;
- $TANG = S_m$ – maximum current rate rise on the front.

On above basis, Berger's original data has been re – analysed and the resultant cumulative frequency distributions of these parameters were presented in literature. Statistical tests for normality were applied to these distributions (after log – transformations) and proved significant in the majority of cases at the 5 percent level. The means μ and standard deviations of the logarithm of the variates ($\sigma_{\log 10}$) in these distributions, together with the 95 percent, 50 percent and 5 percent probability intercepts – as determined from log – normal approximations are summarized in literature.

A.2. Bipolar Lightning Current Shapes

It is known that most of the bipolar lightning events were identified in direct current measurements on tall grounded objects. In this section bipolar lightning events recorded on Corsica (at the telecom base station Miluccia) are shown. During observation period of one and a half year, thirteen bipolar events have been recorded by SADOVIC measurement system. Shapes of bipolar lightning currents are represented in figures from figure A.2.1 to figure A.2.13. Amount of positive and negative charge transfer, current peaks and duration of positive and negative parts of bipolar events, are calculated and presented.

Bipolar lightning event 1 – recorded on the 8th of June 2011



The negative part has the peak current of - 3.05 kA and the positive part has the peak current of + 17.09 kA, with the total charge transfers being -0.1448 As and +0.1345 As, respectively.

Bipolar lightning event 2 – recorded on the 8th of June 2011

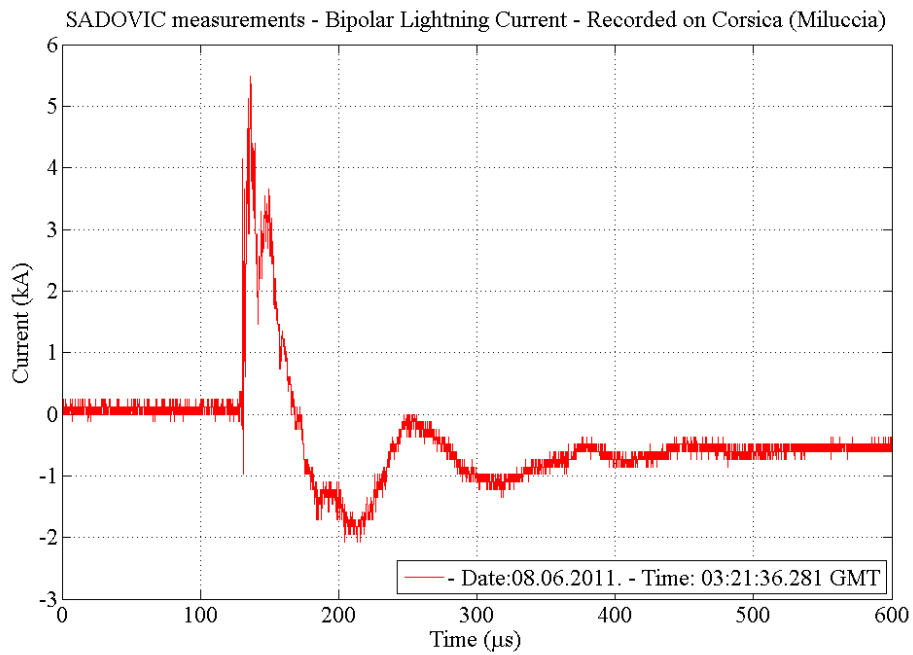


Figure A.2.2. Shape of bipolar current for event 2

The negative part has the peak current of -2.07 kA and the positive part has the peak current of + 5.49 kA, with the total charge transfers being -0.3191 As and +0.1464 As, respectively.

Bipolar lightning event 3 – recorded on the 8th of June 2011

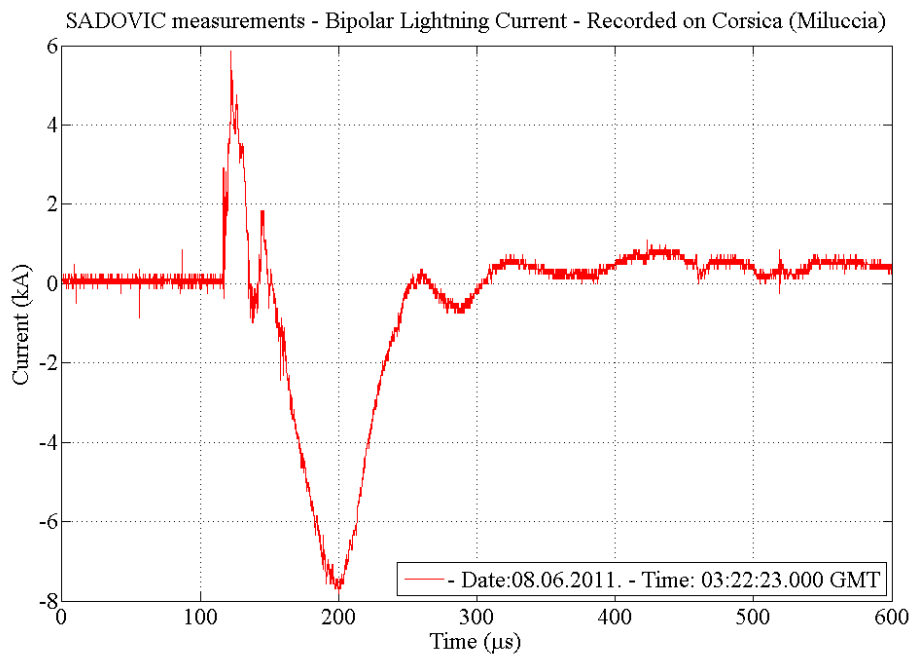


Figure A.2.3. Shape of bipolar current for event 3

The negative part has the peak current of - 7.81 kA and the positive part has the peak current of + 5.86 kA, with the total charge transfers being -0.4174 As and +0.2139 As, respectively.

Bipolar lightning event 4 – recorded on the 8th of June 2011

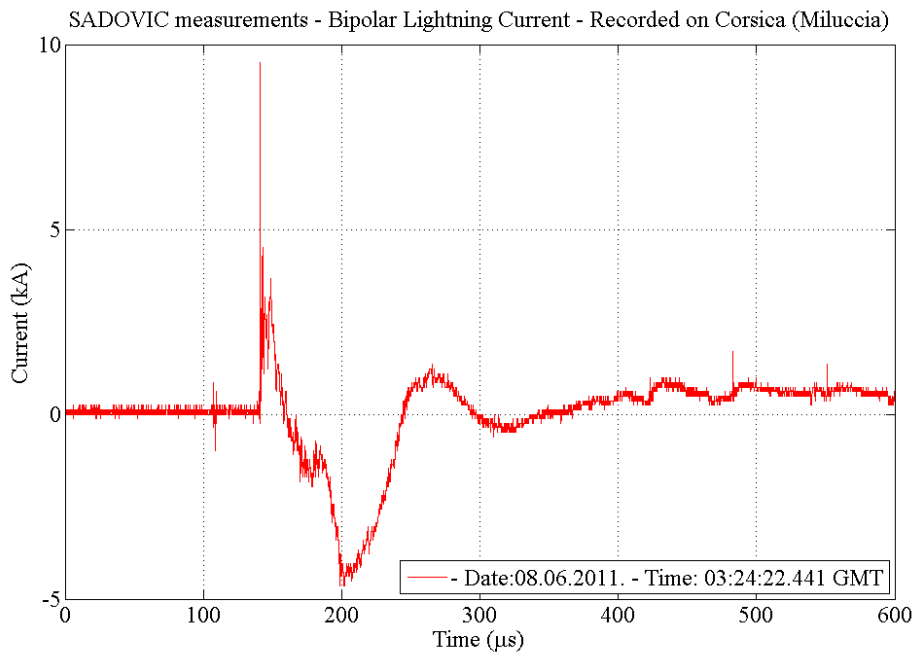


Figure A.2.4. Shape of bipolar current for event 4

The negative part has the peak current of -4.64 kA and the positive part has the peak current of $+9.52$ kA, with the total charge transfers being -0.1885 As and $+0.2280$ As, respectively.

Bipolar lightning event 5 – recorded on the 8th of June 2011

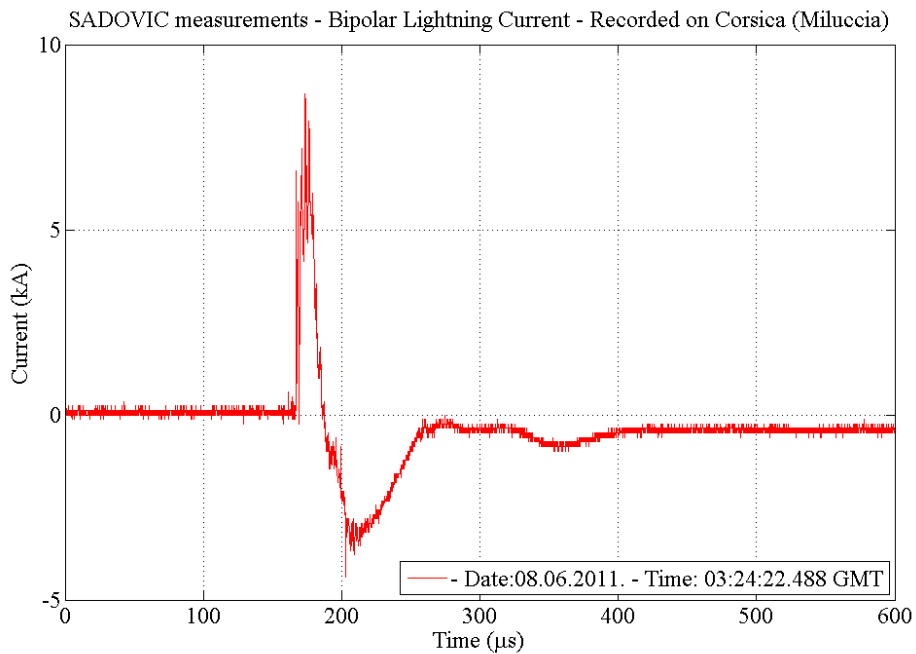


Figure A.2.5. Shape of bipolar current for event 5

The negative part has the peak current of -4.40 kA and the positive part has the peak current of $+8.67$ kA, with the total charge transfers being -0.3304 As and $+0.0780$ As, respectively.

Bipolar lightning event 6 – recorded on the 8th of June 2011

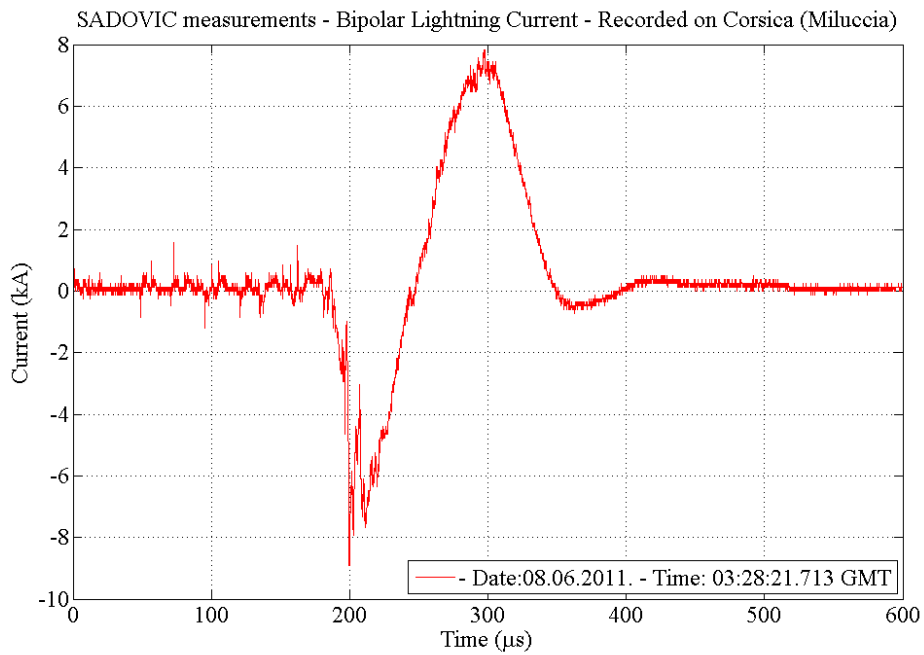


Figure A.2.6. Shape of bipolar current for event 6

The negative part has the peak current of -8.91 kA and the positive part has the peak current of $+7.581$ kA, with the total charge transfers being -0.3019 As and $+0.4804$ As, respectively.

Bipolar lightning event 7 – recorded on the 18th of September 2011

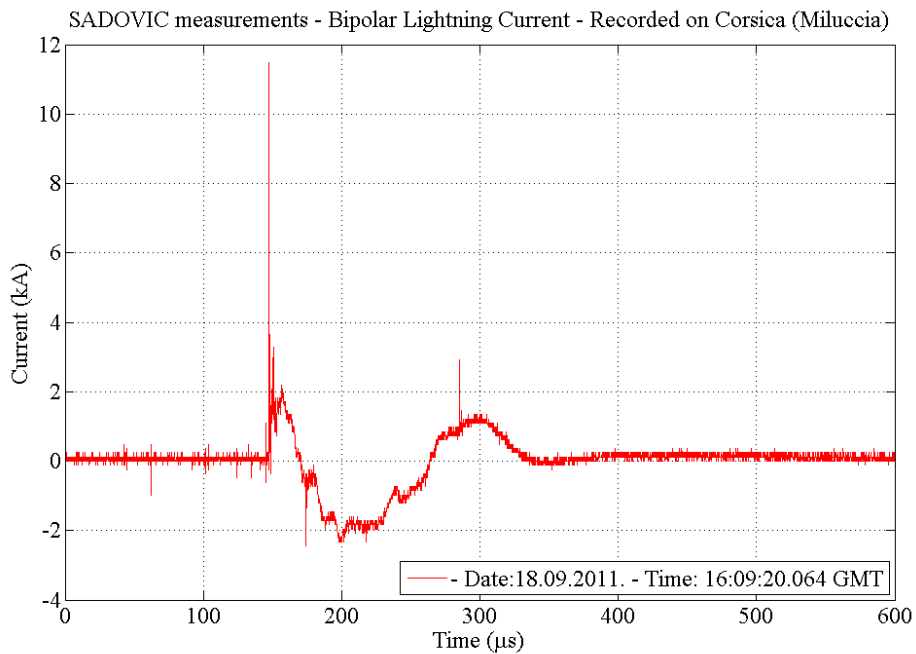


Figure A.2.7. Shape of bipolar current for event 7

The negative part has the peak current of -2.44 kA and the positive part has the peak current of $+11.48$ kA, with the total charge transfers being -0.1314 As and $+0.2024$ As, respectively.

Bipolar lightning event 8 – recorded on the 14th of October 2011

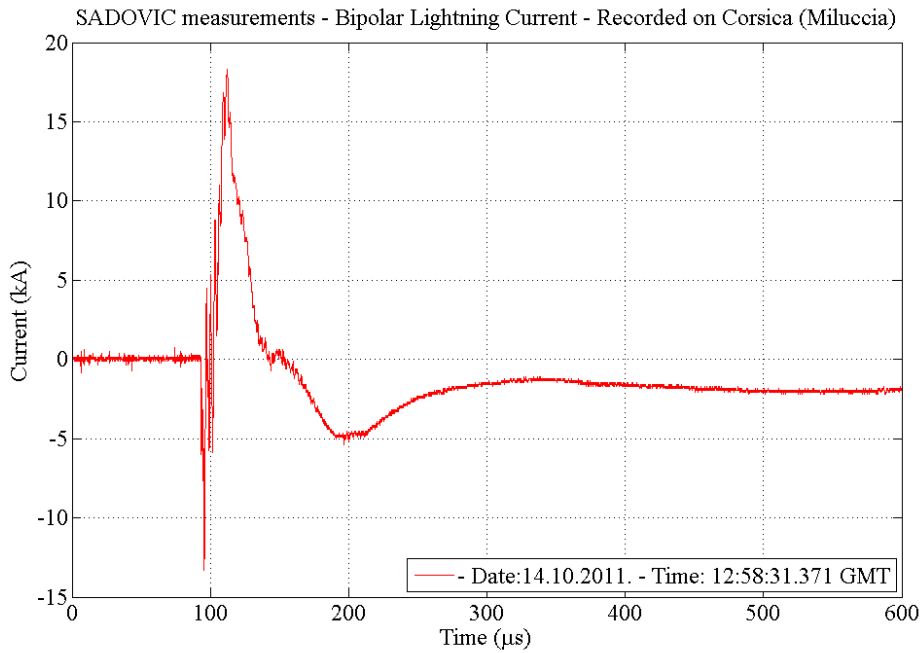


Figure A.2.8. Shape of bipolar current for event 8

The negative part has the peak current of -13.3 kA and the positive part has the peak current of $+18.31$ kA, with the total charge transfers being -0.9913 As and $+0.3531$ As, respectively.

Bipolar lightning event 9 – recorded on the 14th of October 2011

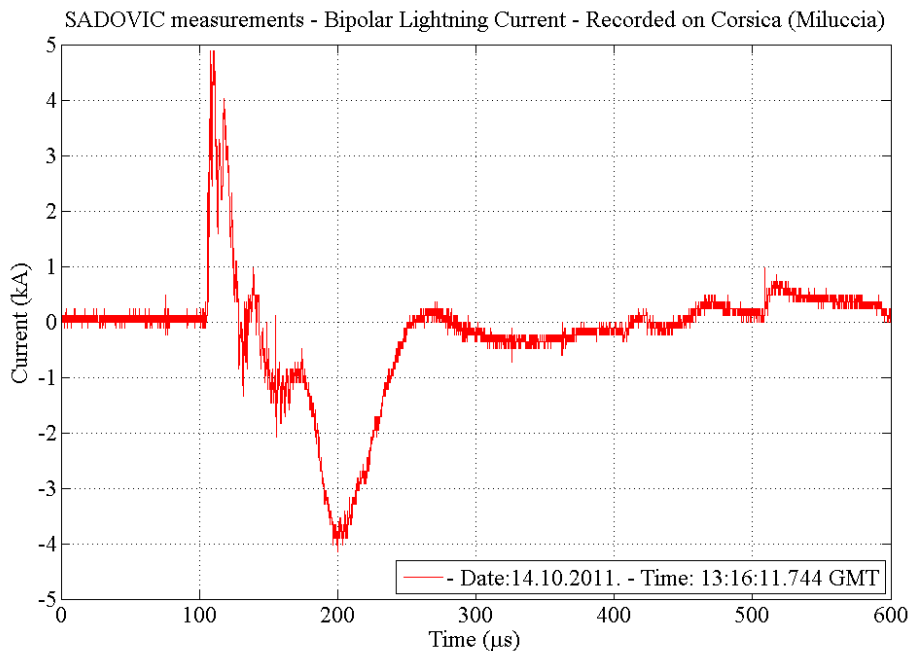


Figure A.2.9. Shape of bipolar current for event 9

The negative part has the peak current of -4.19 kA and the positive part has the peak current of $+4.88$ kA, with the total charge transfers being -0.2892 As and $+0.0612$ As, respectively.

Bipolar lightning event 10 – recorded on the 14th of October 2011

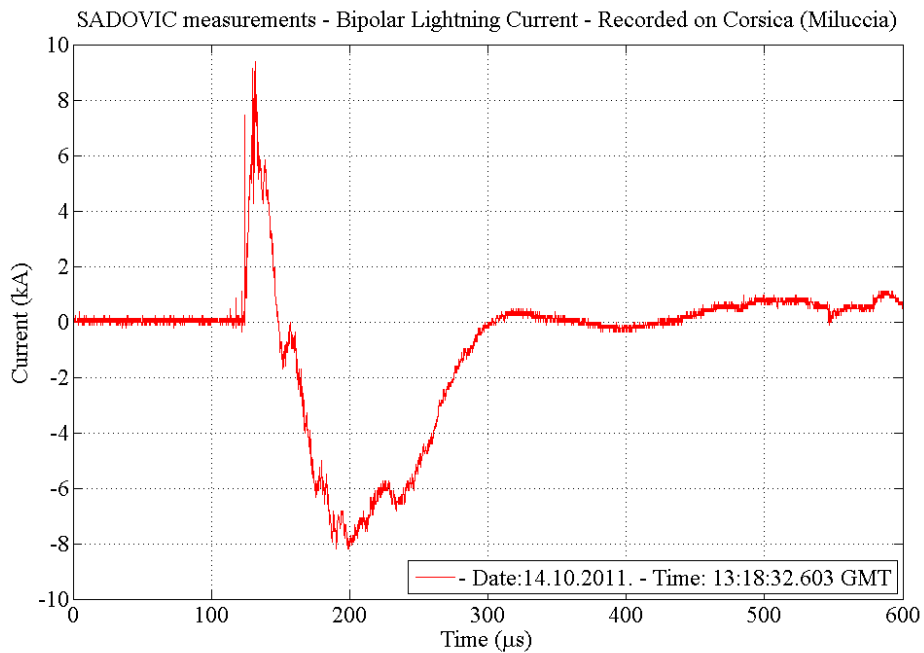


Figure A.2.10. Shape of bipolar current for event 10

The negative part has the peak current of -8.82 kA and the positive part has the peak current of $+9.40$ kA, with the total charge transfers being -0.696 As and $+0.2480$ As, respectively.

Bipolar lightning event 11 – recorded on the 5th of November 2011

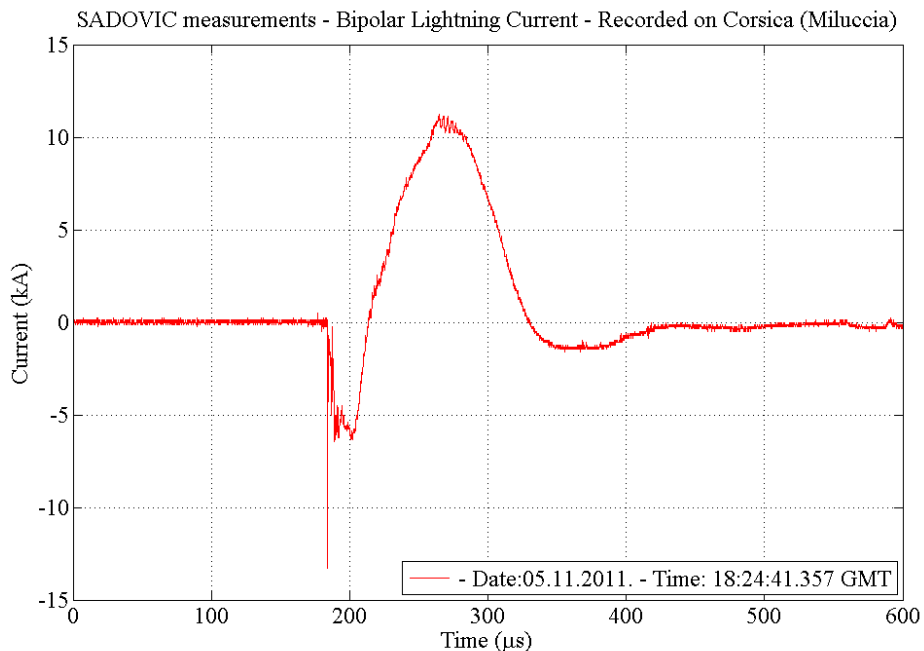


Figure A.2.11. Shape of bipolar current for event 11

The negative part has the peak current of -13.30 kA and the positive part has the peak current of $+11.23$ kA, with the total charge transfers being -0.2670 As and $+0.7544$ As, respectively.

Bipolar lightning event 12 – recorded on the 11th of December 2011

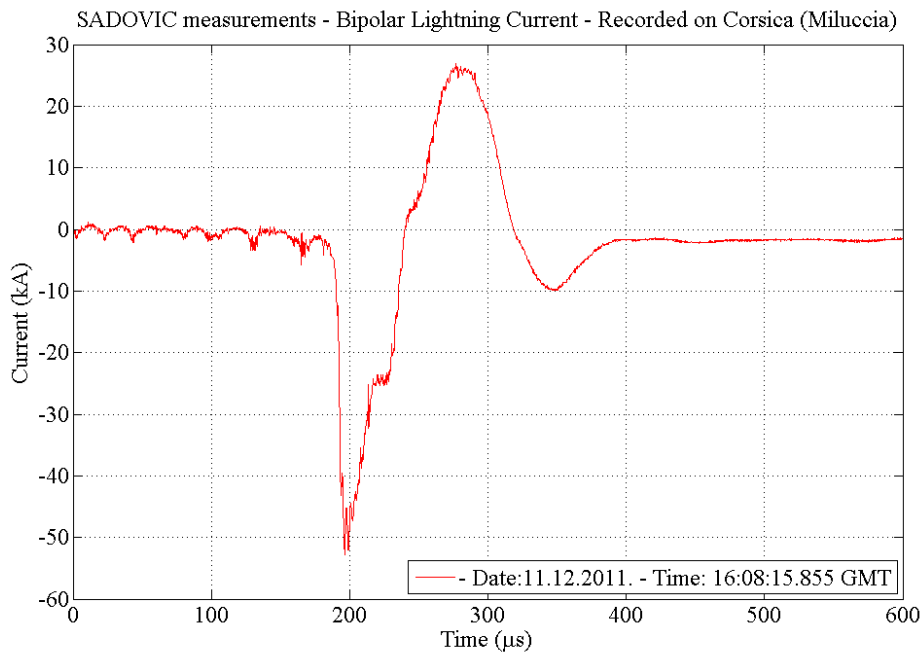


Figure A.2.12. Shape of bipolar current for event 12

The negative part has the peak current of -52.86 kA and the positive part has the peak current of $+26.90$ kA, with the total charge transfers being -2.4062 As and $+1.2487$ As, respectively.

Bipolar lightning event 13 – recorded on the 11th of December 2011

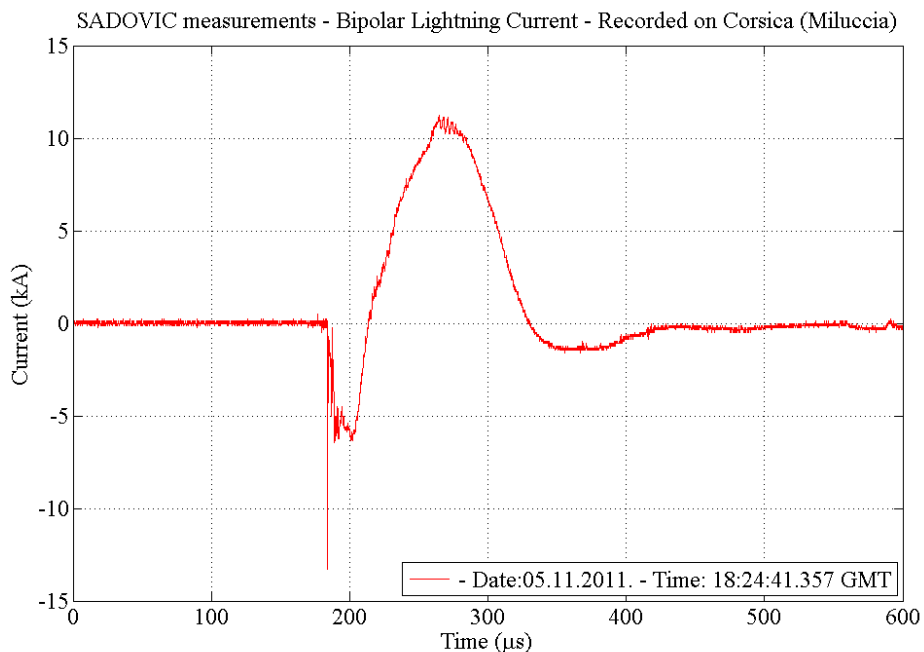


Figure A.2.13. Shape of bipolar current for event 13

The negative part has the peak current of -8.79 kA and the positive part has the peak current of $+2.93$ kA, with the total charge transfers being -0.5086 As and $+0.0793$ As, respectively.

Figure A.2.14 represents histogram of the current peaks for positive part of bipolar lightning currents. Most of the positive current peaks are under 15 kA. Only one current peak is greater than 25 kA.

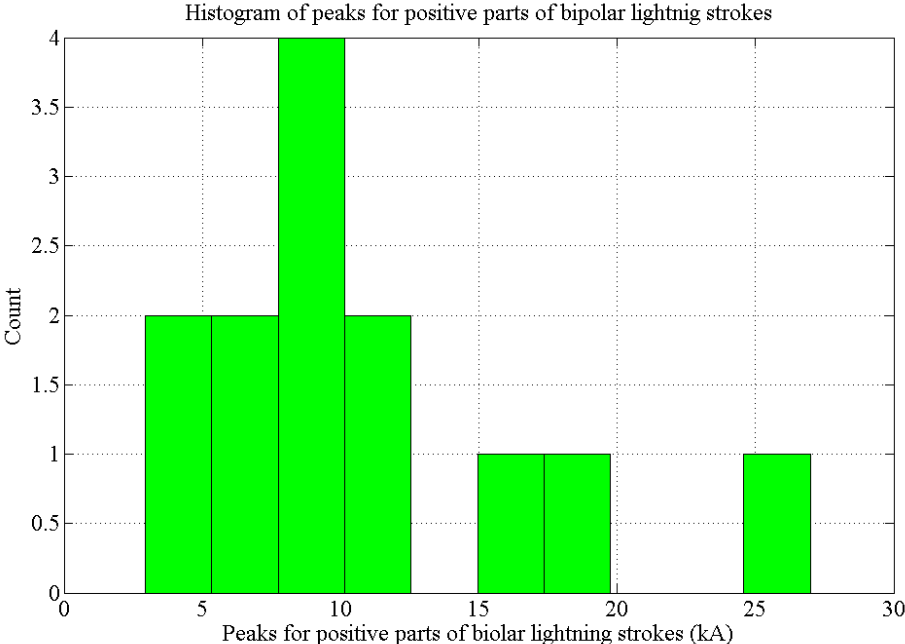


Figure A.2.14. Histogram of current peaks for positive parts of bipolar lightning currents

Figure A.2.15 represents histogram of the current peaks for negative part of bipolar lightning currents. Most of the positive current peaks are under -15 kA. Only one current peak is greater than -50 kA.

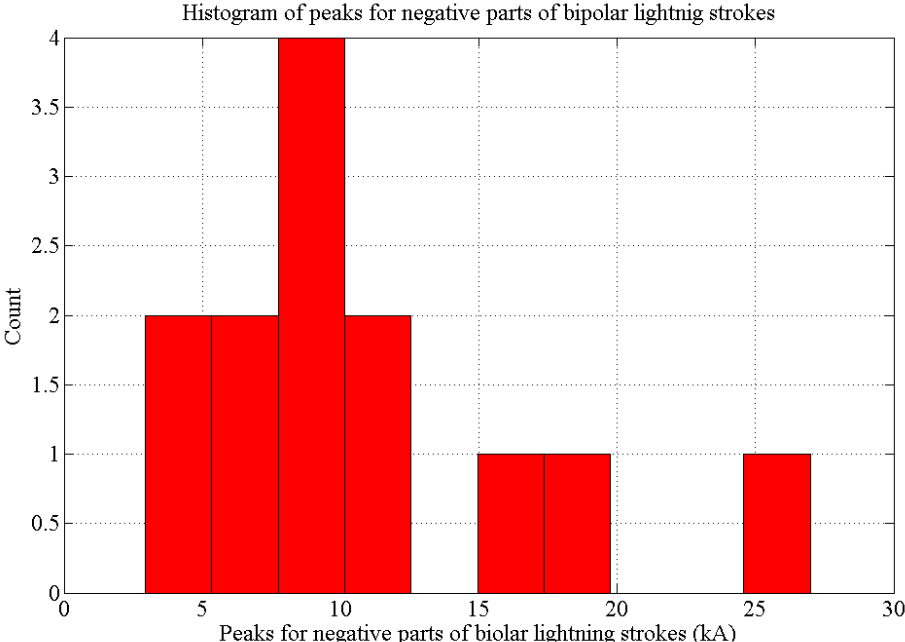


Figure A.2.15. Histogram of current peaks for negative parts of bipolar lightning currents

Figure A.2.16 represents histogram of positive charge transfer of bipolar lightning strokes. Most of the positive current strokes have charge transfer up to 0.8 As (except 1).

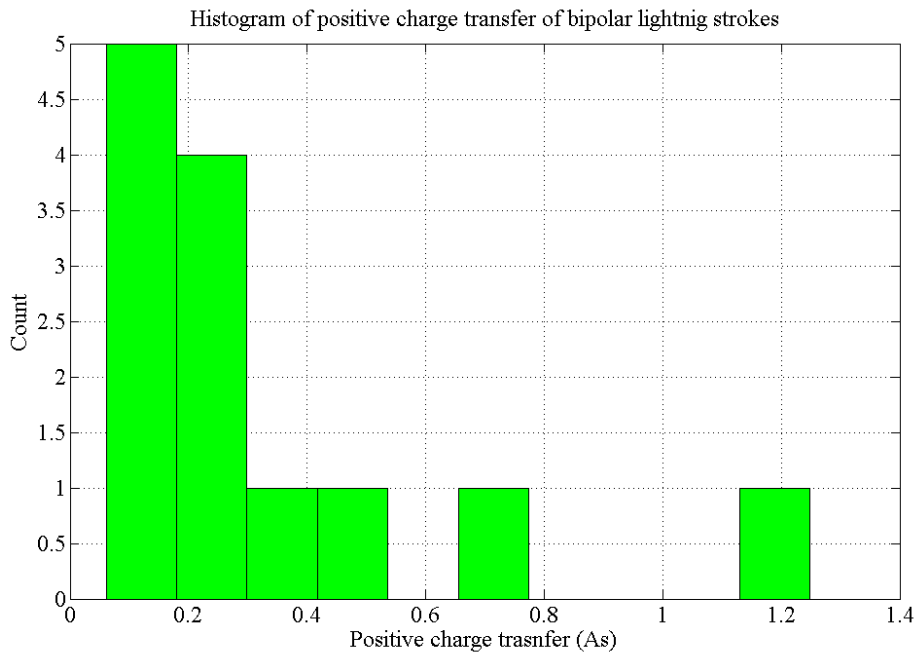


Figure A.2.16. Histogram of positive charge transfer of bipolar lightning strokes

Figure A.2.17 represents histogram of negative charge transfer of bipolar lightning strokes. Most of the negative current strokes have charge transfer up to 1 As (except 1).

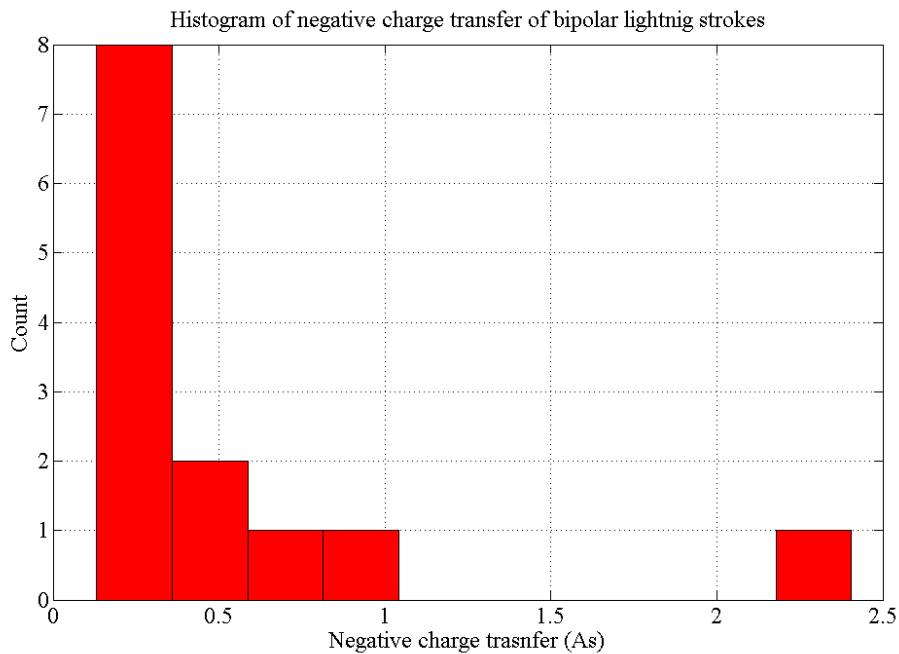


Figure A.2.17. Histogram of negative charge transfer of bipolar lightning strokes

Figure A.2.18 represents histogram of time duration for positive parts of bipolar lightning strokes. Most of the positive current strokes have time duration up to 50 μs .

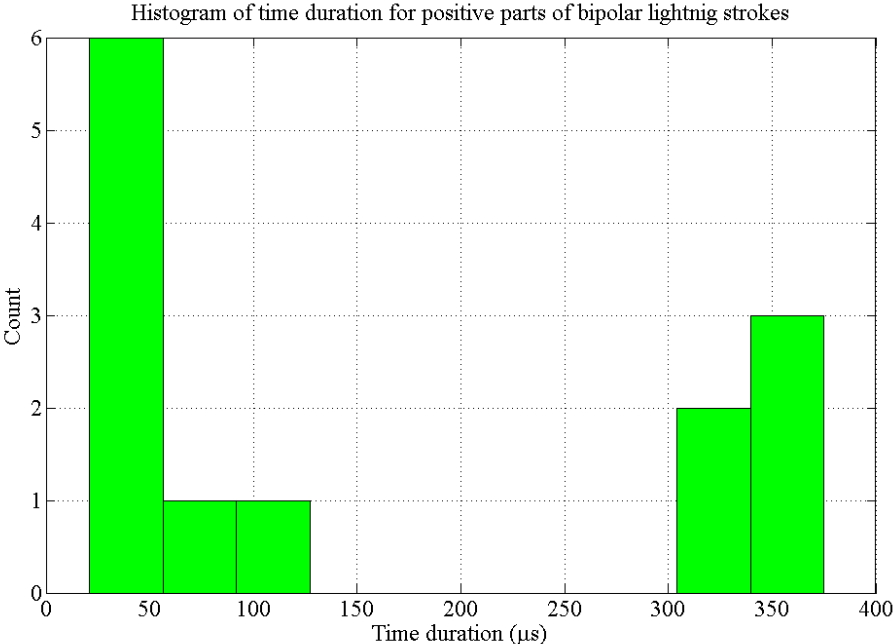


Figure A.2.18. Histogram of time duration for positive parts of bipolar lightning strokes

Figure A.2.19 represents histogram of time duration for positive parts of bipolar lightning strokes. Most of the positive current strokes have time duration up to 50 μs .

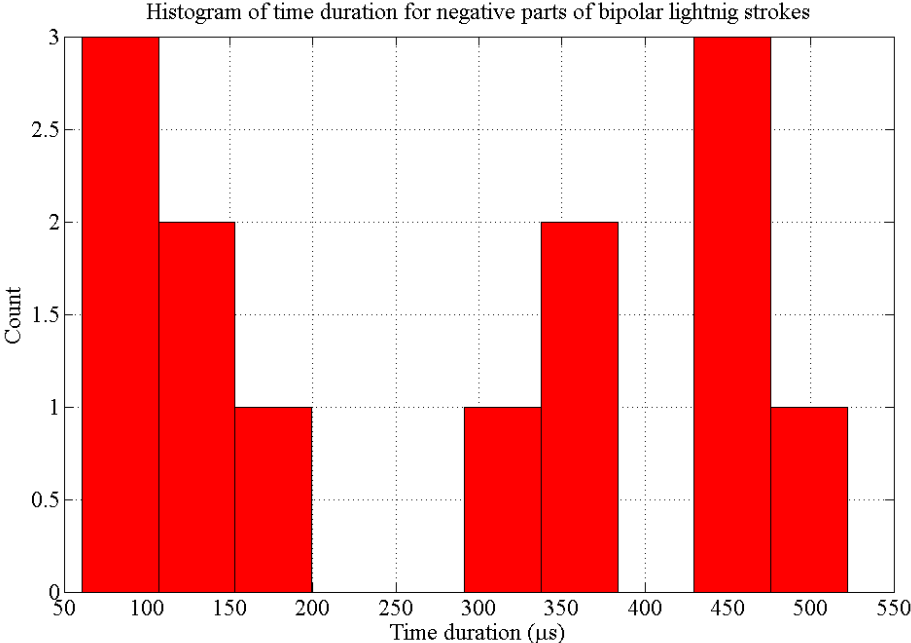


Figure A.2.19. Histogram of time duration for negative parts of bipolar lightning strokes

On telecom base station of Miluccia bipolar lightning events of the first type were recorded, while LINET provides bipolar lightning events of the third type. In eight bipolar events positive current part appears first and after that negative, but in 5 bipolar events first is negative and then positive component. For thirteen recorded bipolar lightning strokes minimum and maximum values of positive current component peaks are 2.93 kA and 26.98 kA, respectively. Mean value and standard deviation are 10.47 kA and 6.61 kA, respectively. Minimum and maximum values of negative current component peaks are -52.86 kA and -2.08 kA, respectively. Mean value and standard deviation are -10.30 kA and 13.32 kA, respectively. Positive charge transfer varies from 0.0612 As to 1.2487 As. Mean value and standard deviation are 0.3253 As and 0.3372As, respectively. Total positive charge transfer is 4.2283 As. Negative charge transfer varies from -0.0612 As to -2.4062 As. Mean value and standard deviation are -0.5358 As and 0.6091 As, respectively. Total negative charge transfer is -6.9654 As. The range variation of total absolute charge transfer is from 0.2793 As to 3.6550 As with a mean value of 0.8611 As and standard deviation of 0.8962 As. Positive current component duration varies from 20.9250 μ s to 375.1000 μ s with a mean value of 166.5023 μ s and standard deviation of 151.5607 μ s. Negative current component duration varies from 60.8000 μ s to 521.9500 μ s with a mean value of 271.4688 μ s and standard deviation of 166.9994 μ s.

A.3. Multicomponent Flashes Data

Flash 1 – recorded on the 28th of November 2012 (flash number 376 in 2012)

Flash 1 is recorded at the location of broadcasting center of Montenegro. LINET data for flash 1 are represented in table A.3.1.

Table A.3.1. LINET data for flash 1

NO.	Date	Time	Latitude	Longitude	Type	Peak (kA)
1	20121128	17:12:29.958	42.3966	18.82	CG	56.3
2	20121128	17:12:30.195	42.3965	18.8174	CG	-17.7

Flash 1 consists of two components. First stroke is positive with current peak of 56.3 kA and second stroke is negative with current peak of -17.7 kA. It is known that third type of bipolar discharge involves return strokes of opposite polarity. So, flash 1 belongs to bipolar lightning type 3. It is very important to emphasize that lightning location systems can only detect bipolar flashes of the type 3 because the slowly varying current components of type 1 and type 2 do not radiate sufficient electromagnetic fields to be detected by the sensors of lightning location systems. Flash duration is 237 ms.

Flash 2 – recorded on the 1st of June 2012 (flash number 237 in 2013)

Flash 2 is recorded at the location of broadcasting centre of Montenegro. LINET data for flash 2 are represented in table A.3.2.

Table A.3.2. LINET data for flash 2

NO.	Date	Time	Latitude	Longitude	Type	Peak (kA)
1	20130601	14:17:58.936	42.393	18.8167	CG	-24.4
2	20130601	14:17:58.948	42.4012	18.8175	CG	6.2

In flash 2 first stroke is negative with current peak of -24.4 kA and second stroke is positive with current peak of 6.2 kA. As well as flash 1, flash 2 belongs to bipolar lightning type 3. Duration of flash 2 is 12 ms.

Flash 3 – recorded on the 27th of August 2013 (flash number 32 in 2013)

Flash 3 is recorded at the of location Njegoš's Mausoleum in Montenegro. LINET data for flash 3 are represented in table A.3.3.

Table A.3.3. LINET data for flash 3

NO.	Date	Time	Latitude	Longitude	Type	Peak (kA)
1	20130827	07:33:54.550	42.3924	18.8392	CG	-35.3
2	20130827	07:33:54.560	42.3925	18.8351	CG	-11.6
3	20130827	07:33:54.609	42.392	18.8391	CG	-22.8
4	20130827	07:33:55.040	42.394	18.842	CG	-9.3
5	20130827	07:33:55.080	42.3921	18.8395	CG	-11.4
6	20130827	07:33:55.144	42.3917	18.8396	CG	-7.9
7	20130827	07:33:55.199	42.3945	18.8418	CG	-7.9
8	20130827	07:33:55.265	42.395	18.8365	CG	-10.5
9	20130827	07:33:55.299	42.3917	18.8396	CG	-14.1
10	20130827	07:33:55.325	42.3918	18.8393	CG	-9
11	20130827	07:33:55.437	42.3916	18.8394	CG	-7.8
12	20130827	07:33:55.471	42.3949	18.8419	CG	-7.3
13	20130827	07:33:55.501	42.3948	18.8418	CG	-8.2
14	20130827	07:33:55.545	42.3950	18.8362	CG	-9.3

All components in flash 3 are negative and current peaks for each component are given in table A.3.3. Interstroke time intervals are represented in table A.3.4. Table A.3.5 represents summary of basic data for flash 3. In this case first stroke have larger current peak than subsequent strokes.

Table A.3.4. Interstroke time interval for flash 3

Time interval between components	Interval duration (ms)	Time interval between components	Interval duration (ms)	Time interval between components	Interval duration (ms)
1 and 2	10.0000	6 and 7	55.0000	11 and 12	34.0000
2 and 3	49.0000	7 and 8	66.0000	12 and 13	30.0000
3 and 4	431.0000	8 and 9	34.0000	13 and 14	44.0000
4 and 5	40.0000	9 and 10	26.0000		
5 and 6	64.0000	10 and 11	112.0000		

Table A.3.5. Summary of basic data for flash 3

Number of components in flash	14
Type	CG
Polarity	all negative
Peak (kA)	-35.3
Flash duration (ms)	995
Minimum duration between components (ms)	10
Maximum duration between components (ms)	431
Mean value of interstroke time interval (ms)	76.5385
Standard deviation of interstroke time interval (ms)	109.3737

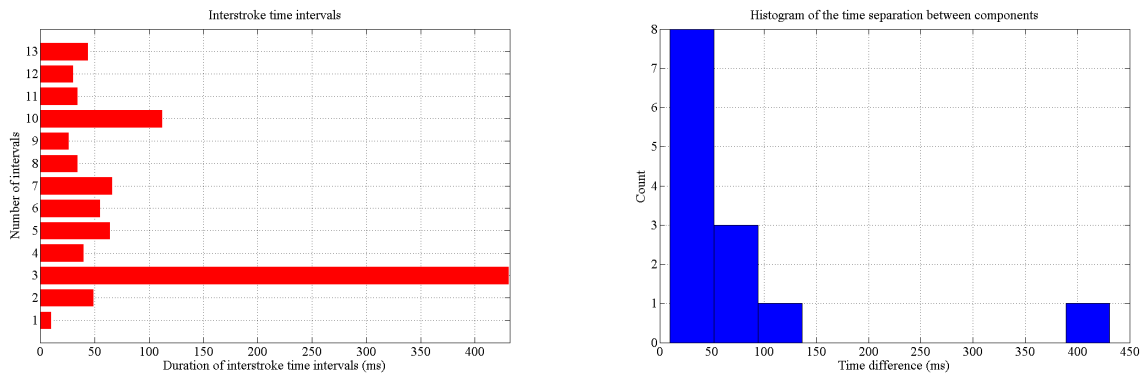


Figure A.3.1. Display and histogram of interstroke time interval data for flash 3

Display and histogram of interstroke time interval data are shown in figure A.3.1. In this histogram most of interstroke intervals (eight intervals) are up to 50 ms, but all of interstroke intervals (except one) are up to 110 ms.

Flash 4 – recorded on the 3rd of February 2012 (flash number 98 in 2012)

Flash 4 is recorded at the location of broadcasting centre of Montenegro. LINET data for flash 4 are represented in table A.3.6. All components in flash 4 are negative and current peaks for each component are given in table A.3.6. Interstroke time intervals are represented in table A.3.7. Table A.3.8 represents summary of basic data for flash 4. This flash is example of the case when first stroke does not have larger current peak than subsequent strokes. Display and histogram of interstroke time interval data for flash 4 are shown in figure A.3.2.

Table A.3.6. LINET data for flash 4

NO.	Date	Time	Latitude	Longitude	Type	Peak (kA)
1	20120203	14:47:04.0790457	42.3958	18.8184	CG	-8.9
2	20120203	14:47:04.1000549	42.3958	18.8181	CG	-4.3
3	20120203	14:47:04.1430843	42.3948	18.8158	CG	-30.9
4	20120203	14:47:04.1572068	42.396	18.817	CG	-10.3
5	20120203	14:47:04.1754401	42.3977	18.8136	CG	-16.5
6	20120203	14:47:04.1794631	42.3965	18.8159	CG	-11.9
7	20120203	14:47:04.1927085	42.3962	18.8171	CG	-8.9
8	20120203	14:47:04.1980295	42.3957	18.8165	CG	-12.3
9	20120203	14:47:04.2248881	42.3959	18.817	CG	-10
10	20120203	14:47:04.2370639	42.3952	18.8158	CG	-22.4
11	20120203	14:47:04.2650966	42.3958	18.8174	CG	-16.7
12	20120203	14:47:04.2779066	42.396	18.8184	CG	-7.5
13	20120203	14:47:04.2810023	42.396	18.8172	CG	-6
14	20120203	14:47:04.2967785	42.3955	18.8171	CG	-13
15	20120203	14:47:04.3067932	42.3963	18.8164	CG	-9.3
16	20120203	14:47:04.3305529	42.3962	18.8167	CG	-7.5
17	20120203	14:47:04.3413539	42.3952	18.8166	CG	-16.1
18	20120203	14:47:04.3494425	42.396	18.8159	CG	-11.3
19	20120203	14:47:04.3520621	42.3959	18.8161	CG	-8.3
20	20120203	14:47:04.3767579	42.3963	18.8165	CG	-12.5
21	20120203	14:47:04.3979001	42.3952	18.8166	CG	-14.7
22	20120203	14:47:04.4033752	42.3973	18.8156	CG	-17.1
23	20120203	14:47:04.4358198	42.3954	18.8169	CG	-27.5
24	20120203	14:47:04.4551659	42.3962	18.8178	CG	-5.1
25	20120203	14:47:04.4614704	42.3967	18.8168	CG	-12.4
26	20120203	14:47:04.4845443	42.3961	18.8165	CG	-10.1
27	20120203	14:47:04.5363155	42.3953	18.8146	CG	-18
28	20120203	14:47:04.5557635	42.3957	18.8152	CG	-11.1
29	20120203	14:47:04.5868977	42.3958	18.8149	CG	-11.9
30	20120203	14:47:04.6675913	42.3958	18.8147	CG	-15.5
31	20120203	14:47:04.7052179	42.3961	18.8158	CG	-10.3
32	20120203	14:47:04.8656488	42.3959	18.8151	CG	-12.9
33	20120203	14:47:04.8974373	42.3961	18.8153	CG	-16

Table A.3.7. Interstroke time interval for flash 4

Time interval between components	Interval duration (ms)	Time interval between components	Interval duration (ms)	Time interval between components	Interval duration (ms)
1 and 2	21.0092	12 and 13	3.0957	23 and 24	19.3461
2 and 3	43.0294	13 and 14	15.7762	24 and 25	6.3045
3 and 4	14.1225	14 and 15	10.0147	25 and 26	23.0739
4 and 5	18.2333	15 and 16	23.7597	26 and 27	51.7712
5 and 6	4.0230	16 and 17	10.8010	27 and 28	19.4480
6 and 7	13.2454	17 and 18	8.0886	28 and 29	31.1342
7 and 8	5.3210	18 and 19	2.6196	29 and 30	80.6936
8 and 9	26.8586	19 and 20	24.6958	30 and 31	37.6266
9 and 10	12.1758	20 and 21	21.1422	31 and 32	160.4309
10 and 11	28.0327	21 and 22	5.4751	32 and 33	31.7885
11 and 12	12.8100	22 and 23	32.4446		

Table A.3.8. Summary of basic data for flash 4

Number of components in flash	33
Type	CG
Polarity	all negative
Peak (kA)	-30.9
Flash duration (ms)	818.3916
Minimum duration between components (ms)	2.6196
Maximum duration between components (ms)	160.4309
Mean value of interstroke time interval (ms)	25.5747
Standard deviation of interstroke time interval (ms)	29.4224

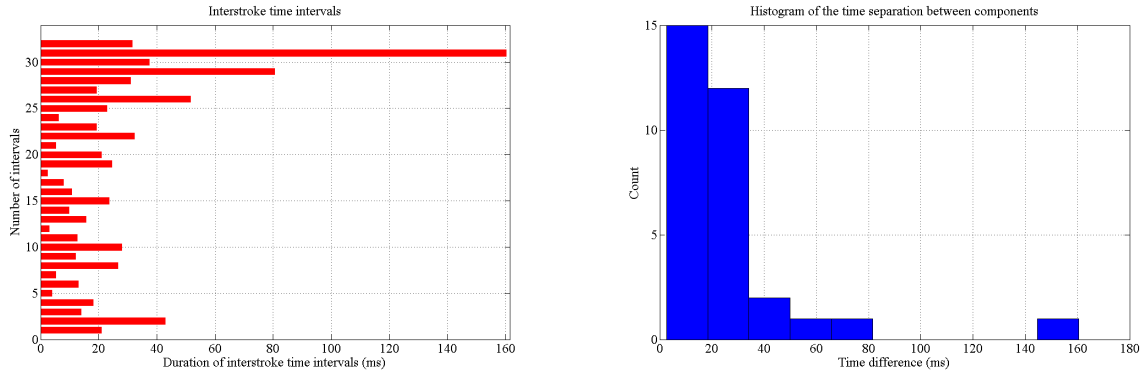


Figure A.3.2. Display and histogram of interstroke time interval data for flash 4

In histogram all of interstroke intervals (except one) are up to 80 ms.

Flash 5 – recorded on the 4th of February 2012 (flash number 186 in 2012)

Flash 5 is recorded at the location of broadcasting center of Montenegro. LINET data for flash 5 are represented in table A.3.9. All components in flash 5 are negative and current peaks for each component are given in table A.3.9. Interstroke time intervals are represented in table A.3.10. Table A.3.11 represents summary of basic data for flash 5.

Table A.3.9. LINET data for flash 5

NO.	Date	Time	Latitude	Longitude	Type	Peak (kA)
1	20120204	01:57:23.8718542	42.3951	18.8179	CG	-5.8
2	20120204	01:57:23.8941698	42.3959	18.8178	CG	-6.9
3	20120204	01:57:23.9373682	42.3953	18.8171	CG	-8
4	20120204	01:57:23.9392176	42.3953	18.817	CG	-8
5	20120204	01:57:23.9529402	42.3961	18.8167	CG	-8.6
6	20120204	01:57:23.9621019	42.3953	18.817	CG	-9.2
7	20120204	01:57:23.9931445	42.3961	18.8171	CG	-5.8
8	20120204	01:57:23.9995558	42.3944	18.8158	CG	-11.7
9	20120204	01:57:24.0075524	42.3955	18.8165	CG	-8.6
10	20120204	01:57:24.0121430	42.3961	18.8175	CG	-5.3
11	20120204	01:57:24.0207327	42.3958	18.8179	CG	-6.9
12	20120204	01:57:24.0357921	42.3956	18.8165	CG	-10.3
13	20120204	01:57:24.0436689	42.3961	18.8166	CG	-11
14	20120204	01:57:24.0470212	42.3956	18.8165	CG	-12.4
15	20120204	01:57:24.0643977	42.3958	18.818	CG	-7.1
16	20120204	01:57:24.0673937	42.3961	18.8173	CG	-7.5
17	20120204	01:57:24.0888633	42.3955	18.8177	CG	-4.5
18	20120204	01:57:24.0927201	42.3957	18.8172	CG	-6.1
19	20120204	01:57:24.1153518	42.3954	18.8183	CG	-12.4
20	20120204	01:57:24.1200273	42.3949	18.8164	CG	-11.8

NO.	Date	Time	Latitude	Longitude	Type	Peak (kA)
21	20120204	01:57:24.1222307	42.3959	18.8173	CG	-9.7
22	20120204	01:57:24.1518185	42.3956	18.8177	CG	-9.4
23	20120204	01:57:24.1562672	42.3957	18.8168	CG	-11.1
24	20120204	01:57:24.1577798	42.3962	18.8174	CG	-7.2
25	20120204	01:57:24.1863772	42.3962	18.8177	CG	-5.9
26	20120204	01:57:24.1928735	42.3956	18.8183	CG	-7.2
27	20120204	01:57:24.1945725	42.3956	18.8161	CG	-13.9
28	20120204	01:57:24.1961165	42.3963	18.817	CG	-6.5
29	20120204	01:57:24.2228447	42.3958	18.8176	CG	-8.8
30	20120204	01:57:24.2334993	42.3956	18.8169	CG	-9.5
31	20120204	01:57:24.2511776	42.3951	18.8174	CG	-11.1
32	20120204	01:57:24.2784858	42.3957	18.8165	CG	-8.8
33	20120204	01:57:24.2971717	42.3956	18.818	CG	-11.3
34	20120204	01:57:24.3036042	42.3961	18.8169	CG	-5.7
35	20120204	01:57:24.3078557	42.3952	18.8166	CG	-16.9
36	20120204	01:57:24.3560298	42.3958	18.8173	CG	-9.5
37	20120204	01:57:24.3597654	42.3973	18.815	CG	-14.1
38	20120204	01:57:24.3832785	42.3954	18.8171	CG	-13.4
39	20120204	01:57:24.4109983	42.3967	18.8176	CG	-10.7
40	20120204	01:57:24.4288106	42.3956	18.8164	CG	-12.4
41	20120204	01:57:24.4825190	42.3977	18.816	CG	-19.9
42	20120204	01:57:24.5140882	42.3963	18.817	CG	-15.1

Table A.3.10. Interstroke time interval for flash 5

Time interval between components	Interval duration (ms)	Time interval between components	Interval duration (ms)	Time interval between components	Interval duration (ms)
1 and 2	22.3156	15 and 16	2.9960	29 and 30	10.6546
2 and 3	43.1984	16 and 17	21.4696	30 and 31	17.6783
3 and 4	1.8494	17 and 18	3.8568	31 and 32	27.3082
4 and 5	13.7226	18 and 19	22.6317	32 and 33	18.6859
5 and 6	9.1617	19 and 20	4.6755	33 and 34	6.4325
6 and 7	31.0426	20 and 21	2.2034	34 and 35	4.2515
7 and 8	6.4113	21 and 22	29.5878	35 and 36	48.1741
8 and 9	7.9966	22 and 23	4.4487	36 and 37	3.7356
9 and 10	4.5906	23 and 24	1.5126	37 and 38	23.5131
10 and 11	8.5897	24 and 25	28.5974	38 and 39	27.7198
11 and 12	15.0594	25 and 26	6.4963	39 and 40	17.8123
12 and 13	7.8768	26 and 27	1.6990	40 and 41	53.7084
13 and 14	3.3523	27 and 28	1.5440	41 and 42	31.5692
14 and 15	17.3765	28 and 29	26.7282		

Table A.3.11. Summary of basic data for flash 5

Number of components in flash	42
Type	CG
Polarity	all negative
Peak (kA)	-19.9
Flash duration (ms)	642.2340
Minimum duration between components (ms)	1.5156
Maximum duration between components (ms)	53.7084
Mean value of interstroke time interval (ms)	15.6642
Standard deviation of interstroke time interval (ms)	13.4916

Flash 5 is also example of the case when first stroke does not have larger current peak than subsequent strokes. Display and histogram of interstroke time interval data for flash 5 are shown in figure A.3.3.

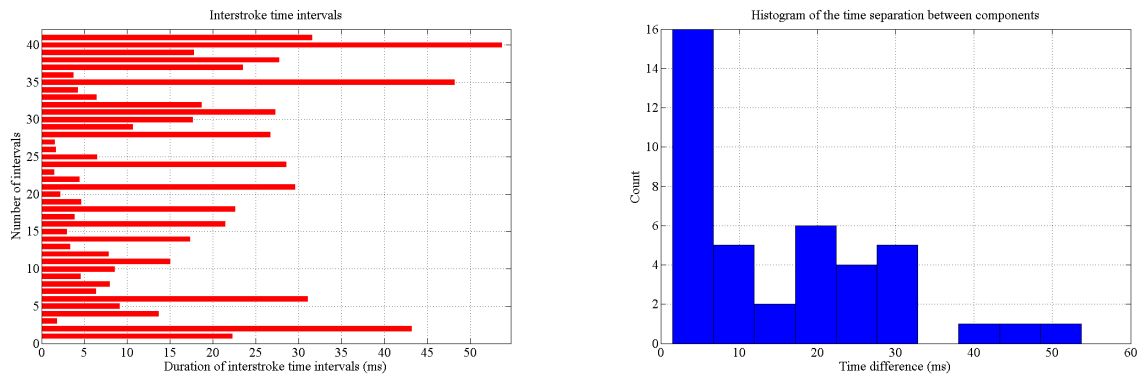


Figure A.3.3. Display and histogram of interstroke time interval data for flash 5

In this histogram all of interstroke intervals are up to 60 ms, most of them are up to 30 ms (36 interstroke intervals).

Flash 6 – recorded on the 18th of the March 2013 (flash number 1891 in 2013)

Flash 6 is recorded for location broadcasting center of Montenegro. LINET data for flash 6 are represented in table A.3.12. All components in flash 6 are negative and current peaks for each component are given in table A.3.12. Interstroke time intervals are represented in table A.3.13. Table A.3.14 represents summary of basic data for flash 6.

Table A.3.12. LINET data for flash 6

NO.	Date	Time	Latitude	Longitude	Type	Peak (kA)
1	20130318	19:40:01.619	42.3986	18.8176	CG	-11.8
2	20130318	19:40:01.634	42.3962	18.8174	CG	-6.6
3	20130318	19:40:01.666	42.3968	18.8163	CG	-16.7
4	20130318	19:40:01.683	42.3956	18.8179	CG	-3.9
5	20130318	19:40:01.703	42.3965	18.8171	CG	-10.5
6	20130318	19:40:01.726	42.3958	18.8178	CG	-5.4
7	20130318	19:40:01.734	42.3957	18.8184	CG	-4.1
8	20130318	19:40:01.756	42.3966	18.8171	CG	-11.9
9	20130318	19:40:01.764	42.3973	18.8177	CG	-15.1
10	20130318	19:40:01.766	42.3964	18.8172	CG	-7.2
11	20130318	19:40:01.783	42.397	18.8171	CG	-7.6
12	20130318	19:40:01.789	42.3974	18.8173	CG	-16.2
13	20130318	19:40:01.804	42.3971	18.8169	CG	-9.5
14	20130318	19:40:01.809	42.3964	18.8168	CG	-10
15	20130318	19:40:01.817	42.3978	18.8168	CG	-12
16	20130318	19:40:01.828	42.3967	18.817	CG	-7.4
17	20130318	19:40:01.842	42.3963	18.8183	CG	-4.5
18	20130318	19:40:01.846	42.3966	18.8172	CG	-4.5
19	20130318	19:40:01.865	42.3971	18.8171	CG	-10.5
20	20130318	19:40:01.870	42.3986	18.8212	CC	-4
21	20130318	19:40:01.874	42.3975	18.8139	CG	-24.1
22	20130318	19:40:01.886	42.3964	18.8169	CG	-5.7
23	20130318	19:40:01.897	42.397	18.817	CG	-8
24	20130318	19:40:01.910	42.3966	18.8167	CG	-6.4
25	20130318	19:40:01.913	42.3973	18.8145	CG	-11
26	20130318	19:40:01.929	42.3965	18.8183	CG	-3.6
27	20130318	19:40:01.955	42.3976	18.8172	CG	-10.4
28	20130318	19:40:02.001	42.3974	18.817	CG	-9.3

NO.	Date	Time	Latitude	Longitude	Type	Peak (kA)
29	20130318	19:40:02.010	42.3974	18.8177	CG	-11.5
30	20130318	19:40:02.040	42.3971	18.8173	CG	-9.8
31	20130318	19:40:02.048	42.3975	18.8169	CG	-9
32	20130318	19:40:02.059	42.3962	18.8172	CG	-4.4
33	20130318	19:40:02.071	42.3974	18.8169	CG	-10.8
34	20130318	19:40:02.097	42.3968	18.8177	CG	-10.1
35	20130318	19:40:02.113	42.397	18.8178	CG	-21
36	20130318	19:40:02.135	42.3964	18.818	CG	-6.6
37	20130318	19:40:02.140	42.397	18.8167	CG	-15.6
38	20130318	19:40:02.162	42.3963	18.8173	CG	-6.2
39	20130318	19:40:02.179	42.3963	18.8171	CG	-7.5
40	20130318	19:40:02.205	42.396	18.8182	CG	-4.7
41	20130318	19:40:02.229	42.3972	18.8176	CG	-16.3
42	20130318	19:40:02.246	42.3974	18.8174	CG	-10.7
43	20130318	19:40:02.437	42.3975	18.8161	CG	-18.5
44	20130318	19:40:02.466	42.3972	18.8173	CG	-8.9
45	20130318	19:40:02.514	42.3974	18.8168	CG	-12.5

Table A.3.13. Interstroke time interval for flash 6

Time interval between components	Interval duration (ms)	Time interval between components	Interval duration (ms)	Time interval between components	Interval duration (ms)
1 and 2	15.0000	16 and 17	14.0000	31 and 32	11.0000
2 and 3	32.0000	17 and 18	4.0000	32 and 33	12.0000
3 and 4	17.0000	18 and 19	19.0000	33 and 34	26.0000
4 and 5	20.0000	19 and 20	5.0000	34 and 35	16.0000
5 and 6	23.0000	20 and 21	4.0000	35 and 36	22.0000
6 and 7	8.0000	21 and 22	12.0000	36 and 37	5.0000
7 and 8	22.0000	22 and 23	11.0000	37 and 38	22.0000
8 and 9	8.0000	23 and 24	13.0000	38 and 39	17.0000
9 and 10	2.0000	24 and 25	3.0000	39 and 40	26.0000
10 and 11	17.0000	25 and 26	16.0000	40 and 41	24.0000
11 and 12	6.0000	26 and 27	26.0000	41 and 42	17.0000
12 and 13	15.0000	27 and 28	46.0000	42 and 43	191.0000
13 and 14	5.0000	28 and 29	9.0000	43 and 44	29.0000
14 and 15	8.0000	29 and 30	30.0000	44 and 45	48.0000
15 and 16	11.0000	30 and 31	8.0000		

Table A.3.14. Summary of basic data for flash 6

Number of components in flash	45
Type	CG
Polarity	all negative
Peak (kA)	-24.1
Flash duration (ms)	895
Minimum duration between components (ms)	2
Maximum duration between components (ms)	191
Mean value of interstroke time interval (ms)	20.3409
Standard deviation of interstroke time interval (ms)	28.2982

Flash 6 is also example of the case when first stroke does not have larger current peak than subsequent strokes. Display and histogram of interstroke time interval data for flash 6 are shown in figure A.3.4.

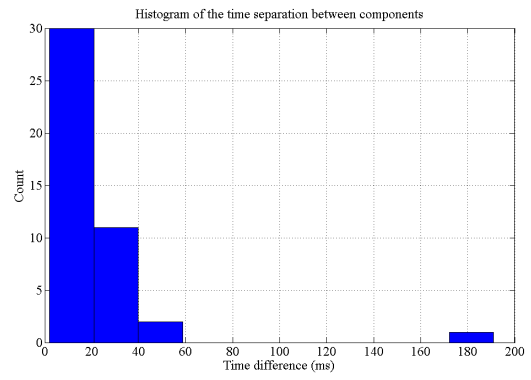
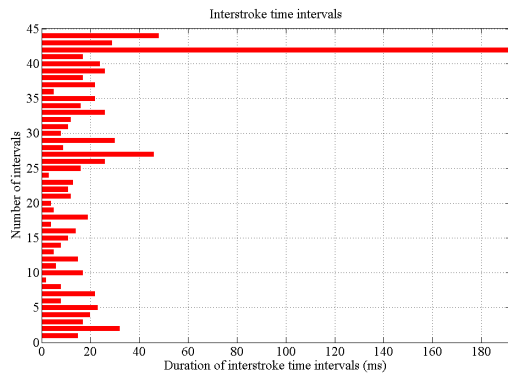


Figure A.3.4. Display and histogram of interstroke time interval data for flash 6

In the histogram shown above all of the interstroke intervals (except one) are up to 60 ms. For multicomponent flashes with large number of components, interstroke intervals ranges from 60 ms to 80 ms.

A.4. Basic Flowcharts of Software for Lightning Data Analyses

Basic flowchart of software for measured bipolar lightning current analysis is shown in figure A.4.1.

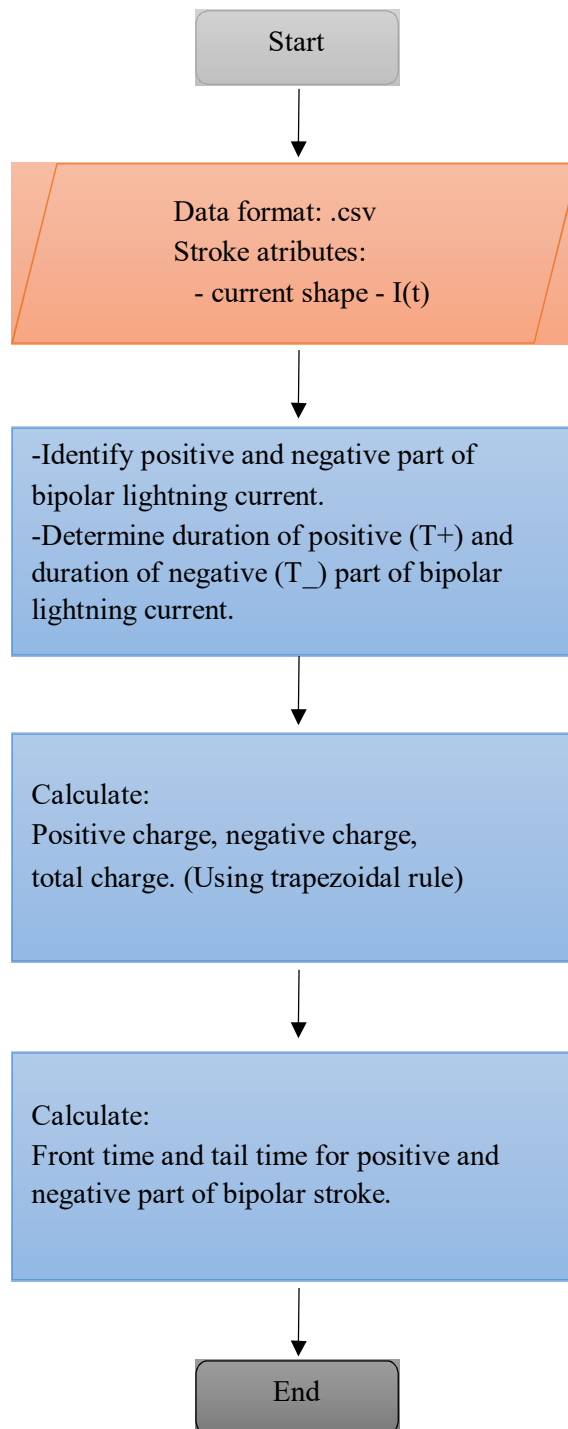


Figure A.4.1. Basic flowchart for measured bipolar lightning current analysis

Basic flowchart of software for extraction of specific multicomponent lightning flashes from lightning location system data is given in figure A.4.2.

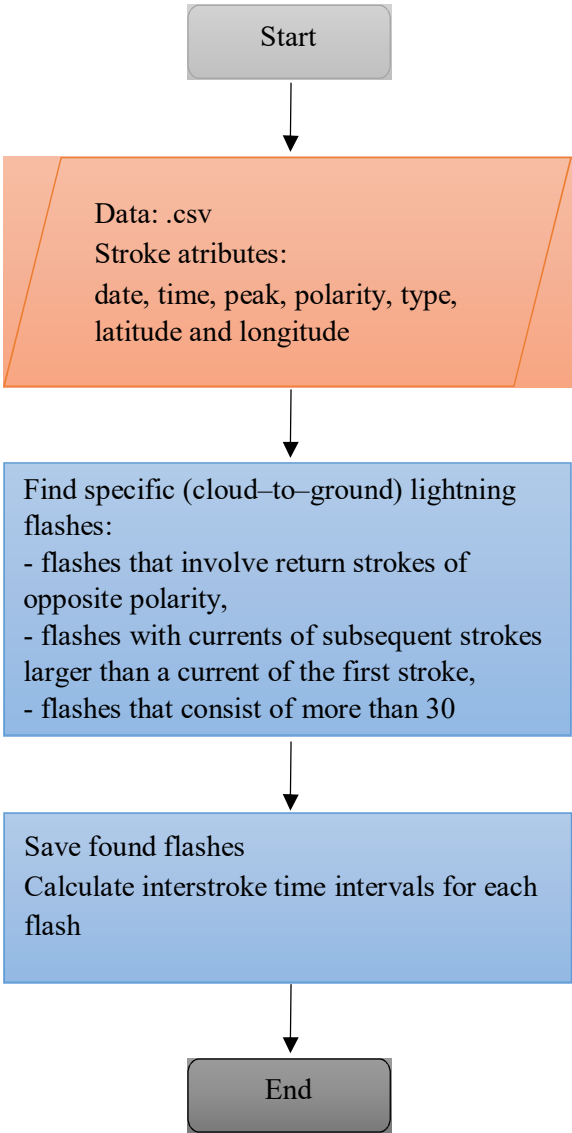


Figure A.4.2. Basic flowchart of software for extraction of specific multicomponent lightning flashes

Appendix B

MATLAB CODE FOR LINE SURGE ARRESTER ENERGY DUTY CALCULATION

An analogy between calculation of line surge arrester energy duty in EMTP – RV and MATLAB is given in Chapter 5. MATLAB code for line surge arrester energy duty calculation and for comparison between line surge arrester energy duty calculation in EMTP – RV and MATLAB is given below.

```
% © Selma GREBOVIC

clc
clear all
load('Ea.mat');
load('Iar_a.mat');
load('Uar_a.mat');
load('t.mat');

%V/I of Line Surge Arrester
ik=[-40000 -20000 -10000 -5000 -2500 -1000 1000 2500 5000
10000 20000 40000];
uk=[-357000 -324000 -291000 -275000 -252000 -239000 239000
252000 275000 291000 324000 357000];

%Interpolated voltage (from V/I and arrester curretn)
uint=[];
for k=1:length(t)
    uint(k)=interp1(ik,uk,Iar_a(k),'spline','extrap');
end

%Plot arrester curretn, voltage from EMTP - RV and
interpolated voltage from MATLAB

figure(1)
subplot(2,1,1)
plot(t*10^6,Iar_a/1000,'-g'); grid on;
set(gca,'FontName','Times New Roman');
set(gca,'FontSize',18);
title('Arrester Current');
xlabel('Time (\mus)');
ylabel('Current (kA)');
```

```

subplot(2,1,2);
plot(t*10^6,uint/1000,'-r'); hold on;
plot(t*10^6,Uar_a/1000,'-b'); grid on;
set(gca,'FontName','Times New Roman');
set(gca,'FontSize',18);
title('Arrester Voltage');
xlabel('Time (\mus)');
ylabel('Voltage (kV)');
legend('Interpolated voltage using arresters V - I
characteristic','Voltage calculated using EMTP - RV');

FigHandle = figure(1);
set(FigHandle, 'Position', [100, 100, 1100, 700]);

%Energy calculation in MATLAB

u=[uint(1)];
i=[Iar_a(1)];
p=[0];
eint=[0];
t1=[0];
et=[0];

for k=2:1:length(t)
    t1=[t1,t(k)];
    u=[u,uint(k)];
    i=[i,Iar_a(k)];
    p=[p,uint(k)*Iar_a(k)];
    eint=[eint,trapz(t1,p)];

end

% Energy comparison

figure (2)
plot(t1*1000000,eint/1000,'-r',t*1000000,e_ZnOT15_a/1000,'-
b');
grid on
set(gca,'FontName','Times New Roman');
set(gca,'FontSize',18);
title('Line surge arrester energy duty calculation in EMTP -
RV and MATLAB');
xlabel('Time (\mus)');
ylabel('Energy (kJ)');
legend('Energy calculated using MATLAB','Energy calculated
using EMTP - RV');

FigHandle = figure(2);
set(FigHandle, 'Position', [100, 100, 1100, 700]);

```